Synthesis, Characterization, and Reactivity of Heterogeneous Boron-Containing Cobalt Catalysts for Catalytic Transfer Hydrogenation

A Dissertation Presented for the

Doctor of Philosophy

Degree

The University of Tennessee, Knoxville

Michael Valentyn Kandziolka, III

May 2019

Copyright © 2019 Michael Kandziolka

All rights reserved

Dedication

This dissertation is dedicated to everyone that has supported me in my life, especially my parents. Without their love and support I would not have come this far.

Acknowledgements

There are many people I need to thank, without whom this dissertation would not be possible. First and foremost, I would like to thank my advisor Dr. Craig Barnes and co-advisor Dr. Steve Chmely for their mentorship in training me to become the scientist that I am today. I also thank my committee members, Dr. Joe Bozell, Dr. Sheng Dai, and Dr. Mark Dadmun for committing their time, patience, and effort to participating on my committee.

I would also like to thank my past and current group members that have made the past six years fun and rewarding: Dr. Austin Albert, Dr. Lena Elenchin, Dr. Ales Styskalik, Michael Orick, Jordan Travis, Christian Scott, and Breanna Vestal.

I also want to thank my friends in other research groups with whom I've shared both the challenges and good times of graduate school: Dr. Kaitlyn McDonald, Matthew McDonald, Missy Bailey, Mark Hipshire Jr., Melinda Howard, and Morgan Higgins.

I also graciously acknowledge Dr. Shawn Campagna and Dr. George Schweitzer for their help, mentorship, and dedication to helping students. I also want to thank past mentors from my undergraduate and post-graduate studies at both the University of Tennessee and Oak Ridge National Laboratory: Dr. Ben Xue, Dr. Michael Sepaniak, Dr. Aditya Savara, and Dr. Nickolay Lavrik. Their mentorship laid the foundational groundwork for me to successfully pursue a career in science.

Finally, I graciously thank my parents. Without their love and support this dissertation would not have been possible.

Abstract

The primary focus of this work was to synthesize and characterize boron-containing cobalt catalysts for selective catalytic transfer hydrogenation (CTH) of several reducible substrates in the interest of lignin valorization applications. Lignin is of interest because it is the most abundant natural source of aromatic nuclei, and a potential competitor with non-renewable petroleum as a source of fuels and value-added chemicals. CTH reactions are a potential route towards effectively reducing lignin's oxygen content. Most CTH catalysts involve expensive noble metals, thus there is interest in discovering earth-abundant catalysts based on Fe, Co, and Ni. Two types of heterogeneous B-containing Co catalysts ("CoB") that exhibit high activity and selectivity for catalytic transfer hydrogenation of carbonyl groups.

CoB catalysts were synthesized using a facile aqueous reduction protocol under air-free conditions and are highly responsive to a strong magnet. The as-synthesized batch was exposed to air ("oxidized" CoB (CoB_{oxi}), and the rest was stored in an inert atmosphere glovebox ("reduced" CoB (CoB_{red})). They were characterized using inductively coupled plasma-optical emission spectroscopy (ICP-OES), powder X-ray diffraction (PXRD) and scanning transmission electron microscopy-energy dispersive X-ray spectroscopy (STEM-EDX). Product distributions and catalyst parameters were quantified by gas chromatography-mass spectrometry (GC-MS). PXRD indicated that both catalysts are amorphous and ICP-OES showed the atomic ratios of CoB_{oxi} are $Co_{1.7}BO_{1.7}$ and CoB_{red} are $Co_{1.7}B$. TEM revealed that both consist of amorphous particles of various sizes encased in a 2-3 nm layer of an amorphous coating. EDX showed that cobalt and boron are uniformly distributed throughout the particles. Post-reaction characterization with STEM revealed the formation of crystalline Co and Co_3O_4 phases on the catalyst surfaces.

CoB_{red} was shown to be the most active catalyst under all conditions tested. The activity of CoB_{oxi} was significantly lower, suggesting that the active site may be a reduced species. A pretreatment protocol was used to enhance the activity of both catalysts. All CoB catalysts were shown to be active at 100 °C, and their selectivities can be tuned in certain cases by modifying the reaction parameters. The results described in this work reveal that B-containing Co materials are selective catalysts for CTH.

Table of Contents

Chapter 1 – Introduction to Heterogeneous Catalysis 1
Introduction to Catalysis 3
Homogeneous vs. Heterogeneous Catalysts 7
Strategies for Synthesizing Heterogeneous Catalysts 8
Evaluation of Catalyst Performance 19
The Catalyst Ensemble – Defining the Active Site 26
Single Site Heterogeneous Catalysts 27
SSHCs and Boron-Containing CoB Catalysts 35
Overview of Future Chapters 39
Chapter 2 – Heterogeneous Catalysts for Transfer Hydrogenolysis and Lignin Valorization 40
Lignocellulosic Biomass, Lignin Structure, and Challenges with Lignin Valorization 40
Reductive Catalytic Fractionation & Sustainable Routes Towards Lignin Valorization 45
Hydrogenation & Catalytic Transfer Hydrogenation 46
Heterogeneous Catalysts for Transfer Hydrogenation 51
Screening of Other Substrates 54
Chapter Summary 56
Chapter 3 – Experimental Methods 59
General Experimental 59
Synthesis of CoB Catalysts 59
Characterization of CoB Catalysts 61
Use of Gravimetric Analysis in ICP-OES and GC-MS Analysis 61
Elemental Analysis with ICP-OES 63
Catalysis Reactor Preparation 67
Gas Chromatography-Mass Spectrometry (GCMS) 68
Catalysis Analysis: Quantitative GCMS 73
Calculation of Catalysis Parameters: % Conversion, % Selectivity, % Yield, and % Mass Balance 78
Catalyst Recycling 86
Catalyst Activation by Pretreatment with i-PrOH 88
Chapter Summary 89
Chapter 4 – Results and Discussion – Spectroscopic and Catalytic Characterization of CoB Catalysts 90
Characterization of As-synthesized CoB_{oxi} and CoB_{red} 90
Catalysis: Possible Reaction Pathways for Reduction of Acetophenone, Acetovanillone, and Guaiacol 95

Catalysis: Comparison of Catalytic Performance of CoB_{oxi}, CoB_{red}, and Co powder 101
Catalysis: Acetophenone 103
Catalysis: Acetovanillone 103
Catalysis: Guaiacol 107
Comparison of CoB_{oxi} and CoB_{red} with a Mixture of Acetophenone, Acetovanillone, and Guaiacol 107
Discussion on the Temperature Study of Catalysis of Acetophenone, Acetovanillone, and Guaiacol 114
Reduction of Acetophenone, Acetovanillone, and Guaiacol in EtOH 125
Stability of CoB_{red} for Conversion of Acetophenone 126
Pretreatment with I-PrOH: Activation of CoB_{oxi} and CoB_{red} 131
Comparison of CoB_{oxi} and CoB_{red} for Catalysis at 100 °C 134
Comparison with Other Heterogeneous Cobalt Catalysts for Reduction of Acetophenone 139
Chapter Summary 144
General Conclusions 148
Future Work 148
The Role of Oxidation States in Catalysis: X-Ray Photoelectron Spectroscopy (XPS) 148
Counting the Active Sites: Gas Chemisorption Analysis 149
Other Chemical Transformations 150
Continuous Flow Reactor 150
Attacking Lignin: Evaluating CoB Catalysts with Real Lignin Feedstocks 150
Nanocrystalline Metal Borides 151
References 152
Vita 159

List of Tables

Table 1. Measured concentrations of Co and B present in CoB_{red} and CoB_{oxi} 66
Table 2. Total errors estimated from the calculated relative response factor errors and the estimated peak area integration errors for all components. 80
Table 3. Summary of the main experiments done in this work. 106
Table 4. Summary of the blanks and controls with acetophenone. 109
Table 5. Screening of catalysts with acetophenone, acetovanillone, and guaiacol in i-PrOH 113
Table 6. Numerical values for comparison of CoB_{oxi} and CoB_{red} with all three substrates. 116
Table 7. Catalytic screening of acetophenone, acetovanillone, and guaiacol in EtOH with CoB_{red} 130
Table 8. Recycling study over 10 runs with CoB_{red} and acetophenone substrate. 133
Table 9. Comparison of CoB_{oxi} and CoB_{red} with and without pretreatment with i-PrOH. 136
Table 10. Comparison of CoB_{red} and CoB_{oxi} after 0, 1, and 2 hours of pretreatment with i-PrOH. 138
Table 11. Comparison of CoB_{red} and CoB_{oxi} with acetophenone, acetovanillone, and guaiacol at 100 °C with and without pretreatment with i-PrOH. 143
Table 12. Comparison of CoB catalysts in this work with some other reported heterogeneous Co catalysts for reduction of C=O bonds. 145

List of Figures

Figure 1. Illustration of a petroleum and natural gas reservoir (top) and an oil refinery schematic (bottom). Figure adapted from reference 1. 2
Figure 2. Activation energy (E_a) plot showing energy (in arbitrary units) vs. the reaction coordinate for an uncatalyzed (smooth blue line) and uncatalyzed (dotted blue line) reaction. The catalyst increases the rate of the reaction by lowering the activation energy. Note that in both cases, the total thermodynamic free energy (ΔG) between reactants and products remains unchanged. 5
Figure 3. Illustration depicting several pincer-type ligands and their influence on properties of the metal atom. Figure reprinted from reference 5. 6
Figure 4. Illustration of the particle nucleation and growth process a) without a capping agent and b) with a capping agent. 10
Figure 5. Reaction schemes illustrating condensation of a) silica, b) alumina, and c) co-condensation to form silica-alumina (reference 9). 13
Figure 6. Two examples of zeolite crystal structures, a) Zeolite A, and b) Zeolite X. Figure reprinted from reference 22. 15
Figure 7. Illustration of the templating process using a surfactant template. Surfactants in aqueous media spontaneously self-assembly into micelle structures which organize into hexagonal assemblies. Addition of a silicate precursor creates surfactant-templated silica, which must be calcined to remove the remaining organic template. 17
Figure 8. Illustration of incipient wetness impregnation. Larger pores result in formation of larger particles than those formed in smaller channels, resulting in catalyst particle size variation. 18
Figure 9. Illustration of the fundamental adsorption-transformation-desorption steps involved in heterogeneous catalysis using the classic example of nickel-catalyzed ethylene hydrogenation. 20
Figure 10. Illustrations of a) poisoning, b) fouling, c) sintering, and d) leaching. 24
Figure 11. Illustrations of a) solid migration, b) support pore collapse), and c) volatilization. 25
Figure 12. Conceptualization of catalyst ensembles in a) a simple case of a single four-coordinate metal atom anchored to a silica surface via two linkages and two ligands (L = -OH, -OR, capping agent, etc.), and b) a more complex example showing a particle of surface-anchored metal oxide, consisting of a multitude of ensembles and possible active sites. The degree of saturation, nature of the coordinating ligand, and distortion of the coordination geometry are all factors that can influence catalytic activity. 28
Figure 13. Illustration of several types of single site heterogeneous catalysts a) as an isolated, embedded atom, b) as an isolated ion, c) as a metallocene complex used for olefin polymerization (reference 34), and d) as a noncovalently anchored species via hydrogen bonding between surface hydroxyl groups and a sulfonate ion. 29
Figure 14. Illustration of a) different types of surface silanols, b) structure of $TiCl_4$, and c) examples of possible titanium sites after reaction of $TiCl_4$ with the various silanol types. 31
Figure 15. Illustration of modification of a silica surface via reaction of surface silanols with $TiCl_4$ a) before silica dehydroxylation, b) after dehydroxylation, and c) after over-dehydroxylation where all silanols have been removed. Note that in case (a), many different surface-titania species are formed. In case (b), more isolated titania species exist but different types can still be formed. In (c), no silanols are available, thus no functionalization occurs, and the surface must be re-hydroxylated to regenerate surface silanols. 32

Figure 16. Reaction scheme showing copolymerization of divinylbenzene and sodium p-styrenesulfonate to form the corresponding copolymer. The sodium ion is then exchanged with a proton by reaction with sulfuric acid to form the heterogeneous acid catalyst. Figure adapted from reference 39. 34
Figure 17. Examples of the many different types of POSS structures. Figure reprinted from reference 42. 36
Figure 18. Illustration of synthesis of poly-POSS-styrene materials. Figure adapted from reference 43. . 37
Figure 19. Example of a crosslinking metathesis reaction between trimethyltin-capped POSS cubes and a metal chloride. 38
Figure 20. Illustration of components of lignocellulosic biomass. Figure reprinted from reference 52. ... 41
Figure 21. Simplified reaction scheme illustrating enzymatic biosynthesis of monolignols, followed by monolignol polymerization to form lignin. 43
Figure 22. Reaction scheme illustrating oxidative radicalization of coniferyl alcohol and several possible dimerization products. Figure adapted from reference 53. 44
Figure 23. Illustration of traditional refining routes (red and blue lines), and more direct, sustainable route (green line) towards refining crude biomass to advanced products. 47
Figure 25. Illustration of catalytic transfer hydrogenation of a several reducible functionalities in the presence of catalyst and isopropanol as the H-donor: A) reduction of a ketone to an alcohol through transfer hydrogenation, B) reduction of an alcohol to an alkane through transfer hydrodeoxygenation, and C) cleavage of a methoxy group to an alkane and MeOH. 49
Figure 24. Illustration of catalytic hydrogenation of several reducible functionalities in the presence of catalyst and hydrogen gas: A) reduction of a ketone to an alcohol through hydrogenation, B) reduction of an alcohol to an alkane through hydrodeoxygenation, and C) cleavage of a methoxy group to an alkane and MeOH. 50
Figure 26. Simplified illustrations of the Meerwein-Ponndorf-Verley reduction reactions catalyzed by A) a homogeneous aluminum alkoxide catalyst and B) a heterogeneous analogue consisting of Lewis basic and acidic active sites. 52
Figure 27. Illustration of the various reducible moieties of acetophenone, acetovanillone, and guaiacol. 55
Figure 28. Summary of various substrates and their product distributions after CTH with CoB catalysts. All reactions were conducted in *i*-PrOH unless otherwise indicated. Red text refers to “minor” and “major” products. However, these products were not quantified and these assignments are entirely qualitative. 57
Figure 29. Images illustrating the steps for synthesizing CoB catalysts. 60
Figure 30. Photographs showing the response of CoB catalysts to a strong neodymium magnet. 62
Figure 31. ICP-OES calibration curves for Co and B. 65
Figure 32. Photographs illustrating the steps for preparing reactors used as the catalysis reaction vessels: A) separated reactor components, B) hex nipple threading secured to a vice and wrapped in Teflon tape, C) one cap securely attached to the taped threading, D) rotation of the reactor and taping of the opposite side, E) reactor that is ready to be charged with catalyst and reaction solution, and F) the final, sealed reactor ready for catalysis. 69
Figure 33. Images showing the heat bath setup used for catalysis. 70
Figure 34. Temperature ramp profiles of the reactors at 165, 200, and 300 °C. 71
Figure 35. Example of the mass chromatogram (top) and mass spectrum (bottom) of acetovanillone. .. 74

Figure 36. Response factor curves for acetophenone (top), 1-phenylethanol (middle), and ethylbenzene (bottom). 75
Figure 37. Response factor curves for acetovanillone (top) and 4-ethylguaiacol (bottom). 76
Figure 38. Response factor curves for guaiacol, phenol, and cyclohexanol. 77
Figure 39. Illustration of chromatograms of acetovanillone before (left) and after (right) catalysis. The large values in red indicate the elution times. 81
Figure 40. Illustration of the error associated with peak area integrations. The large values in red indicate the elution times 85
Figure 41. Chromatogram of a post-reaction mother liquor (top) and the isopropanol wash solution after the third wash (bottom). Vertical scales are $x10^6$. 87
Figure 42. PXRD spectra of as-synthesized CoB_{oxi} (left) and CoB_{red} (right). 91
Figure 43. TEM Micrographs of CoB_{oxi} (left) and CoB_{red} (right). 92
Figure 44. EDX maps of as-synthesized CoB_{oxi} showing Co (red), O (green), B (blue), and all three elemental maps overlaid. 93
Figure 45. EDX maps of as-synthesized CoB_{red} showing Co (red), O (green), B (blue), and all three elemental maps overlaid. 94
Figure 46. PXRD spectra CoB_{oxi} (left) and CoB_{red} (right) after reaction with acetophenone 96
Figure 47. TEM micrograph of CoB_{oxi} after reaction with acetophenone at 165 °C for 15 minutes. The red box indicates the area in which the 2D fast Fourier transform FFT (top left) was taken. 97
Figure 48. EDX maps of CoB_{oxi} after reaction with acetophenone at 165 °C for 15 minutes showing Co (red), O (green), B (blue), and all three elemental maps overlaid. 98
Figure 49. TEM micrograph of CoB_{red} after 10 recycling runs with acetophenone at 165 °C for 15 minutes. The red box indicates the area in which the 2D fast Fourier transform FFT (top left) was taken. 99
Figure 50. EDX maps of CoB_{red} after 10 reactions with acetophenone at 165 °C for 15 minutes showing all maps overlaid (top left), Co (red), O (green), and B (blue). 100
Figure 51. Reaction schemes for some possible reduction pathways of A) acetophenone, B) acetovanillone, C) guaiacol. Substrates are highlighted in blue. Species highlighted in red were not observed in GCMS analysis. 102
Figure 52. Example of the bar chart illustration of catalytic performance. 104
Figure 53. Bar illustration depicting the catalysis parameters for conversion of acetophenone at 300° C at 15 minutes in the presence of CoB_{oxi}. 105
Figure 54. Blanks and controls with acetophenone. Conditions: 10 mg catalyst, 0.5 mmol acetophenone, 2 mL i-PrOH, 200 °C, 15 minutes. Numerical values shown in Table 4. 108
Figure 55. Catalytic results of acetophenone substrate at 300, 200, and 165 °C. Conditions: 10 mg catalyst, 0.5 mmol substrate, 2 mL i-PrOH, 15 minutes. Numerical values shown in Table 5. 110
Figure 56. Catalytic results of acetovanillone substrate at 300, 200, and 165 °C. Conditions: 10 mg catalyst, 0.5 mmol substrate, 2 mL i-PrOH, 15 minutes. Numerical values shown in Table 5. 111
Figure 57. Catalytic results with guaiacol substrate at 300, 200, and 165 °C. Conditions: 10 mg catalyst, 0.5 mmol substrate, 2 mL i-PrOH, 15 minutes. Numerical values shown in Table 5. 112
Figure 58. Catalytic results of CoB_{red} and CoB_{oxi} with a mixture of all three substrates at 200 °C. Conditions: 10 mg catalyst, 0.5 mmol of each substrate, 2 mL i-PrOH, 15 minutes. Numerical values shown in Table 6. 115
Figure 59. Possible reduction pathway of acetophenone to ethylbenzene 118

Figure 60. Catalytic results showing comparison between 4-ethylguaiacol and guaiacol as substrates at 200 °C in the presence of CoB_{red}. Conditions: 10 mg CoB_{red}, 0.5 mmol substrate, 2 mL i-PrOH, 15 minutes. 121
Figure 61. Tautomerization of phenol to cyclohexa-2,4-diene-1-one and subsequent hydrogenation to cyclohexanone and cyclohexanol. 122
Figure 62. Proposed reduction schemes showing the major products formed from each substrate at 200 °C for 15 min in i-PrOH. 123
Figure 63. Illustration of possible surface interactions of various functional groups of each substr 124
Figure 64. Possible reduction pathways over CoB catalysts. 127
Figure 65. Catalysis results with acetophenone, acetovanillone, and guaiacol in the presence of CoB_{red} at 200 °C. Conditions: Conditions: 10 mg CoB_{red}, 0.5 mmol substrate, 2 mL EtOH, 3 hours. n.r. = "no reaction." Numerical values shown in Table 7. 128
Figure 66. Catalysis results with acetophenone, acetovanillone, and guaiacol in the presence of CoBoxi or CoBred at 200 °C. Conditions: Conditions: 10 mg catalyst, 0.5 mmol substrate, 2 mL EtOH, 18 hours. Numerical values shown in Table 7. 129
Figure 67. Recycling of CoB_{red} over 10 runs. Conditions: 10 mg catalyst, 0.5 mmol acetophenone, 2 mL i-PrOH, 165 °C, 15 minutes. Numerical values shown in Table 8. 132
Figure 68. Comparison of CoB_{oxi} and CoB_{red} after activation with isopropanol at 250 °C for 1 hour, and no activation for conversion of acetophenone (left), acetovanillone (middle), and guaiacol (right). Conditions: 10 mg catalyst, 0.5 mmol substrate, 2 mL i-PrOH, 165 °C, 15 minutes. Numerical values shown in Table 9. 135
Figure 69. Comparison of activity of CoB_{oxi} and CoB_{red} with acetophenone after 2 hours of pretreatment at 250 °C, 1 hour of pretreatment at 250 °C, and no pretreatment. Catalysis conditions: 10 mg catalyst, 0.5 mmol acetophenone, 2 mL i-PrOH, 165 °C, 15 minutes. Numerical values shown in Table 10. 137
Figure 70. Comparison of CoB_{oxi} and CoB_{red} for conversion of acetophenone with and without pre-activation with isopropanol. Catalysis conditions: 10 mg catalyst, 0.5 mmol acetophenone, 2 mL i-PrOH, 100 °C, 18 hours. Numerical values shown in Table 11. 140
Figure 71. Comparison of CoB_{oxi} and CoB_{red} for conversion of acetovanillone with and without pre-activation with isopropanol. Catalysis conditions: 10 mg catalyst, 0.5 mmol acetovanillone, 2 mL i-PrOH, 100 °C, 18 hours. Numerical values shown in Table 11. 141
Figure 72. Comparison of CoB_{oxi} and CoB_{red} for conversion of guaiacol with and without pre-activation with isopropanol. Catalysis conditions: 10 mg catalyst, 0.5 mmol guaiacol, 2 mL i-PrOH, 100 °C, 18 hours. Numerical values shown in Table 11. 142
Figure 73. Flow-chart summary of CoB catalysts that were studied in this work. Red text indicates which samples were amorphous and which samples showed crystalline features as determined by TEM. 147

Chapter 1 – Introduction to Heterogeneous Catalysis

Catalysts are responsible for generating approximately $10 trillion USD annually by driving many industrial chemical processes that propel and sustain our standard of living. One of the most important applications of catalysts is for upgrading crude petroleum feedstocks, in which high molecular weight hydrocarbons are reduced to lower molecular hydrocarbons at elevated temperatures in the presence of a solid acid catalyst. Crude oil and natural gases are extracted from natural reservoirs, which have accumulated primarily from ancient deceased microbial organisms. Once extracted, the oil is then converted in refineries *via* catalytic cracking, which creates upgraded small-molecule derivatives that can be used as fuels, fuel additives, lubricants, olefins, and other fine chemicals (Figure 1). Petroleum-derived hydrocarbons are grouped into several categories such as paraffins, olefins, aromatics, and various nitrogen and sulfur-containing heteroatomic molecules.[1] The solid acid catalysts used for petroleum cracking are a class of silica-alumina based catalysts known as *Zeolites* and are responsible for generating most of the world's supply of gasoline.

Another key application of catalysis is in the development and use of *catalytic converters* which are found in every modern automobile. Catalytic converters consist of a ceramic or metallic support (usually referred to as the "converter monolith"), whose surface is decorated with a layer of finely dispersed palladium, platinum, and rhodium.[2] These three precious metals are the catalytically active components of the "three-way" catalytic converter and are responsible for converting carbon monoxide (CO) and nitrogen oxides (NO_x), which are extremely environmentally hazardous gases emitted out of conventional combustion engines, to benign carbon dioxide (CO_2), nitrogen (N_2), and water.[3] In many modern catalytic converters, the ceramic support is made into a tubular, honeycomb structure. The honeycomb structure is specifically designed to optimally increase its surface area, which in turn increases the surface area of the fine coating of precious metals, and therefore enhances the overall activity of the catalytic converter by exposing more catalytically active metal to the targeted gaseous species as they pass through. The notion of supporting catalytically active components onto a high-surface area support is a common and important motif in the design of heterogeneous catalysts in general and is discussed in more detail later in this chapter.

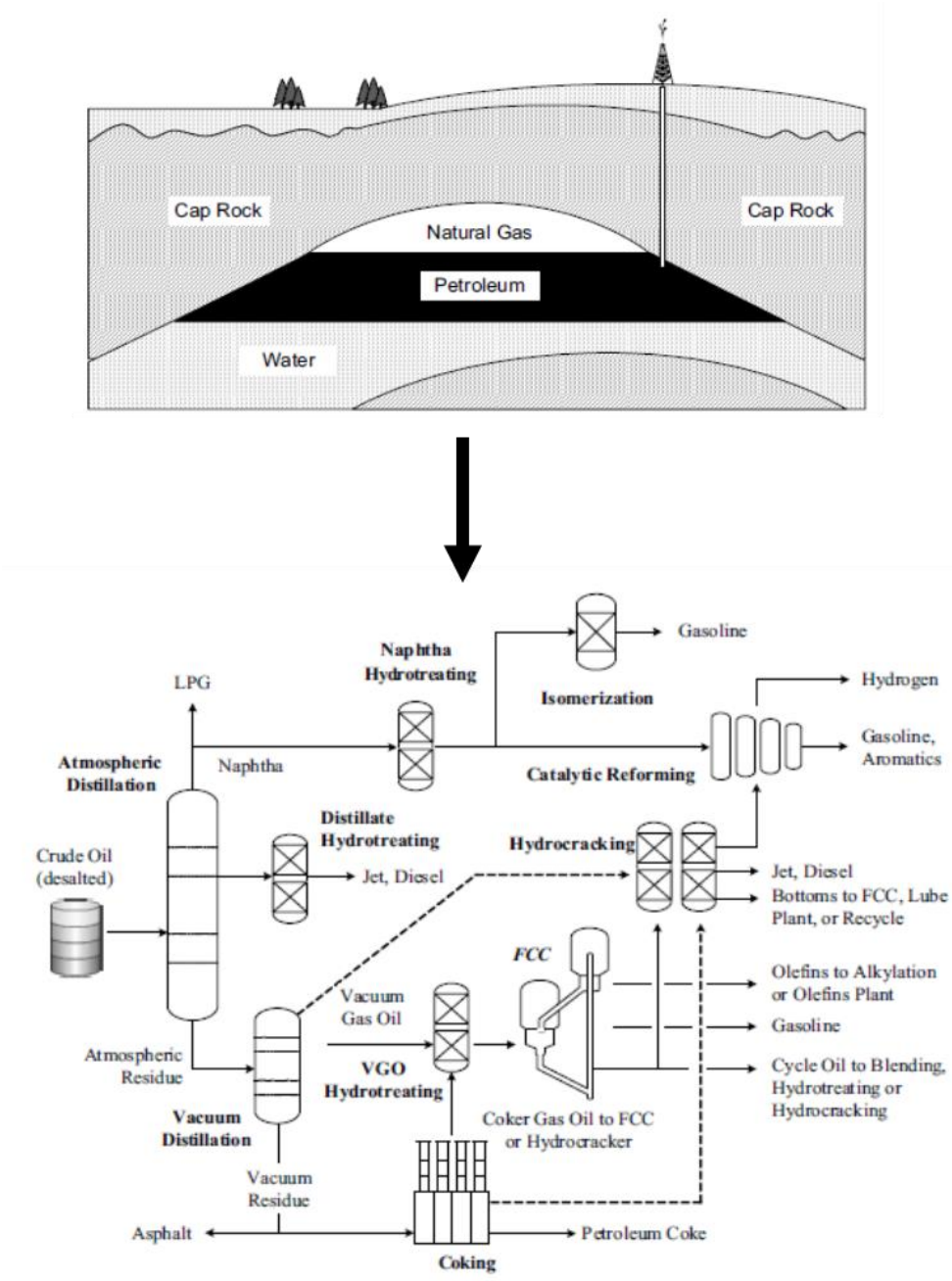


Figure 1. Illustration of a petroleum and natural gas reservoir (top) and an oil refinery schematic (bottom). Figure adapted from reference 1.

Though petroleum is the primary source of global fuel, fossil fuels contribute the largest fraction of human-generated CO_2 into the atmosphere which causes significant concern over global climate change. However, fossil fuels are expected to become less viable as the primary global fuel source within a few decades chiefly due to non-renewability and declining natural reserves which will also result in substantial increases in energy costs. It is noteworthy that the advent of hydraulic fracturing (i.e. "fracking"), a petroleum and natural gas extraction technique in which pressurized fluid is used to crack rocks deep in the earth, has abated many concerns over declining natural fuels. However, use of fracking is a political hot-button topic due to concerns over the possibility of environmental contamination of drinking water sources and environmental pollution.[4] As previously mentioned, fossil fuels also contribute the majority of CO_2 emissions which continues to raise concerns over the effects of climate change. For these reasons, significant effort is now being made to make available alternative sources of energy such as wind, solar, and biomass.

Using plant biomass as a renewable feedstock for fuels and high-value chemicals has become the focus of significant research efforts. The cell walls of plants are comprised of cellulose, hemicellulose, and lignin, the three of which are collectively referred to as lignocellulosic biomass. The primary focus of this work was to study the catalytic behavior of support-free boron-containing cobalt catalysts (referred to here as "CoB" catalysts) with several simple lignin models in the interest of lignin valorization. These earth-abundant catalysts are inexpensive, are readily synthesized *via* facile reduction of high valent solubilized cobalt with sodium borohydride, and easily magnetically separated from reaction solutions. The catalytic behavior of CoB catalysts was studied for reduction of acetophenone, acetovanillone, and guaiacol *via catalytic transfer hydrogenation* to illustrate the potential utility of these catalysts for biomass upgrading. These are the topics of future chapters. First, this chapter briefly introduces the basics of catalysis with a focus on heterogeneous catalysts, including common synthesis strategies, parameters for evaluating catalyst efficiency, and some of the challenges associated with developing heterogeneous catalysts.

Introduction to Catalysis

Catalysis is a field concerned with the synthesis, characterization, and optimization of *catalysts*. Catalysis is a multi-disciplinary field which combines facets of organic chemistry, inorganic chemistry, materials science, chemical engineering, and physics. A catalyst is defined as a substance that increases the rate of a reaction without itself being consumed. Catalysts increase reaction rates by decreasing the activation energy but do not alter the thermodynamic free energy (ΔG) for the reaction. In other words,

catalysts only enhance the kinetics of a reaction, and not the thermodynamics. Catalysts decrease activation energies by providing stability to reactive intermediates that are otherwise too energetic and unstable and make available alternative mechanistic pathways for chemically transforming substances into desired products. Some of the major (and often very challenging) goals in catalysis science are to identify these mechanistic pathways, identify which components of the catalyst are responsible for inducing chemical transformations, determine catalytic cycles, and use this knowledge to make predictions towards developing more efficient catalysts. Figure 2 illustrates a typical activation energy plot for a catalyzed and uncatalyzed reaction.

There are several classes of catalysts. The three main classes include 1) homogeneous and 2) heterogeneous catalysts, which are produced synthetically, and 3) enzymatic catalysts, which are naturally occurring biological catalysts.

1) Homogeneous catalysts are in the same phase as the reactants, most commonly in the liquid phase. Modern homogeneous catalysts are organometallic complexes consisting of a transition metal center coordinated with multiple organic ligands. Organic ligands bind to the Lewis acidic metal center *via* chelating sites, which are usually Lewis basic atoms such as N, O, S, or P. The transition metal is the active site, and the coordinating ligands serve to modify the shape and electronic structure of the metal center, which modifies its activity. Figure 3 illustrates several examples of pincer-type homogeneous catalysts.[5]
2) Heterogeneous catalysts are in a different phase than the reactants and are most commonly a solid interacting with liquid or gaseous phase reactants. Heterogeneous catalysts are the most common type of catalyst used for industrial chemical processes and account for 90% of all catalysts used in industry.
3) Enzymatic catalysts are biological catalysts that exist in all living organisms and are necessary for facilitating the chemical reactions that sustain life. Enzymes are protein macromolecules whose amino acid residue backbone is precisely folded around its active site, which may or may not contain metal atoms. A combination of the shape and chemical nature of the enzyme's active site allows enzymes to exhibit remarkable activity and selectivity for converting reactants to products with extreme specificity.

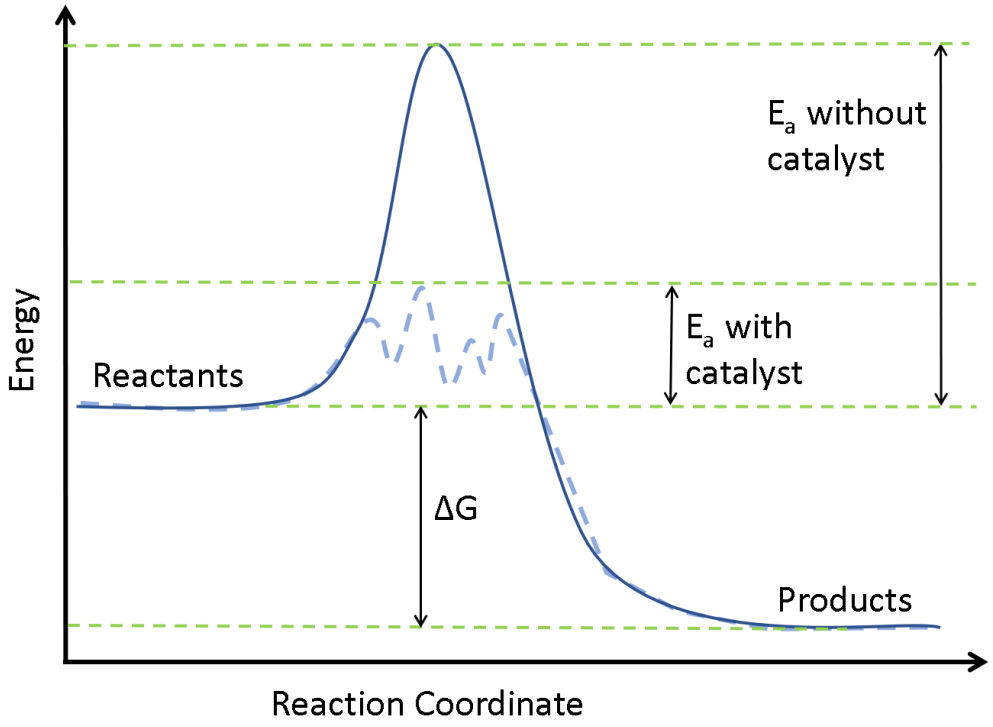


Figure 2. Activation energy (E_a) plot showing energy (in arbitrary units) vs. the reaction coordinate for an uncatalyzed (smooth blue line) and uncatalyzed (dotted blue line) reaction. The catalyst increases the rate of the reaction by lowering the activation energy. Note that in both cases, the total thermodynamic free energy (ΔG) between reactants and products remains unchanged.

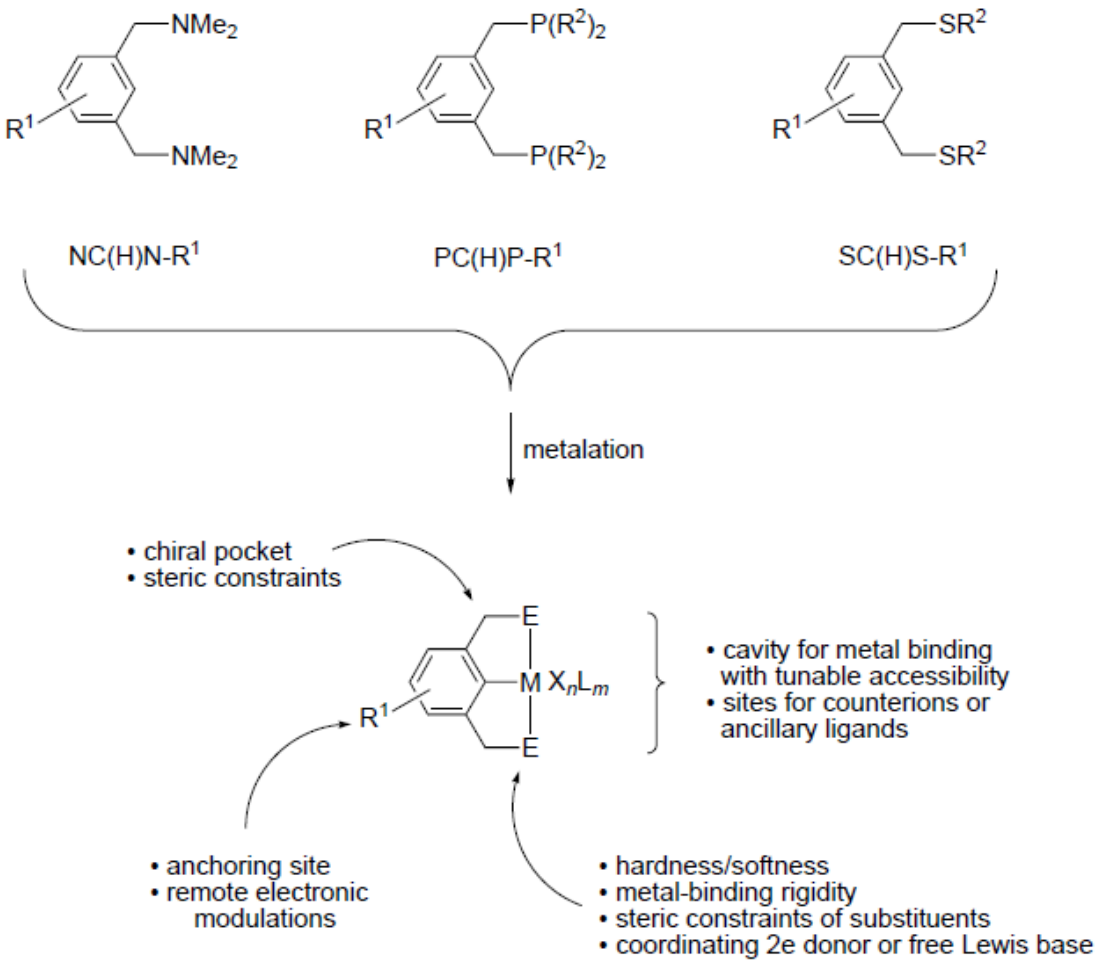


Figure 3. Illustration depicting several pincer-type ligands and their influence on properties of the metal atom. Figure reprinted from reference 5.

Homogeneous vs. Heterogeneous Catalysts

Homogeneous catalysts readily dissolve in solution which makes them amenable to a suite of solution-based spectroscopic characterization techniques that can provide data for the precise determination and characterization of the active catalyst precursor. A few of the conventional "work-horse" spectroscopic techniques include Fourier transform infrared spectroscopy (FTIR), nuclear magnetic resonance spectroscopy (NMR), and X-ray crystallography. FTIR is used to determine molecule structure by probing vibrational modes of molecules. NMR is often well-suited for quantitative applications and allows both structural determination and quantification of molecules without the use of any external calibration. X-ray crystallography uses X-ray diffraction to map out molecular structure in single crystals.

These features present several distinct advantages of homogeneous catalysts over heterogeneous catalysts. Due to their insolubility, gaining structural information of heterogeneous catalysts is a formidable challenge that requires multiple characterization strategies. Powder X-ray diffraction (PXRD) is the most common technique of choice for characterizing crystalline phases of solid materials but is only applicable if the material in question possesses crystalline domains. Inductively coupled plasma – optical emission spectroscopy is a valuable technique for determining and quantifying atomic composition with sensitivity into the parts-per-billion (ppb) regime but provides no structural information because the sample must be completely digested in aqueous acid prior to analysis. X-ray absorption fine structure (XAFS) is an advanced X-ray spectroscopic technique that can provide information about the coordination sphere around the target atom.

The surface of a heterogeneous catalyst is where the active sites ultimately reside, and surface characterization is a non-trivial task. The techniques just described generally only provide information for an averaged structure of the sample, and not necessarily the surface structure, where actual catalysis occurs in heterogeneous catalytic reactions. One method to characterize surfaces involves chemisorption strategies in which a probe molecule (such as CO, ethylene, CO_2, NH_3, etc.) is adsorbed onto the active site, and the sample is then analyzed spectroscopically (typically by FTIR). Changes in the spectroscopic features of the adsorbed materials due to their interactions with the surface can be used to make assessments of the catalyst surface composition and to "count" surface active sites. Although gas sorption techniques can often be informative, they do not necessarily provide direct information about the nature of the heterogeneous active site.

In the face of all the challenges of heterogeneous catalysts present, one might ask why anybody would ever bother using heterogeneous catalysts at all. With this question in mind, almost paradoxically, most catalysts used in industrial processes are heterogeneous. There are two main reasons: 1) heterogeneous catalysts are often much more stable at high temperatures than homogeneous catalysts, which often decompose above 200 °C, and 2) heterogenous catalysts are much more easily separated and recycled from reaction solutions. Despite their disadvantages, these two features make heterogeneous catalysts much more industrially relevant because many industrial processes involve elevated temperatures (200-1000 °C). Furthermore, separating products from homogeneous solutions is extremely costly and can account for up to half of all operating costs. Easy separation and recycling of heterogeneous catalysts dramatically reduces processing costs and decreases generation of waste.

Heterogeneous catalysts can either be supported or non-supported. In the case of the supported catalyst, the active component (i.e. the metal or metal oxide responsible for catalysis) is bound to an inert material, such as silica gel (SiO_2). In the case of non-supported catalysts, the active component exists as a free particle. However, because free active particles typically possess highly reactive and energetic surfaces, free particles tend to lower their surface energy by aggregating into larger particles. This may severely diminish their active surface area and thus the number of available active sites, resulting in decreased activity, or even total deactivation. To prevent undesirable aggregation, the active component can be finely dispersed onto, or embedded into, an inert support. Embedded active sites are generally desired over surface-confined active sites because embedded sites interact with the support much more intimately, which helps prevent undesirable loss of the active component through “leaching” under catalytic reaction conditions. General strategies for synthesizing heterogeneous catalysts and incorporating the active component with an inert support can be accomplished in numerous ways and are discussed in the following section.

Strategies for Synthesizing Heterogeneous Catalysts

Simple wet synthesis, deposition-precipitation, sol-gel condensation, hydrothermal synthesis, templating, and incipient wetness impregnation are some of the most common strategies for producing heterogeneous catalysts. The choice of synthetic strategy depends on factors such as the desired application of the catalyst, costs associated with the reagents and processing required to synthesize the catalyst, the desired final composition of the solid material, and whether surface active sites or embedded active sites are desired. Strategies to create surface active sites can involve reduction or precipitation of a solubilized catalyst precursor onto a pre-synthesized support, as in the case of

deposition-precipitation. Embedding strategies typically involve simultaneous precipitation of both catalyst precursor and support precursors together, as in the case of sol-gel condensation.

Simple wet synthesis refers to the synthesis of solid materials by inducing their precipitation from a solution containing a soluble precursor. This is one of the most common and facile methods to produce nanoparticles.[6] The process of particle formation occurs by initial spontaneous creation of a seed particle from solution, referred to as nucleation, followed by particle growth. *Nucleation and growth* (Figure 4) is the most commonly cited operative mechanism by which solids form out of solution.[7] It involves formation of solid particles by either the physical process of recrystallization, in which solid crystals are formed by supersaturating a solution containing solubilized precursor, or by simple mixing of two solutions, one consisting of the solubilized catalyst precursor (typically a high-valent metal cation), and the other consisting of a reducing or precipitating agent. The mechanisms of nucleation and growth are classically described by Lamellar nucleation[8] followed by Ostwald ripening.[9] Strictly speaking, nucleation is defined as the process by which a distinct thermodynamic phase spontaneously forms. In general, the formed phase can either be solid (i.e. crystal growth), liquid (i.e. droplet condensation), or gaseous (i.e. bubble formation). In the context of this dissertation and of heterogeneous catalysis, nucleation will be discussed specifically in the context of liquid-to-solid transitions. Nucleation can either be homogeneous or heterogeneous (not to be confused with homogeneous or heterogeneous catalysts).[9] In homogeneous nucleation, particles form uniformly throughout a specified volume. In heterogeneous nucleation, particles form on structural features such as pre-existing seed particles, container walls, or surface inhomogeneities and defects. Nucleation is also categorized as either primary, in which nucleation occurs *via* spontaneous self-assembly of solubilized precursors, or secondary, in which nucleation is initiated by a pre-existing seed template. Growth is the second step in particle formation, the rate of which is a function of the diffusion rate of precursor to the particle surface and the rate of the reaction at the surface. During nucleation and growth, the soluble precursors are continuously consumed, and growth stops when insufficient precursor remains.

In many cases, this strategy is the most straightforward for producing catalysts, but generally offers little fine control over synthesis conditions which can lead to poor batch-to-batch reproducibility and poor consistency in the catalysts produced. Further, as previously mentioned, as-synthesized particles often contain highly energetic surfaces and rapidly aggregate. A strategy to circumvent

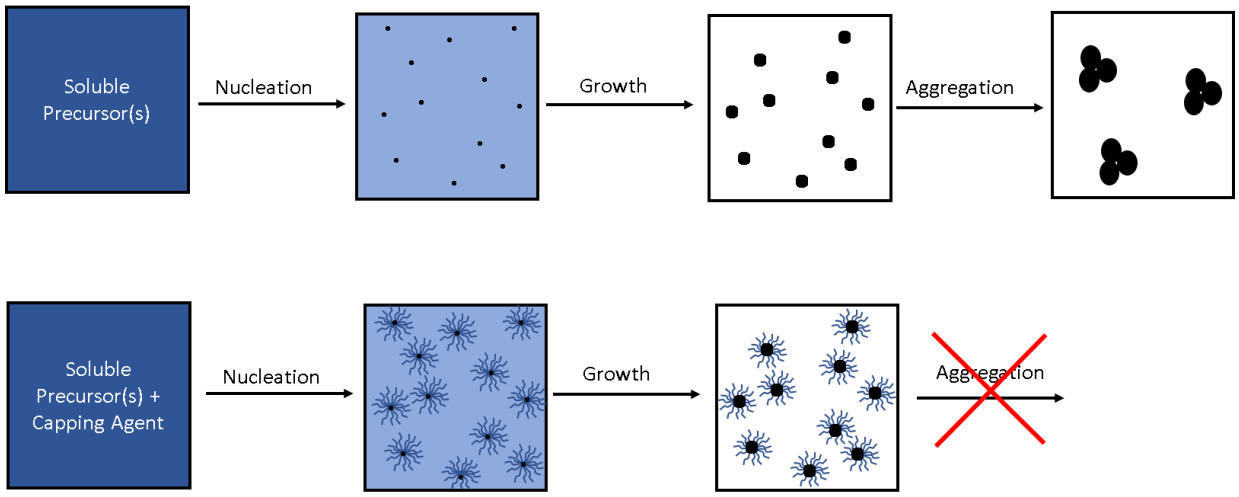


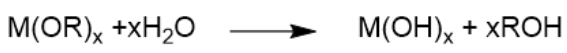
Figure 4. Illustration of the particle nucleation and growth process a) without a capping agent and b) with a capping agent.

aggregation and create more stable, uniform, and well-separated particles can be accomplished by the addition of a stabilizing capping agent such as a surfactant or polymer. The capping agent acts by directly coordinating with the surface of the particle as it grows, preventing inter-particle interaction and subsequent aggregation. However, as catalysis occurs on the surface of the particle, the surfactant often must be removed before catalysis *via* either solvent washings or calcination at elevated temperatures (>500 °C). Removal of the capping agent by calcination often leads to catalyst sintering which may render it inactive.

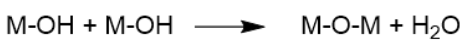
Multi-component alloy or ceramic particles can be produced using nucleation and growth strategies *via* co-precipitation or co-reduction, in which a solution consisting of multiple metal precursors are simultaneously mixed with a reducing or precipitating agent.[10] Alloys are compounds consisting of at least two different metals, whereas ceramics are compounds consisting of a combination of metal and non-metal, such as carbon, nitrogen, or oxygen. This strategy does not always proceed quantitatively nor necessarily generate a uniform, atomically intermixed material, especially if the reduction potentials or pH of precipitation of the precursors significantly differ from one another.

Deposition-precipitation is a strategy to deposit active catalyst onto a support surface by precipitating the metal precursor in the presence of a solid support. This can be accomplished by suspending a pre-synthesized support material, which acts as a nucleation site for the catalyst, in a solution containing dissolved metal precursor and subsequently precipitating the metal precursor as a metal oxide by increasing the pH of the solution, or reducing it with a reducing agent.

Sol-gel synthesis is one of the most commonly used strategies for synthesizing heterogeneous catalysts. The popularity of this technique is due to its ability to create a wide array of metal and ceramic oxide materials with controlled pore sizes from relatively inexpensive precursors under mild conditions.[11] Observation of the sol-gel phenomena first occurred in the 19th century by Ebelman and Graham, who discovered that tetraethyl orthosilicate (TEOS) spontaneously condenses into a glassy material after hydrolysis in acid. In the sol gel process, metal alkoxide monomer precursors are condensed to form colloidal metal oxides *via* aqueous hydrolysis. The metal alkoxides first react with water to form the corresponding metal hydroxide and alcohol, and the metal hydroxides subsequently condense to form the corresponding metal oxide solid and water. The general equations are as follows (Figure 5A):



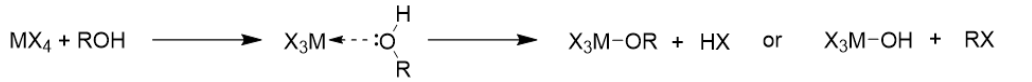
Equation 1.1



Equation 1.2

Properties such as morphology and pore size of the resulting sol-gel material can be tuned by varying precursor concentrations. In some cases, this method can also be used to create mixed matrices consisting of multiple metals, such as silica-alumina, one example of which was demonstrated by Narula and Rokosz.[12] In this example, silica-alumina sol-gels were synthesized by co-condensing TEOS and aluminum *sec*-butoxide. Figure 5C illustrates an example of silica, alumina, and silica-alumina condensation reactions. Creating mixed-metal oxides using sol-gel is, however, only feasible in cases where the hydrolysis rates of the reactive alkoxide precursors are similar. For example, the rate of hydrolysis of silicon alkoxide is much slower than that of titanium alkoxide, thus co-hydrolysis results in preferential formation of segregated Si-O-Si and Ti-O-Ti units, instead of co-condensed Si-O-Ti groups.[13]

Hydrolytic sol-gel condensation of metal alkoxides is an effective strategy for rapidly creating metal oxide materials at low temperatures, but poor control over the micro- and nanoarchitecture of the final sol-gel material is a common problem because the reaction rate of metal alkoxide condensation initiated by water is extremely fast.[14] An alternative sol-gel strategy uses nonhydrolytic sol-gel processes in which alkoxide condensation is initiated not by water, but either by aprotic reagents such as ethers, or non-aqueous protic reagents such as alcohols.[15] The most straightforward method to accomplish nonhydrolytic condensation is by simple thermal decomposition, although this method requires elevated temperatures (>200 °C). In cases where an alcohol is used to initiate condensation, the Lewis basic lone pair of the alcohol oxygen atom directly coordinates to the metal center, followed by



Equation 1.1

formation of either the metal alkoxide derivative and hydrogen halide, or metal hydroxide derivative and alkyl halide. The direction towards formation of M-OR or M-OH can be controlled by choice of alcohol.[16] Non-hydrolytic sol-gel routes can also be accomplished through a variety of other oxygen donors including esters[17], ethers, carboxylic acids, and carboxylates.

Hydrothermal synthesis is a strategy in which crystalline materials are synthesized at elevated temperature (>25 °C) and pressure (>1 atm). Hydrothermal synthesis works by exploiting the fact that a

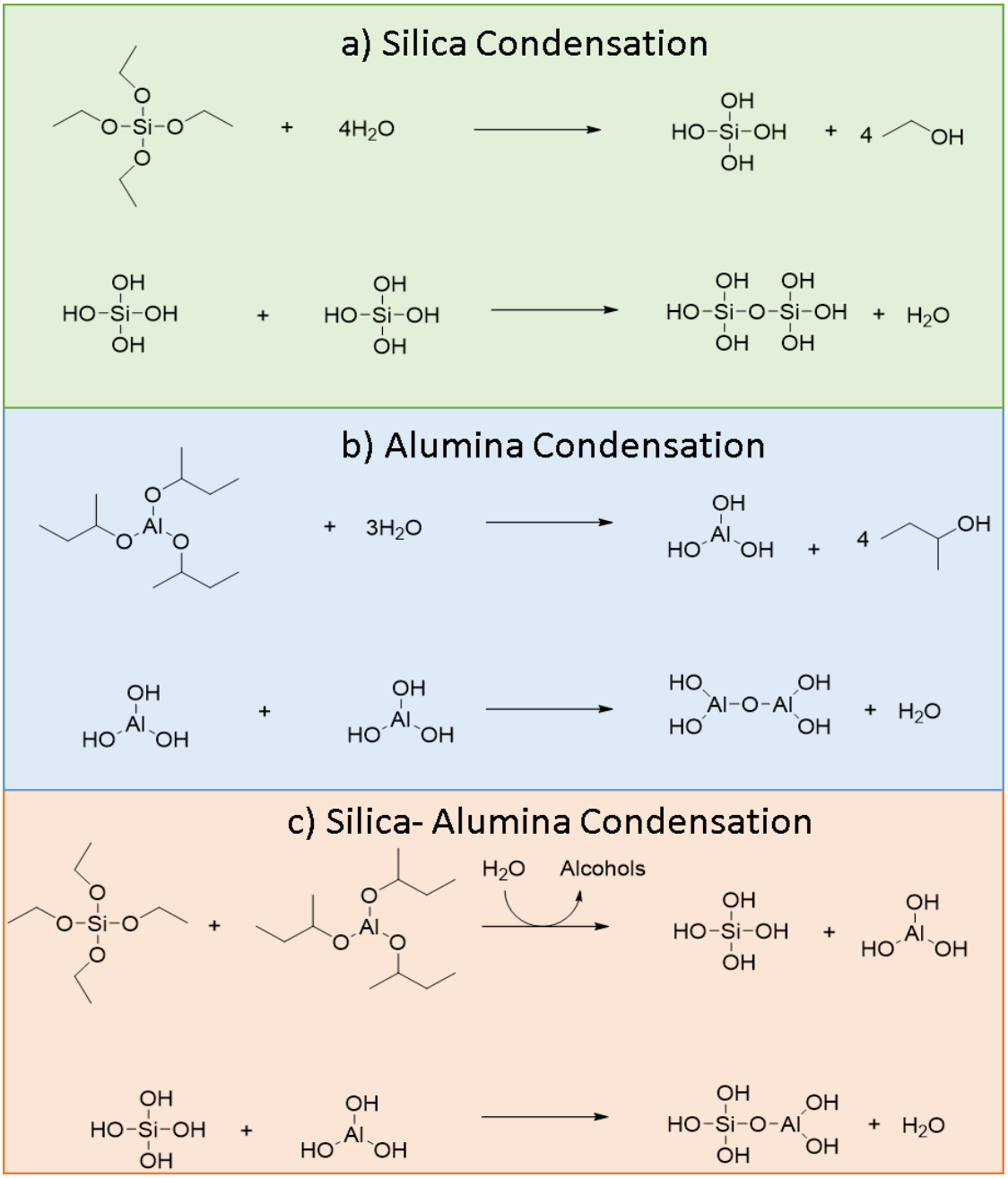


Figure 5. Reaction schemes illustrating condensation of a) silica, b) alumina, and c) co-condensation to form silica-alumina (reference 9).

solvent's dielectric constant and solubilizing capability changes with temperature.[18] The main disadvantages of this technique include long reaction times often requiring hours or days, and that steel autoclaves must be use which prevents observation of the reaction as it proceeds.

Hydrothermal synthesis is the most common method for synthesizing zeolites, which are an important class of porous crystalline silica-alumina materials that are extensively used for their catalytic[19,20] and adsorptive[21-23] properties. An example of a typical zeolite hydrothermal preparation procedure involves adding a suspension of amorphous silica and alumina in basic media (>7 pH) to an autoclave and subjecting the suspension to elevated temperatures (>200 °C) and pressures (>1 MPa).[24] Zeolites constitute one of the most commonly used industrial catalysts and, as previously mentioned, are chiefly used for catalytic cracking of high molecular weight hydrocarbons in crude petroleum into lower molecular weight hydrocarbons that are ultimately used for a large portion of the world's supply of fuels, though they possess numerous other applications as well.[25] An additional advantage of zeolites is that a multitude of metals, such as Ti, Fe, Co, or Ga, to name a few, can be incorporated into the zeolite framework by replacing a tetrahedral silicon in a SiO_4 unit. In the context of catalysis, this means that the catalytic properties of the zeolites can be specifically tailored toward different types of reactivity.

The zeolite structure is comprised of a crystalline microporous network of silica and alumina tetrahedra, where silicon and aluminum atoms are bridged by oxygen atoms.[26] Figure 6 illustrates two examples of zeolite A and zeolite X. The sizes of the channel that comprise the microporous network are usually in the 1 to 2-nanometer diameter regime. The small pore sizes impart molecular size discrimination capabilities to zeolites, referred to as the *molecular sieving effect*. The microporous size regime is small enough to allow small molecules to enter, but prevent larger ones from entering, with near atom-size specificity.[27] Depending on the desired application, the sieving properties of zeolites may be advantageous, such as for analytical separations, or disadvantageous, such as in catalytic decomposition of feedstocks of large molecules, where substrate molecules are too large to enter zeolite pores and interact with active sites. To improve pore accessibility and limit the negative effects of steric hindrance, strategies towards creating mesoporous (2-50 nm pores) zeolites are actively being developed. The most common way to synthesize mesoporous zeolites is *via* templating, which is another general synthesis strategy and is discussed next.

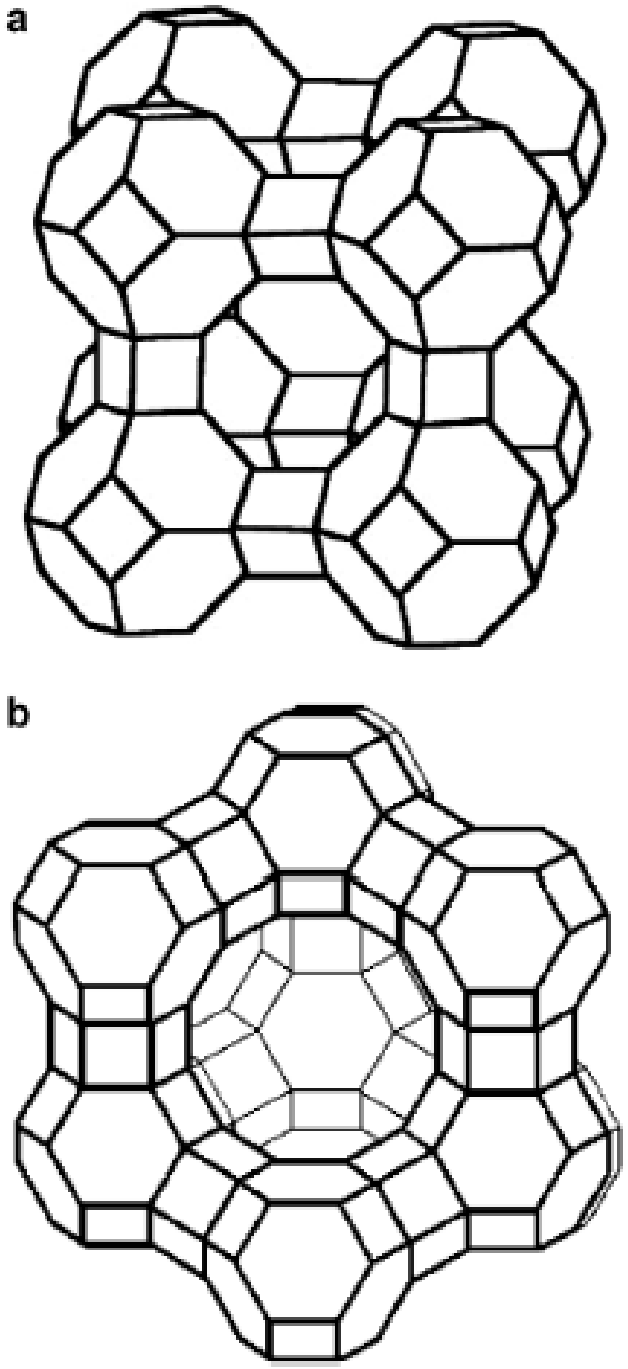


Figure 6. Two examples of zeolite crystal structures, a) Zeolite A, and b) Zeolite X. Figure reprinted from reference 22.

Templating is a synthetic strategy in which precipitation of reactive precursors is carried out in the presence of a template. The template serves as a structure directing agent which controls the final size, shape, porosity, and morphology of the solid material. Templating has been used to create a vast array of nanostructures including hollow spheres, crescents, rods, cubes, and porous materials, to name a few examples. It can be either a physical process, such as physical adsorption of a species onto a template surface, or a chemical process, such as grafting species onto the template surface *via* functionalizable moieties such as surface alcohols, thiols, or vinyl groups. In most cases the template is a sacrificial species that is removed post-reaction either by dissolution or calcination, assuming the synthesized material can survive the removal process. Templates are conventionally nano-size compounds or particles and can be classed as either hard or soft. Examples of hard templates include "3-dimensional" colloidal particles such as alumina or silica whose surface is chemically or physically modified by the desired precursor, or "2-dimensional" surfaces with nanostructures onto which precursor substrate can be cast. Examples of soft templates include emulsions, micelles, surfactants or polymers which are often removed post-reaction *via* calcination.

Incipient wetness impregnation is a method for synthesizing heterogeneous catalysts in which a porous support is wetted with a solution containing the catalyst precursor such as a high-valent metal cation (Figure 8). If the volume of solution added to the porous support is greater than the support pore volume, it is referred to as "wet" impregnation, whereas if the volume of solution is less than the support pore volume, it is referred to as "dry" impregnation. Solution is drawn into the support pores *via* capillary action wherein cations can interact with the pore walls *via* either physical adsorption or ion exchange with acidic surface protons. Once inside the pores, the solution is then evaporated from the pores and the soluble precursor is precipitated onto the surface.

One of the main advantages of incipient wetness impregnation is that the final amount of precipitated catalyst can be precisely controlled by varying the concentration of dissolved precursor. Ideally, the solid active catalyst will be uniformly distributed throughout the support after evaporation of the volatiles. However, the crystallite size can be affected by the pore size. Larger pores that contain large volumes of solution will precipitate larger crystallites than smaller ones, which can result in an uneven distribution of solid precipitate. Larger crystallites are generally undesirable as more catalytically active metal will be confined to the bulk of the particles which prevents their utilization during catalysis.

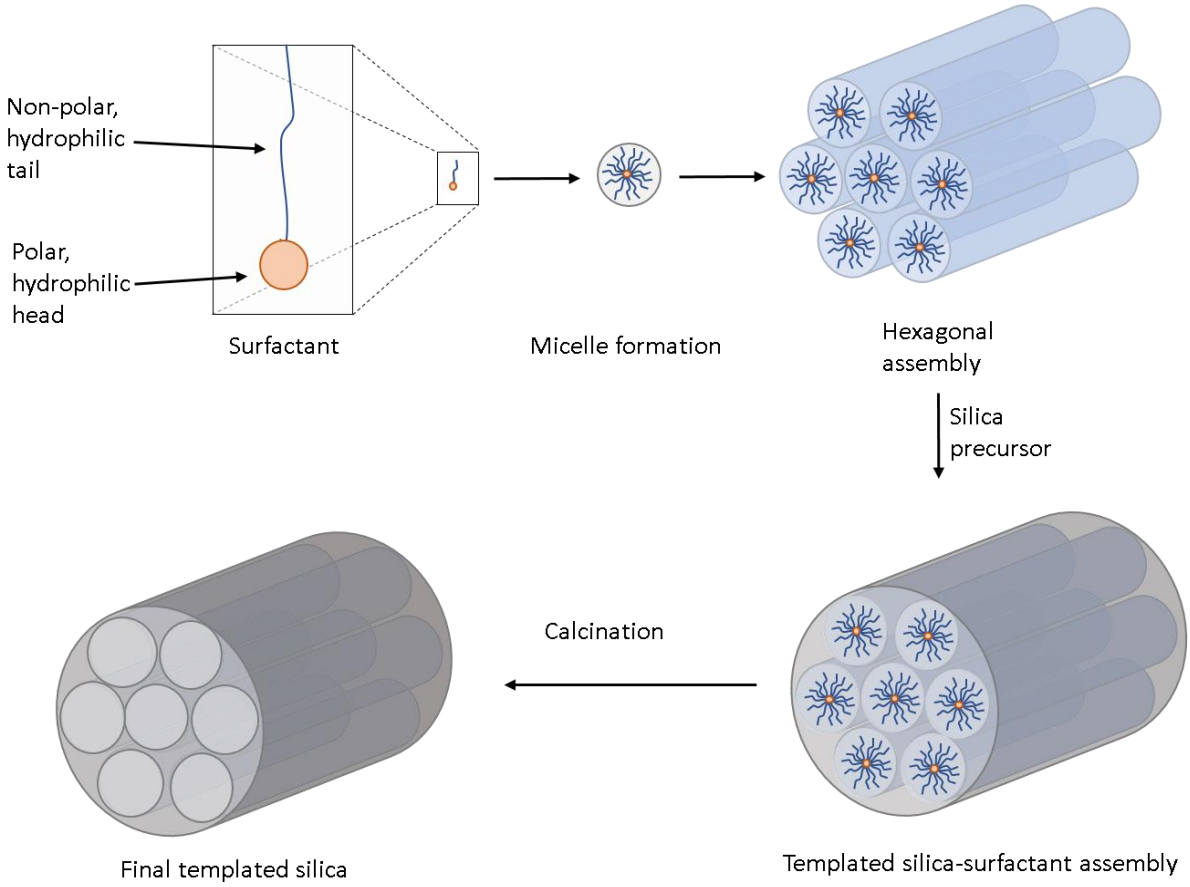


Figure 7. Illustration of the templating process using a surfactant template. Surfactants in aqueous media spontaneously self-assembly into micelle structures which organize into hexagonal assemblies. Addition of a silicate precursor creates surfactant-templated silica, which must be calcined to remove the remaining organic template.

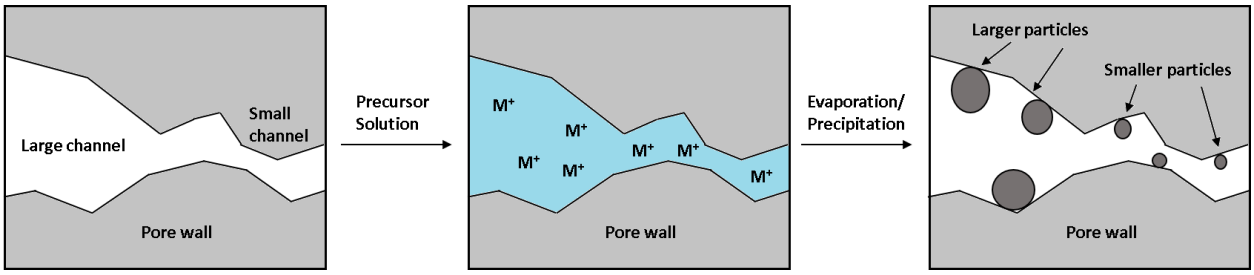


Figure 8. Illustration of incipient wetness impregnation. Larger pores result in formation of larger particles than those formed in smaller channels, resulting in catalyst particle size variation.

Further, if evaporation is carried out too quickly there may be an uneven distribution of solid towards pore openings, which can result in pore blockage.[28]

Evaluation of Catalyst Performance

Catalyst performance is evaluated based on the following parameters: activity, yield and selectivity, stability, and overall cost.

Activity is defined as the degree to which the catalyst enhances the rate of a chemical reaction. For heterogeneous catalysts, reactions occur at the surface, and catalyst particles are not necessarily uniformly dispersed in solution like homogeneous catalysts. Rate of conversion therefore in this case is not only a function of time, temperature, and pressure, but also of catalyst surface area, and mass transfer of the reaction components. Substrate conversion in heterogeneous catalysis occurs in three fundamental steps:

1) The substrate(s) adsorbs onto an active site on the catalyst surface
2) The catalyst induces a chemical transformation of the substrate(s) into the product(s)
3) The product molecule(s) desorbs from the surface

Figure 9 illustrates these fundamental steps with the example of ethylene hydrogenation catalyzed by a solid nickel catalyst. Ethylene and molecular hydrogen concomitantly adsorb to the nickel surface. The surface-adsorbed activated ethylene and hydrogen species then react to form ethane which subsequently desorbs from the surface.

Catalytic activity can be expressed mathematically as the rate of conversion of substrate to product per unit amount of catalyst. The unit amount of catalyst is ideally expressed on a per-mole basis of available active sites per unit of time. Activity can be quantified by calculating the *turnover frequency* (TOF). TOF is derived from the *turnover number*, which defined as the number of moles of substrate converted per mole of catalytic active site and is a measure of catalyst longevity (equation 1), and the *turnover frequency* (TOF), which is the turnover number per unit time (equation 2).

$$TON = \frac{moles\ of\ substrate\ converted}{moles\ of\ catalytic\ active\ sites} \qquad \text{Equation 1.4}$$

$$TOF = \frac{TON}{time} \qquad \text{Equation 1.5}$$

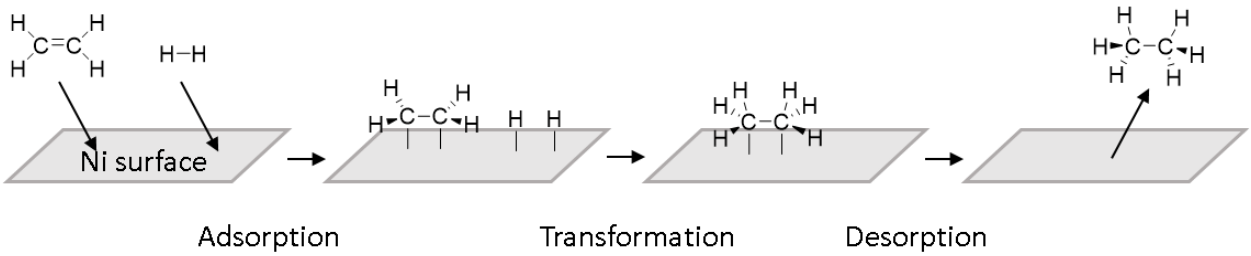


Figure 9. Illustration of the fundamental adsorption-transformation-desorption steps involved in heterogeneous catalysis using the classic example of nickel-catalyzed ethylene hydrogenation.

However, because the exact number and type of active sites are typically unknown for heterogeneous catalysts, quantifying activity on a per-mole basis is frequently impossible, and arbitrary units must be defined instead. This makes comparing heterogeneous catalysts a considerable challenge. Conventionally, the activity of heterogeneous catalysts is expressed as the rate of substrate conversion per unit mass of catalyst, though unfortunately this is only an approximation based on the average contribution of all possible active sites. Still, defining activity for heterogeneous catalysts in this way provides a useful method for benchmarking by which researchers can compare catalysts.

Selectivity and yield are measures of the efficiency of a catalyst for converting a given substrate or feedstock to target product(s) and are measures of mass conservation. Selectivity is defined as the number of moles of a given product formed per moles of substrate converted relative to other products. In other words, selectivity of a desired product is its mole fraction compared to the sum of moles of all products formed.

$$Selectivity = \frac{moles\ of\ product\ X\ formed}{sum\ of\ moles\ of\ products\ formed} \qquad \text{Equation 1.6}$$

Yield is defined as the number of moles of product formed relative to the amount of substrate converted. Here, it is simply calculated as the product of the conversion of substrate and selectivity of the product.

$$Yield = Conversion * Selectivity \qquad \text{Equation 1.7}$$

A catalyst that exhibits low selectivity generates waste and increases overall process costs, and post-reaction separations and work-up steps must be done to isolate the target product(s).

A single-site catalyst generally catalyzes one reaction leading to a single product, therefore leading to high selectivity in heterogeneous catalysis. This “single-site” hypothesis will be discussed in more detail later in the chapter. Homogeneous catalysts typically exhibit high selectivity because of the uniformity of the active site. For heterogeneous catalysts, because the active site is often non-uniform, achieving high selectivity is often a challenge. Further, the high temperatures required for many heterogeneously catalyzed processes can open mechanistic pathways toward undesired products.

Stability refers to the length of time a catalyst remains active over one or more successive catalytic cycles. Most catalyst research found in the literature focuses primarily on designing and

optimizing catalyst activity and selectivity, but longevity is another critical parameter for a catalyst to be industrially relevant. A hypothetical "flash-in-the-pan" catalyst that is both extremely active and selective may appear attractive, but ultimately may not have much utility away from the research laboratory if its lifetime is short-lived. A major challenge in industrial processes is that they often involve catalytically converting complex feedstocks, such as crude oil or vehicle exhaust gases, which can contain an assortment of contaminants that may dramatically impede or cause catalyst performance to completely cease. Catalyst longevity is important for both environmental and economic purposes, as short catalyst lifetimes lead to increased waste associated with disposing of inactive catalyst, and overall costs associated with synthesizing fresh catalyst. There are several mechanisms by which catalysts can deactivate, three major categories of which include poisoning, fouling, and degradation (Figure 10 and Figure 11).

Poisoning refers to the strong chemisorption of an atom or molecule to catalyst active sites such that catalyst activity decreases or ceases entirely.[29] Such binding may also result in irreversible structural changes to the catalyst's surface which can change its catalytic properties and make catalyst regeneration impossible.[30,31] In many cases, poisoning is irreversible, but can be reversible in some cases where the poison can be converted to gaseous compounds and volatilized by O_2 or H_2. Catalyst poisons are usually compounds that contain highly electronegative p-block atoms such as nitrogen, oxygen, sulfur, phosphorous, arsenic, and selenium. Sulfur is an especially notorious catalyst poison as it is often present in, for example, petroleum feedstocks as H_2S or organosulfur compounds. Due to its strong binding to many catalytically active metals, it is capable of irreversibly deactivating catalysts even in parts-per-billion (ppb) quantities.[32] It is noteworthy that although poisoning is usually undesired, there are some industrial processes in which a highly active catalyst is intentionally poisoned in order to temper its activity and increase selectivity. In some cases, sulfur can even act as a catalyst promoter. One example involves a carbon-supported Fisher-Tropsch iron catalyst which was dosed with sodium and sulfur to enhance its selectivity towards light olefins from syngas.[33]

Fouling refers to physical adsorption of materials onto the catalyst surface which results in blockage of active sites. Catalyst deactivation by coking, the process by which intractable carbonaceous material forms on a catalyst surface and blocks active sites, is one of the most common forms of fouling. To regenerate the catalyst, it must be treated with oxygen at >500 °C to reliably convert the coke into gaseous CO_2 and re-expose catalyst active sites.[29] A risk of high temperature calcination is that it may induce catalyst sintering, which is a form of catalyst degradation discussed below. It should also be

noted that coke adsorption can either be physical or chemical, and thus in certain cases coking can be classed as a poisoning process as well.

Degradation refers to catalyst deactivation due to physical or chemical destruction of the catalyst itself. There are numerous ways in which catalysts can degrade, including 1) sintering, 2) pore collapse, 3) leaching, 4) vaporization, 5) solid migration, and 6) mechanical degradation.

1) *Sintering* is the aggregation and compaction of smaller particles into larger ones by heat or pressure without reaching the melting point of the material. Sintering results in loss of surface area and catalyst activity. Sintering can also refer to transformation of the catalyst surface into inactive crystallite phases due to interactions with gaseous molecules. This is known as chemical sintering.
2) *Pore collapse* refers to collapse of the porous support structure, consequently resulting in loss of surface area and entrapment of active sites which can no longer be accessed by substrates. Pore collapse occurs most often as a result of thermal or external mechanical stresses.
3) *Leaching* is the process by which catalyst active sites are dislodged and solubilized from the support and released into solution by one or more reactive components in the system. Leaching often occurs *via* solvolysis in which the solvent itself reacts with the active metal such that it forms a soluble species, or by destroying the bonds that anchor the active component to the support.
4) *Vaporization* is the process by which the active catalyst reacts with a component in the system that results in formation of a volatile metal derivative species which subsequently evaporates away from the system. Vaporization commonly occurs in high temperature processes where CO is present, which subsequently forms volatile metal carbonyl species. Examples include formation of nickel carbonyl during CO methanation,[34] or ruthenium carbonyl formation from catalytic converters.[35]
5) *Solid migration* refers to migration, diffusion, or separation of atoms into distinct, less active (or inactive) phases.
6) *Mechanical degradation* refers to catalyst deactivation from physical breakdown due to mechanical stress from the reactor itself, such as pulverization by mechanical stirring or grinding apparatuses, interparticle collisions, or erosion caused by flow of the reaction solution.

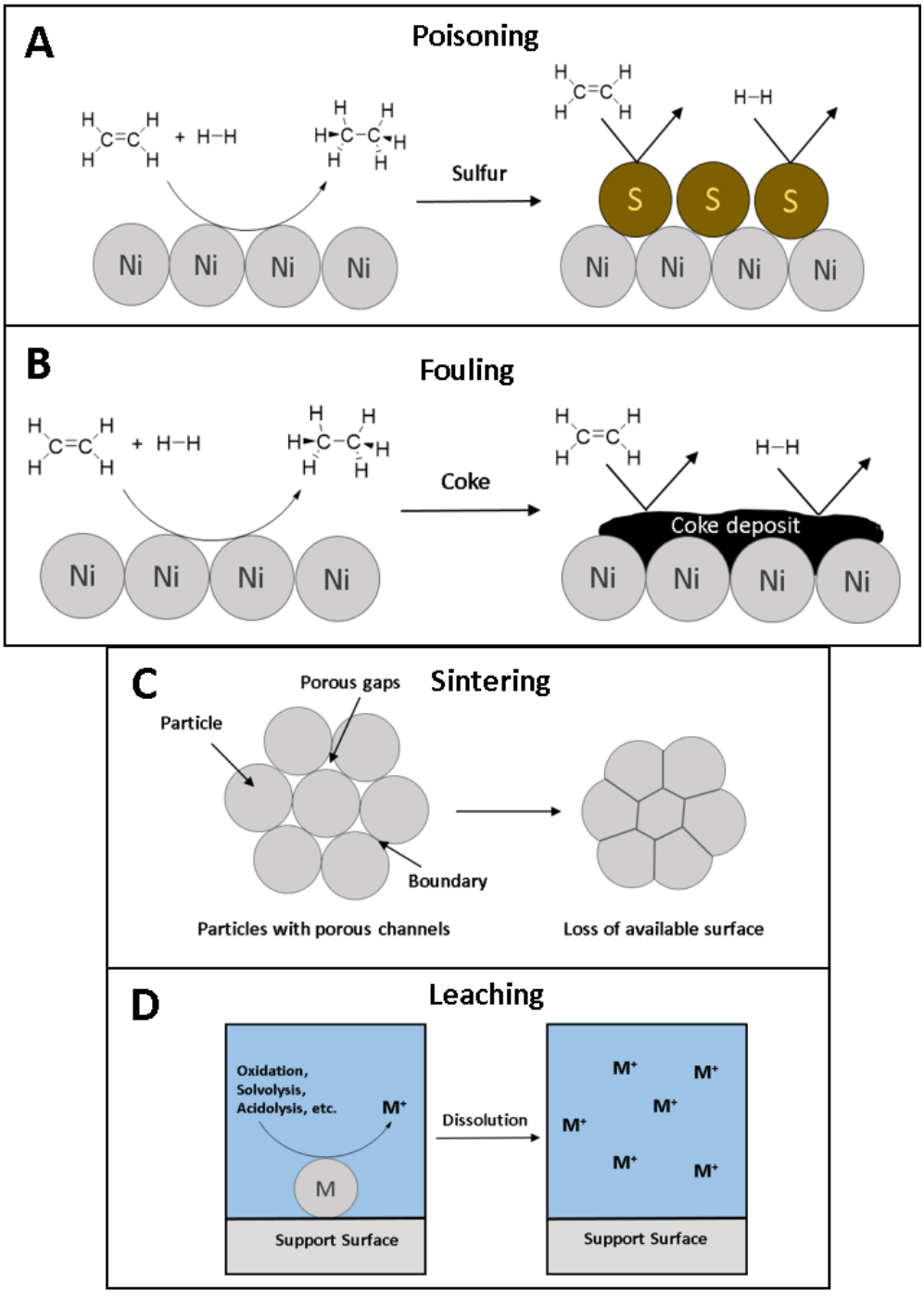


Figure 10. Illustrations of a) poisoning, b) fouling, c) sintering, and d) leaching.

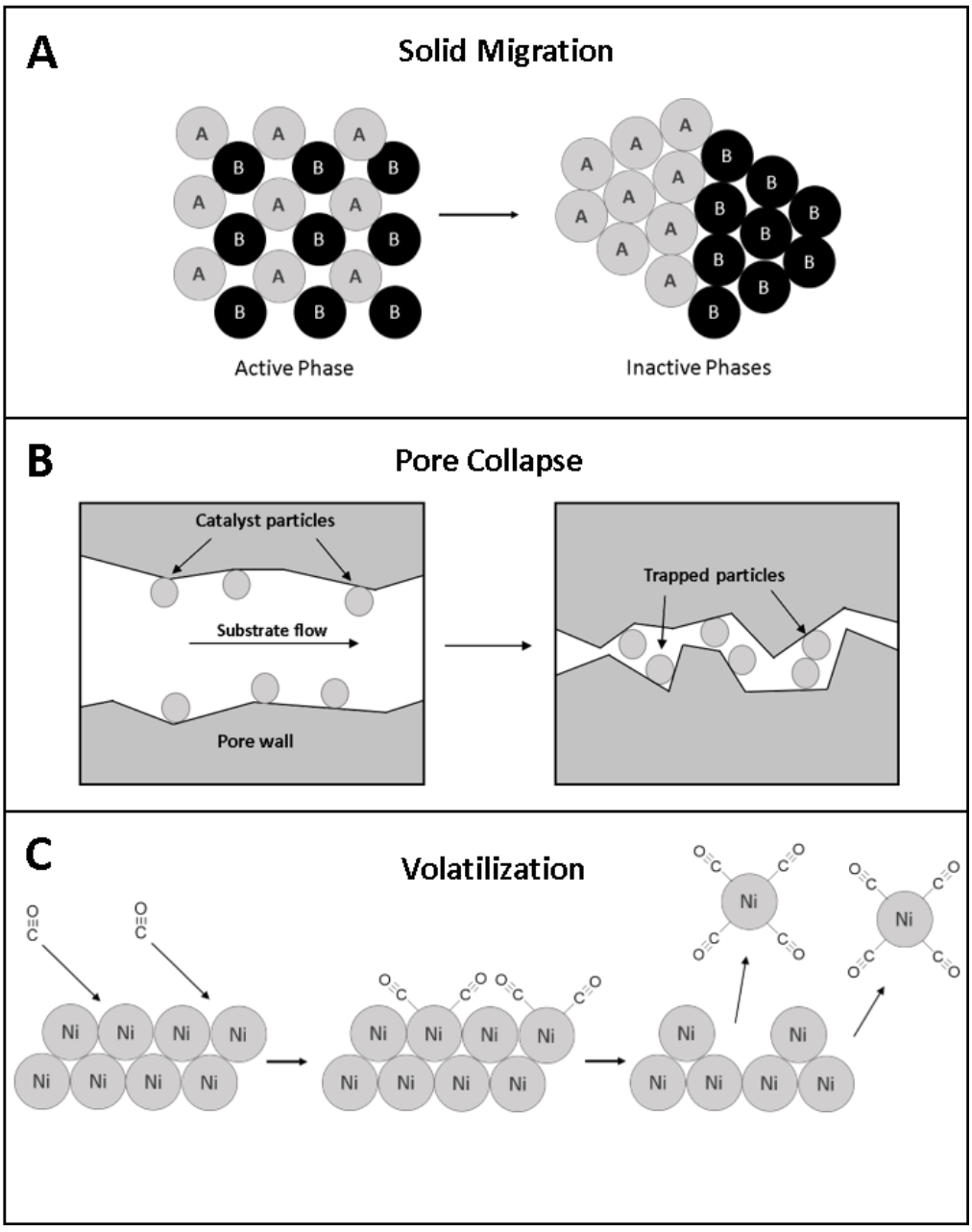


Figure 11. Illustrations of a) solid migration, b) support pore collapse), and c) volatilization.

In most cases, catalyst deactivation is irreversible. However, there are some situations where the catalyst can be regenerated. Most cases involve removal of adsorbed coke deposits by volatilizing it to CO_2 in the presence of O_2/H_2O fluidized streams at elevated temperatures (>500 °C). Regeneration in this way must often be treated delicately to prevent or minimize catalyst sintering.

Finally, the overall *cost* of the catalyst itself plays a crucial role in determining its use for industrial purposes. Factors that influence the economic viability of heterogeneous catalyst includes cost of the reactive precursors, solvents and chemicals required for synthesis, longevity and recyclability (as previously discussed), and energy input required to drive their synthesis. Efficient catalysts based on, for example, silica, alumina, and iron are highly sought after due to their low cost. However, in cases where high activity, selectivity, and stability are required, such as in the case of automobile catalytic converters, noble metal-based catalysts are used. Due to scarcity and inherent high cost of noble metals, there is significant research being done towards replacing noble metal-based catalysts with cheaper earth-abundant analogues for these purposes, such as Fe, Ni, and Co.

The Catalyst Ensemble – Defining the Active Site

The atomic and morphological structure at the surface of heterogeneous catalysts can be rather complex, in comparison to homogeneous catalysts in which the catalytic precursor is often discrete and well-defined. The structure of organometallic homogeneous catalyst active sites can be specifically tailored depending on the nature of the ligands that are bound to the metal center. The attached ligands alter the electron density of the active metal's HOMO-LUMO frontier orbitals, depending on the electron donating or withdrawing strength of the ligand. The size, shape, and bonding geometry of the ligands also alters the steric environment around the metal center and can also aid in the binding characteristics of substrates to the active site. Therefore, the activity and selectivity of the metal center can be specifically tuned towards desired reactivity based on choice of ligand. These properties of homogeneous catalysts, in addition to their relatively easy synthesis and characterization, allows for readily attainable kinetic information, which in turn can allow for the determination of reaction mechanisms, reactive intermediates, and establishing catalytic cycles.

The identity of the catalytically active species and its coordinating environment are collectively referred to as the *catalyst ensemble* (a couple examples of hypothetical heterogeneous ensembles are depicted in Figure 12). The active component of the heterogeneous catalyst is not necessarily confined to just the active species itself, but also contributions from the active site's immediate environment, such as synergistic electronic effects due to interaction with ligands or adjacent atoms, or surface

functionalities of the support. The catalytic nature of the active site can also be influenced by factors such as strained coordination geometry at the surface, neighboring surface defects, or coordinatively unsaturated surface functional groups which are stabilized by electronic contributions from the bulk. As previously discussed, the active sites for heterogeneous catalysts are often difficult to define because of the general lack of synthetic control and challenges with characterization. These challenges have led to significant research efforts towards discovering *single site heterogeneous catalysts* (SSHCs), wherein the heterogeneous catalyst ensemble is uniform and well-defined.

Single Site Heterogeneous Catalysts

Historically, progress in the world of heterogeneous catalysis has been largely the result of "Edisonian" trial-and-error approaches instead of theory-based strategies based on predictive models. A recurring point made in previous sections of this chapter is that heterogeneous catalyst ensembles are frequently non-uniform and ill-defined. These issues make it especially challenging to identify structure-function relationships between the solid catalyst and its activity. For these reasons, researchers are actively seeking routes towards creating single site heterogeneous catalysts that possess the combined advantages of both homogeneous and heterogeneous catalysts, and minimization of the disadvantages of each.

To be classified as an SSHC, a catalyst's active sites must be identical and spatially isolated from one another. Types of SSHCs include single isolated atoms or ions, or molecular species that are covalently or non-covalently tethered to the surface (Figure 13). Isolated atoms as single sites are usually embedded into supports by occupying a vacancy. A classic example of this is isolated palladium atoms embedded into magnesium oxide which cyclotrimerize acetylene.[36] Other examples of catalytically active ions include transition metals such as Ti(IV) or Zr(IV), which can typically be anchored to the surface *via* their metal halide or metal alkoxide precursors. "Molecular species" refers to molecules or metal complexes that are anchored to the surface *via* an inert linker. Molecules in this context refers to organic species such as surfactants, polymers, small molecules, lipids, etc. that possess a non-metal active site (a subtle distinction is made here to emphasize that not all catalysts are necessarily based on metals, e.g. sulfonic acid catalysts). Metal complexes here specifically refers to catalytically active metal coordination complexes, which may or may not be organometallic molecules. Frequently, organometallic species used for heterogeneous catalysis are heterogenized analogues of homogeneous catalysts (e.g. metallocene catalysts),[37] whereby one or more coordinating ligands possesses a reactive functional group anchor that allows the species to become surface-immobilized. As

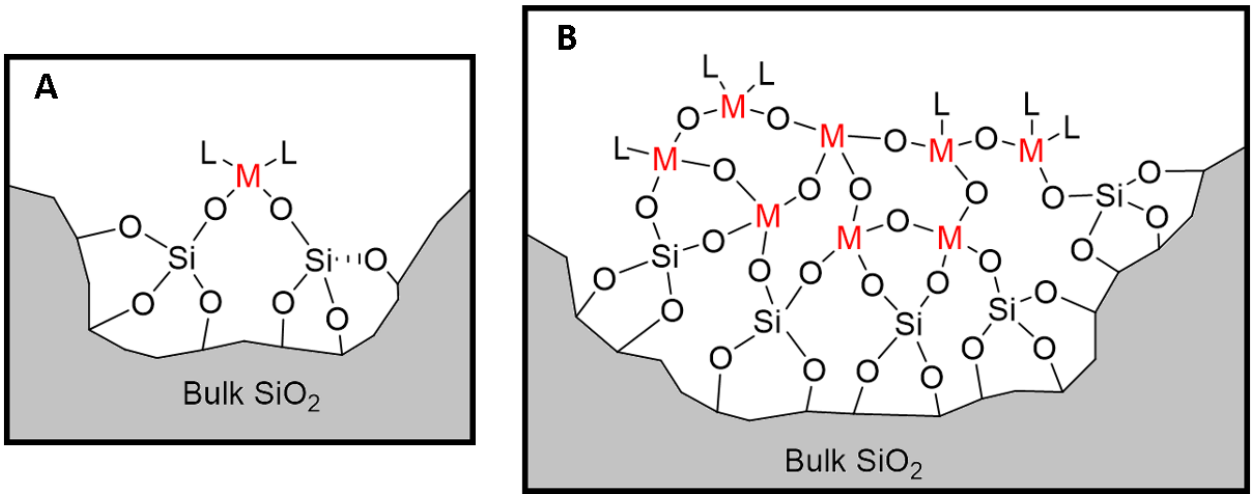


Figure 12. Conceptualization of catalyst ensembles in a) a simple case of a single four-coordinate metal atom anchored to a silica surface via two linkages and two ligands (L = -OH, -OR, capping agent, etc.), and b) a more complex example showing a particle of surface-anchored metal oxide, consisting of a multitude of ensembles and possible active sites. The degree of saturation, nature of the coordinating ligand, and distortion of the coordination geometry are all factors that can influence catalytic activity.

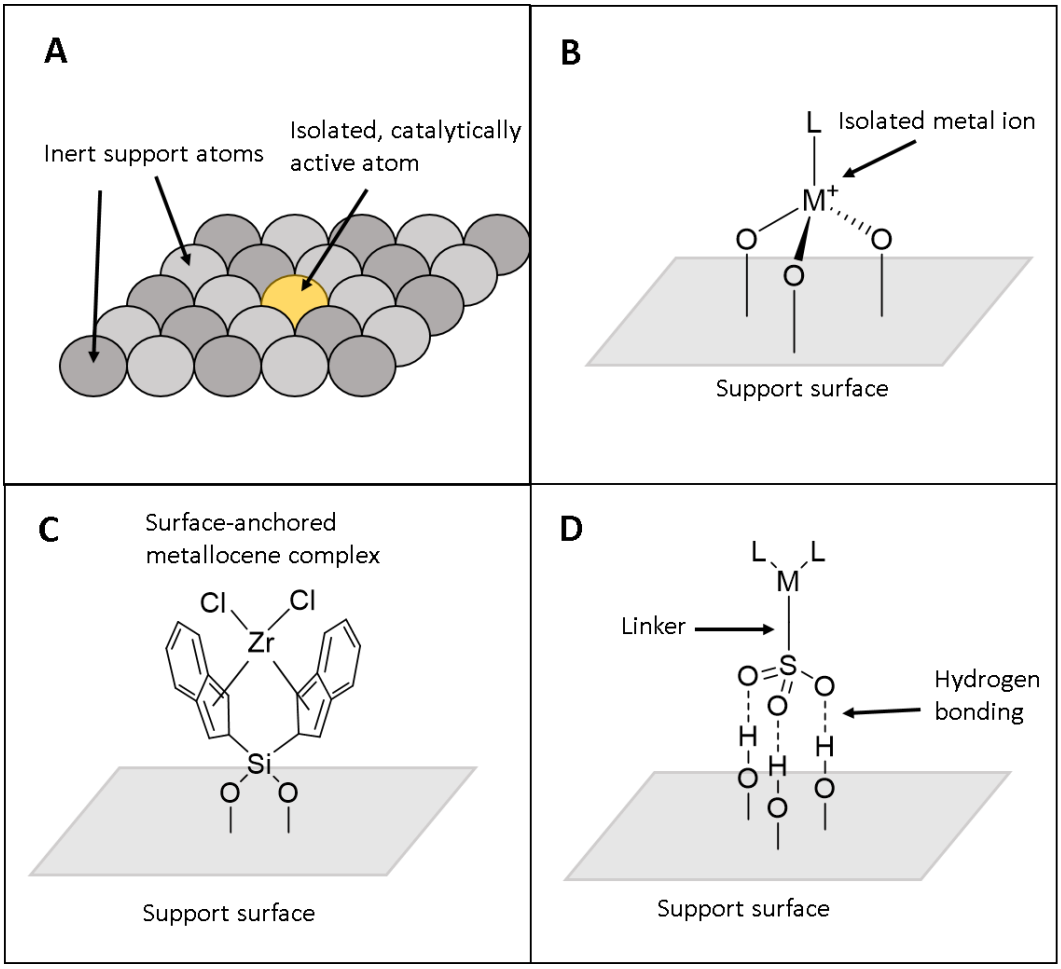


Figure 13. Illustration of several types of single site heterogeneous catalysts a) as an isolated, embedded atom, b) as an isolated ion, c) as a metallocene complex used for olefin polymerization (reference 34), and d) as a noncovalently anchored species via hydrogen bonding between surface hydroxyl groups and a sulfonate ion.

many homogeneous catalysts possess regioselectivity, heterogenizing organometallic complexes has important applications in asymmetric chemistry where enantiomeric selectivity is desired. As previously mentioned, the active species is anchored (covalently or non-covalently) to a support, usually either by grafting, tethering, or embedding it, and the final active sites should be spatially isolated from one another. SSHC synthesis often involves reacting a well-defined precursor that possesses reactive functional groups onto a pre-existing support that possesses reactive pendant moieties. As a simple illustrative example, an early transition metal halide such as titanium tetrachloride, which possesses highly reactive Ti-Cl bonds, can be reacted with a silica support (prepared by e.g. sol-gel or templating protocols) whose surface possesses reactive pendant surface hydroxyl (silanol) groups. Ti-Cl bonds readily react with protic functional groups to form the corresponding titanium derivative. Figure 14 illustrate the various types of surface silanol groups (either isolated, geminal, or vicinal) and possible resultant surface titanium species after surface modification. Although free silanol groups are highly reactive and rapidly condense with one another to form Si-O-Si bonds and water, the surface-confined Si-O bonds of neighboring silanols are too distant from one another to react through the necessary condensation reaction. However, they still may be close enough to one another to interact *via* hydrogen bonding between one silanol hydrogen and a neighboring silanol oxygen.

Reaction of titanium tetrachloride with surface silanols produces titanium derivatives which are anchored to the surface by Ti-O-Si bonds. However, if the area density of resident surface silanol groups is too high, as is typically the case with freshly-synthesized silica gels, they will reside close enough to one another such that $TiCl_4$ can react to form anchored titania species with varied connectivities to the surface. To reduce the density of surface silanols, the silica is dehydroxylated by heating it to high temperatures (typically >500 °C), which decomposes surface -OH groups into water molecules that subsequently volatilize. Dehydroxylation reduces the density of surface silanols and creates more isolated silanols. Figure 15 illustrates the effect of dehydroxylation on surface silanols and its effects on surface modification with $TiCl_4$. However, despite dehydroxylation treatment there still may be a significant number of non-isolated silanols which can result in multiple active sites after surface modification. Further, if the surface is dehydroxylated too far, no silanols will remain and thus surface modification in the manner described above cannot occur, and the surface must be rehydroxylated with water.

The synthetic strategy towards SSHCs described above represents the general logic behind many conventional “top-down” immobilization strategies, in which molecular species are combined with pre-

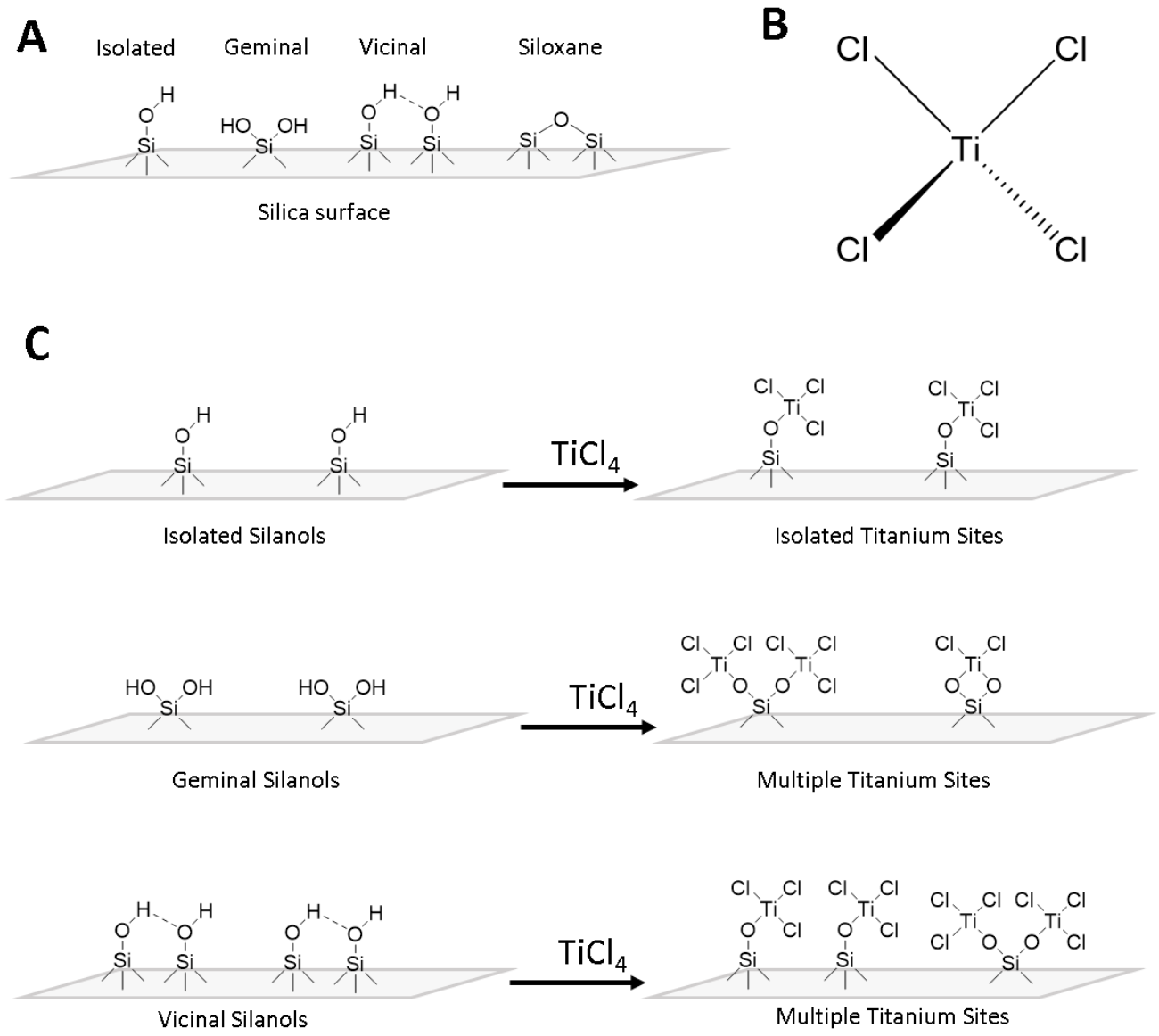


Figure 14. Illustration of a) different types of surface silanols, b) structure of $TiCl_4$, and c) examples of possible titanium sites after reaction of $TiCl_4$ with the various silanol types.

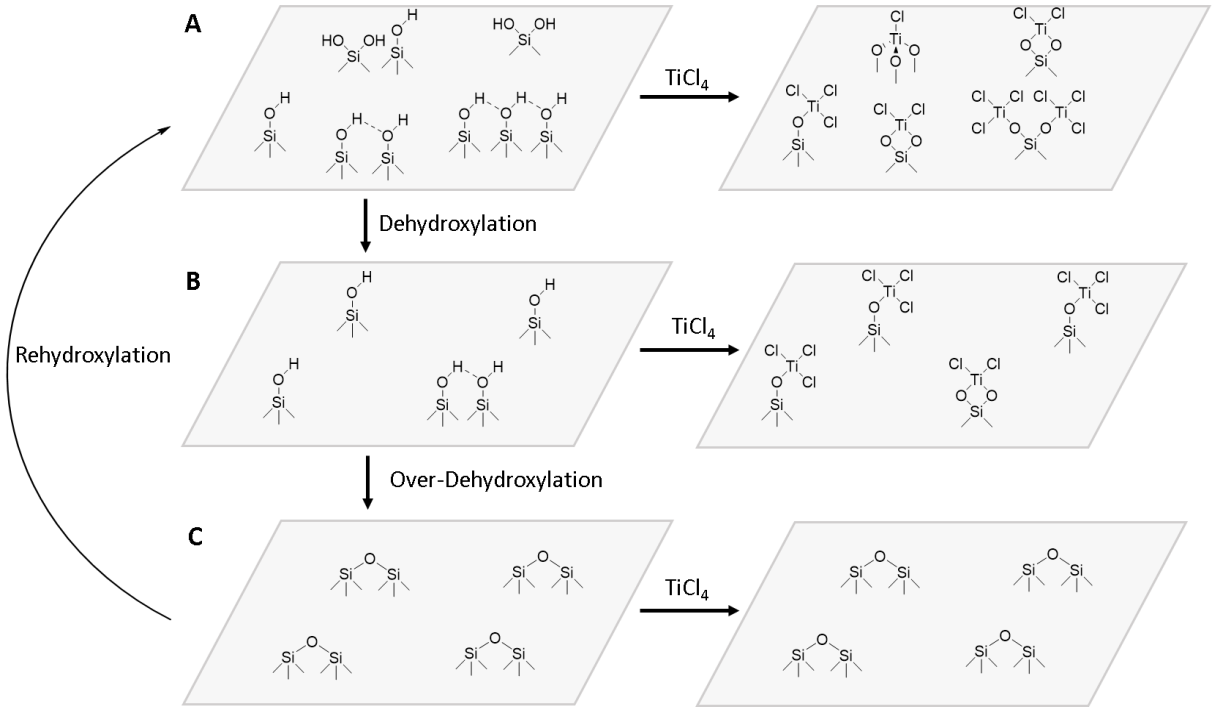


Figure 15. Illustration of modification of a silica surface via reaction of surface silanols with $TiCl_4$ a) before silica dehydroxylation, b) after dehydroxylation, and c) after over-dehydroxylation where all silanols have been removed. Note that in case (a), many different surface-titania species are formed. In case (b), more isolated titania species exist but different types can still be formed. In (c), no silanols are available, thus no functionalization occurs, and the surface must be re-hydroxylated to regenerate surface

existing supports in some fashion and illustrates some of the challenges associated with these approaches. “Bottom-up” strategies in which catalysts are built from small molecule building block precursors is an attractive alternative approach towards creating SSHCs, because the building blocks can be precisely defined using convenient solution-based spectroscopic techniques prior to their assembly into macrostructures. Bottom-up approaches provide the opportunity to rationally design and synthesize well-defined small molecule precursors with specific functionalities, that can be used to tune the properties of the final catalyst.

SSHCs based on organic polymers can be synthesized by co-polymerizing a small molecule monomer (or “linker”) with a monomer that possesses the desired catalytically active moiety. An enormous array of polymer materials can be created with tunable porosity from the microporous (<2 nm pores) to above the macroporous (>50 nm) depending on the choice of monomer.[38] The number of active sites can also be tuned by varying the ratio of monomer precursors. A vast library of monomers and their combinations to create functional polymer materials exists and have been discussed in detail in several recent reviews.[38-40] One example demonstrated by Liu *et. al.*[41] involves synthesis of mesoporous sulfonic acid-based polymer catalysts for acid-catalyzed esterification. Catalyst synthesis was done by copolymerization of divinylbenzene (DVB) and sodium *p*-styrene sulfonate, followed by post-reaction acidification of the sodium sulfonate groups with sulfuric acid (Figure 16). Although organic polymer heterogeneous catalysts are attractive due to the wide array of possible monomers and tunable functionalities, carbon-based materials tend to decompose at high temperatures, which are often necessary for many industrial processes. Many organic polymers are also vulnerable to swelling, in which solvent molecules diffuse into the polymer and may negatively influence its physical properties. Silica-based materials as supports are desired because of their thermal stability and structural rigidity, though, as previously discussed, synthetic routes towards silica-based single site heterogeneous catalysts is a challenge. However, polyhedral oligomeric silsesquioxanes (POSS) provide an opportunity to rationally synthesize numerous silica-based functional materials, as well as a route towards silica-based single site heterogeneous catalysts.

POSS are a class of silica-organic hybrid molecules (empirical formula $RSiO_{1.5}$) which form a variety of structures including cages, partial cages, ladders, or random polymeric structures, and whose silicon vertices can be functionalized by a variety of reactive or unreactive organic moieties and functional groups (Figure 17).[42] POSS structures exhibit high thermal stability (>500 °C) and, due to the wide range of possible functionalities, can be rationally tailored for a variety of applications, such as use

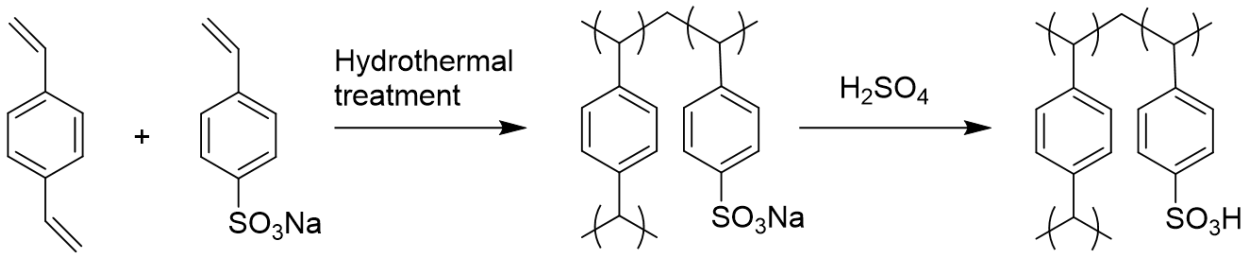


Figure 16. Reaction scheme showing copolymerization of divinylbenzene and sodium p-styrenesulfonate to form the corresponding copolymer. The sodium ion is then exchanged with a proton by reaction with sulfuric acid to form the heterogeneous acid catalyst. Figure adapted from reference 39.

in electronics, protective inert coatings, drug delivery, and catalysis. POSS structures are usually synthesized by hydrolyzing and condensing alkoxysilane or chlorosilane precursors, similar to sol-gel synthesis. One of the key advantages of POSS materials is that they are soluble in a variety of organic solvents, which makes them amenable to solution-based spectroscopies such as NMR and allows them to be precisely defined prior to macromolecular assembly.

One example demonstrated by Haddad *et. al.*[43] involves synthesis of several POSS-organic polymers in which a cubic POSS serves as a pendant functional group on a polystyrene backbone (Figure 18). To accomplish this, a partial-cage POSS with an open trisilanol corner is reacted with p-trichlorosilylstyrene in tetrahydrofuran (THF) in the presence of triethylamine (TEA) (TEA serves as a soft base to capture hydrochloric acid (HCl) that is evolved by the condensation of Si-O-Si bonds from reaction of Si-OH and Si-Cl bonds). The resulting macromer is then co-polymerized with styrene to form the corresponding poly-POSS-styrene materials.

In the context of single site heterogeneous catalysis, another example of POSS materials is one pioneered by the Barnes group, in which a cubic POSS whose corners are functionalized by trialkyltin functional groups is reacted with reactive metal chlorides to form highly dispersed, embedded single site catalysts (The trialkyltin groups serve as good leaving groups for metathesis reactions with metal chlorides (Figure 19). This reaction can be accomplished under mild conditions (<100 °C) and does not require the any additional reagents such as a base or a catalyst to drive the reaction.

SSHCs and Boron-Containing CoB Catalysts

Although the previous section focused primarily on a general introduction and discussion on SSHCs, the work here involves synthesis of boron-containing cobalt materials. As will be discussed in Chapters 3 and 4, unfortunately their structures are poorly defined and difficult to characterize. But as will be shown in Chapter 4, these catalysts exhibit very high selectivity for reduction of carbonyl moieties. In the context of SSHCs, one can postulate that a heterogeneous catalyst that exhibits high selectivity possesses only one (or a few) types of active sites and can be approximated as a single site catalyst.

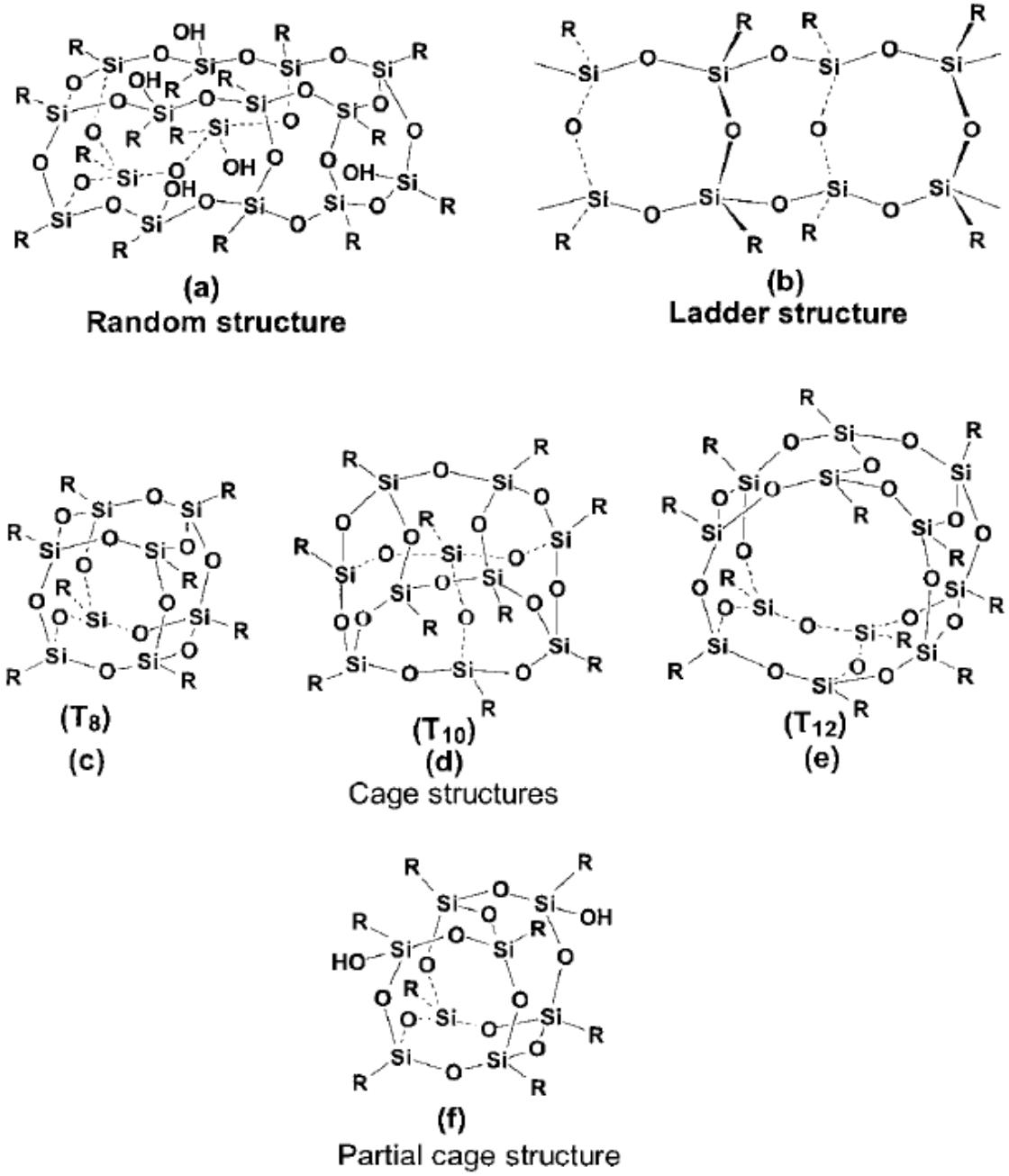


Figure 17. Examples of the many different types of POSS structures. Figure reprinted from reference 42.

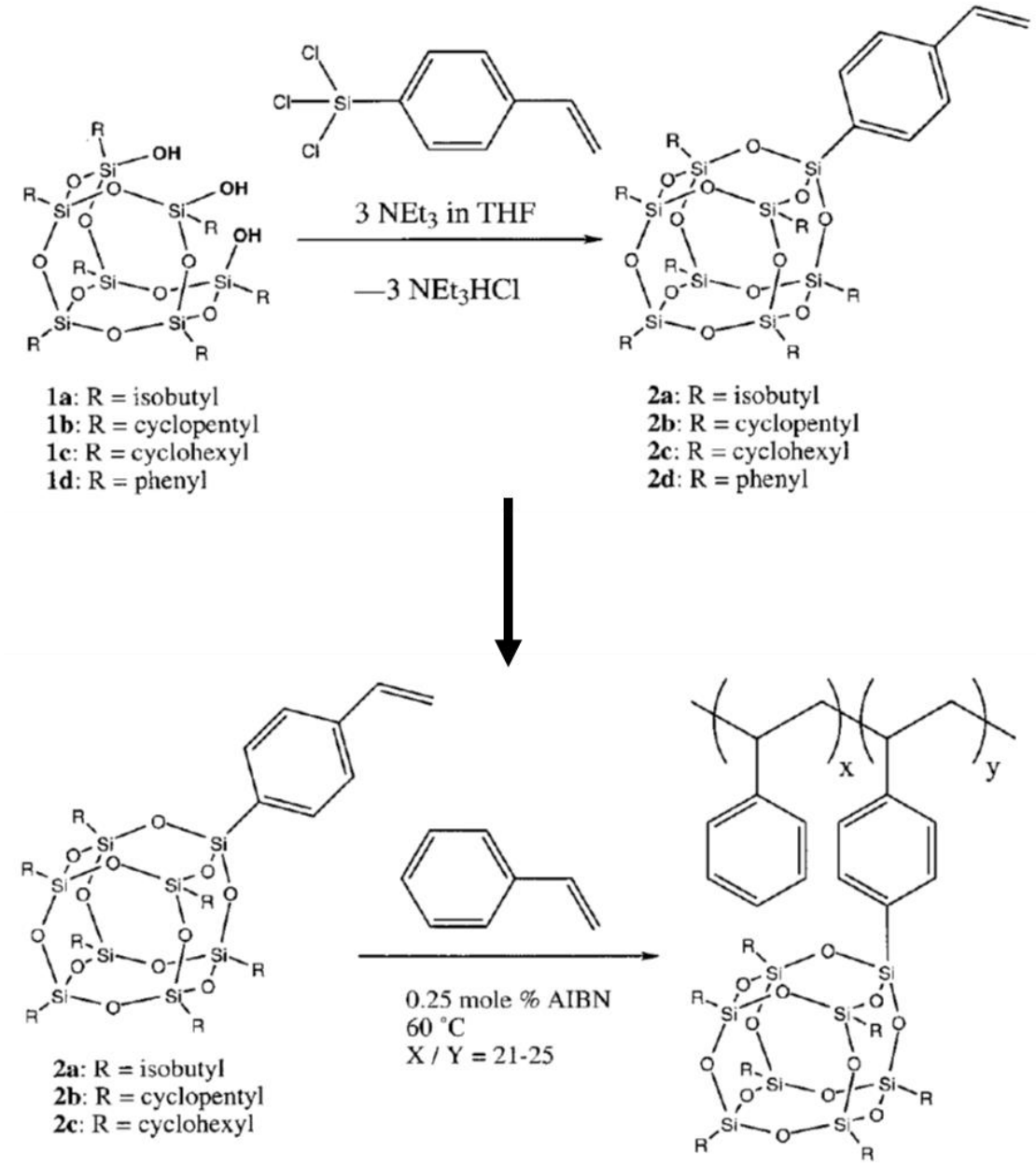


Figure 18. Illustration of synthesis of poly-POSS-styrene materials. Figure adapted from reference 43.

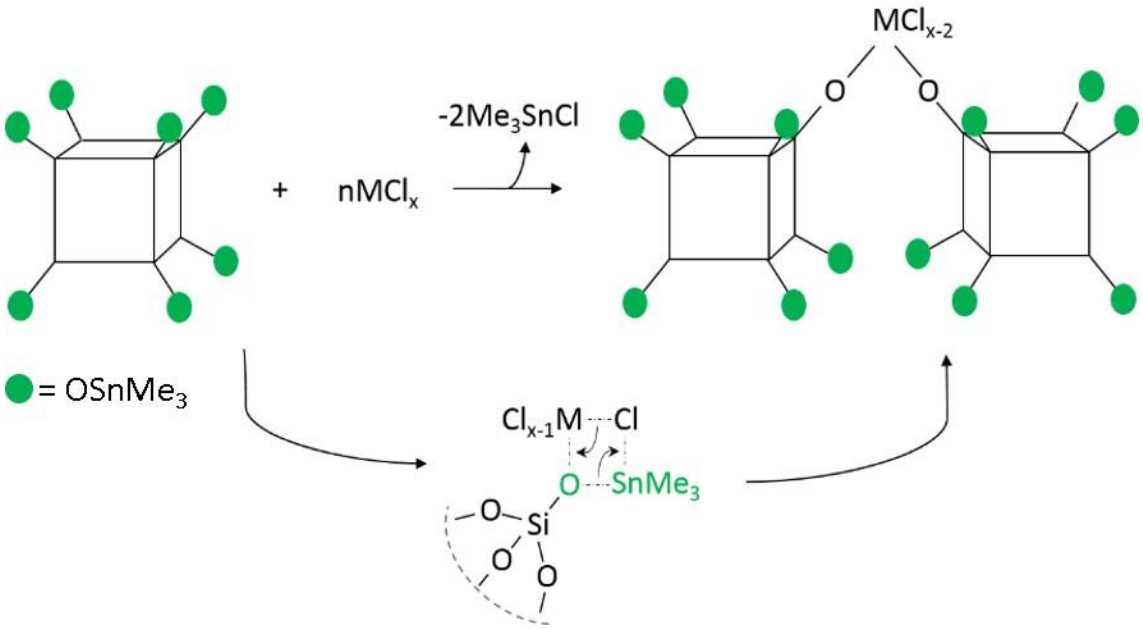


Figure 19. Example of a crosslinking metathesis reaction between trimethyltin-capped POSS cubes and a metal chloride.

Overview of Future Chapters

Chapter 1 broadly covered the basics of heterogeneous catalysis, including the definition of a catalyst, the importance and utility of heterogeneous catalysts, general synthetic routes, and some of the challenges associated with utilizing and studying heterogeneous catalysts. Lignocellulosic biomass as a renewable source of useful chemicals was briefly mentioned at the beginning of this chapter.

Chapter 2 briefly introduces biomass with special focus on lignin valorization and highlights some of the associated challenges. Catalytic transfer hydrogenation using earth-abundant catalysts is introduced as an attractive reduction strategy for biomass upgrading. The molecules acetophenone, acetovanillone, and guaiacol, are introduced as reducible probe molecules used in this work to evaluate the catalytic efficiency of earth-abundant boron-containing cobalt (CoB) catalysts.

Chapter 3 describes the synthesis and characterization of CoB catalysts, as well as the protocols used for reactor preparation, and the equipment used to run test reactions. Quantitative gas chromatography-mass spectrometry (qGCMS) was used to quantify all the reaction components. Finally, the quantitative methodology used to measure and calculate several key catalysis parameters such as % conversion, % selectivity, % yield, and % mass balance to evaluate catalyst performance is described.

Chapter 4 discusses the characterization and catalysis results of acetophenone, acetovanillone, and guaiacol in the presence of CoB catalysts with i-PrOH and EtOH as H-donors at various elevated temperatures using the protocols and methodologies described in Chapter 3.

Chapter 5 presents general conclusions and discusses future work.

Chapter 2 – Heterogeneous Catalysts for Transfer Hydrogenolysis and Lignin Valorization

Lignocellulosic Biomass, Lignin Structure, and Challenges with Lignin Valorization

Petroleum-derived fossil fuels are the current mainstay of global energy consumption, comprising 80% of all energy produced and consumed. As the global population increases, demand for energy will also increase. However, fossil fuels are considered non-renewable, and their combustion is also the primary source of CO_2 emissions which raises concerns over global climate change. For these reasons, alternative strategies for cleaner, renewable energy sources such as solar, hydrothermal, wind, and plant biomass are actively being researched.[44] Of these energy sources, lignocellulosic biomass is currently the most amenable to incorporation into current energy infrastructure because many of its components are structurally similar to petroleum.

Use of plant biomass has drawn significant attention of researchers as it is viewed as a renewable alternative to petroleum and is considered "carbon neutral." In this context, the term carbon neutral refers to the notion that plant biomass consumed or burned for fuel generates a proportional amount of CO_2, which is in turn recycled from the atmosphere to generate new plants, such that the net change in total CO_2 content in the atmosphere is negligible.

Plant biomass consists of three primary components: cellulose, hemicellulose, and lignin (Figure 20). Lignin comprises approximately 5-30% of biomass, but its recalcitrance towards transformation into value-added chemicals has hindered its translation into use as an industrial feedstock and is typically simply burned as low-quality fuel. However, because lignin comprises a significant fraction of plant biomass, and because it is the most abundant natural source of heteroaromatic nuclei, significant research attention has been brought towards lignin valorization as a feedstock for fuels and platform chemicals.[45] Detailed information on lignin valorization can be found in numerous reviews.[46-51]

Many methods for processing lignin require harsh conditions such as high temperatures and pressures, which often unfortunately lead to condensation and formation of refractory C-C bonds that cannot be readily upgraded.[52] Thus, many efforts in recent years have looked towards catalytic solutions for lignin upgrading to prevent C-C condensation and enhance yields for value-added chemicals and materials. Many such catalysts are based on heterogeneous late transition noble metals. While noble metals are powerful catalysts, their scarcity, toxicity, and high cost makes them less desirable. Much research effort has attempted to elucidate efficient catalysts based on earth-abundant transition metal catalysts, such as iron (Fe), nickel (Ni), and cobalt (Co) because they are inexpensive, relatively non-toxic, and readily abundant.

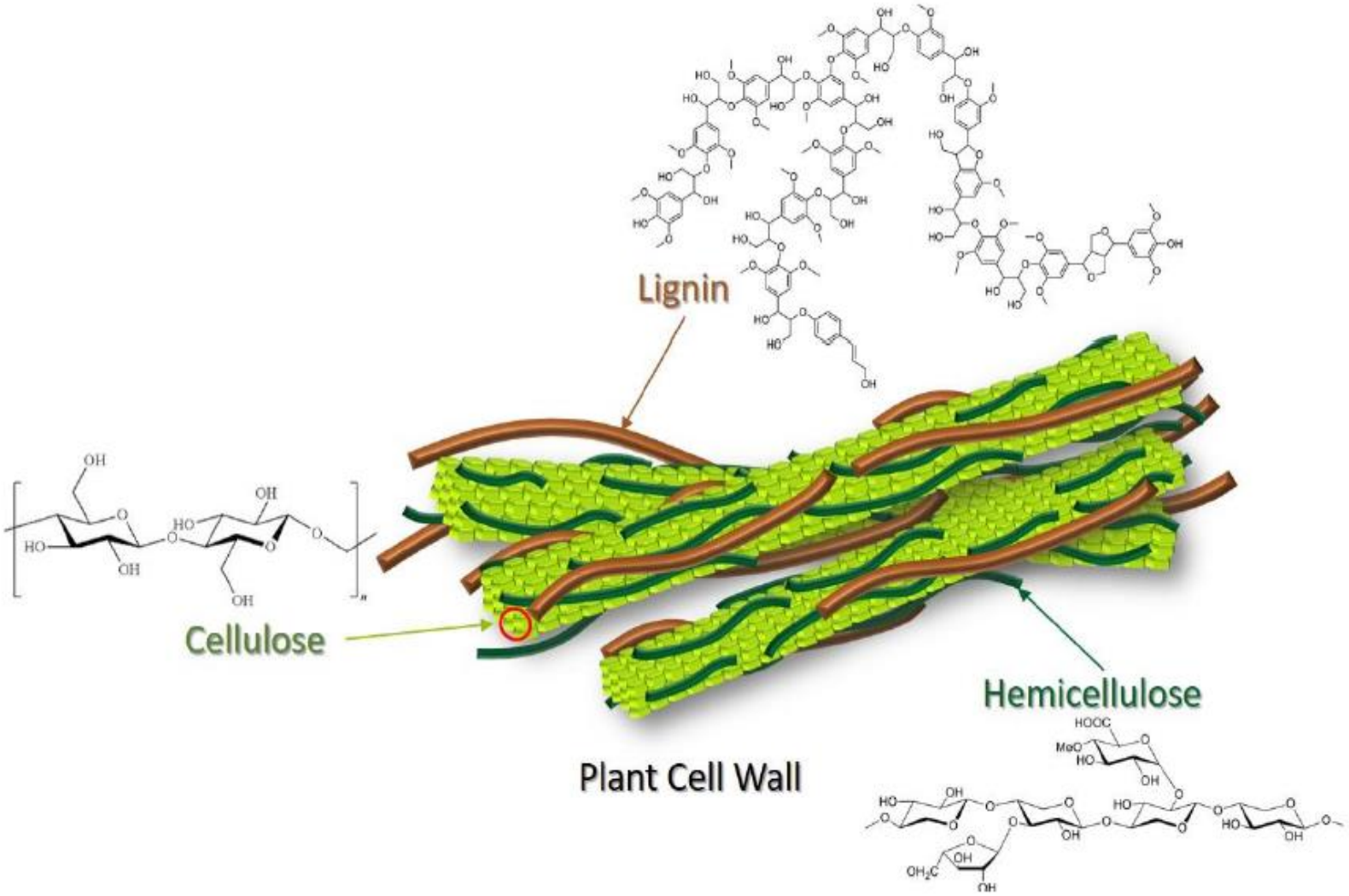


Figure 20. Illustration of components of lignocellulosic biomass. Figure reprinted from reference 52.

The structure of lignin is a complex heteropolymer comprised of propyl phenolic nuclei that are interlinked by β-O-4 ether bonds. In nature, lignin is biosynthesized by the oxidative coupling of small 4-hydroxyphenylpropanoids, primarily *p*-coumaryl, coniferyl, and sinapyl alcohols (generally referred to as H-, S-, and G-lignin, respectively), which are derived from phenylalanine (Figure 21).[53] These three alcohols are collectively referred to as *monolignols*, which are the primary structural units that comprise the macroscopic polymer structure of lignin. These monolignols then condense *via* oxidative radical polymerization to form the final lignin polymeric structure. An example of several types of linkages present in lignin is illustrated in Figure 22 using the dimerization of coniferyl alcohol as an example. It is important to note that, although lignin is referred to here in a singular manner, "lignin" is actually a broad class of heteroaromatic natural polymers, though lignin polymers possess certain functional groups that are ubiquitous to all forms of lignin.

Lignin's complicated structure makes it resistant to both microbial and chemical attack, which consequently makes it challenging to process and upgrade. For this reason, it is often simply burned as a low-quality fuel. However, because lignin is a significant component of biomass and the most abundant natural source of renewable aromatic moieties, research efforts towards its valorization have recently accelerated. "Lignin-first" biorefining strategies which involve taking greater processing precautions to preserve lignin during biomass refining and maintain it in a usable form have received renewed interest in the past decade, despite lignin's recalcitrance.[54]

Some current strategies to process lignin begin with separation of lignin from native lignocellulosic biomass by fractionation, followed by its decomposition into lower molecular weight species. The most common method for fractionating lignocellulosic biomass is *via* the Kraft process in which native lignocellulosic biomass is treated with sodium hydroxide (NaOH) and sodium sulfide (Na_2S). Other common lignin fractionation strategies include for example alkali or acid hydrolysis, [55] steam gasification,[56] hydrothermal treatment,[57] ionic liquids,[58] and pyrolysis[59]. However, these methods often require harsh conditions and frequently lead to undesirable condensation side-reactions in which the lignin C-O ether linkages transform and form unreactive C-C bonds. Because of this, the yield for aromatic products is often low (5-10%).[60] Milder conditions can be employed to reduce condensation and preserve more β-O-4 linkages, but ultimately result in the compromise of reduced delignification.

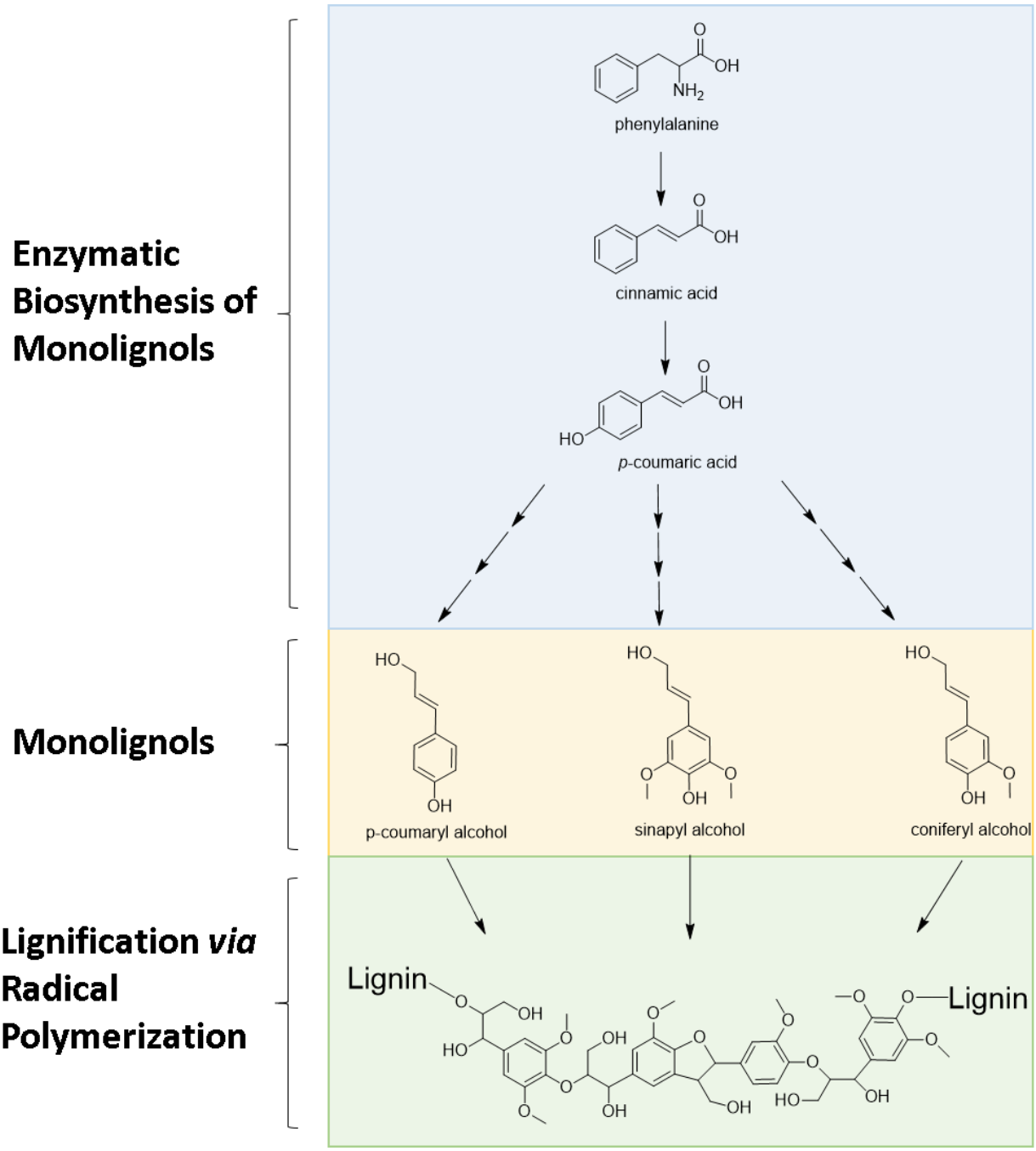


Figure 21. Simplified reaction scheme illustrating enzymatic biosynthesis of monolignols, followed by monolignol polymerization to form lignin.

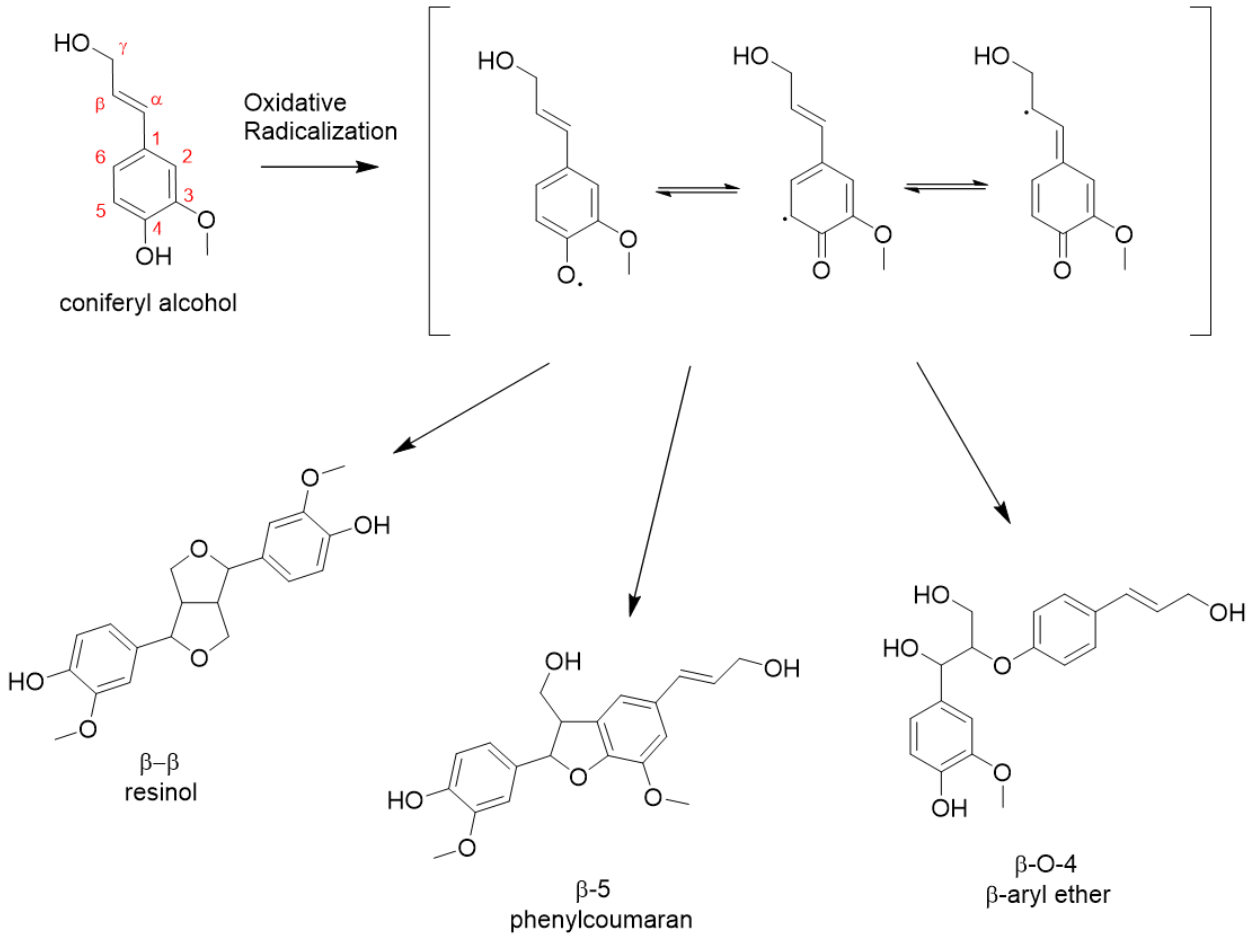


Figure 22. Reaction scheme illustrating oxidative radicalization of coniferyl alcohol and several possible dimerization products. Figure adapted from reference 53.

Reductive Catalytic Fractionation & Sustainable Routes Towards Lignin Valorization

Many conventional decomposition processes involve transforming native biomass into platform chemicals such as syngas which can then be upgraded *via* for example Fischer-Tropsch processes to higher value molecules (Figure 23). However, such processes involve complete degradation, followed by energy-intensive upgrading of the platform molecules. Thus it may be desirable to develop more energy-efficient biomass degradation routes in which many of the native functionalities are retained, which can be used for the production of higher value products such as monomeric precursors for advanced polymers and resins.[50] Reductive catalytic fractionation (RCF) is an up-and-coming approach in which lignin fractionation and depolymerization is simultaneously promoted in the presence of a solid reducing catalyst. Lignin is extracted from whole biomass *via* solvolysis and subsequently reduced in the presence of a catalyst. The catalyst serves to both promote delignification under milder conditions than conventional fractionation strategies, and to stabilize the highly reactive fractionation intermediates and thus prevent undesirable condensation.[61] RCF is an attractive alternative to conventional biomass pretreatment strategies and is one of the strategical foundations for the "lignin-first" biorefinery.[62]

There are numerous challenges associated with decomposing a solid feedstock such as lignin with a heterogeneous catalyst:

1) A strong solid-solid interaction between the catalyst and substrate is required. If the interaction is insufficient, the interaction between the substrate and catalyst surface may be too weak to reliably promote the reaction.
2) The opposite issue could also be true. Lignin possesses a high oxygen content which may cause lignin to interact too strongly with the catalyst such that it simply coats the catalyst surface and render it inert.
3) Reduction of lignin often affords numerous products which may complicate product separation processes and be economically deleterious to process costs.

Despite these issues, several recent reports in the literature have demonstrated significant progress for selective reduction of lignin from whole biomass. Anderson *et. al.*[63] recently reported a flow-through reactor setup for fractionation of biomass. They studied the hydrogenation of poplar wood over a 15% wt. Ni/C catalyst. The flow reactor allowed them to study the changing product profiles: namely, monomeric products were initially formed, but over time, higher MW species eventually began forming in higher yields.

Luterbacher *et. al.*[64] developed a methodology in which lignin is stabilized and extracted from whole biomass using various aldehydes. The aldehydes react with α,γ-diol groups on lignin side chains and form cyclical dioxane protecting groups. They found that hydrogenating the functionalized lignin leads to almost 80% monomer yield with a relatively narrow product slate (i.e. a few products as opposed to hundreds). Among the protecting groups tested, hydrogenolysis of acetaldehyde- and proprionaldehyde-treated lignin afforded the highest selectivity and most narrow product distribution for monomeric products.

However, both these strategies involve hydrogenation reactions in which exogeneous hydrogen gas is used as the reductant under high temperatures and pressures. Hydrogen gas under these conditions is a potential fire hazard. For these reasons this work focuses on use of *transfer hydrogenation* in which hydrogenations are promoted without the addition of hydrogen gas (an introduction to *hydrogenation*s with H_2 gas and *catalytic transfer hydrogenation* reactions is provided in the following sections). The work described in this dissertation focuses on evaluation of CoB catalysts for reducing several simple lignin models to screen each catalyst's potential as a transfer hydrogenation catalyst. With the strategies described above in mind, future investigations in our laboratory will involve combining the flow reactor technology and the lignin extraction protocol and attack lignin *via* catalytic transfer hydrogenation using CoB catalysts.

Hydrogenation & Catalytic Transfer Hydrogenation

Catalytic hydrogenation reactions comprise an important class of chemical transformations which involve either reduction of unsaturated double or triple bonds, or cleavage of single heteroatom bonds by the addition of hydrogen in the presence of a catalyst. Figure 25 illustrates the reduction of several reducible moieties; a ketone, an alcohol, and a methoxy group in the presence of catalyst and hydrogen gas. One of the largest-scale applications involves hydrogenation of the long, unsaturated hydrocarbon tails of plant and animal-derived fatty acids into their saturated derivatives to create margarine. Another important application involves asymmetric hydrogenation to produce chiral molecules from e.g. ketones, esters, carboxylic acids, imines or enamines.[65,66] In the context of biomass upgrading, catalytic hydrogenation using hydrogen gas (H_2) is a common approach to reductively depolymerize lignin. Oxygen-containing functional groups are removed *via*, for example, dehydration, dehydroxylation, and demethoxylation reactions. Hydrogenation is also used for converting complex and unstable oxygen-containing post-pyrolysis bio-oil derivatives into upgraded platform chemicals such as lignin-derived lower aromatics and hydrocarbons.

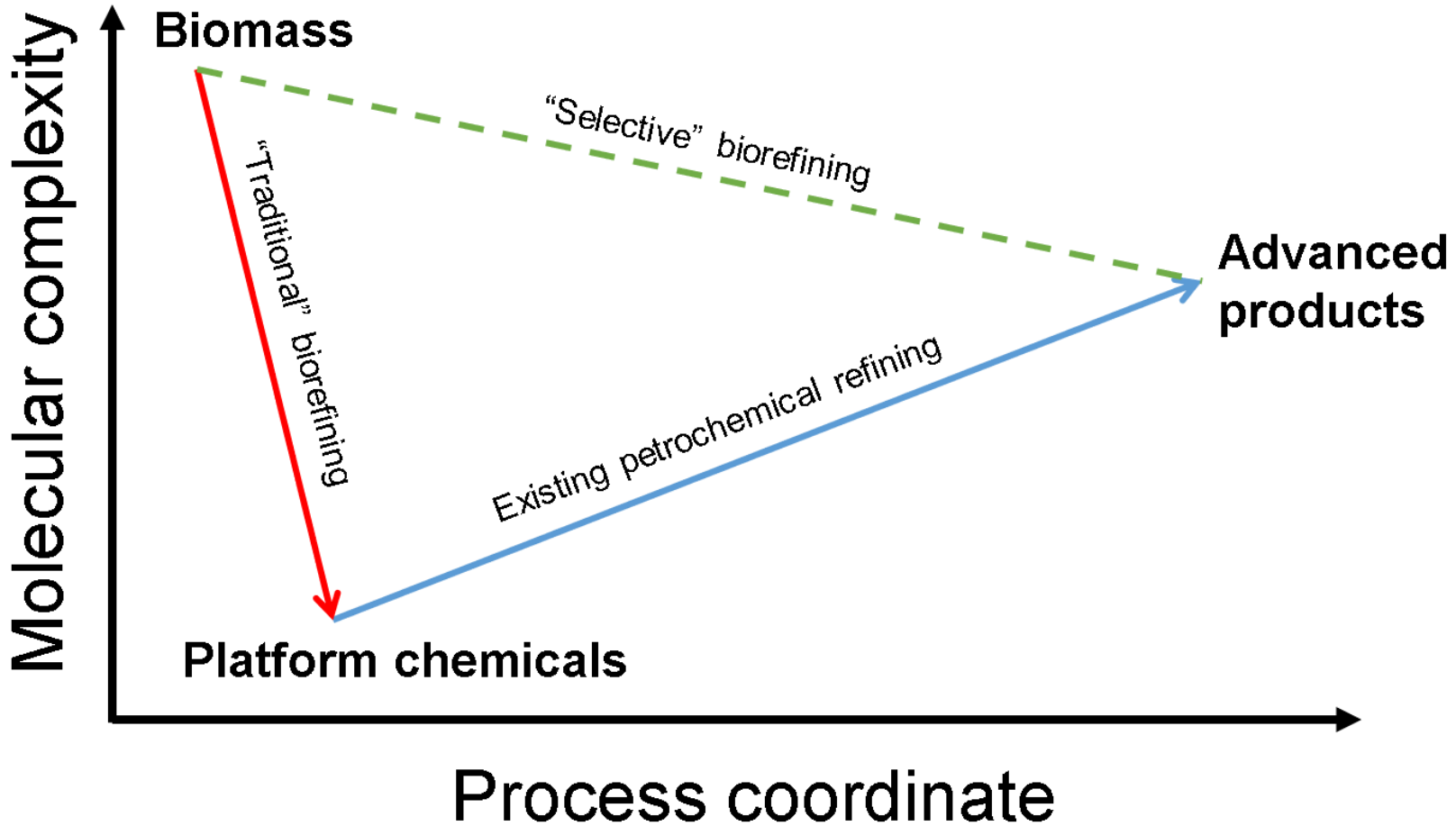


Figure 23. Illustration of traditional refining routes (red and blue lines), and more direct, sustainable route (green line) towards refining crude biomass to advanced products.

Hydrogenation reactions are conventionally mediated by late transitional metal catalysts such as nickel, platinum, palladium, or ruthenium. However, the gaseous nature of H_2, as well as the high temperatures and pressures required, substantially increase operational costs at large scale, and present significant safety concerns due to the potentially flammable nature of molecular H_2. An alternative strategy to circumvent these issues is known as catalytic transfer hydrogenation.

Catalytic transfer hydrogenation (CTH) is a variant of hydrogenation in which the hydrogen atoms are derived from a source that is not molecular H_2 (Figure 24). The hydrogen donor (abbreviated now as H-donor) is often a liquid-phase component which usually includes small alcohols such as isopropanol (i-PrOH), though a variety of other molecules such as *sec*-butyl alcohol, ethers such as dioxane, amines such as tripropylamine, or heteroaromatics such as napthalene have been reported as H-donors.[67] In practice, any hydrogen-containing molecule with a high reduction potential can serve as an H-donor.[68] Because the choice of H-donor can be varied, and because they are almost always liquid-phase species, two distinct advantages of CTH over conventional hydrogenation are apparent: first, pressurizing reactions is often not required, thus alleviating many concerns associated with possible explosion hazards, and second, the H-donor can simultaneously act as both solvent and reactant.

A well-known classic example of CTH is known as the Meerwein-Ponndorf-Verley (MPV) reduction. Figure 26A shows the mechanism of an MPV reduction of an alcohol to a ketone catalyzed by an aluminum alkoxide. In the MPV reduction, an alcohol donates its hydroxyl and α-carbonyl protons *via* a hydride shift to an acceptor molecule such as a ketone or aldehyde in the presence of an aluminum alkoxide catalyst. The reaction proceeds first with direct coordination of the acceptor molecule to the aluminum center *via* its carbonyl oxygen. A neighboring alkoxy species then transfers its α-carbonyl hydrogen to the α-carbon of the acceptor molecule *via* a 6-membered pericyclic transition state in which the hydrogen transfer step occurs concomitantly with transfer of electron density from the C=O bond of the acceptor molecule to the O-Al bond, and from the Al-O bond to the C-O bond of the neighboring alkoxy species which subsequently dissociates as the corresponding ketone or aldehyde. The coordinated acceptor molecule is then displaced by a solvent alcohol to regenerate the original aluminum alkoxide catalyst and form the target alcohol. Consequently, the H-donor alcohol is converted into its ketone or aldehyde derivative while the acceptor is converted to the corresponding primary or secondary alcohol. It should be noted that MPV reductions specifically refer to reactions where the target product is formation of an alcohol from a ketone or aldehyde, the reverse of which is referred to as an Oppenauer oxidation.

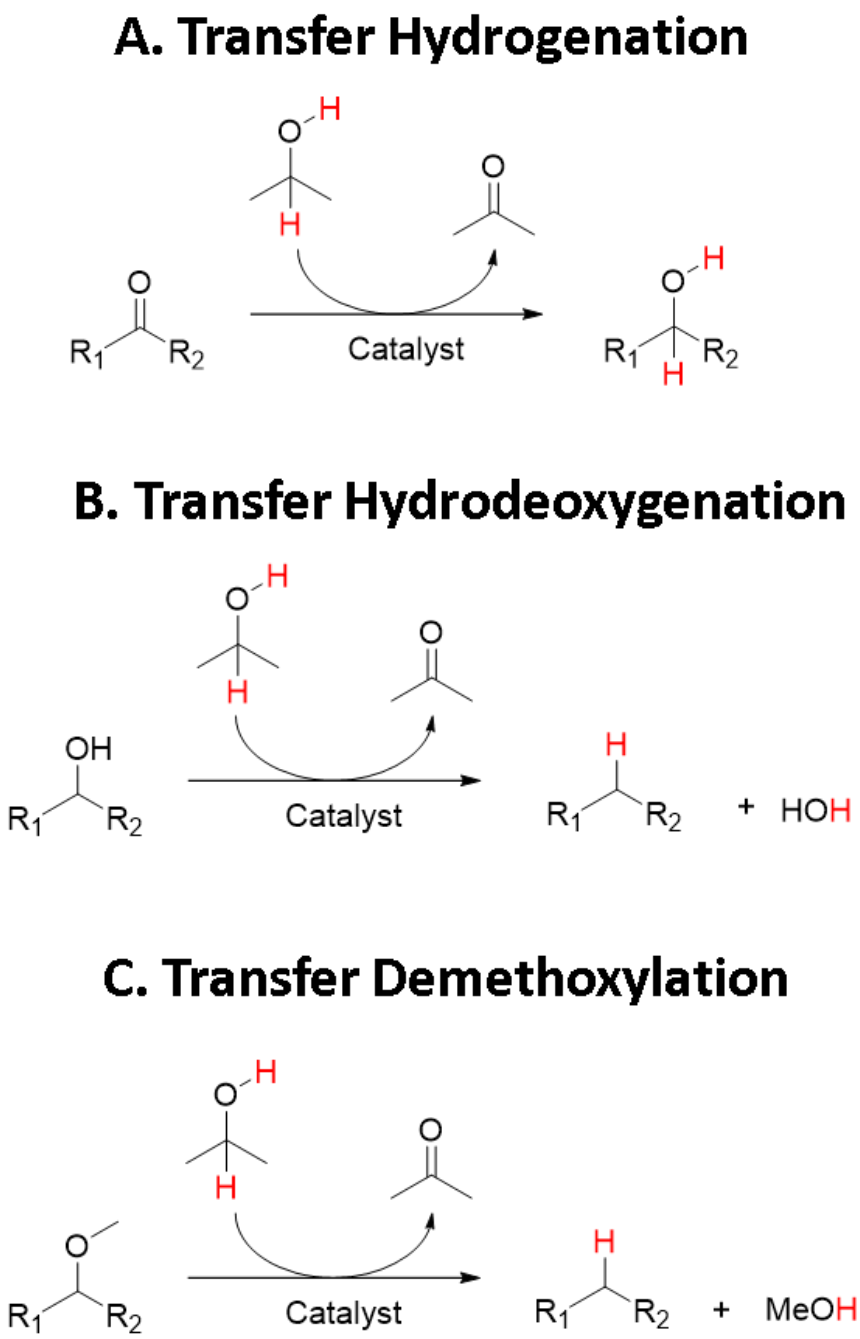


Figure 24. Illustration of catalytic transfer hydrogenation of a several reducible functionalities in the presence of catalyst and isopropanol as the H-donor: A) reduction of a ketone to an alcohol through transfer hydrogenation, B) reduction of an alcohol to an alkane through transfer hydrodeoxygenation, and C) cleavage of a methoxy group to an alkane and MeOH.

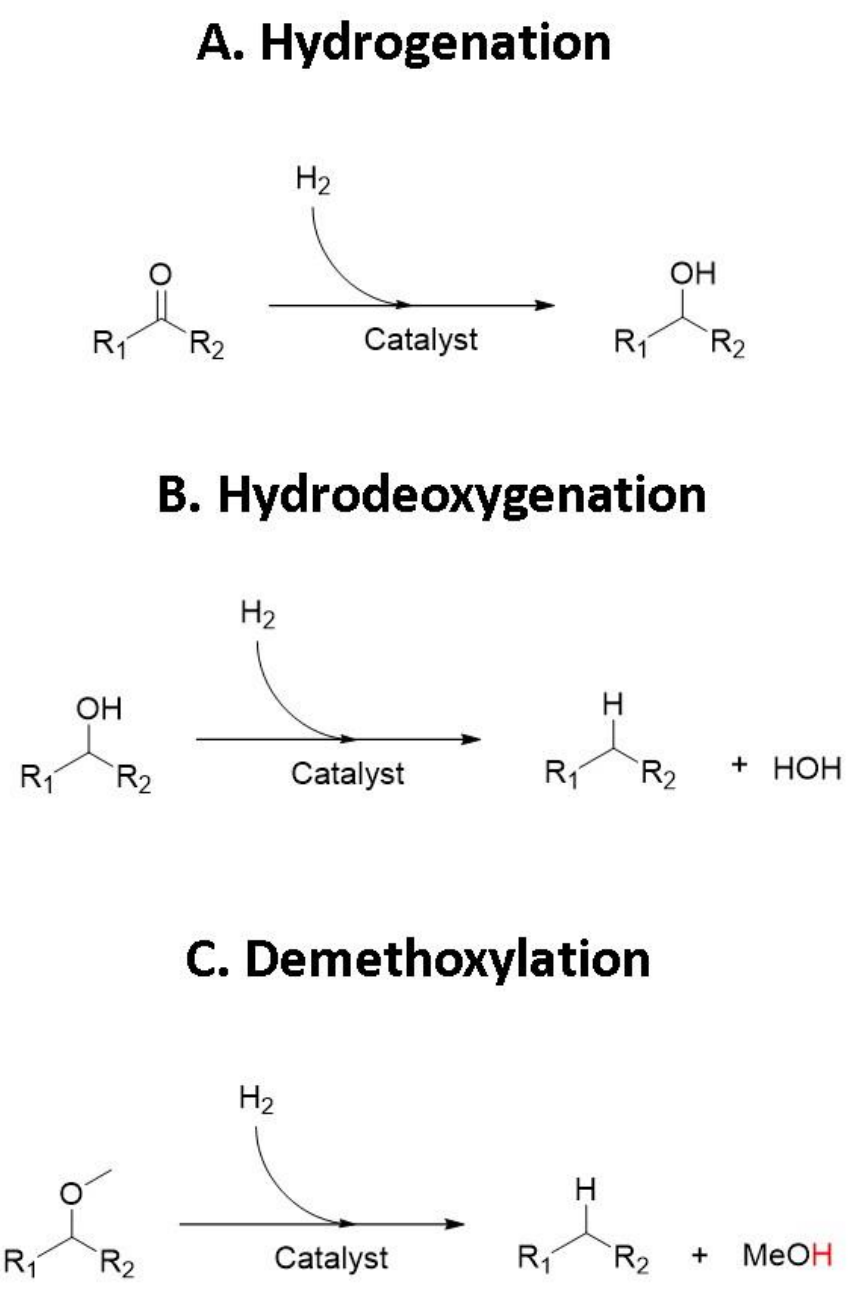


Figure 25. Illustration of catalytic hydrogenation of several reducible functionalities in the presence of catalyst and hydrogen gas: A) reduction of a ketone to an alcohol through hydrogenation, B) reduction of an alcohol to an alkane through hydrodeoxygenation, and C) cleavage of a methoxy group to an alkane and MeOH.

Figure 26B shows mechanism of the MPV reduction of a ketone to an alcohol by a heterogeneous catalyst. In this case, the donor alcohol is first deprotonated by a Lewis basic site, which then adsorbs to an adjacent Lewis acid site together with the acceptor ketone. The hydrogen of the α-carbon of the donor alkoxide is then transferred to the acceptor ketone through an analogous concerted metallocyclic transition state.[69] One possible alternative pathway involves generation of H_2 *in situ* in which the H-donor is first transformed into the reduced derivative with generation of H_2 or a surface metal hydride species, which in turn promote hydrogenolysis.

Heterogeneous Catalysts for Transfer Hydrogenation

Heterogeneous catalysts used to mediate CTH in past decades include surface-supported aluminum, lanthanum, zirconium, and hafnium alkoxides, hydrotalcites, magnesium oxide, and zirconia, among others.[70] Though these catalysts are active for carbonyl reductions under relatively mild conditions, their activity is generally only modest, and high catalyst loadings must be used in most cases. Further, many of these catalysts, particularly the metal alkoxides, are also highly sensitive to water.

Late transition metal catalysts comprising the platinum group metals (PGMs) have shown wide use as powerful CTH catalysts, with many examples converting substrates with high efficiency, and substrate-to-catalyst ratios at catalytic amounts. Most examples of such catalysts are homogeneous derivatives based on the PGMs iridium, ruthenium, rhodium, palladium, and osmium complexes, though their homogeneity renders them disadvantaged by the usual pitfalls such high cost, toxicity, instability at elevated temperatures, and costly separations from reaction solutions.

Lignin upgrading is conventionally mediated by late transition metal, transition metal oxide, or transition metal-ceramic solid catalysts.[71] One method for catalytically treating lignin involves combining palladium immobilized on a carbon support (usually denoted Pd/C) combined with an acidic zeolitic catalyst such as H-ZSM-5.[72] The Pd/C catalyst serves as a hydrogenation catalyst, whereas the zeolitic catalyst acts as the C-C cracking catalyst. However, this method still employs a noble catalyst with conventional hydrogenation. Fewer examples in the literature involving catalytic transfer hydrogenation in the context of lignin or lignin models are available, as most reports detail use of conventional hydrogenation.[69] H-donor molecules in this context often include simple, inexpensive alcohols such as i-PrOH.

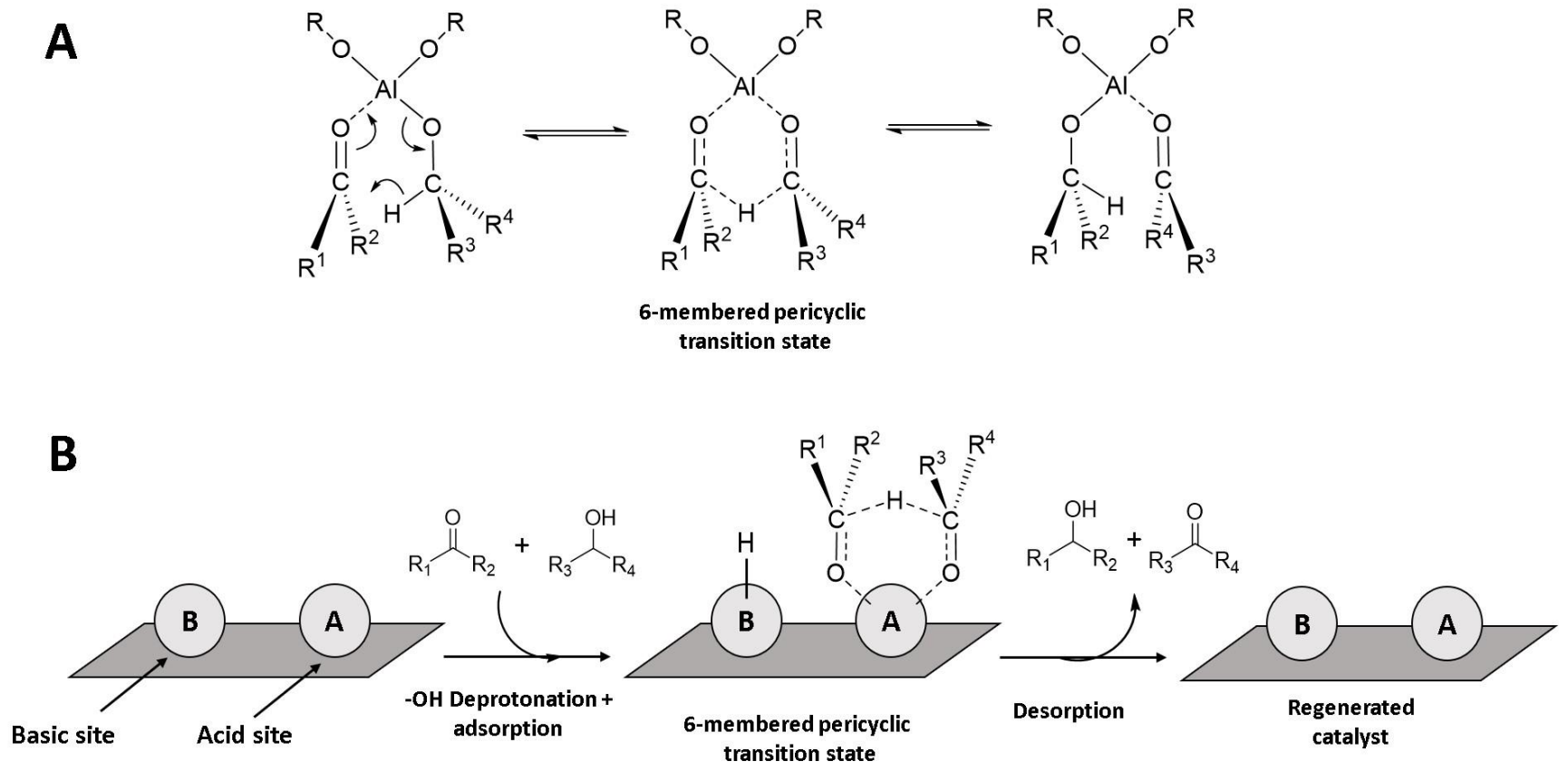


Figure 26. Simplified illustrations of the Meerwein-Ponndorf-Verley reduction reactions catalyzed by A) a homogeneous aluminum alkoxide catalyst and B) a heterogeneous analogue consisting of Lewis basic and acidic active sites.

Because of the inherent cost and scarcity of platinum group metals, there is significant effort to find catalysts based on earth-abundant catalysts such as iron, cobalt, and nickel. Luo[73] *et. al.* recently reported a carbon-supported nickel catalyst for hydrogenation of Miscanthus lignin. With regard to cobalt-based hydrogenation catalysts, Chen *et. al.*[74] reported α-Al_2O_3-supported Co catalysts as effective hydrogenation catalysts for reduction of C=O to alcohols and C≡N to amines in the presence of other reducible moieties for a variety of substrates. The authors also note significant enhancement of selectivity for reduction of C≡N to amines with addition of ammonia, which suggests the importance of base addition to promote these reactions. Zhang *et. al.*[75] recently demonstrated that cobalt supported on high surface area mesoporous carbon converts acetophenone to ethylbenzene with high selectivity under mild conditions.

There are also several examples of heterogeneous cobalt catalysts for transfer hydrogenation reactions. Long *et. al.*[76] synthesized Co@C-N catalysts by pyrolysis of a Co-containing metal organic frameworks and demonstrated their activity towards CTH of C=O, C=C, N=O, and C≡N bonds in i-PrOH under mild conditions. The authors also demonstrated that higher surface basicity of the catalyst results in higher activity and selectivity for conversion of acetophenone to 1-phenylethanol, highlighting the potential importance of catalyst surface basicity for CTH reactions. Chen *et. al.*[77] also demonstrated high selectivity of N-doped cobalt nanoparticles towards reduction of a variety of N-heteroarenes using formic acid as the hydrogen source without the addition of base. Their results also indicate that the presence of nitrogen may play an important role in catalytic activity. Kumar *et. al.*[78] demonstrated that cobalt nanoparticles (NPs) immobilized on carbon-coated iron oxide nanospheres (Co NPs@HCCs) are active for C=O reduction to alcohols for a variety of compounds in the presence of KOH.

Boron-containing metal compounds have been extensively studied for their electronic, catalytic, and refractory properties.[79] Boron-containing cobalt ("CoB") compounds and cobalt borides CoB, Co_2B, and Co_3B have been studied for use in alkaline batteries,[80] and for catalytic hydrogenation of organic double bonds, and have been shown to be more resistant to poisoning than the isolated metal.[81] Several types of binary, ternary, and quaternary boron-containing compounds have been reported for use as conventional hydrogenation catalysts as well. Wang *et. al.*[82] reported a Co-Ni-Mo-B catalyst for hydrodeoxygenation of phenol and revealed that the presence of Co enhanced catalytic activity, as compared to Ni-Mo-B. The same group demonstrated Co-Mo-B catalysts are active catalysts for hydrodeoxygenation of several bio-oil model compounds.[83] Li *et. al.*[84] reported amorphous mesoporous Co-B catalyst are active for hydrogenation of cinnamaldehyde to cinnamyl alcohol.

Although several examples of B-containing metal catalysts are known for conventional hydrogenation, to the best of our knowledge boron-containing cobalt catalysts have not been employed for *transfer hydrogenation*. However, Regmi *et. al.* recently demonstrated Fe-Ni-B catalysts are active for hydrodeoxygenation of acetophenone to ethyl benzene in super-critical EtOH, which highlights the potential of boron-containing metal materials as active CTH catalysts.

Inspired by their results, the synthesis and investigations into the structure and catalytic properties of two forms of CoB are the focus of the work described in this dissertation. The catalytic reactions investigated were for catalytic transfer hydrogenation of acetophenone, acetovanillone, and guaiacol (each of which are illustrated in Figure 27) using i-PrOH and EtOH (EtOH) as the hydrogen donors. These substrates were chosen for several reasons: each are commercially available and inexpensive, each possess several reducible moieties in the presence of others, and each substrate and their reduced derivatives are readily amenable to quantitative analysis *via* gas chromatography-mass spectrometry (qGCMS), which is a powerful tool for analyzing complex mixtures of volatile organic species. The ability to readily quantify the catalytic reaction mixtures allows for rapid evaluation of catalytic performance as potential candidates for use as CTH catalysts.

Numerous routes towards synthesizing boron-containing metal nanoparticles and metal borides are known. Carenco *et. al.*[85] thoroughly described these methods in a detailed review. Synthetic routes generally involve reacting a transition metal, metal oxide, or metal salt with a boron-containing compound such as elemental boron, boron oxide, boric acid, boron halogenides, boranes, or alkali borohydrides. Most of these strategies require extremely high temperatures (500-1500 °C) and some require use of highly toxic gaseous boron sources such as diborane (B_2H_6) or boron halogenides such as BCl_3, and often require use of Mg(0) or I_2 to promote reduction of the precursors.[86] For these reasons, the synthetic strategy used in this work involves room-temperature reduction of $CoCl_2$ with $NaBH_4$. This method is quick, simple, scalable, and requires non-toxic and inexpensive precursors, and can be carried out in aqueous media. The synthetic procedure is described in Chapter 3.

Screening of Other Substrates

Although this work focuses on acetophenone, acetovanillone, and guaiacol, CoB catalysts described here were also previously screened against variety of substrates for CTH. These substrates included eugenol, syringol, catechol, vanillin, benzamide, α-ketoglutaric acid, and levulinic acid. These species were chosen as candidates for several reasons. Eugenol, syringol, catechol, and vanillin are common lignin-derived post-pyrolysis bio-oil components.

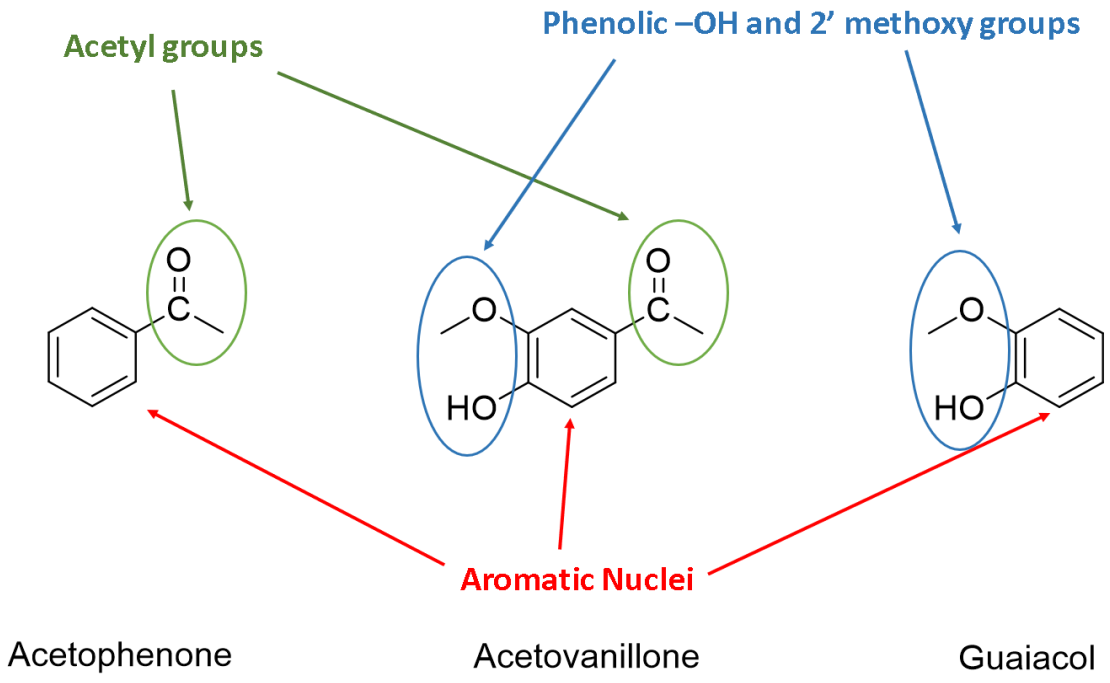


Figure 27. Illustration of the various reducible moieties of acetophenone, acetovanillone, and guaiacol.

Benzamide was chosen to because of the presence of an amide functional group. α-ketoglutaric acid and levulinic acid were chosen because of the presence of one or more carboxylic acid functionalities (it is noteworthy that levulinic acid is an important platform chemical which can be derived from cellulose).

A qualitative summary of these substrates and their products are shown in Figure 28. The products in each case are described as either “major” or “minor” (indicated in the red text). However. it should be noted that these species were identified using GCMS but were not quantified. “Major” simply means “large peak area intensity” and “minor” simply means “small peak intensity” and are entirely qualitative. Although these systems were not quantified, several conclusions can be drawn from these results. Namely, CoB catalysts appear to be active and stable for transformation of a relatively wide variety of functional groups. While the focus of this work, as discussed in Chapters 3 and 4, was on selective carbonyl reduction, these preliminary studies indicate that CoB catalysts are functional group tolerant and potentially applicable to numerous types of reductions. In the context of biomass valorization, this could be important as numerous functional groups are present or formed during reduction of these highly functionalized feedstocks.

Although CoB catalysts were active for these transformations, a decision was made to narrow the substrate scope to acetophenone, acetovanillone, and guaiacol to conduct more in-depth studies. These three were specifically chosen because of their structural similarity, which allows for more direct comparisons of the catalytic effects of the presence of absence of certain functional groups.

Chapter Summary

This chapter briefly discusses biomass conversion in the context of lignin valorization and highlights some of the associated challenges. Lignin is a recalcitrant material which, until recently, was not considered an economically viable feedstock and simply burned as low-quality fuel. However, upgrading and utilizing lignin in recent years has become a highly sought-after endeavor because lignin is a major component of lignocellulosic biomass and is the most abundant source of naturally occurring aromatic nuclei with great potential to become a feedstock for advanced, value-added materials. Many contemporary processes towards upgrading lignin involve harsh conditions which frequently result in low yields of desirable products and high yields for unusable C-C condensation products.

Reductive catalytic fractionation is an up-and-coming strategy which involves treating native lignocellulosic biomass in the presence of a catalyst under milder conditions to enhance yields for desired value-added products. However, many commonly-used catalysts involve the scarce and

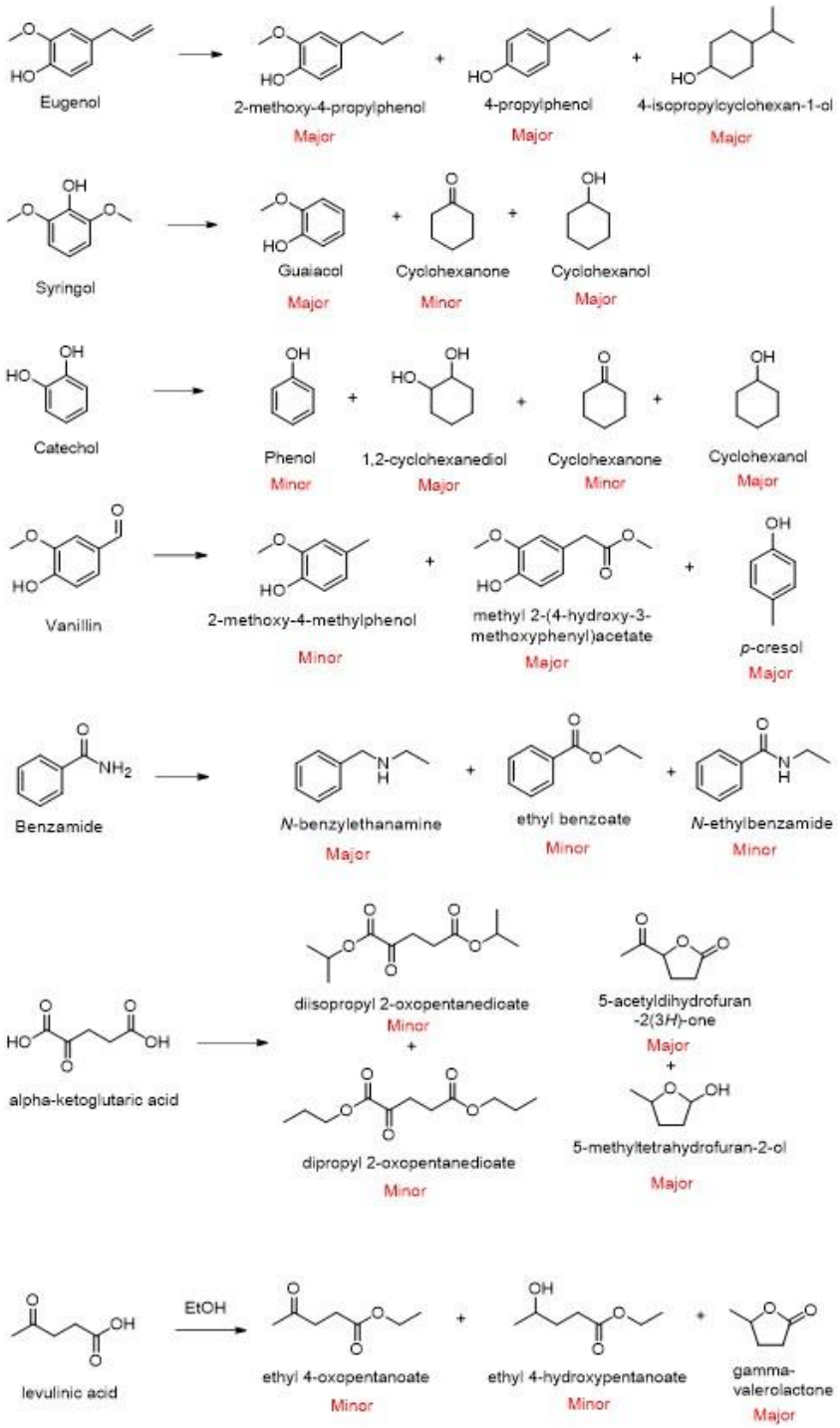


Figure 28. Summary of various substrates and their product distributions after CTH with CoB catalysts. All reactions were conducted in *i*-PrOH unless otherwise indicated. Red text refers to “minor” and “major” products. However, these products were not quantified and these assignments are entirely qualitative.

expensive platinum group metals which negatively impacts the economic viability of biomass conversion processes. To this end, there is significant effort towards discovering catalysts based on inexpensive, earth-abundant catalysts such as iron, cobalt, and nickel. Various hydrogenation and transfer hydrogenation catalysts based on heterogeneous cobalt were discussed. The work described here involves the synthesis, characterization, and catalytic evaluation of boron-containing cobalt (CoB) catalysts for transfer hydrogenolysis reactions in the interest of lignin valorization. The following chapter describes the experimental protocols for catalyst synthesis, characterization, and the protocols used to quantify catalytic reaction mixtures.

Chapter 3 – Experimental Methods

General Experimental

All reagents were purchased from commercial vendors and used as received. Powder x-ray diffraction (PXRD) spectra were obtained using a Panalytical Empyrean diffractometer with a Cu K_α source (λ = 0.15406 nm) with a current of 40 mA. Inductively coupled plasma-optical emission spectroscopy (ICP-OES) analyses were performed using an Agilent 5110 ICP-OES with an Agilent SPS 4 autosampler. GCMS data were obtained using an Agilent 7820A GC system with an Agilent 5977B mass spectrometry detector (MSD). Scanning transmission electron microscopy-electron dispersive X-ray spectroscopy (STEM-EDX) data were obtained using a Tecnai Osiris STEM equipped with a SuperX EDX system that allows for detection of light elements down to boron.

Synthesis of CoB Catalysts

Figure 29 shows photographs of the steps in synthesizing CoB catalysts. A 2 Liter three-neck round bottom flask was charged with a solution of $CoCl_2 \cdot 6H_2O$ (40.0 g, 168 mmol) in 1 Liter of 18 MΩ H_2O. N_2 was passed over the solution while N_2 was also simultaneously sparged directly through the solution for several minutes to remove ambient O_2. A molar excess of $NaBH_4$ (50.0 g, 1.32 mol) was then added to 500 mL of 18 MΩ H_2O in a beaker and vigorously stirred for several minutes until completely dissolved. The bubbling solution was then carefully poured into a dropper funnel which was attached to the central neck of the three-neck round bottom flask containing the $CoCl_2 \cdot 6H_2O$ solution. N_2 was passed over the solution (the flow should start at the Schlenk arm and pass through the top of the attached dropper funnel) while N_2 was simultaneously sparged through the $NaBH_4$ solution for several minutes.

The $NaBH_4$ solution was then added dropwise over the course of one hour to the $CoCl_2 \cdot 6H_2O$ solution. Upon addition of the first drop, the solution color rapidly changed from a deep reddish-purple to black and the solution bubbled vigorously. Once the $NaBH_4$ solution was completely added, the resulting black powder was stirred until gas evolution decreased. The black powder was then separated with a strong magnet and the reaction solution was decanted and discarded. The black powder was then washed 3 times with a large volume (500 mL each) of 18 MΩ H_2O followed by 3 more washings with a large volume of i-PrOH. All washings were done under a N_2 blanket. The powder was then dried under vacuum overnight at 80 °C.

The resulting powder was then taken into an inert atmosphere glovebox, ground using mortar and pestle and weighed. Approximately 10 g of black powder was recovered. A small amount was lost

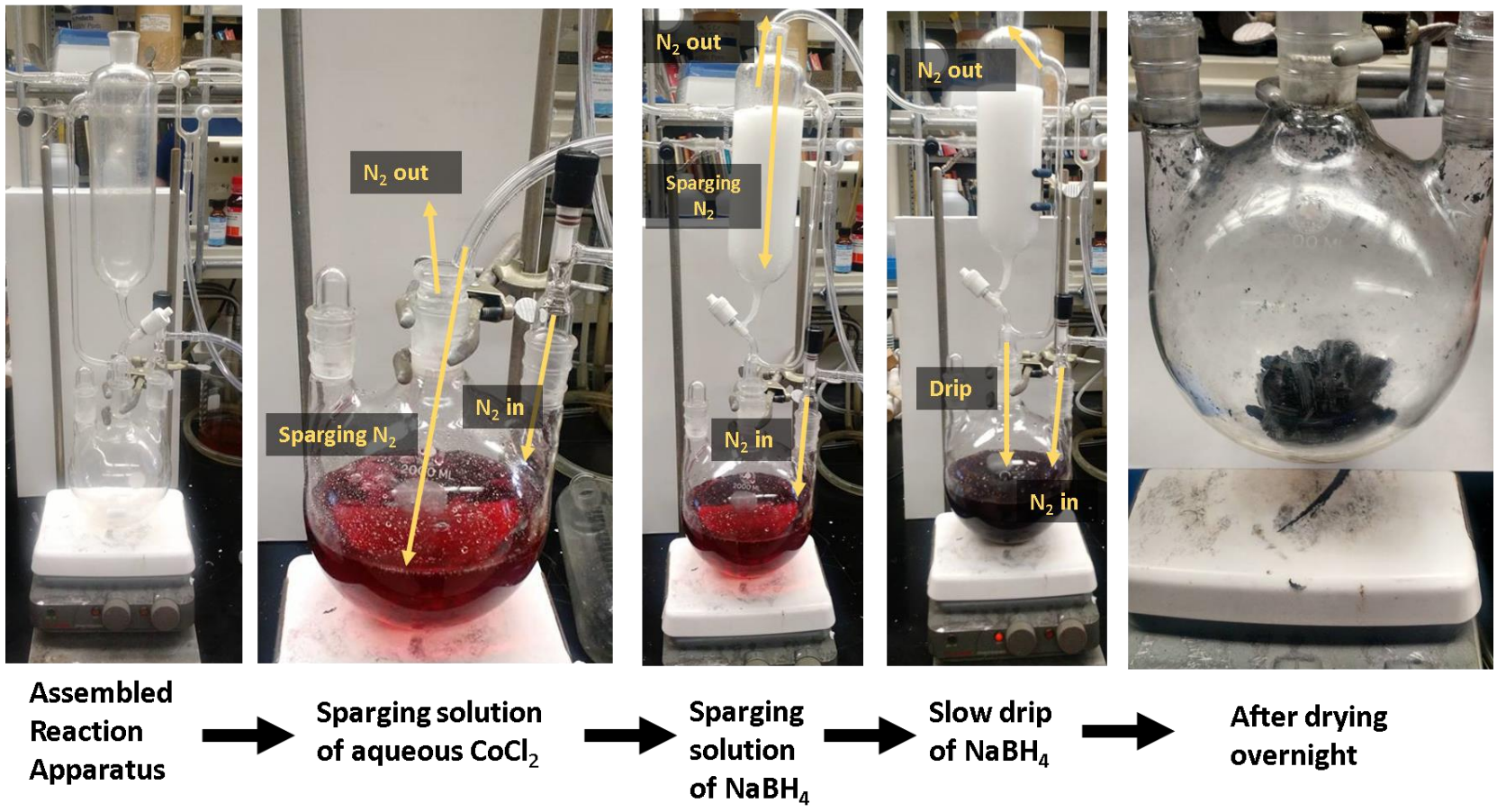


Figure 29. Images illustrating the steps for synthesizing CoB catalysts.

during the washing steps, during transfer of the powder out of the three-neck flask, and after grinding with mortar and pestle. The powder was then partitioned into two separate batches. One batch was stored in the glovebox (now referred to as "reduced" CoB (CoB_{red})), and the other was removed from the glovebox and exposed to air overnight in an oven at 100 °C (now referred to as "oxidized" CoB (CoB_{oxi}).

Characterization of CoB Catalysts

Characterization of CoB catalysts was done by powder X-ray diffraction (PXRD), inductively coupled plasma-optical emission spectroscopy (ICP-OES), and transmission electron microscopy-electron dispersive X-ray spectroscopy (TEM-EDX). The sample is highly response to a strong magnet, as shown in Figure 30. The magnetic properties of the catalyst can be used in purification strategies which helps circumvent the need for filtration or centrifugation.

Use of Gravimetric Analysis in ICP-OES and GC-MS Analysis

For ICP-OES and GC-MS analysis, all quantities were measured gravimetrically using a calibrated laboratory scale. All liquid samples, including liquid substrates, solution aliquots, dilutions, calibration curve aliquots, and calibration curve dilutions were transferred *via* pipetting using a calibrated Fisherbrand™ Elite™ adjustable-volume pipette (100-1000 µL), and the pipetted samples were all weighed gravimetrically. To test the accuracy of the scale, 0.5, 2, 5, and 10 g calibration weights were weighed, which gave values of 0.5001, 2.0007, 5.0007, and 10.0008, respectively. Since the weighing error was found to be much less than 1%, the error associated with weighing was not considered a dominating source of error and was thus excluded from error analyses. To test the accuracy of the pipette, 0.25, 0.5, and 1 mL aliquots of ultra-pure H_2O were pipetted into a glass vial which was tared on the previously mentioned calibrated balance. The measured values were 0.2490, 0.5007, and 1.0007 g, respectively. Thus, the error associated with pipetting *aqueous* solutions was not considered a dominating source of error and was also excluded from error calculations for aqueous samples. However, it should be noted that pipetting in this fashion was only accurate for aqueous samples.

For non-aqueous liquid samples such as hexadecane, acetophenone, guaiacol, i-PrOH, and solution aliquots derived from i-PrOH solutions, pipetting was less accurate. For example, for generating GCMS response factor curves using hexadecane as the internal standard, approximately 100 µL of hexadecane was pipetted into five tared vials. The measured weights were

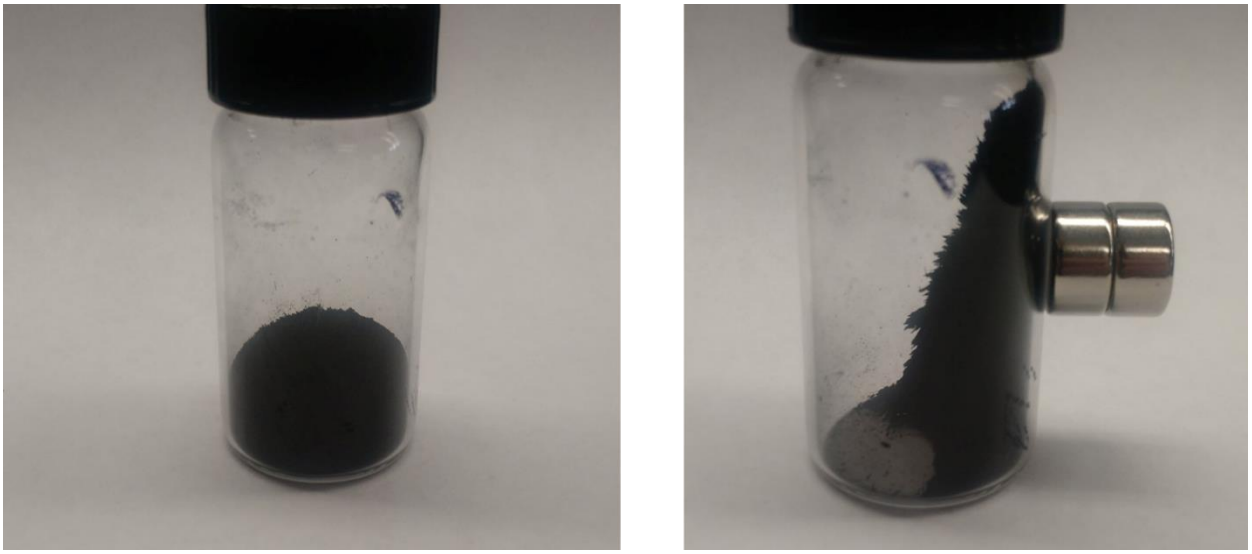


Figure 30. Photographs showing the response of CoB catalysts to a strong neodymium magnet.

determined to be 0.0733, 0.0770, 0.0746, 0.0759, and 0.0745 g. The volumes were then calculated using the density of hexadecane (0.770 g mL^{-1}), and were found to be 0.0952, 0.100, 0.0969, 0.0986, and 0.0968 mL, respectively.

This disparity is likely due to the differences in density and viscosity of these components relative to water, which may negatively impact the volumetric pipetting accuracy. It is thus critically important that non-aqueous liquids should be measured gravimetrically to eliminate error associated with pipetting.

Elemental Analysis with ICP-OES

ICP-OES is a technique used for the determination of the elemental composition of substances. It consists of two main components: an induction coil that generates a plasma torch (T = 8000-10,000 K) by electromagnetic induction, and a spectrometer that measures photons emitted from elements that are passed through the plasma torch. ICP-OES samples are analyzed by first digesting the sample in acidic media, and the resulting solution is then drawn through a capillary tube by a peristaltic pump and aerosolized by a nebulizer into a spray chamber. A stream of argon carries a small portion of the aerosol into the plasma. The extreme temperatures in the plasma promote electronic excitations of the elements in the sample, which subsequently relax and emit photons whose wavelengths and intensities are recorded by a spectrometer. One of the main advantages of ICP-OES is that most elements on the periodic table can be accurately quantified down to concentrations in the parts-per-billion concentration regime. However, no structural information is gained using this technique since the analyte must be destroyed by digestion in acidic media prior to analysis. In cases of complex samples that consist of many components, quantification may be difficult if there is significant overlap of spectral features.

Prior to sample analysis, an external calibration curve must be created for each element believed to be present in the material being analyzed. Calibration curves are generated by preparing serial dilutions from a stock solution containing a precisely known concentration of the element being analyzed. Stock solutions used here were commercially purchased (Fisher Scientific™) 1000 ppm stock solutions of Co and B. The intensities of the calibration standards are then plotted as a linear function of intensity versus concentration.

To prepare a sample for ICP-OES analysis, it must be quantitatively digested in acidic aqueous solution. Digestions are commonly done with strong acids such as hydrochloric acid (HCl), nitric acid (HNO_3), or aqua regia (3:1 HCl:HNO_3 mixture). The peak area intensities of the emission peaks

corresponding to the given elements in the analyte are subsequently measured and compared to the corresponding calibration curves to determine elemental concentrations.

As described previously, the as-synthesized CoB was divided into two batches, one of which was kept in an inert atmosphere glovebox, "CoB_{red}", and a second one that was removed from the box and exposed to air, "CoB_{oxi}". To prepare CoB_{red} and CoB_{oxi} for ICP-OES analysis, CoB_{red} (75.3 mg) and CoB_{oxi} (100.6 mg) were digested in 10 mL of 10% HNO_3 overnight. The two solutions were then diluted individually to approximately 50 mL with H_2O (gravimetrically determined). Concentrations of the stock solutions were calculated in parts-per-million based on weight using the following equation:

$$ppm = \frac{Sample\ wt.(g)}{Solvent\ wt.(g)} * 10^6 \qquad \text{Equation 2.1}$$

A 250 µL aliquot of each digestion was taken and further diluted with 10 mL of H_2O.

To prepare the calibration standards, 20.0, 40.0, 60.0, and 80.0 ppm (wt./wt.) serial dilutions were prepared from 1000 ppm Co and B stock solutions that were purchased commercially (Fisher Scientific). To make the dilutions, 1.0, 2.0, 3.0, and 4.0 mL (gravimetrically determined, <0.1% error) of the stock solution were each pipetted into four separate 50 mL plastic volumetric containers and diluted to approximately 50 mL with H_2O. For ICP-OES analysis, two wavelengths for both Co (238.892 and 228.615 nm) and B (249.678 and 182.577 nm) were analyzed. The concentrations determined for each of the wavelengths was then averaged together. The calibration curves for each of these wavelengths are shown in Figure 31. The measured concentrations of Co and B present in CoB_{red} and CoB_{oxi} are reported in Table 1.

For CoB_{red}, the measured concentrations of Co and B were 26.86 ± 0.08 and 2.81 ± 0.01 respectively, and for CoB_{oxi}, the concentrations of Co and B were 27.39 ± 0.12 and 2.81 ± 0.01, respectively. These values were used to back-calculate the concentrations of Co and B in the stock solutions. For CoB_{red}, the stock concentrations of Co and B were calculated to be 1352.82 ppm and 141.20 ppm, respectively. For CoB_{oxi}, the stock concentrations of Co and B were calculated to be 1413.07 ppm and 148.81 ppm, respectively. The digested weights of Co and B were then back-calculated using a rearrangement of equation 2.1:

$$Element\ wt. = \frac{ppm * solvent\ wt.}{10^6} \qquad \text{Equation 2.2}$$

For CoB_{red} the weights of Co and B were calculated to be 68.1 ± 2.0 mg and 0.7 ± 0.02 mg, respectively, with a total weight of 75.2 ± 3.0 mg. For CoB_{oxi}, the weights of Co and B were calculated to be 72.9 ± 2.2 mg and 7.7 ± 2.3 mg, respectively, with a total weight of 80.6 mg. For CoB_{red}, the initial

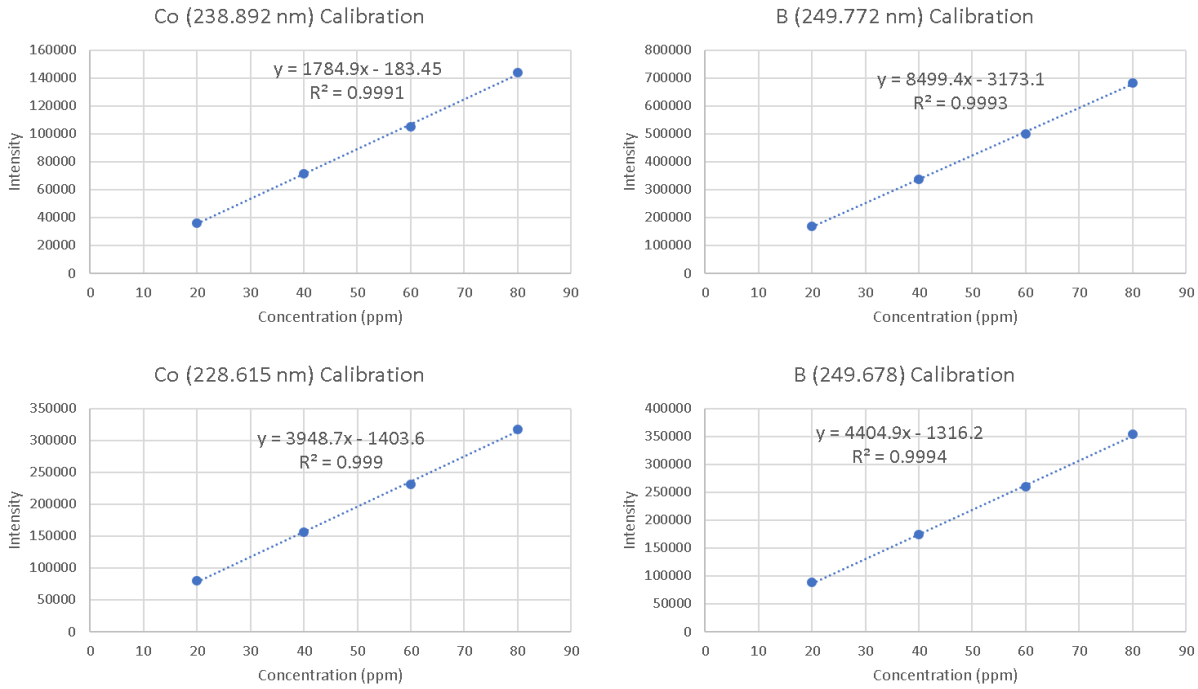


Figure 31. ICP-OES calibration curves for Co and B.

Table 1. Measured concentrations of Co and B present in CoB_{red} and CoB_{oxi}

Element (wavelength, nm)	Concentrations (ppm)	Averaged Concentrations (ppm)
CoB_{red}		
Co (238.892)	26.80	26.86 ± 0.08
Co (228.615)	26.91	
B (249.678)	2.88	2.81 ± 0.01
B (182.577)	2.89	
CoB_{oxi}		
Co (238.892)	27.31	27.39 ± 0.12
Co (228.615)	27.48	
B (249.678)	2.88	2.89 ± 0.01
B (182.577)	2.89	

sample weight was 75.3 mg, whereas the total weight of the components Co and B as determined from by ICP-OES analysis was 75.2 ± 2.3 mg.

For CoB_{oxi}, the initial sample weight was 100.6 mg, whereas the total weight of the components Co and B measured by ICP-OES was determined to be approximately 80.6 mg. From these values, the millimole amounts of Co and B in CoB_{red} and CoB_{oxi} were then calculated. CoB_{red} was calculated to contain 1.15 ± 0.03 mmol Co and 0.66 ± 0.02 mmol B, whereas CoB_{oxi} was calculated to contain 1.24 ± 0.04 mmol Co and 0.71 ± 0.02 mmol B. Thus, the stoichiometric formula for CoB_{red} and CoB_{oxi} is approximately $Co_{1.7}B$ in both cases.

For CoB_{red}, the difference between the gravimetrically determined weight and ICP-OES weight is approximately 0.15 mg, whereas the difference for CoB_{oxi} is approximately 20.0 mg. Because CoB_{oxi} was exposed to air overnight, this weight difference was assumed to be due to the presence of oxygen in the sample, either due to ambient O_2, H_2O, or a combination of both. The following analysis assumes the weight difference is entirely due to the presence of oxygen. Thus, the oxygen content present in the sample is 1.25 ± 0.04 mmol. Thus, the stoichiometric formula based on this analysis is consistent with $Co_{1.7}BO_{1.7}$. It is important to note that, because samples are digested prior to analysis, ICP-OES does not provide structural information, thus these results do not provide information about phases or actual stoichiometry present in the materials.

Assuming oxygen with an oxidation state of -2 has been incorporated into CoB_{oxi}, some portion of the reduced Co and B present in the catalyst must take on higher oxidation states in the form of their corresponding metal oxides in catalyst samples that were exposed to air. The O present in the sample could be formulated as phases of boron oxides or cobalt oxides. This may play a role in catalytic performance, and for this reason, as discussed in Chapter 4, the catalyst performance of CoB_{red} and CoB_{oxi} were compared.

Catalysis Reactor Preparation

All reactions were performed in Swagelok stainless steel reactors comprised of a ¼" male stainless steel hex nipple and two ¼" female stainless steel caps. Figure 32 shows the steps to prepare reactors for catalysis. The hex nipple is first secured in place with a benchtop vice, and one of the threaded sides of the nipple are wrapped in Teflon tape. The taped side is then capped. The cap is first hand-tightened, then a wrench is used to tighten it further (special care should be taken not to overtighten and damage the threading which may result in the caps locking – one full turn is usually

enough). The reactor is then turned over in the vice so that the uncapped side is facing upward, and the uncapped side is then wrapped in Teflon tape. The reactor is then charged with catalyst and 2 mL of the reaction solution, then sealed with the second cap, and the reactor is placed in a constant temperature heat bath set to the desired temperature.

Figure 33 shows the heat bath setup. The heat bath consists of approximately 1 kg of a low temperature eutectic salt mixture containing approximately 53% potassium nitrate (KNO_3), 40% sodium nitrite ($NaNO_2$), and 7% sodium nitrate ($NaNO_3$). The salts were thoroughly mixed in a 3 L stainless steel beaker, and the beaker was insulated by 2" thick ceramic insulation and aluminum foil. The beaker was then placed on a Thermo Scientific™ Cimarec™ hotplate with 7.25 x 7.25 inch surface area. The beaker was then heated until the eutectic mixture was completely melted (m.p. >160 °C). The melted salt mixture temperature was monitored by an external thermocouple. After reaction, reactors were removed from the salt bath and quenched in a large volume of water, the reactor is secured with a benchtop vice, and one of the caps is removed. A 10 µL aliquot is then taken for GCMS analysis as described in the following section. To clean the reactors after reaction, the reactors were disassembled and washed several times with a large volume of acetone and dried in an oven.

Because the reactors are made of relatively thick stainless steel, it was important to determine the heating rate of the solutions inside the reactors from room temperature to the desired temperature after being placed in the heat bath. A reactor with a Swagelok thermocouple adapter (PN SS-100-7-4) was prepared as before, filled with i-PrOH, sealed, and placed into the heat bath at 165, 200, and 300 °C for 15 minutes followed by quenching in room temperature water. The temperature ramp profiles are shown in Figure 34. For all three temperatures, the reactor temperature equilibrates to the desired temperature in approximately 2 minutes

Gas Chromatography-Mass Spectrometry (GCMS)

GCMS is a powerful and sensitive technique for determination of small (<400 molecular weight) and volatile organic molecules with sensitivity in the parts-per-billion regime. As the name suggests, a typical GCMS instrument consists of two main components: a gas chromatograph and a mass spectrometer. The gas chromatograph essentially consists of a temperature-programmable oven which contains a capillary column that has a chemically inert stationary phase deposited on the inside walls of the capillary. A typical commercial capillary column is 20-30 meters in length with an inner diameter approximately 0.25 millimeters and an organo-siloxane stationary phase such as polydimethylsiloxane

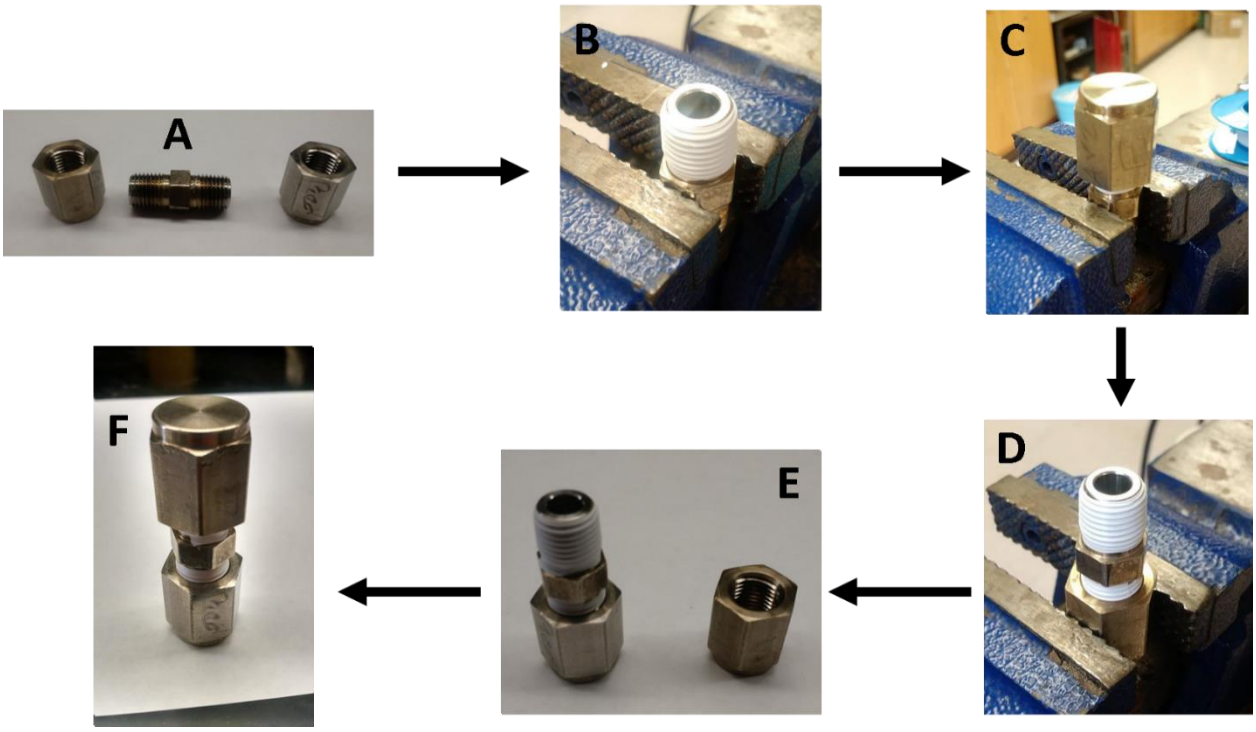


Figure 32. Photographs illustrating the steps for preparing reactors used as the catalysis reaction vessels: A) separated reactor components, B) hex nipple threading secured to a vice and wrapped in Teflon tape, C) one cap securely attached to the taped threading, D) rotation of the reactor and taping of the opposite side, E) reactor that is ready to be charged with catalyst and reaction solution, and F) the final, sealed reactor ready for catalysis.

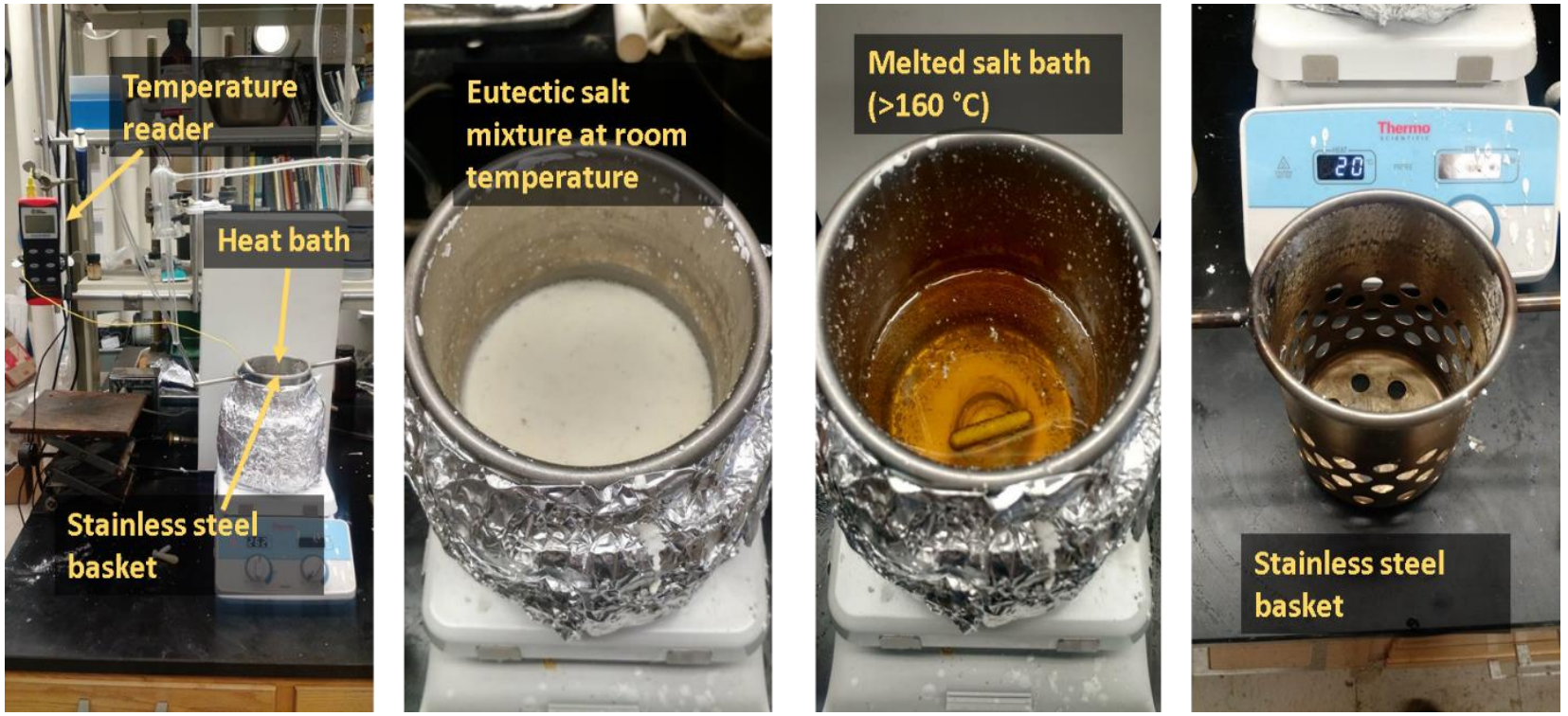


Figure 33. Images showing the heat bath setup used for catalysis.

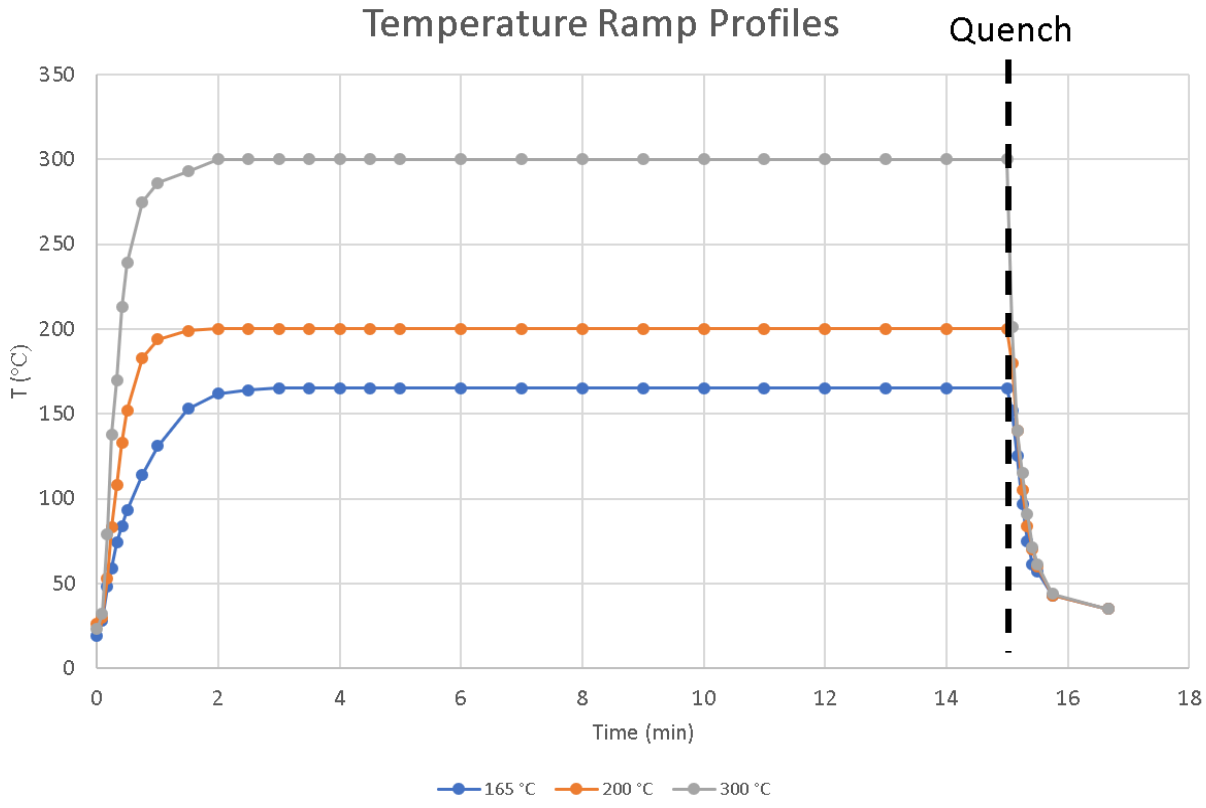


Figure 34. Temperature ramp profiles of the reactors at 165, 200, and 300 °C.

(PDMS). Columns come in a wide variety of lengths, shapes, sizes, and can contain different types of stationary phase materials depending on the type of compounds in the mixture, but the previously-mentioned components are among the most commonly used for routine small-molecule analysis and are the ones used here.

As an illustrative example of a typical GC analysis run, a 1 µL aliquot of a solution containing the analyte is dissolved in a non-aqueous solvent (bulk water may be damaging to the instrument) is drawn into a 10 µL GC syringe and injected into the chromatograph through a septum-sealed injection port. The injected aliquot is then rapidly volatilized in the injection port by a heater (>250 ^{o}C) which is mated to the GC column. The column is initially maintained at a low temperature (e.g. 50-100 ^{o}C). The temperature-programmable oven then gradually heats up to a higher temperature (e.g. 200-300 ^{o}C) at a specified ramp rate (e.g. 1-40 ^{o}C/min). The choice of parameters depends on the nature of the components being analyzed and are all easily varied.

Once in the column, the molecules then traverse the column in the presence of the flow of an inert carrier gas, referred to as the "mobile phase." Helium is the most common mobile phase used for GC analysis, but N_2 and H_2 are also used. The rate at which a molecule moves through the column is dependent on both the inherent volatility of the molecule itself, as well as the dynamic adsorptive interactions between the analyte and the stationary phase. The time it takes a molecule to exit the opposite end of the column is referred to as the *elution time*. In the case of a non-polar stationary phase, such as PDMS mentioned before, non-polar components tend to interact with the stationary phase more strongly than more polar components and thus elute more slowly. At the same time, heavier components tend to elute more slowly than lighter components. Finally, if two components have similar structures and properties, they may have identical or near-identical elution times and thus quantitative separation may prove challenging.

Once a component elutes from the column it is then passed through a high-temperature transfer line and into the ionization chamber of the mass spectrometer. The ionization chamber consists of a filament which generates high energy electrons that ionize and fragment analyte molecules eluted from the chromatograph. The fragmented ions are then passed through a quadrupole mass analyzer which separates ions based on their mass-to-charge (m/z) ratio. The separated fragments are then passed to a detector which then records the intensities of the fragments. A computer then generates a mass spectrum which shows the relative intensities of all mass fragments detected as a function of time. In GCMS, the total ion current (TIC) at each time point may be plotted as a function of time to generate

a mass chromatogram. At each point in a mass chromatogram a measurement of the TIC may be made, and the concentrations of each component can be quantified by integrating the peak area intensities. Figure 35 shows the mass chromatogram of acetovanillone and its corresponding mass spectrum.

Catalysis Analysis: Quantitative GCMS

Because the ratio of the detector response to the analyte concentration is not unity, calibration curves must be generated for each molecular component to be quantified. The protocol used for analysis begins at 50 °C held for three minutes, followed by a temperature ramp of 20 °C min^{-1} to 250 °C which is then held for one minute. Each run is followed by a one-minute ramp to 300 °C to bake out and remove any residual components that may be left in the column before the next analysis. To protect the mass spectrometer, the solvent delay was set to three minutes to allow the bulk i-PrOH to elute prior to data collection.

Calibration curves were generated for the following molecules: acetophenone, 1-phenylethanol, and ethylbenzene (Figure 36), acetovanillone and 4-ethylguaiacol (Figure 37), and guaiacol, phenol, and cyclohexanol (Figure 38). The calibration curves were produced using five serial dilutions of a stock solution of analyte, and an internal standard (hexadecane) in each dilution vial. All quantities described below were weighed on a calibrated balance, including liquid analytes and liquid aliquots.

As an illustrative example, approximately 75 mg (0.3 mmol) hexadecane was added to a series of five vials. As previously mentioned the gravimetrically determined values were found to be 0.0733, 0.0770, 0.0746, 0.0759, and 0.0745 g, respectively. A separate stock solution containing of acetovanillone (83.09 mg, 0.500 mmol) in i-PrOH (1.56 g, 1.98 mL) was prepared. The amounts of the components of the stock solution and the hexadecane in the serial dilutions were chosen such that they closely resemble their respective concentrations in the catalysis reaction solutions being studied. Approximately 100, 200, 300, 400, and 500 µL aliquots were then pipetted into each pre-tared vial containing hexadecane. The weights of each aliquot were recorded, and the volume was calculated from the density of i-PrOH (0.786 g mL^{-1}). The values of each were 0.0788 g (0.100 mL), 0.161 g (0.205 mL), 0.245 g (0.312 mL), 327 g (0.416 mL), 399 g (0.507 mL), respectively. Each vial was then diluted to a total volume of approximately 2 mL with i-PrOH (determined gravimetrically to the nearest mg). The total volumes were calculated from the sum of the stock aliquot and i-PrOH dilution volumes, which were calculated to be 1.99, 2.01, 2.00, 1.99, and 1.99 mL, respectively. Then, 10 µL aliquots from each serial dilution were added to five separate autosampler vials and each was diluted to 1.5 mL with i-PrOH.

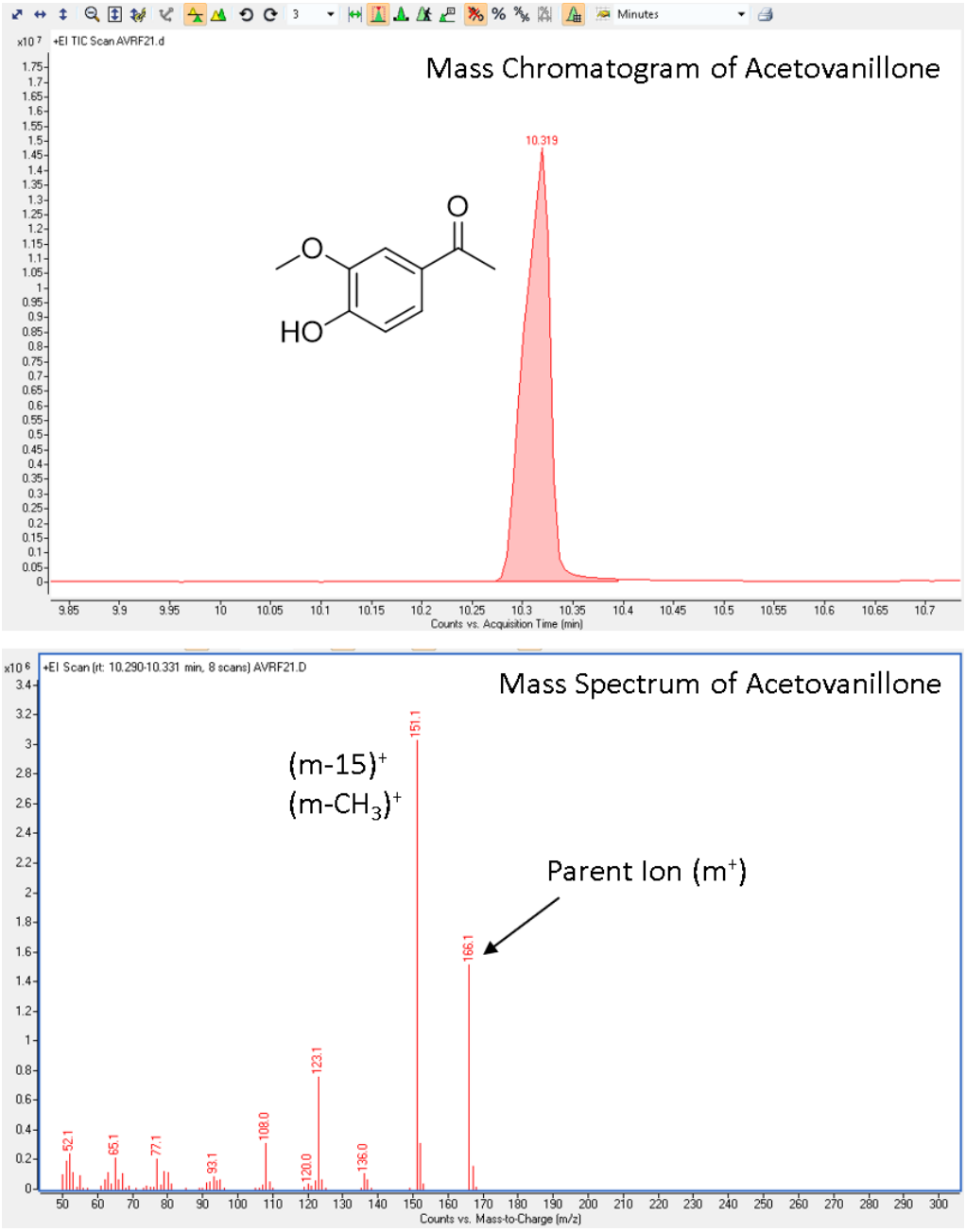


Figure 35. Example of the mass chromatogram (top) and mass spectrum (bottom) of acetovanillone.

Acetophenone System Response Factor Curves

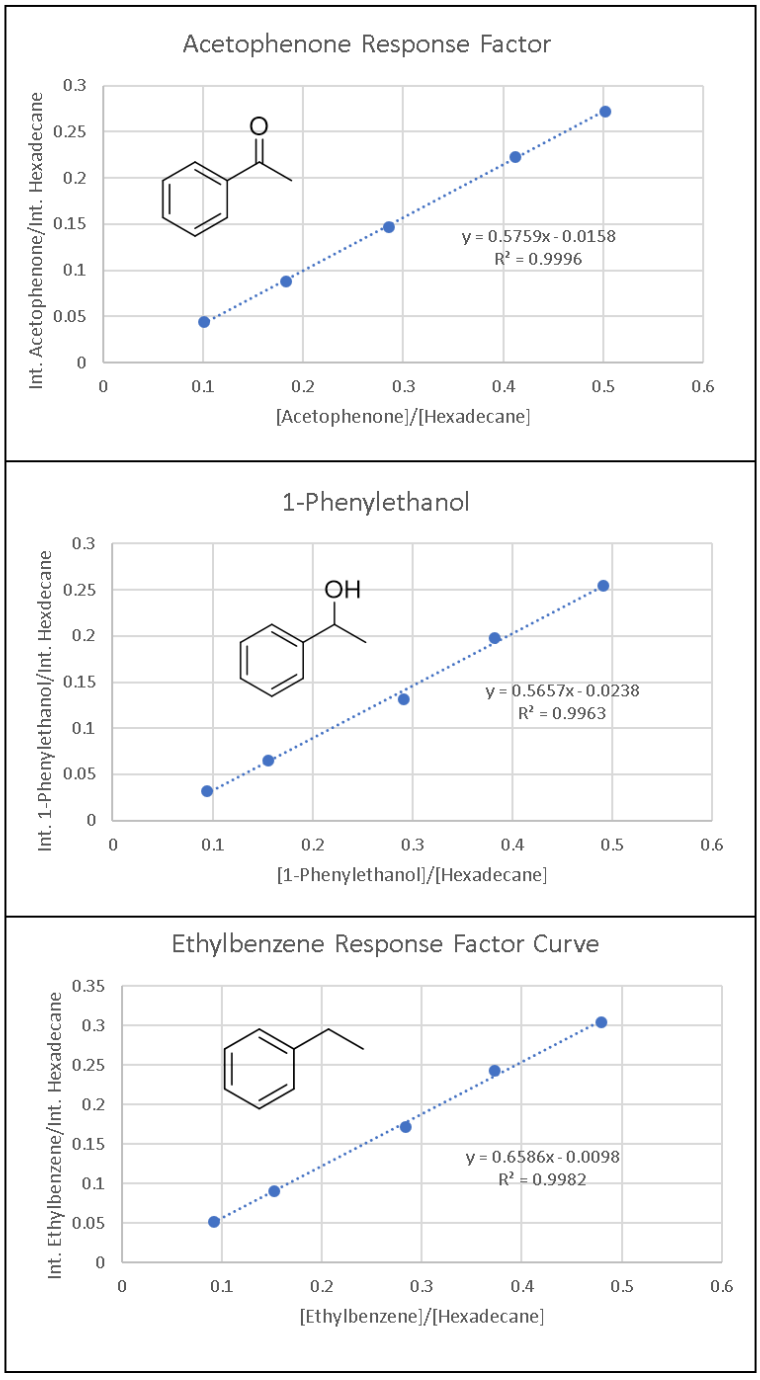


Figure 36. Response factor curves for acetophenone (top), 1-phenylethanol (middle), and ethylbenzene (bottom).

Acetovanillone System Response Factor Curves

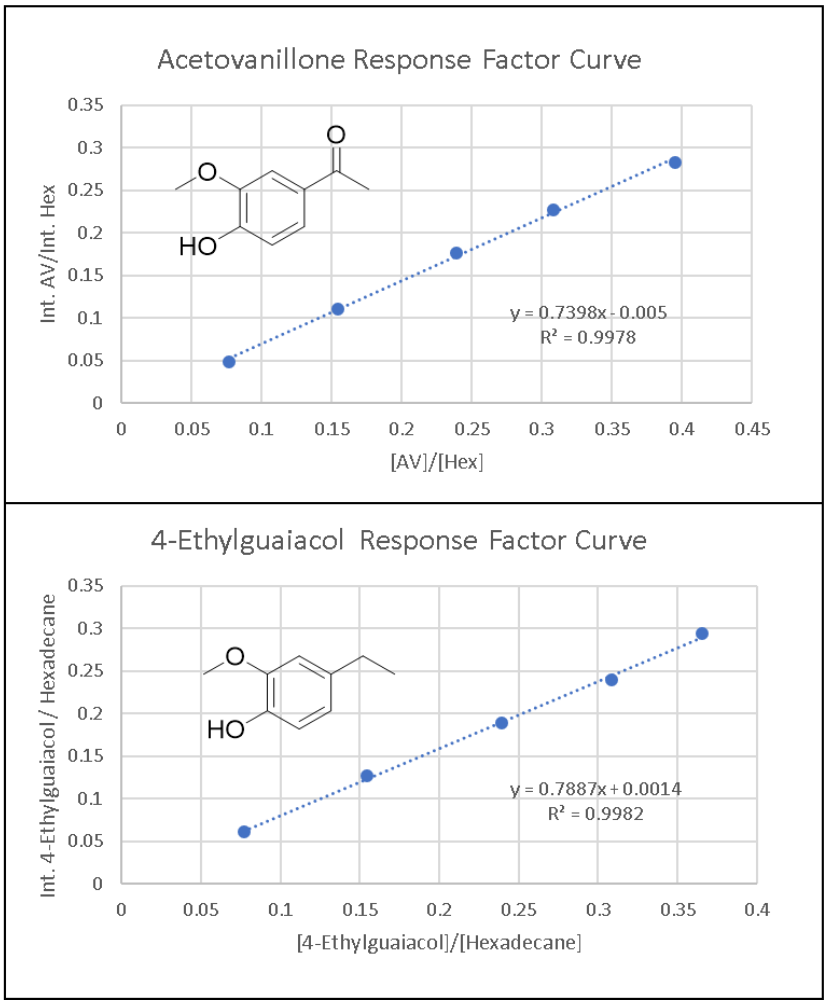


Figure 37. Response factor curves for acetovanillone (top) and 4-ethylguaiacol (bottom).

Guaiacol System Response Factor Curves

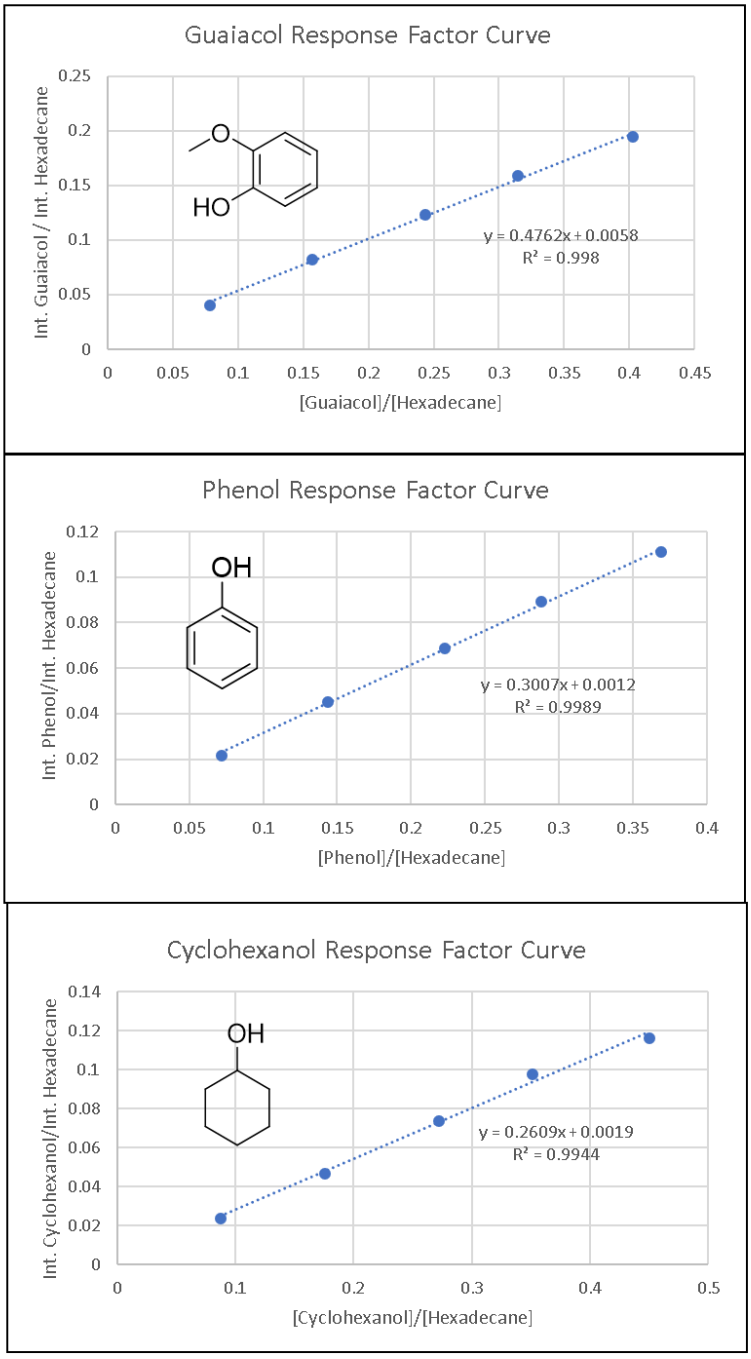


Figure 38. Response factor curves for guaiacol, phenol, and cyclohexanol.

The dilutions were then analyzed by GCMS and the peak area intensities for each component were integrated as previously described.

The peak area intensities of acetovanillone and hexadecane were then ratioed, as well as the measured concentrations of acetovanillone and hexadecane. The ratio of the measured intensities was then plotted against the ratio of the concentrations. The relative slope error for each component ranged from 1 - 4.5% and is believed to be one of the major sources of error in the analysis. For simplicity, the total error for all components was treated as 5%. Another source of error, as will be described below, comes from errors in peak integration. This was estimated to be approximately 3%. Thus, the total error was estimated to be approximately 6%. Table 2 shows the total error derived from the relative response factor error and the estimated peak area integration error.

It is important to note that the autosampler was a significant factor in obtaining acceptable calibration curves and the quantitation of the catalysis results in these studies. Additionally, to account for possible instrument drift that may affect calibrations over time, new calibration curves were generated after five months for acetovanillone and 4-ethylguaiacol. The calibration slope for acetovanillone was 0.740 initially, then 0.781 after five months (~5% difference), whereas 4-ethylguaiacol was initially 0.789 and 0.882 after five months (~9% difference). A significant portion of these differences is likely due to error associated with slope error and peak area integration as just mentioned. For this work, the response factor values 0.740 and 0.789 for acetovanillone and 4-ethylguaiacol, respectively, were used for catalysis quantification.

Calculation of Catalysis Parameters: % Conversion, % Selectivity, % Yield, and % Mass Balance

The catalytic efficiency of CoB catalysts for mediating CTH of acetophenone, acetovanillone, and guaiacol was investigated. To compare the relative activities of the CoB catalysts, three catalysis temperatures were studied: 300 °, 200 °C, and 165 °C. A large molar excess (approximately 50:1 H-donor to substrate) of either i-PrOH or EtOH was used as the solvent and hydrogen donor.

To illustrate how catalysis parameters were determined, the reaction of acetovanillone in i-PrOH in the presence of CoB(oxi) will be used as an illustrative example. To prepare the reaction solution, a stock solution of acetovanillone (0.830 g, 5.0 mmol) and hexadecane (0.759 g, 3.4 mmol) were dissolved in i-PrOH (15.7 g, 19.97 mL) was prepared to give final calculated concentrations of 0.250 M acetovanillone and 0.168 M hexadecane. Then, a stainless steel reactor prepared as previously described was charged with approximately 10 mg of catalyst followed by 2 mL of the stock solution and

placed in a heat bath at the desired temperature. After a set time the reactor was removed from the bath and quenched in water and allowed to cool to room temperature for several minutes. A 10 µL aliquot was then diluted in 1.5 mL of i-PrOH and analyzed by GCMS.

It should be noted that weighing small quantities of CoB_{red} on a scale in the glovebox proved challenging and unreliable. Thus, a weighing protocol was developed in which CoB_{red} was packed into approximately 1 cm into the tip of a Fisherbrand 9" disposable Pasteur pipet and then transferred into the stainless steel reactor. This transfer process is done a total of four times, which amounts to approximately 10 mg. To verify the accuracy of this procedure, CoB_{red} was transferred as just described into pre-weighed vial, removed from the glovebox, and weighed afterwards on a calibrated balance. This accuracy check was repeated three times and the average weight of CoB_{red} using this protocol was 10 $\pm$ 0.2 mg.

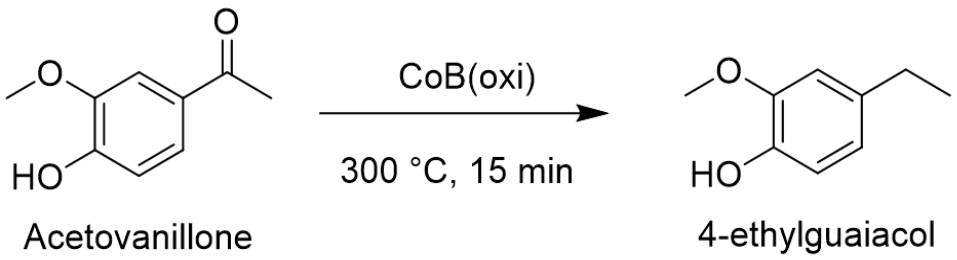
Figure 39 shows the chromatograms of the species present before and after catalysis. The species giving rise to each of the peaks were identified by comparing their mass spectra to NIST software database. The concentrations of each component were determined by the integrated peak area intensities. The integration ranges chosen to define the peak area integrations were chosen manually to integrate as much of the peak area as possible that corresponds to the given component in the chromatogram. In this case, acetovanillone was integrated in the range of retention times from approximately 10.3 to 10.6 minutes, while hexadecane was integrated from approximately 10.9 to 11.1 minutes.

Before catalysis, only acetovanillone and hexadecane are present. After reaction, a new peak with a retention time of approximately 8.9 min was observed and identified as 4-ethylguaiacol. The peak area intensity was measured by integrating from approximately 8.9 to 9.1 minutes. It is important to note that the peaks corresponding to 4-ethylguaiacol and acetovanillone exhibit a some peak tailing, which can introduce error in the final concentrations that are calculated from their respective peak areas. This was studied and is discussed below. First, the method for calculating component concentrations and catalysis parameters will be discussed.

The concentration of hexadecane is calculated from the weighed values of the hexadecane and i-PrOH stock solution. In this case, as mentioned above, 0.759 g (3.4 mmol) of hexadecane was dissolved in (19.97 mL) i-PrOH, giving a final concentration of 0.168 M hexadecane. The stock solution was then

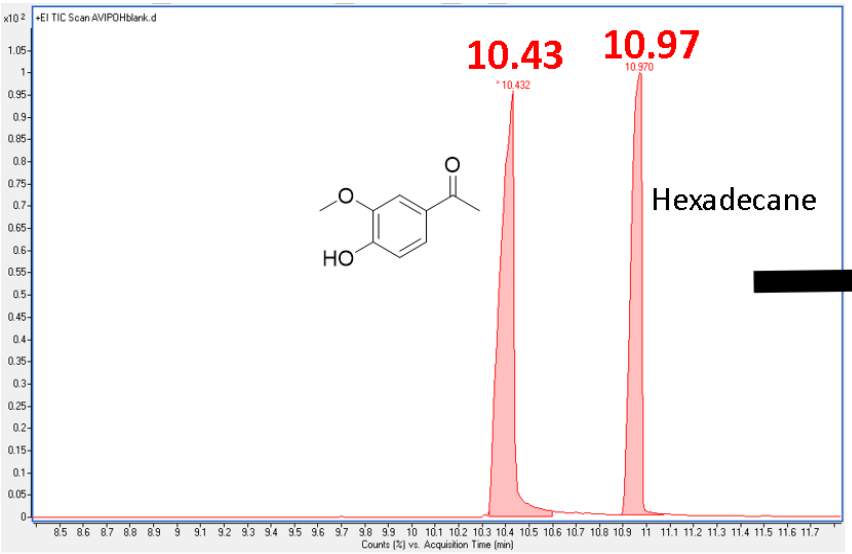
Table 2. Total errors estimated from the calculated relative response factor errors and the estimated peak area integration errors for all components.

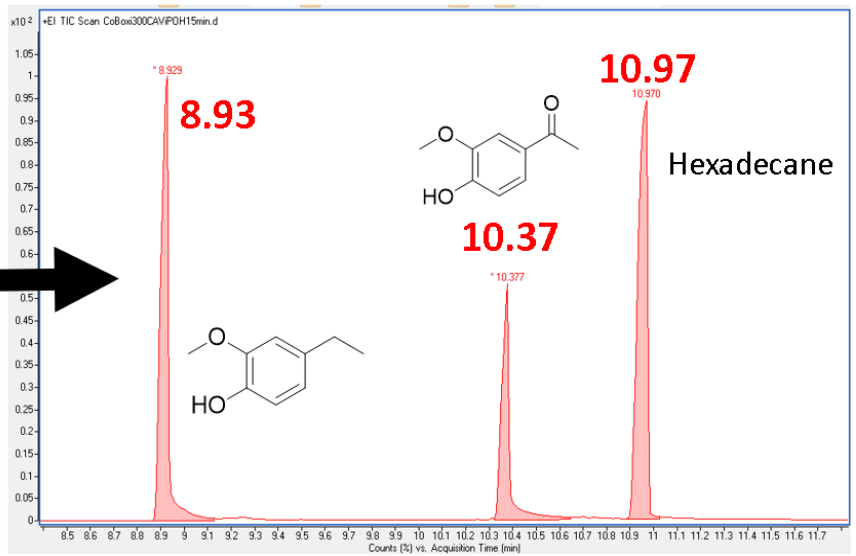
Component	Relative Response Factor Error (%)	Estimated Peak Area Integration Error (%)	Total Error (%)
Acetophenone	1.15	3	3.21
1-Phenylethanol	3.5	3	4.61
Ethylbenzene	2.45	3	3.87
Acetovanillone	2.72	3	4.05
4-Ethylguaiacol	2.42	3	3.85
Guaiacol	2.56	3	3.94
Phenol	1.92	3	3.56
Cyclohexanol	4.43	3	5.35



Acetovanillone

4-ethylguaiacol





Before Catalysis

After Catalysis

Figure 39. Illustration of chromatograms of acetovanillone before (left) and after (right) catalysis. The large values in red indicate the elution times.

analyzed by GCMS and the peak area intensities for acetovanillone (53006454.89) and hexadecane (43083238.66) were recorded. The response factor curves described above give the following equation:

$$\frac{[X]}{[IS]} = \frac{Int.(X)}{Int.(IS)} * RF \qquad \text{Equation 2.3}$$

where *[X]* is the analyte concentration, *[IS]* is the internal standard concentration, *Int.(X)* is the peak area intensity of the analyte, *Int.(IS)* is the peak area intensity of the internal standard, and *RF* is the response factor value for the given component. The intensities of the analyte and hexadecane, and the calculated hexadecane concentration were then used to calculate the concentration of acetovanillone using a rearrangement of equation 2.3:

$$[X] = \frac{Int.(X)*[IS]}{Int.(IS)*RF} \qquad \text{Equation 2.4}$$

Thus, for acetovanillone:

$$[Acetovanillone] = \frac{Int.(Acetovanillone)*[Hexadecane]}{Int.(Hexadecane)*RF_{Acetovanillone}} \qquad \text{Equation 2.5}$$

where *[Acetovanillone]* is the concentration of acetovanillone, *[Hexadecane]* is the concentration of hexadecane, *Int. (Acetovanillone)* is the peak area intensity of acetovanillone, *Int.(hexadecane)* is the intensity of hexadecane, and $RF_{Acetovanillone}$ is the response factor for acetovanillone, as previously determined. Thus, the concentration of acetovanillone of the stock solution is calculated as follows:

$$[Acetovanillone] = \frac{53006454.89*0.168M}{43083238.66*0.740} = 0.279 \pm 0.0167M \qquad \text{Equation 2.6}$$

Note that this value, and the calculated stock concentration (0.250M) differ by approximately 10%, which is outside the previously calculated error (6%). This may be due to errors that were not accounted for in the analysis, although initial concentrations calculated in this way were generally within the calculated error of 6%. To address this, all values for initial concentrations of substrate were derived from the values determined by GCMS from the as-prepared stock solutions, and all subsequent post-catalysis reactions derived from their respective stock solutions were compared to these initial substrate concentrations.

For catalysis, a stainless steel reactor was charged with 2 mL of the previously prepared stock solution and 10 mg of CoB_{oxi} and subjected to the previously mentioned conditions (300 °C for 15 minutes), quenched, and analyzed by GCMS as described above. Using the peak area integration protocol previously described, the peak areas for 4-ethylguaiacol, acetovanillone, and hexadecane were

determined to be 39391593.65, 17244664.23, and 34061262.86, respectively. The final concentrations of acetovanillone and 4-ethylguaiacol were then calculated as above:

$$[Acetovanillone] = \frac{17244664.23 * 0.168M}{39391593.65 * 0.740} = 0.099 \pm 0.0059M \quad \text{Equation 2.7}$$

and,

$$[4 - Ethylguaiacol] = \frac{34061262.86 * 0.168M}{39391593.65 * 0.789} = 0.184 \pm 0.011M \quad \text{Equation 2.8}$$

Thus, the final concentrations for acetovanillone and 4-ethylguaiacol were determined to be 0.099M and 0.184M, respectively. Then, the % conversion, % selectivity, % yield, and % mass balance were each calculated. The % conversion here is defined as the ratio of the final to the initial concentrations of acetovanillone:

$$\%\ Conversion\ (Acetovanillone) = (1 - \frac{[Acetovanillone]_{Final}}{[Acetovanillone]_{Initial}}) * 100 \quad \text{Equation 2.9}$$

thus, from the initial and final concentrations of acetovanillone determined before,

$$\%\ Conversion\ (Acetovanillone) = (1 - \frac{0.099M}{0.279M}) * 100 = 65 \pm 4\% \quad \text{Equation 2.10}$$

The % selectivity is defined here as the ratio of the final concentration of product (in this case, 4-ethylguaiacol) to the difference between the initial and final concentrations of substrate (in this case, acetovanillone), and is shown in the following equation:

$$\%\ Selectivity\ (4 - Ethylguaiacol) = \frac{[4 - Ethylguaiacol]}{[Acetovanillone]_{Initial} - [Acetovanillone]_{Final}} * 100 \quad \text{Equation 2.11}$$

thus,

$$\%\ Selectivity\ (4 - Ethylguaiacol) = \frac{0.184M}{0.279M - 0.0994M} * 100 = 102 \pm 6\% \quad \text{Equation 2.12}$$

Therefore, the selectivity for 4-ethylguaiacol is 102 ± 6%. This means that within experimental error, all of the starting acetovanillone that was converted in the reaction is converted to 4-ethylguaiacol.

The % yield here is simply calculated by multiplying the % conversion of acetovanillone with the % selectivity of 4-ethylguaiacol and dividing by 100. Hence,

$$\%\ Yield\ (4 - ethylguaiacol) = (\%\ Conversion * \%Selectivity)/100 \quad \text{Equation 2.13}$$

thus,

$$\%\ Yield\ (4-ethylguaiacol) = (66\% * 102\%)/100 = 67\ \pm\ 4\% \qquad \text{Equation 2.14}$$

Thus the % yield for 4-ethylguaiacol is 67 $\pm$ 4%, which is within experimental error for conversion of acetovanillone.

Finally, the % mass balance is calculated by dividing the sum of the concentrations of post-reaction components by the initial concentration of substrate, shown by the following equation:

$$\%\ Mass\ Balance = \frac{Acetovanillone_{Final}+4-Ethylguaiacol}{Acetovanillone_{Initial}} * 100 \qquad \text{Equation 2.15}$$

Therefore,

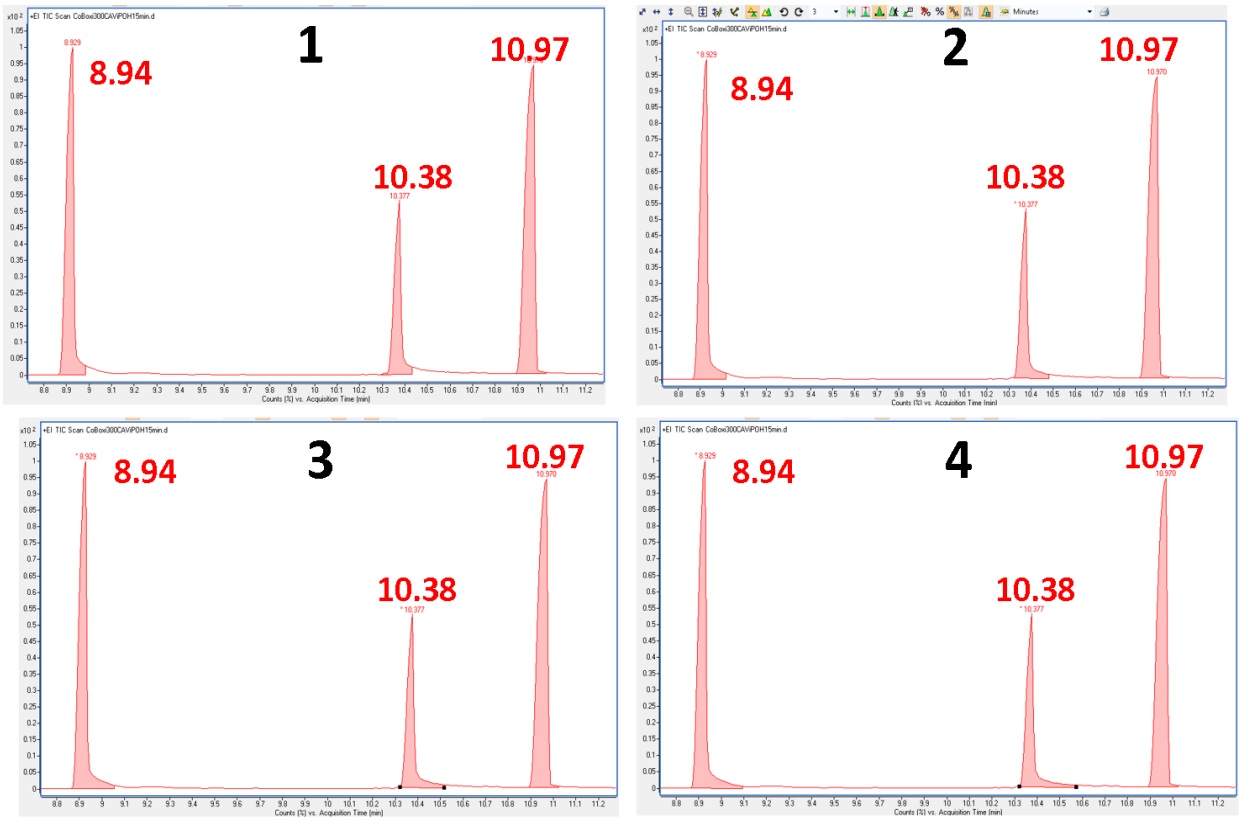
$$\%\ Mass\ Balance = \frac{0.0994M+0.184M}{0.279M} * 100 = 102\ \pm\ 6\% \qquad \text{Equation 2.16}$$

Thus, the total mass balance is 102 ± 6%.

It is important to note that the mass balance calculation used in this work is only based on the species that have been quantified. Sometimes disparities exist where the total mass balance is lower than 100%. In some cases, the disparity is within error of the analysis, whereas in other cases, it is not. This can sometimes be explained by the presence of products observed in the chromatogram that were not quantified. In other cases, no species are observed in the chromatogram that account for the disparity in the mass balance. This could either be due to the possibility that the unaccounted-for species are highly volatile gaseous products such as, for example, methane, propane, or carbon dioxide that escape the post-reaction mother liquors before GCMS analysis, or the species formed are non-volatile oligomeric species that cannot pass through the GC column for GCMS analysis, or a combination of the two possibilities.

As previously mentioned, the choice of the peak area integration range when integrating may introduce error into the analysis. To test this, four sets of integrations were taken of acetovanillone and 4-ethylguaiacol in which the final retention time of the integration range was varied within the tailing region. The integration of hexadecane was not varied. Figure 40 shows four chromatograms labelled 1-4.

The integration values were then averaged for acetovanillone and 4-ethylguaiacol and their respective relative percentage errors, which were calculated to be 3.02% and 2.04%, respectively. Therefore, the percentage error contribution due to integration error is expected to be approximately 3% for all calculations. The error described here (~3%) and the error associated with the response factor



Conversion	% Selectivity 4-EG	% Yield 4-EG	Mass Balance
66.85±1.00	97.79±3.45	65.34±1.33	98.50±2.33

Figure 40. Illustration of the error associated with peak area integrations. The large values in red indicate the elution times

calibration curves (~5%) are thus expected to be the dominating sources of error in the analysis described here, thus the total error is estimated to be approximately 6%.

Catalyst Recycling

To test the stability of CoB_{red} over the course of multiple catalytic reactions, acetophenone was heated in the presence of CoB_{red} and i-PrOH at 165 °C for 15 minutes over 10 successive runs. As will be described in Chapter 4, this temperature was chosen because CoB_{red} shows complete conversion of acetophenone at higher temperatures (>200 °C). Since complete conversion is achieved at this temperature, information on any changes in the reaction kinetics are lost. Thus, the lower temperature 165°C was chosen for these tests, as only moderate conversion was observed, which allows observations of any significant change in the rates of conversion over successive runs.

A stock solution of acetophenone (0.252 M, 5.05 mmol) in i-PrOH (19.97 mL) was prepared. A stainless steel reactor was prepared as before and taken into an inert air glovebox. The reactor was then charged with approximately 10 mg of CoB_{red} and 2 mL of the stock solution using the same calibrated volumetric pipette (100-1000 µL) as before. To prevent undesirable loss of catalyst during cap removal after each reaction, the side of the reactor containing catalyst was marked. The reactor was then capped, hand-tightened, then removed from the box and the cap was further secured with a wrench. The reactor was then heated to 165 °C for 15 minutes in the salt bath as previously described. After 15 minutes, the reactor was removed from the heat bath and cooled in a large volume of water for several minutes.

To prevent ambient air from entering the reactor, the reactor was secured to a benchtop vice and the cap was loosened, but not completely removed to ensure that ambient air could not enter the reactor, but the cap could still be removed by hand. The cap was loosened only enough to prevent undesirable evaporation of the mother liquor while under the low pressure conditions of the glovebox vacuum antechamber. The reactor was then quickly taken into the inert atmosphere glovebox. The catalyst was then held in place within the reactor using a strong magnet and the mother liquor was carefully decanted into a small vial. To wash away the residue of reaction components from the previous run, approximately 2 mL of i-PrOH was added to the reactor, the catalyst was secured to the reactor

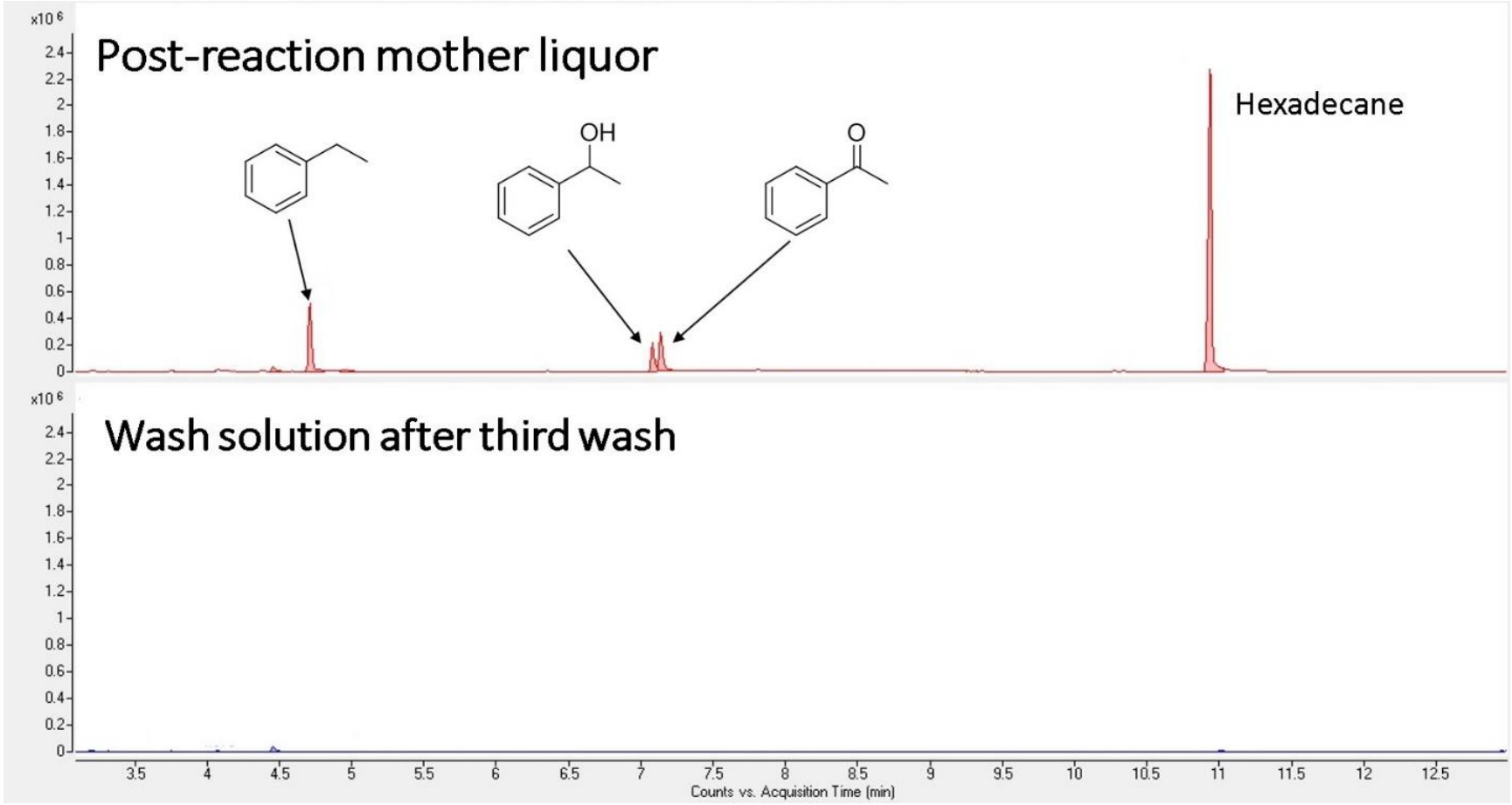


Figure 41. Chromatogram of a post-reaction mother liquor (top) and the isopropanol wash solution after the third wash (bottom). Vertical scales are $x10^6$.

with a strong magnet as before, and the i-PrOH wash solution was decanted into a waste container. This process was repeated two more times for a total of three washings. The decanted mother liquor and i-PrOH washings were carefully inspected for the presence of black powder to ensure no undesired loss of catalyst occurred.

Residual Teflon tape was then removed from the threading, and the hex nipple was then re-taped. The reactor was then charged with approximately 2 mL of acetophenone stock solution, the reactor was then capped and hand-tightened, removed from the box, and tightened with a wrench as before. The reactor was then heated to 165 °C for 15 minutes. This process was repeated for a total of 10 runs. Each mother liquor was collected in a small vial and 10 µL aliquots were taken of each for GCMS analysis. To ensure that all residual components were successfully removed between each reaction, a 10 µL aliquot of the i-PrOH wash solution after the third wash was taken and analyzed by GCMS.

Catalyst Activation by Pretreatment with i-PrOH

Studies were conducted in which the activity of CoB_{oxi} and CoB_{red} were compared after pretreatment with neat i-PrOH at 250 °C for 1 hour. As an illustrative example, a stainless steel reactor was prepared as described previously and charged with 10 mg of either CoB_{oxi} and CoB_{red} and approximately 2 mL of i-PrOH. It should be noted that for CoB_{oxi}, reactors were prepared and charged with CoB_{oxi} outside of the inert atmosphere glovebox. The reactor was then taken into the glovebox and charged with i-PrOH.

Once charged with catalyst and i-PrOH, the reactor was then capped and hand-sealed, removed from the box, secured to a vice, and further sealed with a wrench. The reactor was then heated to 250 °C for 1 hour in a higher temperature salt bath as described before. Afterwards, the reactor was removed from the heat bath and quenched in room temperature water. The reactor was then loosened with a wrench such that it could be removed by hand but was not completely opened. The reactor was then taken into the glovebox, opened, and then solution was decanted from the reactor while the catalyst was held in place with a strong magnet. The catalyst was then washed once with neat i-PrOH and decanted as before. The reactor was then charged with 2 mL of a stock solution containing i-PrOH, hexadecane, and substrate, as described before. The reactor was then heated to 165 °C in the heat bath for 15 minutes. Afterwards, the reactor was removed from the heat bath, quenched in water, opened with a wrench, and the mother liquor was analyzed *via* GCMS.

Chapter Summary

This chapter describes the protocols used to synthesize, characterize, and test the catalytic activity of CoB_{oxi} and CoB_{red}. These catalysts were synthesized using facile reduction of Co^{2+} in aqueous solution with $NaBH_4$. This synthesis protocol requires inexpensive, readily available precursors, is done in aqueous media, and was easily carried out on a 10-gram scale, indicating that CoB catalysts can be readily scaled up. Preliminary characterization of CoB_{oxi} and CoB_{red} shows that they are highly responsive to strong magnets and can be easily separated from the synthesis solution. Elemental analysis by ICP-OES indicates that the atomic formulas of CoB_{oxi} and CoB_{red} are $Co_{1.7}BO$ and $Co_{1.7}B$, respectively.

All catalytic reactions were carried out in stainless steel reaction vessels whose components are inexpensive, commercially available, are easy to prepare and clean, and do not corrode under the reaction conditions. Reactions were heated in a low-temperature eutectic salt bath whose components consist of inexpensive salts KNO_3, $NaNO_3$, and $NaNO_2$. The salt mixture is thermally stable and can be contained in a stainless steel beaker which does not corrode over time. The heat bath also does not corrode the stainless steel reactors. The following chapter presents the results and discussion of the catalytic performance.

Chapter 4 – Results and Discussion – Spectroscopic and Catalytic Characterization of CoB Catalysts

Characterization of As-synthesized CoB_{oxi} and CoB_{red}

Figure 42 shows the PXRD spectra of as-synthesized CoB_{oxi} and CoB_{red}. No evidence of Bragg diffraction is observed for CoB_{red}. Diffraction data CoB_{oxi} reveals possible evidence for some crystalline domains. An unidentified broad feature was also observed at $2\theta = 48°$. ICP-OES analysis, as discussed in the previous chapter, shows that the elemental composition of CoB_{oxi} and CoB_{red} is $Co_{1.7}BO_{1.7}$ and $Co_{1.7}B$, respectively. Exposure to air results in a highly exothermic, pyrophoric reaction of CoB_{red} to form CoB_{oxi}. Thus, the oxygen content is likely due to formation of cobalt and boron oxides on the surface of the catalyst.

Figure 43 shows the TEM micrographs of as-synthesized CoB_{oxi} and CoB_{red}. The micrographs indicate that both catalysts are amorphous and consist of particles of various sizes coated in a 2-3 nm layer of amorphous material. Though PXRD revealed some evidence for diffraction patterns in CoB_{oxi}, crystalline domains were not observed in the TEM. Figure 44 and Figure 45 show the elemental EDX maps for Co, O, and B for as-synthesized CoB_{oxi} and CoB_{red}, respectively. In both cases cobalt and boron appear uniformly distributed throughout the material, whereas oxygen also appears throughout the entire particle, but more oxygen is observed on the outer surface layer of each CoB particle. As just mentioned in the case of the ICP-OES data, the oxygen is likely present in the form of cobalt oxide or boron oxide materials, or a combination of both. Although ICP-OES analysis indicated that very little oxygen is present in CoB_{red}, some evidence for the presence of oxygen layers is present in the EDX images. This may be due to brief (~60 second) oxygen exposure while loading the sample into the TEM instrument.

Post-Catalysis Spectroscopic Characterization

CoB_{oxi} and CoB_{red} were also characterized with PXRD and TEM-EDX after catalytic runs using acetophenone as the substrate at 165 °C for 15 min. Figure 46 shows the PXRD spectra of CoB_{oxi} and CoB_{red} after reaction with acetophenone. For CoB_{red}, no significant differences were observed between the post-reaction diffractograms as compared to the as-synthesized diffractograms shown previously, whereas CoB_{oxi} shows evidence for some crystalline cobalt domains. Figure 47 shows the TEM micrograph of CoB_{oxi} after reaction. As described earlier, care was taken to prevent air exposure of the TEM samples but brief exposure was unavoidable and thus surface oxidation cannot be ruled out. After reaction, CoB_{oxi} showed evidence for the formation of crystalline domains with 2.07 Å lattice spacing which likely corresponds to a Co phase.[87]

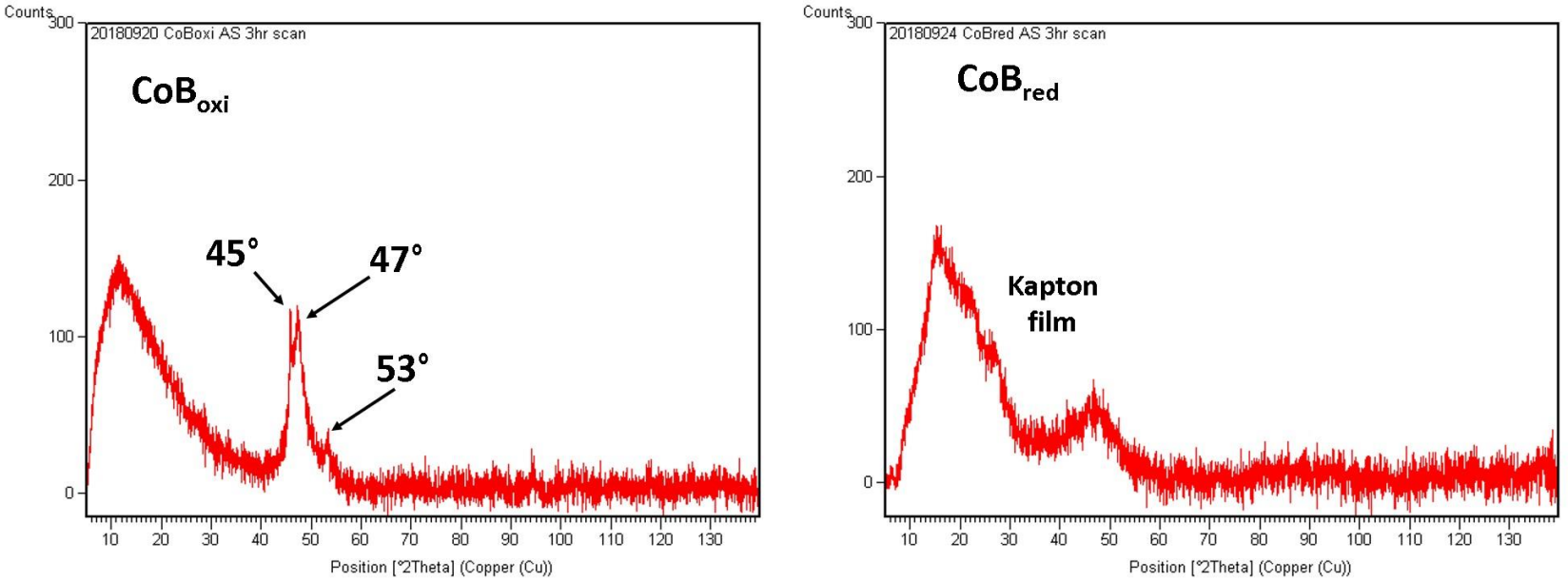


Figure 42. PXRD spectra of as-synthesized CoB_{oxi} (left) and CoB_{red} (right).

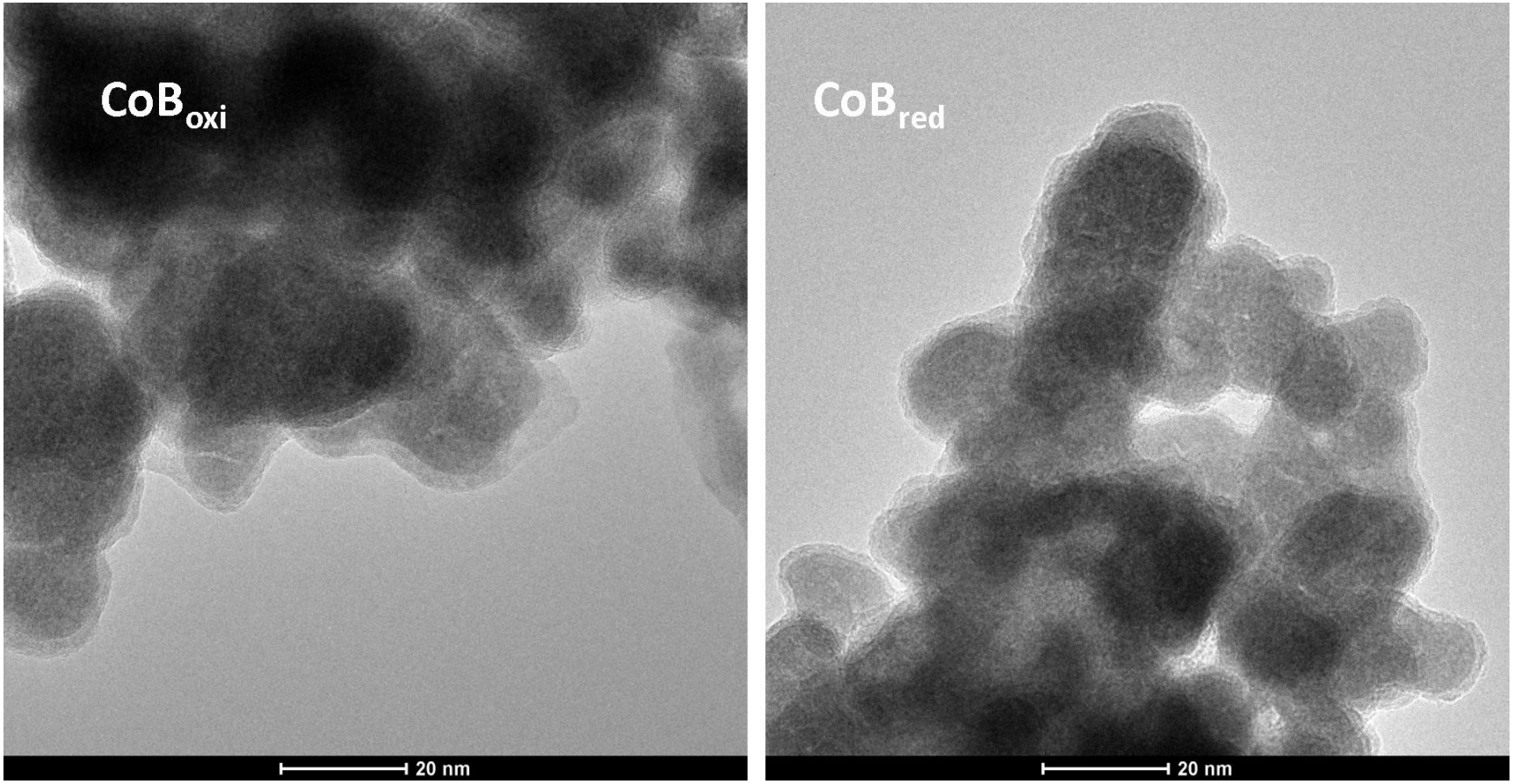


Figure 43. TEM Micrographs of CoB_{oxi} (left) and CoB_{red} (right).

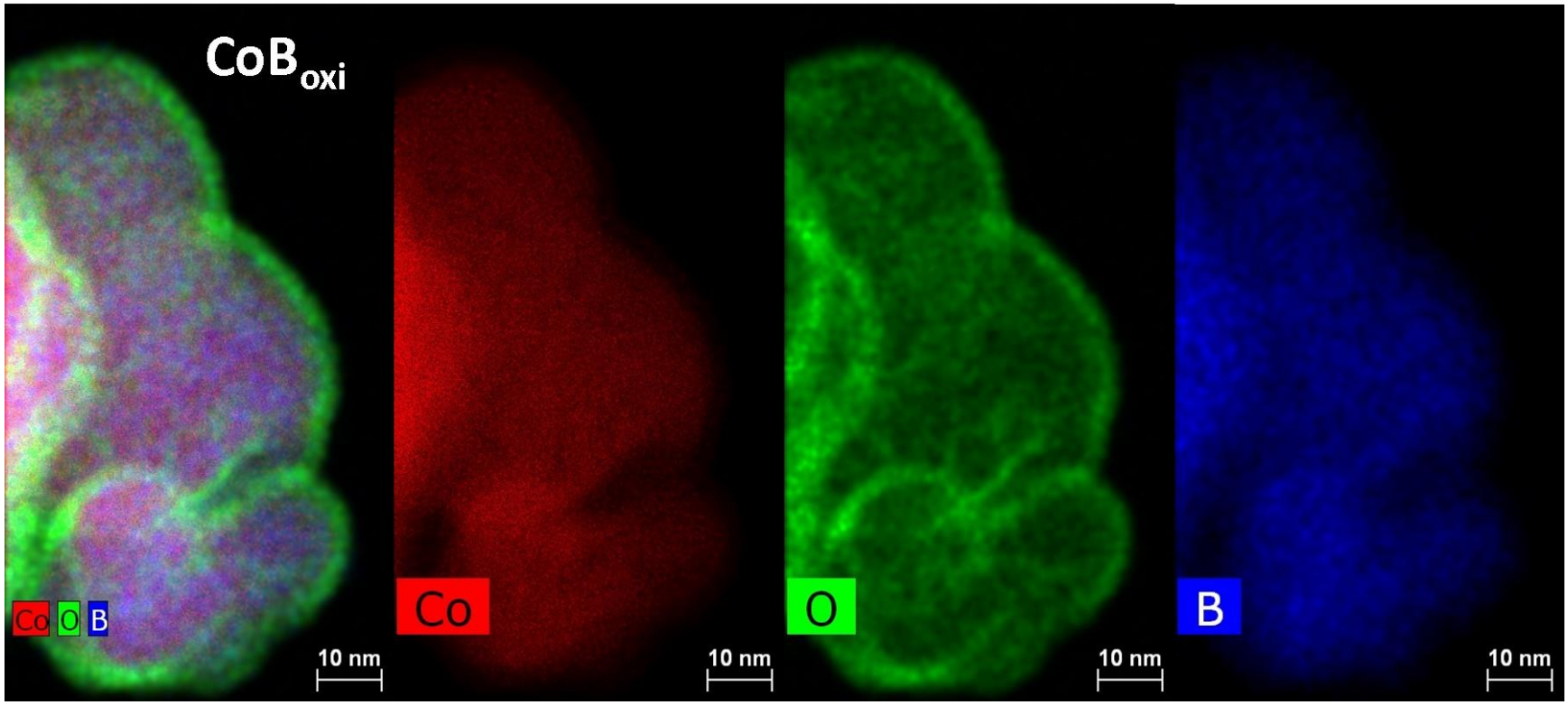


Figure 44. EDX maps of as-synthesized CoB_{oxi} showing Co (red), O (green), B (blue), and all three elemental maps overlaid.

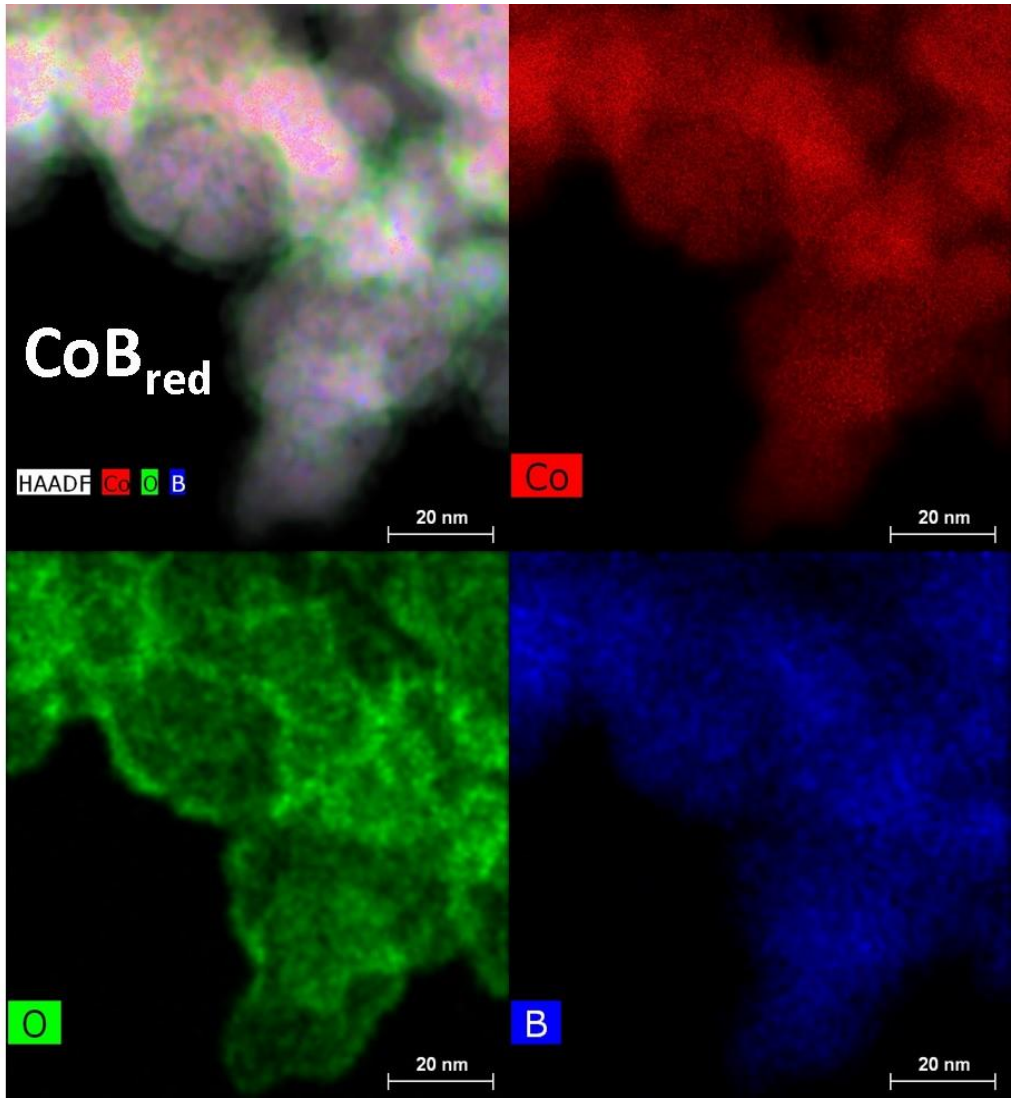


Figure 45. EDX maps of as-synthesized CoB_{red} showing Co (red), O (green), B (blue), and all three elemental maps overlaid.

Figure 48 shows the EDX maps for the elements present in CoB_{oxi} after reaction. Cobalt and boron appear uniformly distributed with a distinct layer of oxygen on the surface.

Figure 49 shows the TEM micrograph of CoB_{red} after 10 recycling runs with acetophenone at 165 °C for 15 minutes each. After recycling, the appearance of crystalline domains in the material is evident with lattice spacings of 1.98 and 2.45 Å. By comparison with literature reports, 1.98 Å is consistent with the Co phases and 2.45 Å is consistent with the Co_3O_4 phases.[88-90] Figure 50 shows the EDX maps for the elements present in CoB_{red} after 10 recycling runs. Co and B appear uniformly distributed within the material, whereas oxygen appears concentration on the surface of particles, as before.

Catalysis: Possible Reaction Pathways for Reduction of Acetophenone, Acetovanillone, and Guaiacol

Many generally-accepted reduction schemes for these substrates can be found in the literature.[91-93] Figure 51A-C shows reaction schemes that illustrate some of the possible reduction pathways for acetophenone, acetovanillone, and guaiacol, each of which are highlighted in blue

For acetophenone, one possible reduction pathway begins with the reversible hydrogenation of the carbonyl moiety to the corresponding alcohol, 1-phenylethanol (k_1), which can then proceed to ethylbenzene either by direct hydrodeoxygenation (k_2), or through an alternative pathway in which the hydroxyl moiety is first converted to styrene *via* dehydration (k_3) followed by hydrogenation of the vinyl moiety (k_4) to ethyl benzene. As will be mentioned later, reactions were done in which 1-phenylethanol and styrene were treated as substrates. In both cases, ethylbenzene was formed in nearly quantitative yield which suggests the dehydration route is the operative pathway. However, the direct hydrodeoxygenation pathway still cannot be ruled out.

Another alternative pathway to ethylbenzene involves single step direct transformation of the carbonyl moiety of acetophenone, directly to ethyl benzene (k_5). This pathway is frequently assumed not to be an important or significant operative pathway. Finally, formation of ethylcyclohexane (indicated in red) by hydrogenation of the aromatic ring of ethyl benzene (k_6) is also possible. However, this species was not observed in this work and therefore the hydrogenation of ethylbenzene is assumed to not occur. Reaction pathways k_2 through k_5 are assumed to be irreversible.

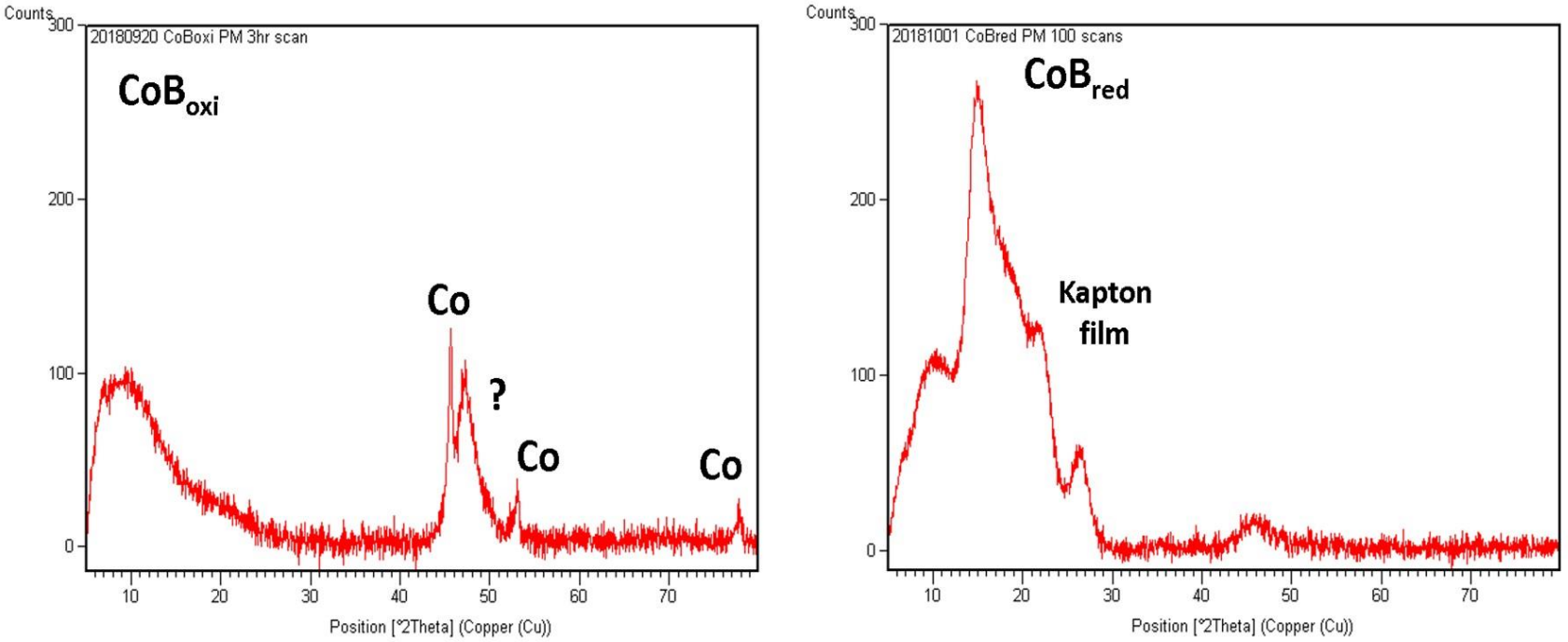


Figure 46. PXRD spectra CoB_{oxi} (left) and CoB_{red} (right) after reaction with acetophenone

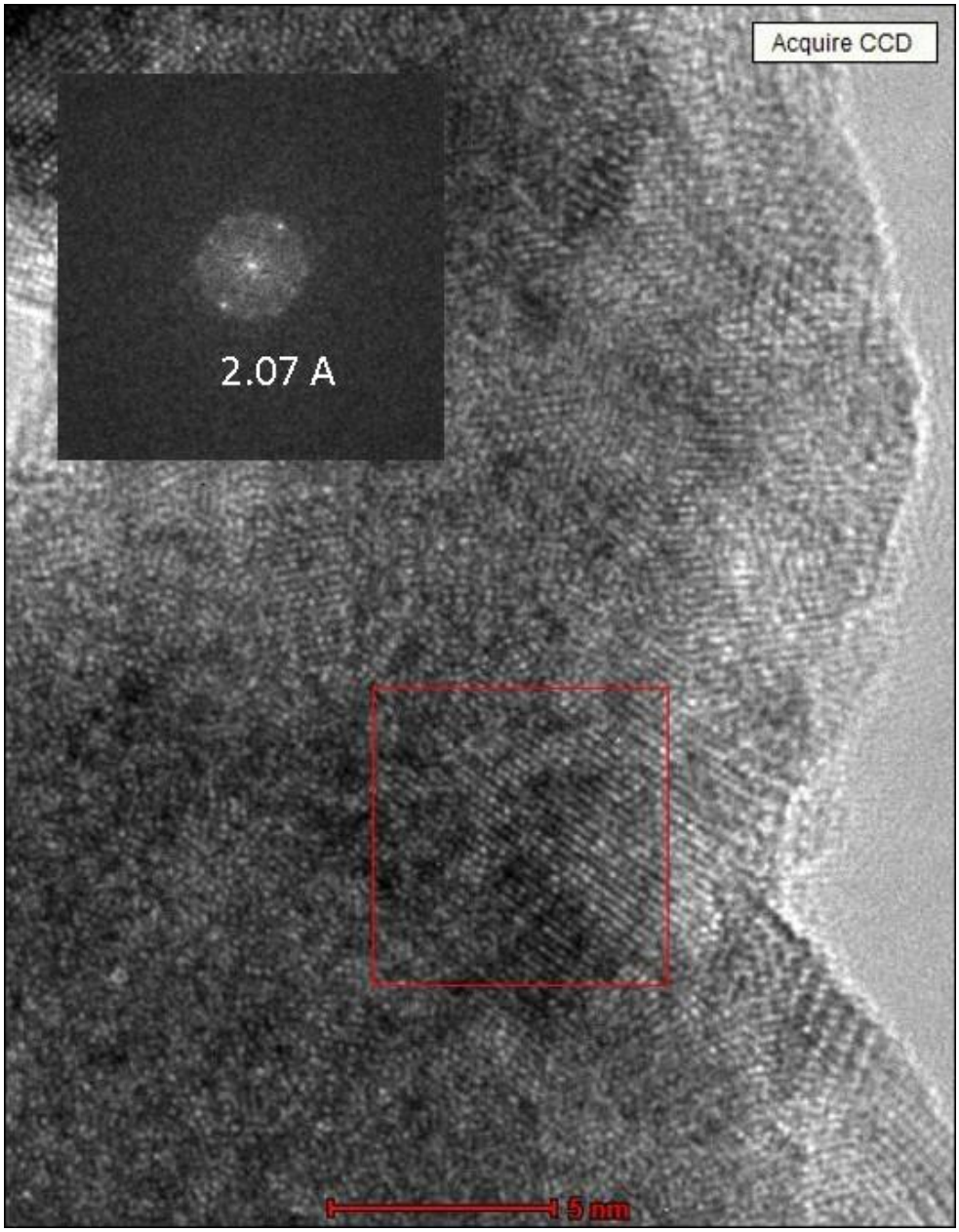


Figure 47. TEM micrograph of CoB_{oxi} after reaction with acetophenone at 165 °C for 15 minutes. The red box indicates the area in which the 2D fast Fourier transform FFT (top left) was taken.

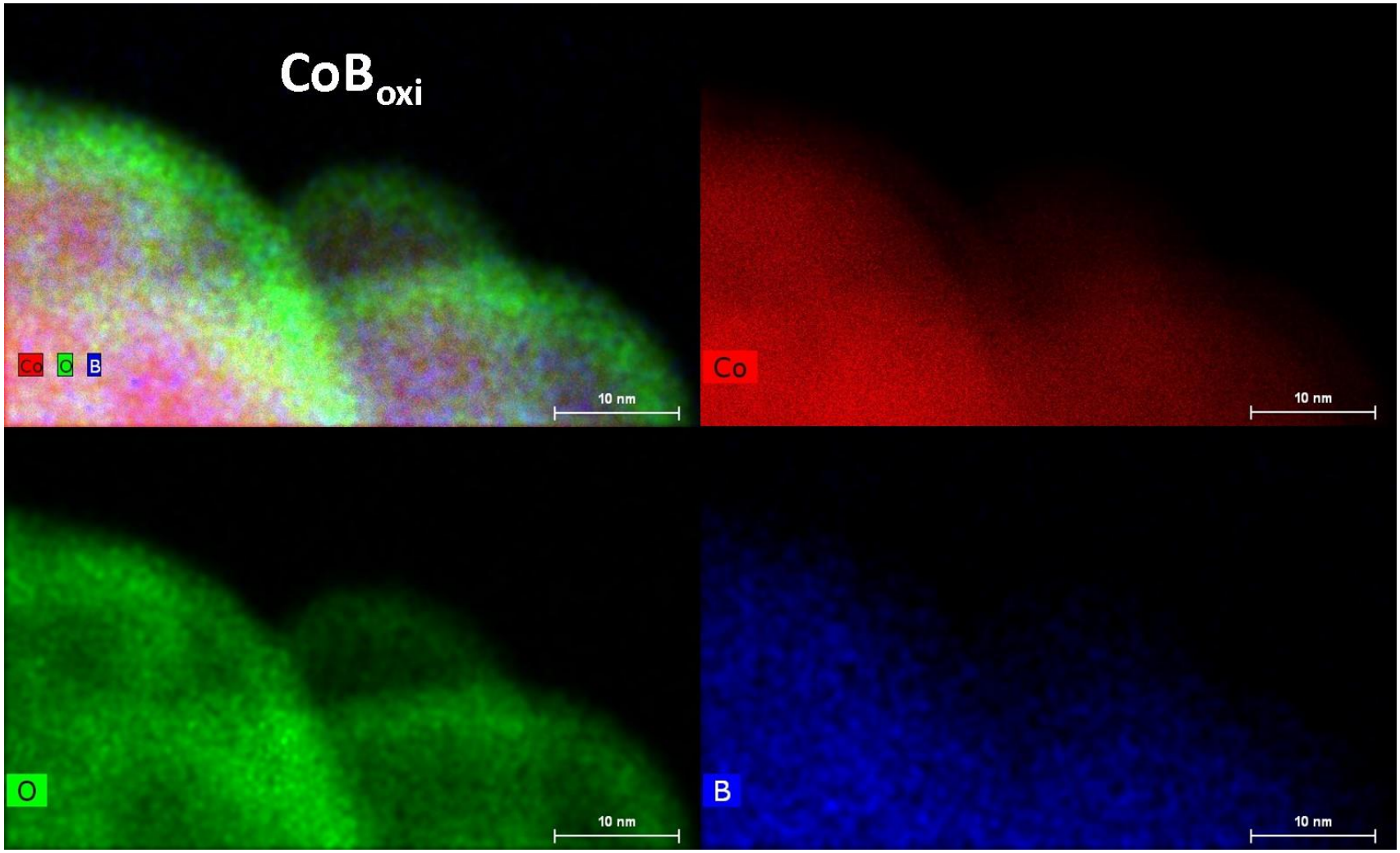


Figure 48. EDX maps of CoB_{oxi} after reaction with acetophenone at 165 °C for 15 minutes showing Co (red), O (green), B (blue), and all three elemental maps overlaid.

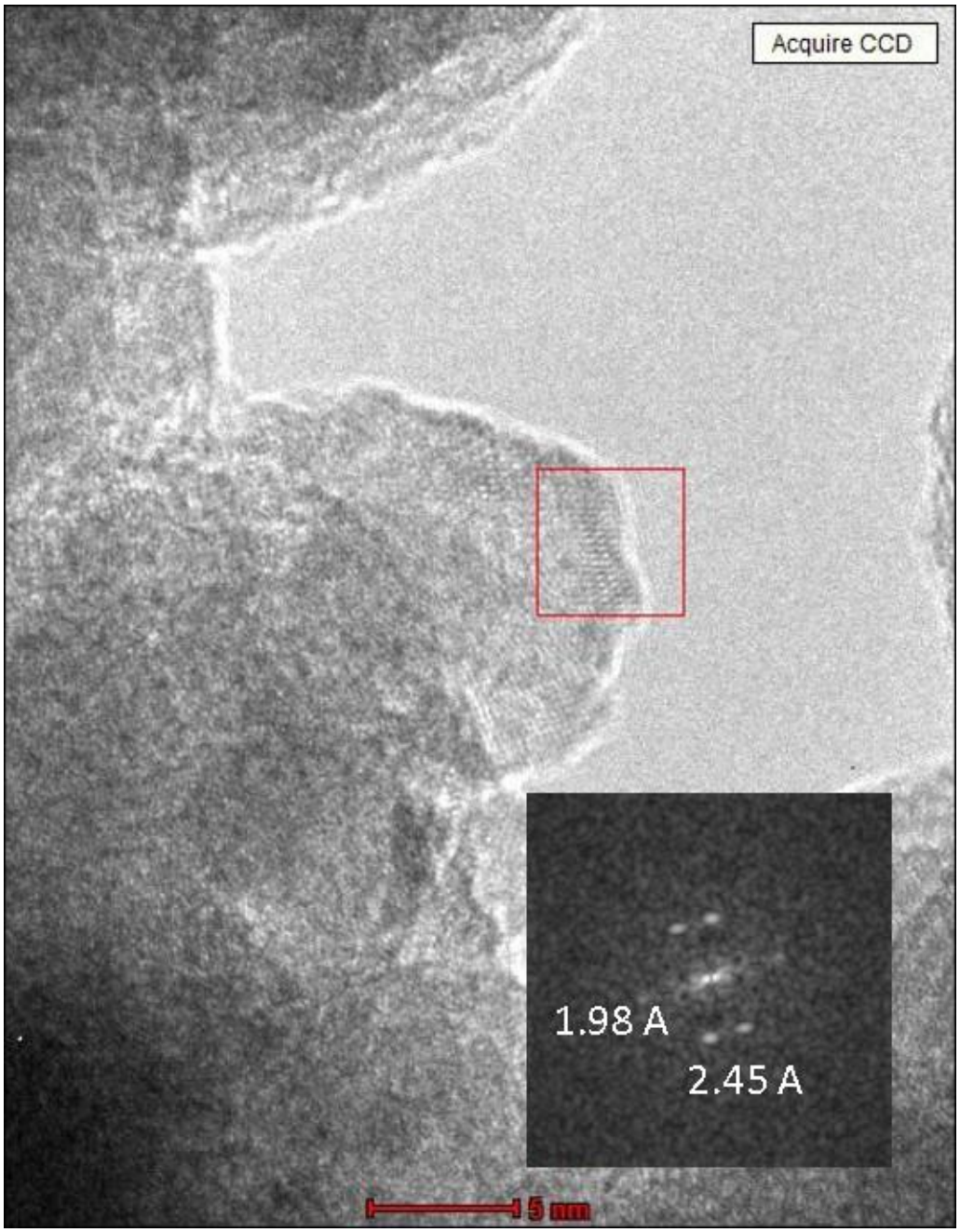


Figure 49. TEM micrograph of CoB_{red} after 10 recycling runs with acetophenone at 165 °C for 15 minutes. The red box indicates the area in which the 2D fast Fourier transform FFT (top left) was taken.

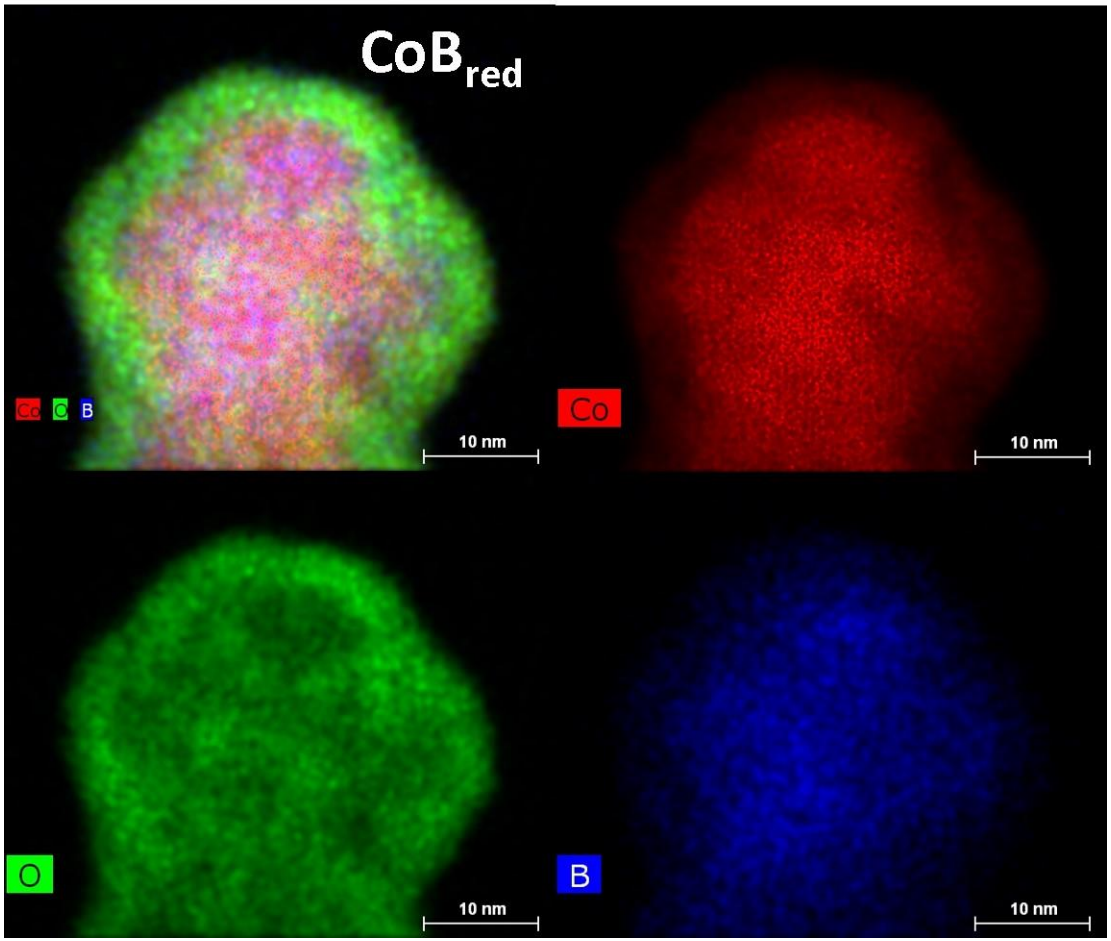


Figure 50. EDX maps of CoB_{red} after 10 reactions with acetophenone at 165 °C for 15 minutes showing all maps overlaid (top left), Co (red), O (green), and B (blue).

For acetovanillone, one possible reduction pathway involves hydrogenation of the carbonyl moiety to the corresponding alcohol derivative (k_1) followed either by hydrodeoxygenation to 4-ethylguaiacol (k_2), or dehydration of the alcohol to 4-vinylguaiacol (k_3). This may be followed by hydrogenation of the vinyl moiety to 4-ethylguaiacol (k_4). The alcohol intermediate (depicted in red) of acetovanillone was not observed in our catalysis studies. Another possible pathway involves formation of 4-ethylguaiacol through direct reduction and deoxygenation of the carbonyl moiety of acetovanillone (k_5), though this is again assumed to not be an operative pathway. Finally, 4-ethylguaiacol can be further reduced to 4-ethylphenol *via* demethoxylation and 4-ethylcyclohexanol *via* hydrogenation of the aromatic ring.

For guaiacol, one possible reduction pathway involves transformation of guaiacol to phenol *via* demethoxylation (k_1) followed by direct hydrogenation of phenol (k_2) to cyclohexanone, and subsequently to cyclohexanol (k_3). Alternatively, phenol can be directly hydrogenated to cyclohexanol (k_4). Finally, cyclohexanol can be converted to cyclohexene *via* dehydration (k_5), followed by subsequent hydrogenation to cyclohexane (k_6). Cyclohexane can also be formed by direct hydrodeoxygenation of cyclohexanol (k_7). However, neither cyclohexene nor cyclohexane were observed in analysis.

Catalysis: Comparison of Catalytic Performance of CoB_{oxi}, CoB_{red}, and Co powder

To compare the catalytic performance of CoB_{oxi} and CoB_{red}, the substrates acetophenone, acetovanillone, and guaiacol were heated in i-PrOH in the presence of each catalyst at 300, 200, and 165 °C for 15 minutes. 165 °C was chosen instead of 150 °C because no appreciable conversion at 150 °C was observed in the timeframe. CoB_{oxi} and CoB_{red} were also compared to commercially purchased Co powder (Fisher Scientific™, -22 mesh, 99.998%, used as received), and blanks in which no catalyst was added to the reaction solutions. The results for all catalysts, substrates, and conditions are summarized in Table 5.

Figure 52 illustrates how the data will be presented in their bar graph forms. Figure 52A shows a bar graph illustration of a pre-catalysis solution that consists of completely unconverted substrate. Figure 52B shows the % yields of the hypothetical products formed as a portion of the total percent of substrate that was converted. Figure 53 shows an example using the example of a post-catalysis reaction mixture of acetophenone at 300 °C for 15 minutes. The remaining substrate is depicted in gray, the 11 % yield of 1-phenylethanol is depicted in blue, the 79 % yield of ethylbenzene is depicted in green, and the % yield of unquantified or unobserved "other products" is depicted in red. For each set of

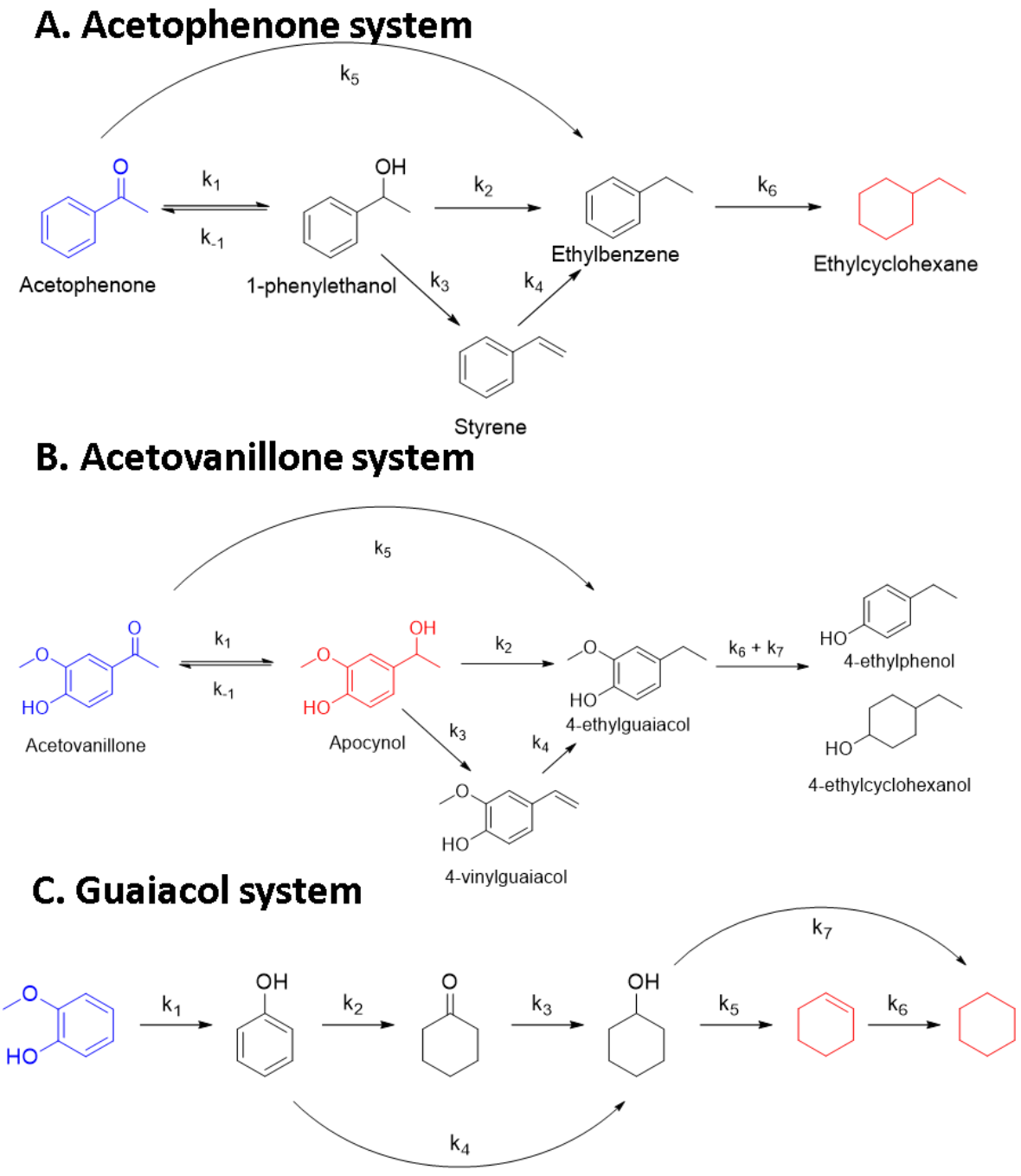


Figure 51. Reaction schemes for some possible reduction pathways of A) acetophenone, B) acetovanillone, C) guaiacol. Substrates are highlighted in blue. Species highlighted in red were not observed in GCMS analysis.

experiments, the data are presented both in the graphical form just described and with tables of the numerical data. Table 3 summarizes the experiments done in this work.

A series of blanks were also run using acetophenone as the test substrate at 200 °C for 15 min. (these blanks were not tested at 300 or 165 °C). The blanks tested were commercially purchased boron powder, boron oxide, cobalt powder, a physical mixture of cobalt powder and boron powder, a physical mixture of cobalt powder and boron oxide, sodium borate, cobalt chloride, and a blank in which no catalyst was added. These data are summarized in Figure 54 and the numerical values are given in Table 4.

Catalysis: Acetophenone

Figure 55 shows the catalysis results with acetophenone at 300, 200, and 165 °C. At 300 °C, high conversion is observed for all cases with high yield for ethyl benzene. For CoB_{oxi}, 88±5% substrate was converted with 12±1% yield 1-phenylethanol and 78±5% yield of ethylbenzene. For CoB_{red}, 100±6% conversion was observed with 86±5% yield for ethylbenzene, and 14±1% yield of other products. Cobalt powder showed 98±6% conversion with 62±4% yield for ethylbenzene, and 38±2% yield for other products. The blank also showed high conversion acetophenone. 96±6% conversion was observed with 90 ± 6% yield for ethylbenzene. Because the blank showed comparable reactivity as all three catalysts at 300 °C, these conditions are not indicative of catalytic activity.

However, at 200 °C, only CoB_{red} showed any significant activity, with 97±6% conversion and 27±2% yield for 1-phenylethanol and 70±4% yield for ethylbenzene. Finally, at 165 °C only CoB_{red} showed any significant activity with 85±5% conversion and 37±2% yield for 1-phenylethanol and 26±2% yield for ethyl benzene.

Catalysis: Acetovanillone

Figure 56 shows the catalysis results with acetovanillone at 300, 200, and 165 °C. At 300 °C, CoB_{oxi}, Co powder, and the blank showed moderate conversion (64±4, 63±4, and 49±3%, respectively) and high yield for 4-ethylguaiacol (66±4, 48±3, and 40±2%, respectively). CoB_{red} however showed complete conversion of substrate (100±6%) and 48±2% yield for 4-ethylguaiacol, and 52±3% yield for other products. Among the other products, 4-ethylphenol and 4-ethylcyclohexanol were observed in the chromatogram after 300 °C as minor products, but their presence alone does not necessarily account for the total amount of other products formed.

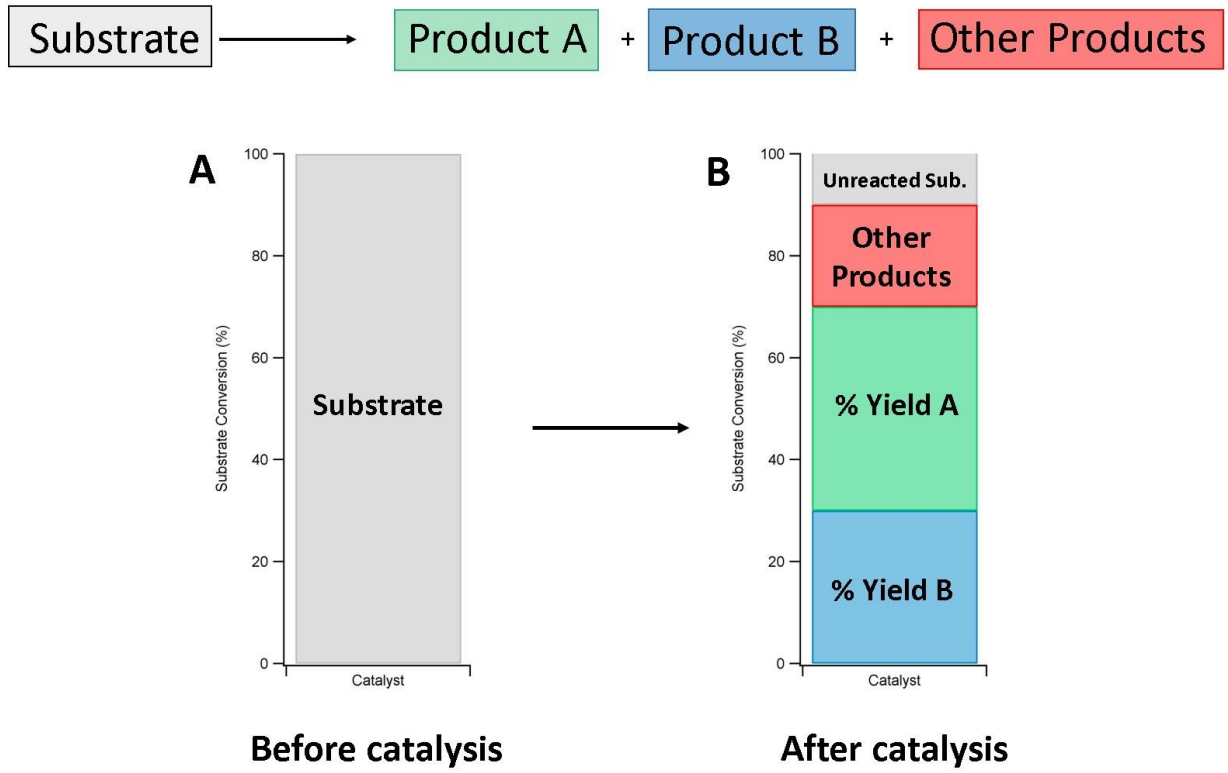
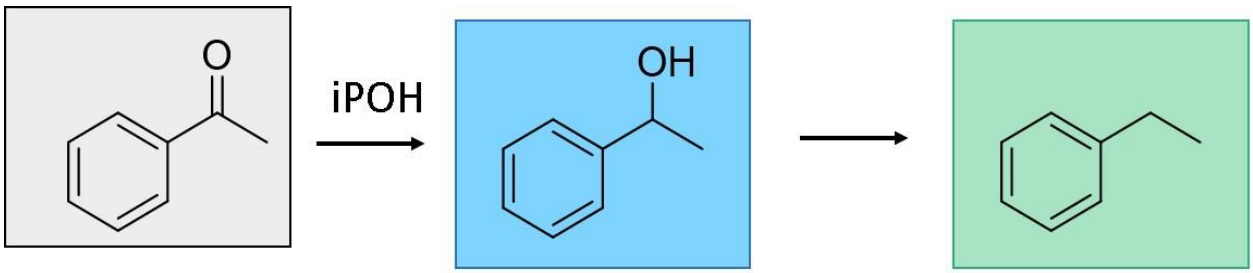


Figure 52. Example of the bar chart illustration of catalytic performance.



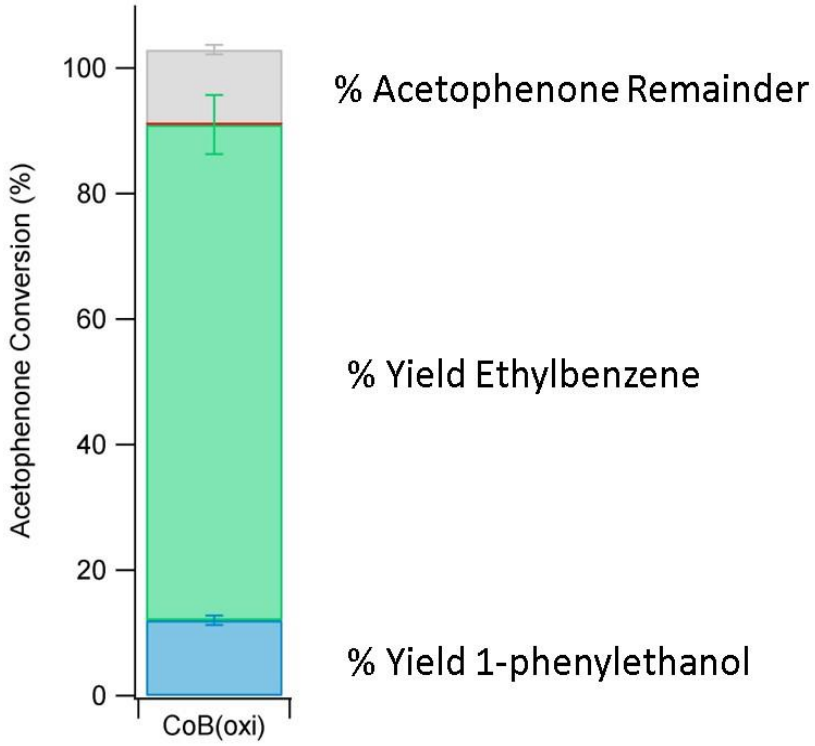


Figure 53. Bar illustration depicting the catalysis parameters for conversion of acetophenone at 300° C at 15 minutes in the presence of CoB_{oxi}.

Table 3. Summary of the main experiments done in this work.

Experiments	H-Donor	Temp. (°C)	Time (hr)	Reasons	Outcomes
Catalyst activity studies	*i*-PrOH	300 200 165	0.25 (15 min)	To compare activity of CoB_{oxi} and CoB_{red} at various temperatures.	CoB_{red} is unanimously most active.
Recyclability study with CoB_{red}		165	0.25 (15 min)	To test catalyst stability over multiple catalytic runs	CoB_{red} is stable over 10 runs.
Activation studies		165	0.25 (15 min)	To test the effects of *i*-PrOH pretreatment and compare to previous catalysis results	Pretreatment with *i*-PrOH significantly enhances activity of both CoB_{oxi} and CoB_{red}.
Low T studies (with and without activation)		100	18	To test the activity of CoB catalysts at low T.	Catalysts are active, **and** selectivity can be modified by using activation protocol.
Ethanol studies	EtOH	200	3, 18	Evaluate EtOH as an H-donor.	EtOH less active than *i*-PrOH, but very selective for C=O w/ CoB_{red} (CoB_{oxi} not very selective).

At 200 °C, only CoB_{oxi} and CoB_{red} showed activity. CoB_{oxi} exhibited low conversion (18±1%) with 20±1% yield for 4-ethylguaiacol. However, CoB_{red} showed almost complete conversion (97±6%) and 84±5% yield for 4-ethylguaiacol and 13±1% yield for other products.

At 165 °C, CoB_{oxi} showed low conversion (2±1%) and 2±1% yield for 4-ethylguaiacol. CoB_{red} showed activity with 17±1% conversion and 14±1% yield for 4-ethylguaiacol.

Catalysis: Guaiacol

Figure 57 shows the catalysis results with guaiacol at 300, 200 and 165 °C. At 300 °C, CoB_{oxi}, Co powder, and CoB_{red} showed activity towards conversion of guaiacol. CoB_{oxi} exhibited 30±2% conversion with 5±1% yield for phenol and 14±1% yield for cyclohexanol, and 11±1% yield for other products. CoB_{red} showed almost complete conversion (98±6%) of guaiacol with 59±4% yield for cyclohexanol and 39±2% yield for other products. Co powder exhibited moderate conversion (66±4%) with 6±1% yield for phenol, 24±1% yield for cyclohexanol, and 35±2% yield for other products. The blank exhibited low conversion (11±1%) and 11±1% yield for other products.

At 200 °C, CoB_{oxi} showed low conversion (6±1%) with 6±1% yield for other products. CoB_{red} showed moderate conversion (56±3%) and 12±1% yield for phenol, 31±2% yield for cyclohexanol, and 16±1% yield for other products. For Co powder and the blank, low conversion was observed (7±1 and 6±1%, respectively) were observed with 7±1% and 6±1% yield for other products.

At 165 °C, CoB_{oxi} showed low conversion (8±1%) and 8±1% yield for other products. CoB_{red} however showed moderate conversion (30±2%) with 5±1% yield for phenol, 13±1% yield for cyclohexanol, and 12±1% yield for other products. Cobalt powder and the blank showed little to no conversion.

Comparison of CoB_{oxi} and CoB_{red} with a Mixture of Acetophenone, Acetovanillone, and Guaiacol

Finally, CoB_{oxi} and CoB_{red} were tested with equimolar mixtures of each substrate at 200 °C for 15 minutes. The results are summarized in Figure 58. CoB_{red} showed moderate conversion for acetophenone and acetovanillone (63% and 65%, respectively) and low conversion of guaiacol (12%). With acetophenone, modest yields for 1-phenylethanol and ethylbenzene (23% and 20%, respectively) were obtained. Moderate yield for 4-ethylguaiacol from acetovanillone (43%) was also obtained. However, low yield for phenol from guaiacol was observed (4%).

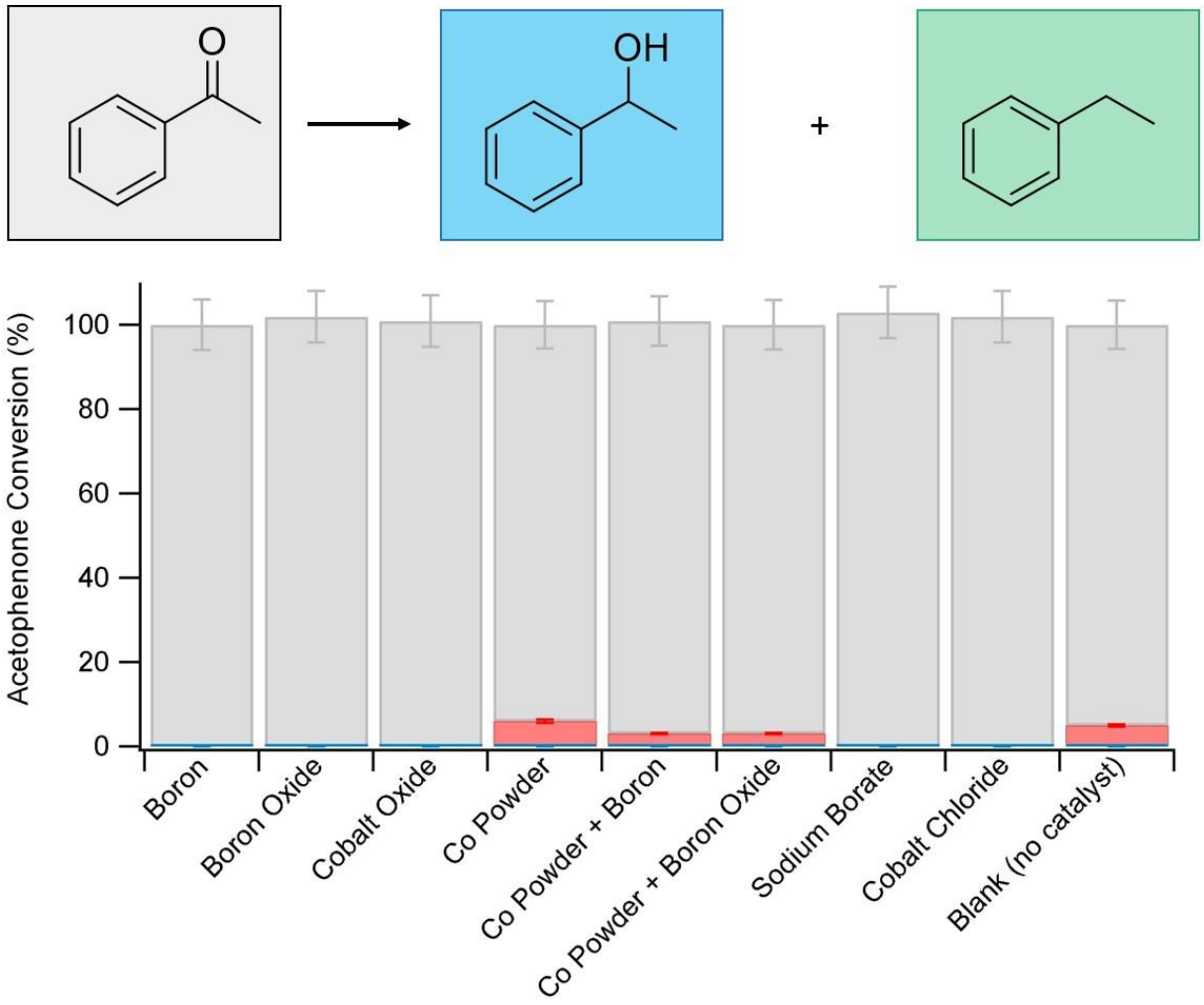


Figure 54. Blanks and controls with acetophenone. Conditions: 10 mg catalyst, 0.5 mmol acetophenone, 2 mL i-PrOH, 200 °C, 15 minutes. Numerical values shown in Table 4.

Table 4. Summary of the blanks and controls with acetophenone.

Catalyst[a]	T (°C)	X (%)[b] 	Y (%)[c] 	Y (%) 
Boron Powder	200	0	N.D.[d]	N.D.
Boron Oxide	200	-2	N.D.	N.D.
Cobalt Oxide	200	-1	N.D.	N.D.
Cobalt Powder	200	6	N.D.	N.D.
Cobalt Powder + Boron Powder	200	3	N.D.	N.D.
Cobalt Powder + Boron Oxide	200	3	N.D.	N.D.
Sodium Borate	200	-3	N.D.	N.D.
Cobalt Chloride	200	-2	N.D.	N.D.
Blank (no catalyst)	200	5	N.D.	N.D.

[a] Reaction conditions: 10 mg catalyst, 0.5 mmol acetophenone, 2 mL i-PrOH, 200 °C, 15 min.

[b] Conversion (X) was measured with GC/MS using hexadecane as the internal standard.

[c] Yield (Y) was measured as above.

[d] N.D. = not detected.

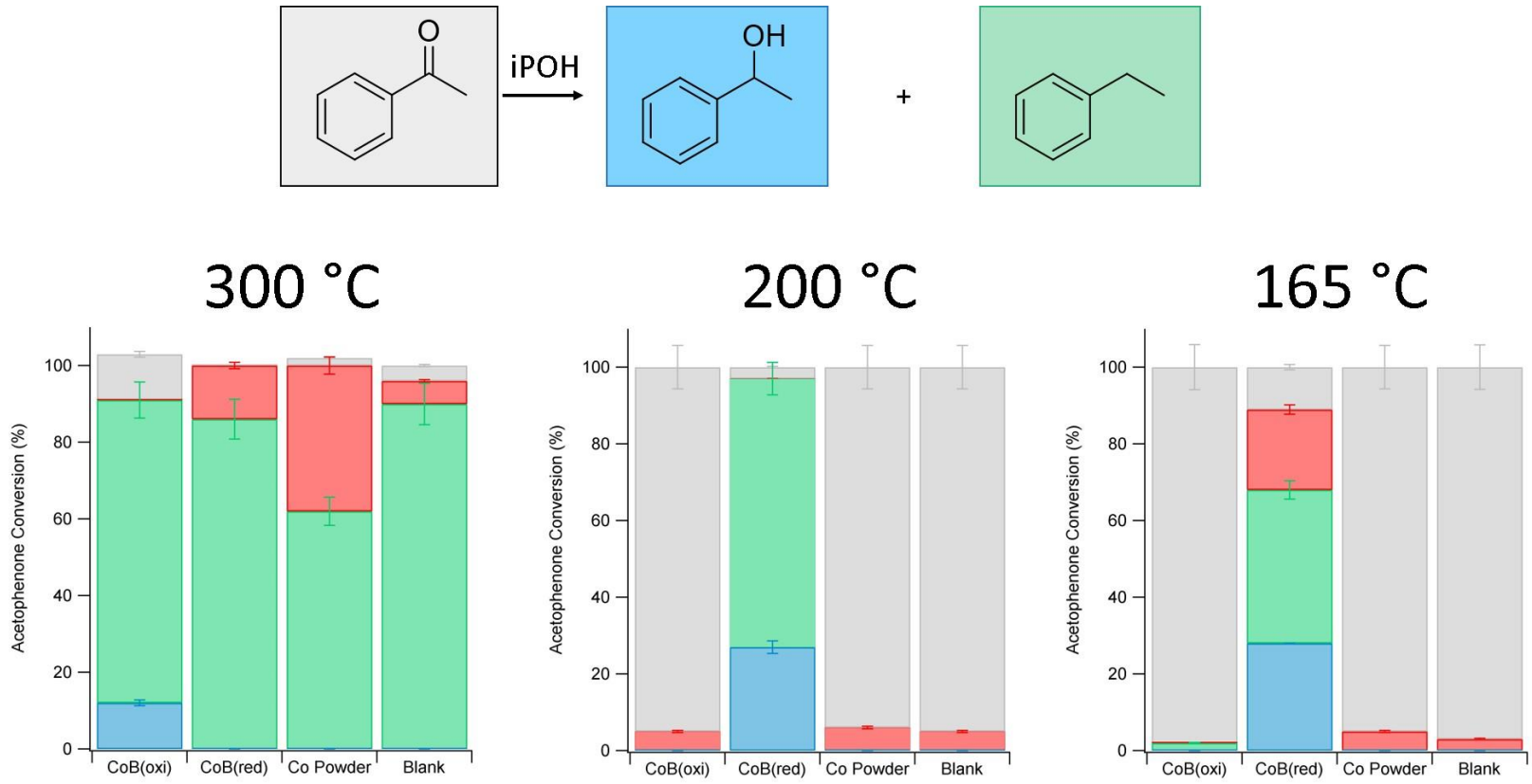


Figure 55. Catalytic results of acetophenone substrate at 300, 200, and 165 °C. Conditions: 10 mg catalyst, 0.5 mmol substrate, 2 mL i-PrOH, 15 minutes. Numerical values shown in Table 5.

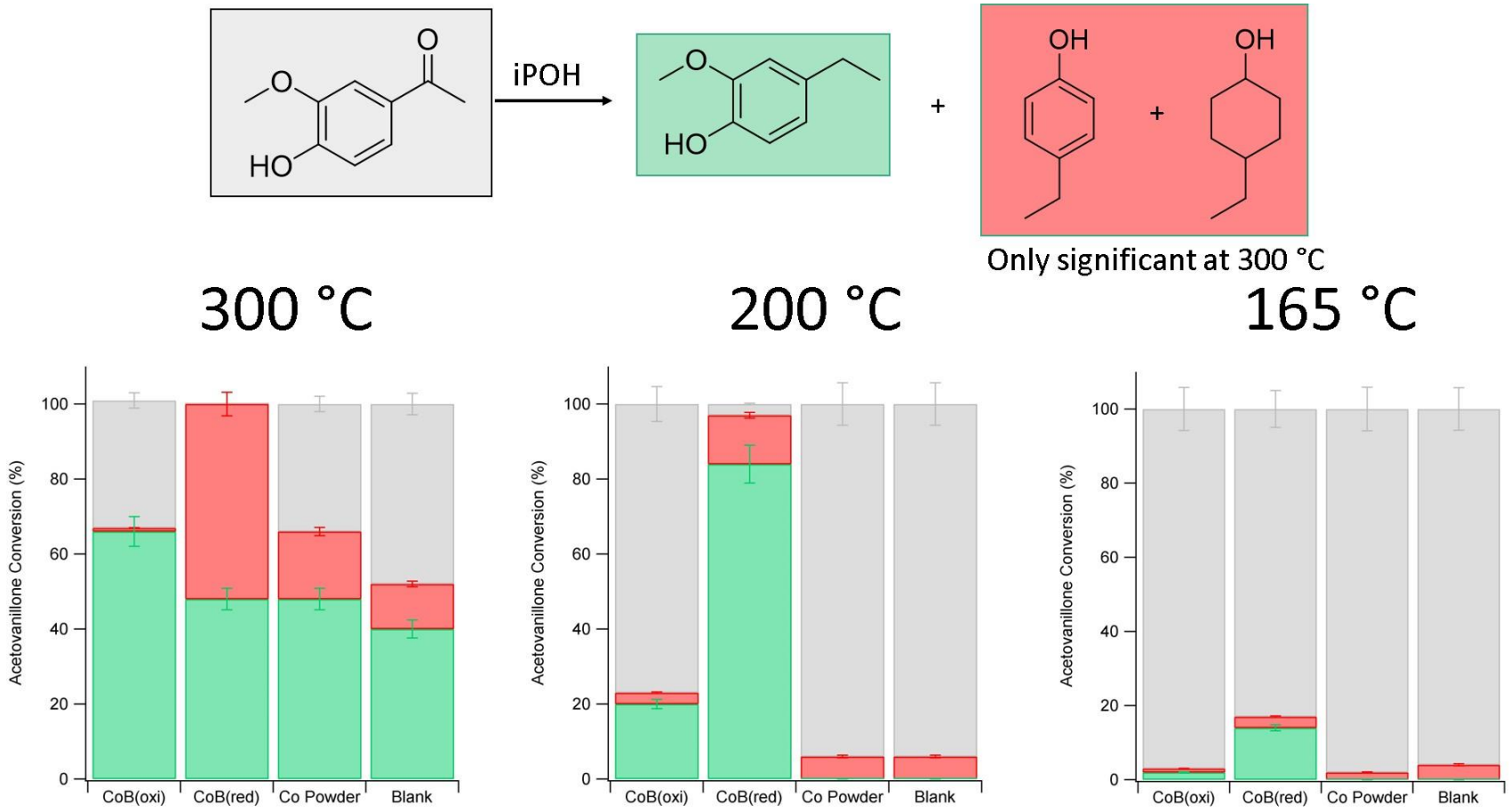


Figure 56. Catalytic results of acetovanillone substrate at 300, 200, and 165 °C. Conditions: 10 mg catalyst, 0.5 mmol substrate, 2 mL i-PrOH, 15 minutes. Numerical values shown in Table 5.

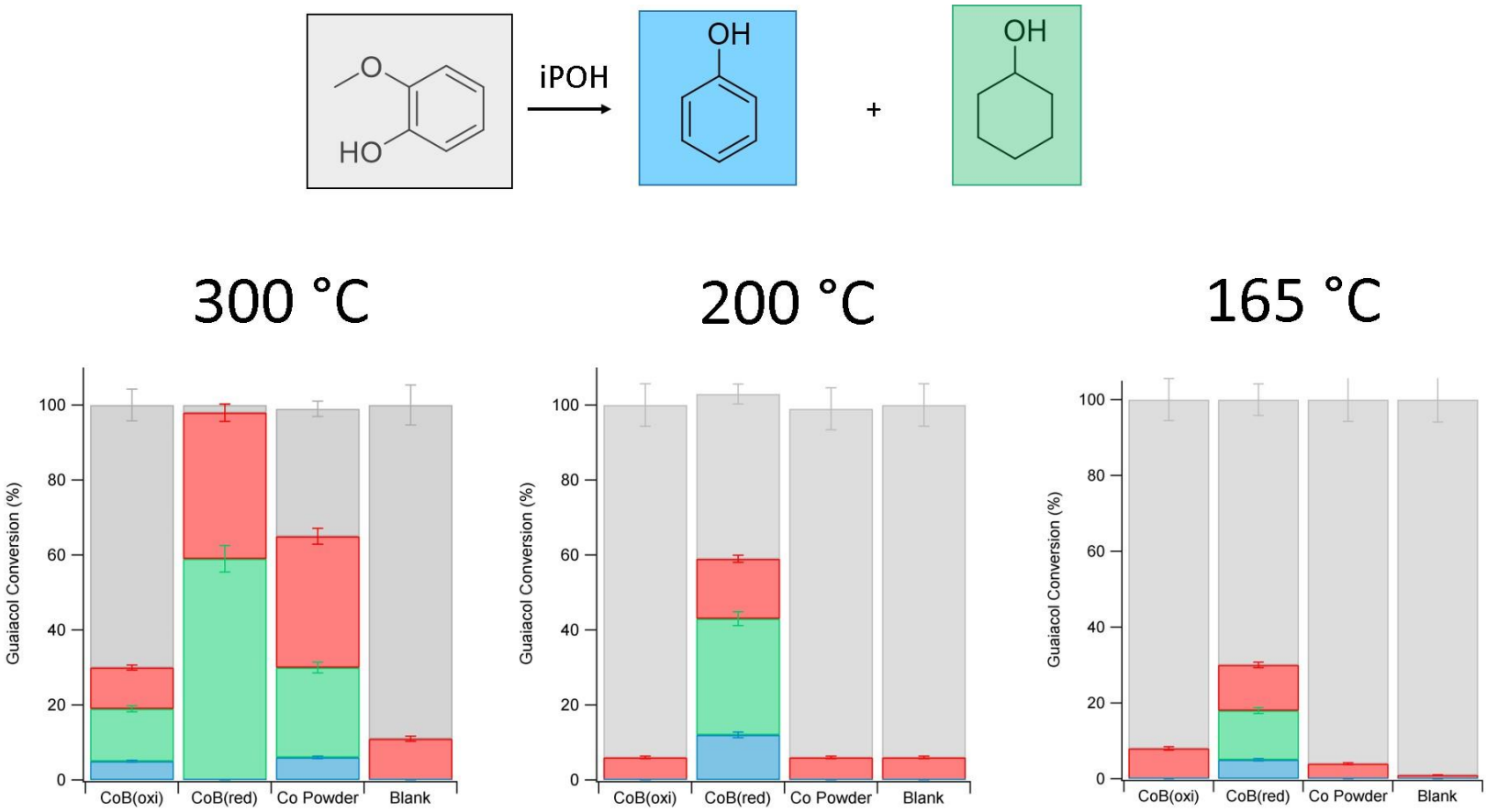
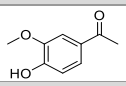
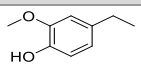
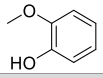


Figure 57. Catalytic results with guaiacol substrate at 300, 200, and 165 °C. Conditions: 10 mg catalyst, 0.5 mmol substrate, 2 mL i-PrOH, 15 minutes. Numerical values shown in Table 5.

Table 5. Screening of catalysts with acetophenone, acetovanillone, and guaiacol in i-PrOH

Catalyst[a]	T (°C)	X (%)[b] 	Y (%)[c] 	Y (%) 
CoB_{oxi}	300	88 ± 5	12 ± 1	78 ± 5
CoB_{red}	300	100 ± 6	N.D.[d]	86 ± 5
Co powder	300	98 ± 6	N.D.	62 ± 4
Blank	300	96 ± 6	N.D.	90 ± 5
CoB_{oxi}	200	5 ± 1	N.D.	N.D.
CoB_{red}	200	97 ± 6	27 ± 2	70 ± 4
Co powder	200	6 ± 1	N.D.	N.D.
Blank	200	5 ± 1	N.D.	N.D.
CoB_{oxi}	165	2 ± 1	N.D.	2 ± 1
CoB_{red}	165	85 ± 5	37 ± 2	26 ± 2
Co powder	165	5 ± 1	N.D.	N.D.
Blank	165	3 ± 1	N.D.	N.D.
				
CoB_{oxi}	300	64 ± 4	66 ± 4	
CoB_{red}	300	100 ± 6	48 ± 2	
Co powder	300	63 ± 4	48 ± 3	
Blank	300	49 ± 3	40 ± 2	
CoB_{oxi}	200	18 ± 1	20 ± 1	
CoB_{red}	200	97 ± 6	84 ± 5	
Co powder	200	6 ± 1	N.D.	
Blank	200	6 ± 1	N.D.	
CoB_{oxi}	165	2 ± 1	2 ± 1	
CoB_{red}	165	17 ± 1	14 ± 1	
Co powder	165	2 ± 1	N.D.	
Blank	165	3 ± 1	N.D.	
				
CoB_{oxi}	300	30 ± 2	5 ± 1	14 ± 1
CoB_{red}	300	98 ± 6	N.D.	59 ± 4
Co powder	300	66 ± 4	6 ± 1	24 ± 1
Blank	300	11 ± 1	N.D.	N.D.
CoB_{oxi}	200	6 ± 1	N.D.	N.D.
CoB_{red}	200	56 ± 3	12 ± 1	31 ± 2
Co powder	200	7 ± 1	N.D.	N.D.
Blank	200	6 ± 1	N.D.	N.D.
CoB_{oxi}	165	8 ± 1	N.D.	N.D.
CoB_{red}	165	30 ± 2	5 ± 1	13 ± 1
Co powder	165	3 ± 1	N.D.	N.D.
Blank	165	1 ± 1	N.D.	N.D.

[a] Reaction conditions: 10 mg catalyst, 0.5 mmol substrate, 2 mL i-PrOH, 15 min.
[b] Conversion (X) was measured with GC/MS using hexadecane as the internal standard.
[c] Yield (Y) was measured as above.
[d] N.D. = not detected.

CoB_{oxi} generally showed lower conversions overall. Acetophenone was converted (15%) with low yields for 1-phenylethanol (4%) and ethylbenzene (7%). Acetovanillone showed moderate conversion (40%) and yield for 4-ethylguaiacol (21%). No conversion of guaiacol was observed.

Discussion on the Temperature Study of Catalysis of Acetophenone, Acetovanillone, and Guaiacol

For acetophenone, at 300 °C, CoB_{oxi}, CoB_{red}, Co powder, and the blank all showed almost complete conversion (>90%) of acetophenone. CoB_{oxi}, CoB_{red}, and the blank all exhibit high selectivity (>80%) for formation of ethylbenzene. Interestingly, Co powder appears to show significantly lower selectivity (~60%) than the other cases. However, because the blank also exhibited comparable activity and selectivity to the reactions done in the presence of catalyst, conversion of acetophenone at 300 °C was not representative of catalyst performance.

One explanation for these observations is that at such high temperatures the *i*-PrOH readily participates in transfer hydrogenations reactions without catalyst. A second explanation is that i-PrOH is not active without catalyst, but the stainless steel reactor itself is able to participate in the reaction at 300 °C. It is possible that the stainless steel surface itself, or microscopic defects are able to promote CTH. For this reason, the activity studies described here are focused on reactions done at 200 and 165 °C, as negligible conversion was evident with the blanks and we observe "true" catalysis from CoB_{red} at these temperatures. The same will be the case for the acetovanillone and guaiacol systems.

At 200 °C, CoB_{red} showed almost complete conversion of acetophenone with high selectivity for ethyl benzene, while CoB_{oxi}, Co powder, and the blank showed almost no conversion. The controls, which consisted of various compounds of cobalt and boron, also showed no activity towards conversion of acetophenone, which illustrates the unique catalytic properties of CoB_{red}.

At 165 °C, only CoB_{red} showed activity with high selectivity for ethyl benzene. At 200 and 165 °C no conversion was observed in the case of the blank. It is noteworthy that, at 165 °C, higher yield for unidentified products was observed as compared to 200 °C. One explanation is that an unidentified reaction pathway is more favored in which a non-volatile, but soluble oligomeric intermediate species is formed in higher yield in 15 min at 165 °C than at 200 °C. Trace amounts of styrene is sometimes observed in GCMS analyses of these reactions and may be a reactive intermediate. To test this hypothesis, styrene was treated as a substrate and reacted in i-PrOH in the presence of CoB_{red} at 165 °C

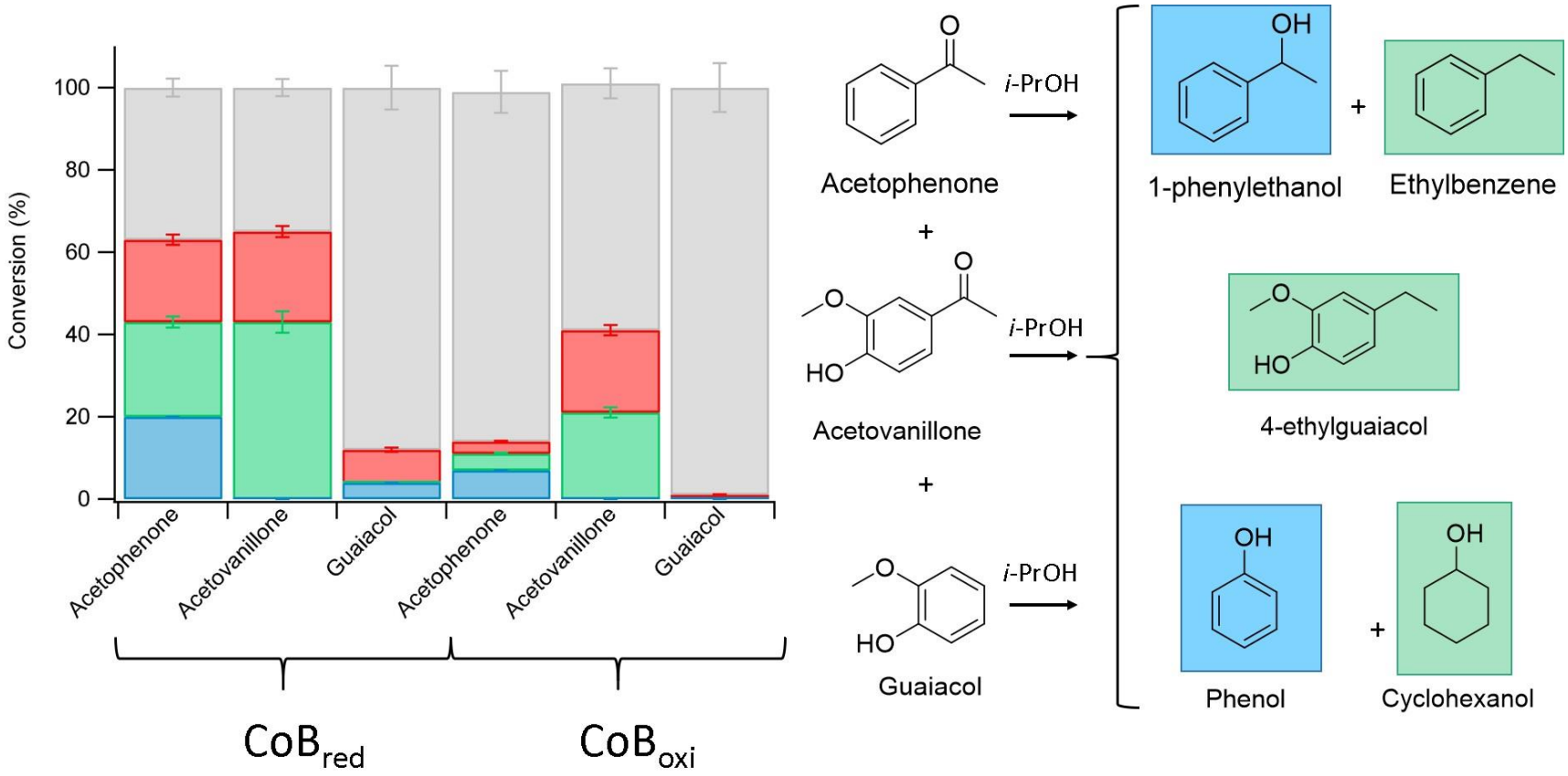
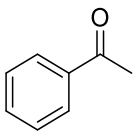
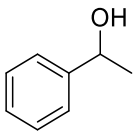
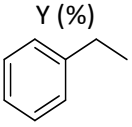
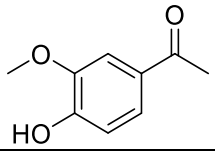
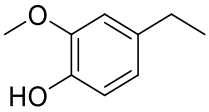
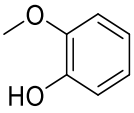
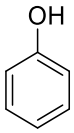
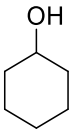


Figure 58. Catalytic results of CoB_{red} and CoB_{oxi} with a mixture of all three substrates at 200 °C. Conditions: 10 mg catalyst, 0.5 mmol of each substrate, 2 mL i-PrOH, 15 minutes. Numerical values shown in Table 6.

Table 6. Numerical values for comparison of CoB_{oxi} and CoB_{red} with all three substrates.

Catalyst[a]	X (%)[b] 	Y (%)[c] 	Y (%) 
CoB_{oxi}	15 ± 1	4 ± 1	7 ± 1
CoB_{red}	63 ± 4	23 ± 1	20 ± 1
			
CoB_{oxi}	40 ± 2	21 ± 1	
CoB_{red}	65 ± 4	43 ± 2	
			
CoB_{oxi}	1 ± 1	N.D.	N.D.
CoB_{red}	15 ± 1	8 ± 1	N.D.

[a] Reaction conditions: 10 mg catalyst, 0.5 mmol of each substrate, 2 mL *i*-PrOH, 200 °C, 15 min.
[b] Conversion (X) was measured with GC/MS using hexadecane as the internal standard.
[c] Yield (Y) was measured as above.
[d] N.D. = not detected.

for 3 hours. Complete conversion of styrene was observed with 98 ± 6% yield for ethylbenzene. However, some white precipitate was also observed in the post-reaction mother liquor which may be due to the formation of insoluble polymers of styrene. Although white precipitates were not observed with reactions using acetophenone as substrate at 165 °C, the possibility that soluble oligomerized styrene species have formed cannot be ruled out and may account for the unobserved products. At 200 °C, the reduction of styrene to ethylbenzene may be favored over styrene polymerization, which could explain the higher selectivity for ethyl benzene under these conditions.

Another experiment was carried out in which 1-phenylethanol was treated as the substrate and reacted in i-PrOH at 165 °C for 3 hours in the presence of CoB_{red}. 97 ± 6% conversion of the alcohol was observed with 90 ± 6% yield for ethylbenzene. Minor amounts of acetophenone were also observed, which demonstrates that conversion of acetophenone to 1-phenylethanol is likely reversible. Finally, these results, taken together with the results for reduction of styrene, suggest that a reaction pathway proceeds in the order acetophenone → 1-phenylethanol → styrene → ethylbenzene (illustrated in Figure 59). However, direct hydrodeoxygenation of 1-phenylethanol to ethylbenzene still cannot be ruled out as a possible pathway.

With acetovanillone at 300 °C, CoB_{oxi}, Co powder, and the blank all showed comparable activity and selectivity, whereas CoB_{red} showed almost complete conversion with lower selectivity for 4-ethylguaiacol and significant formation of non-selective products. At 200 °C, both CoB_{oxi} and CoB_{red} exhibited activity and high selectivity for 4-ethylguaiacol. However, CoB_{red} exhibited almost complete conversion of acetovanillone, whereas CoB_{oxi} showed much lower conversion. At 165 °C, CoB_{oxi} showed almost no conversion whereas CoB_{red} showed low conversion with high selectivity for 4-ethylguaiacol.

For guaiacol, minor conversion was observed for the blank at 300 °C. CoB_{oxi} and Co powder both exhibited some conversion with moderate selectivity for cyclohexanol and low selectivity for phenol, but also showed significant formation of other non-selective products. CoB_{red} again showed the highest activity, exhibiting almost complete conversion of guaiacol, but with only moderate selectivity for cyclohexanol and significant formation of other products as well. At 200 °C, only CoB_{red} showed activity and with moderate selectivity for cyclohexanol and low selectivity for phenol, but still showed significant formation of non-selective products.

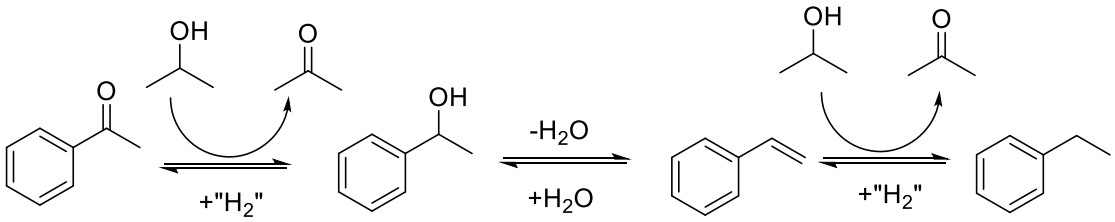


Figure 59. Possible reduction pathway of acetophenone to ethylbenzene

In all cases, CoB_{red} shows the highest catalytic activity compared to CoB_{oxi} and Co powder, with high activity for conversion of acetophenone, acetovanillone, and guaiacol. Interestingly, for acetophenone and acetovanillone at 200 and 165 °C, CoB_{red} shows high selectivity for ethylbenzene and 4-ethylguaiacol, whereas in the case of guaiacol, CoB_{red} shows lower selectivity towards preservation of the aromatic methoxy substituent and the aromatic ring, which is evidenced by the formation of significant amounts of phenol and cyclohexanol. The catalyst also shows much lower selectivity for identifiable products in general for guaiacol.

In the cases in which catalysis was done on a mixture of all three substrates, the degrees of conversion of acetophenone and acetovanillone with CoB_{red} were almost identical. The total yields for quantified products were also nearly identical (that is, the sum of the yields for 1-phenylethanol and ethylbenzene (23% + 20% = 43%), were the same as compared to the yield for 4-ethylguaiacol (43%)). This suggests that, when present together in a mixture, the rates of deoxygenation of the ketone of acetophenone and acetovanillone substrates are similar. Further, guaiacol conversion in the mixed solution was significantly lower than in the case of guaiacol alone. These results suggest that ketone reduction in the cases of acetophenone and acetovanillone is highly favored over guaiacol reduction, which may be the result of competitive inhibition in which the ketone-containing species more favorably interact with the surface as compared to guaiacol. However, in the isolated cases, guaiacol rapidly reduces to phenol and cyclohexanol.

Another observation was made in comparing guaiacol and 4-ethylguaiacol (the main product from acetovanillone): guaiacol readily reduces whereas 4-ethylguaiacol (the primary product from acetovanillone) does not convert as readily. It is notable that 4-ethylguaiacol is structurally similar to guaiacol, though an obvious difference between the two is the presence of an ethyl group in the para-position relative to the phenolic hydroxyl moiety. A rationale for these reactivity differences is suggested in the following:

For comparison, 4-ethylguaiacol was used as a substrate and reacted in i-PrOH at 200 °C for 15 minutes in the presence of CoB_{red} and compared to catalysis with guaiacol, the results of which are summarized in Figure 60. CoB_{red} showed 2±1% conversion of 4-ethylguaiacol, compared to 56±3% conversion of guaiacol. Several recent articles in the literature have described computational modeling that shows that guaiacol preferentially adsorbs to catalyst surfaces *via* interaction of its aromatic ring with the surfaces of some Fe, Ni, and noble metal-based catalysts prior to hydrodeoxygenation and hydrogenation.[94-96] Therefore, one rationale for the difference in selectivity observed between 4-

ethylguaiacol and guaiacol exhibited by CoB_{red} is that the ethyl group of 4-ethylguaiacol may sterically hinder and alter the adsorptive characteristics of 4-ethylguaiacol to the catalyst surface as compared to guaiacol and thus hinder its transformation to the corresponding demethoxylated and aliphatic derivatives.

It is noteworthy that, in the reduction of acetophenone, formation of ethylcyclohexane was never observed, whereas guaiacol readily reduces to form cyclohexanol, which indicates saturation of the aromatic ring. A clear difference in susceptibility of aromatic ring reduction is evident. A simple rationale is as follows: several studies in the literature[97-99] on phenol hydrodeoxygenation suggest that phenol reduction proceeds through a cyclohexadienone tautomerization intermediate (Figure 61). In the context of this work, this mechanism implies that demethoxylation of guaiacol to form phenol is a critical step to saturation of the aromatic ring. It is assumed unlikely that guaiacol itself tautomerizes into the corresponding cyclohexadienone species. This mechanism also suggests that the presence of the phenolic -OH is required to break ring aromaticity and allow further reduction. Figure 62 summarizes possible reduction pathways of each substrate.

In the cases of acetovanillone, guaiacol, or 4-ethyguaiacol (the primary product from acetovanillone), if direct ring adsorption is necessary for demethoxylation, then, in the case of acetovanillone or 4-ethylguaiacol, the presence of the acetyl- or ethyl- groups may sterically hinder the molecule from demethoxylation and thus formation of the corresponding phenol and thus further reduction. It is again noteworthy that, neither acetophenone nor ethylbenzene, despite possessing an acetyl- and ethyl- group, afford ring hydrogenation species such as ethylcyclohexane, though the ring may not be sterically hindered for surface adsorption. Since acetophenone and ethylbenzene do not possess phenolic -OH moieties, aromaticity cannot be broken and is thus resistant to reduction. With respect to ketone reduction, the ring adsorption mechanism may not be operative and may explain the relatively higher rate of ketone reduction as compared to either demethoxylation or aromatic ring reduction. Figure 63 illustrates several possible scenarios of substrate-surface interactions and the implications on reduction.

Taken together, these data indicate that the presence of certain ring functional groups can either behave synergistically or antagonistically for aromatic ring reduction. Several conclusions can therefore be drawn: 1) an aromatic ring with only an alkyl substituent, as in ethylbenzene, does not afford ring saturation products, 2) the presence of a phenolic -OH group is necessary to destabilize

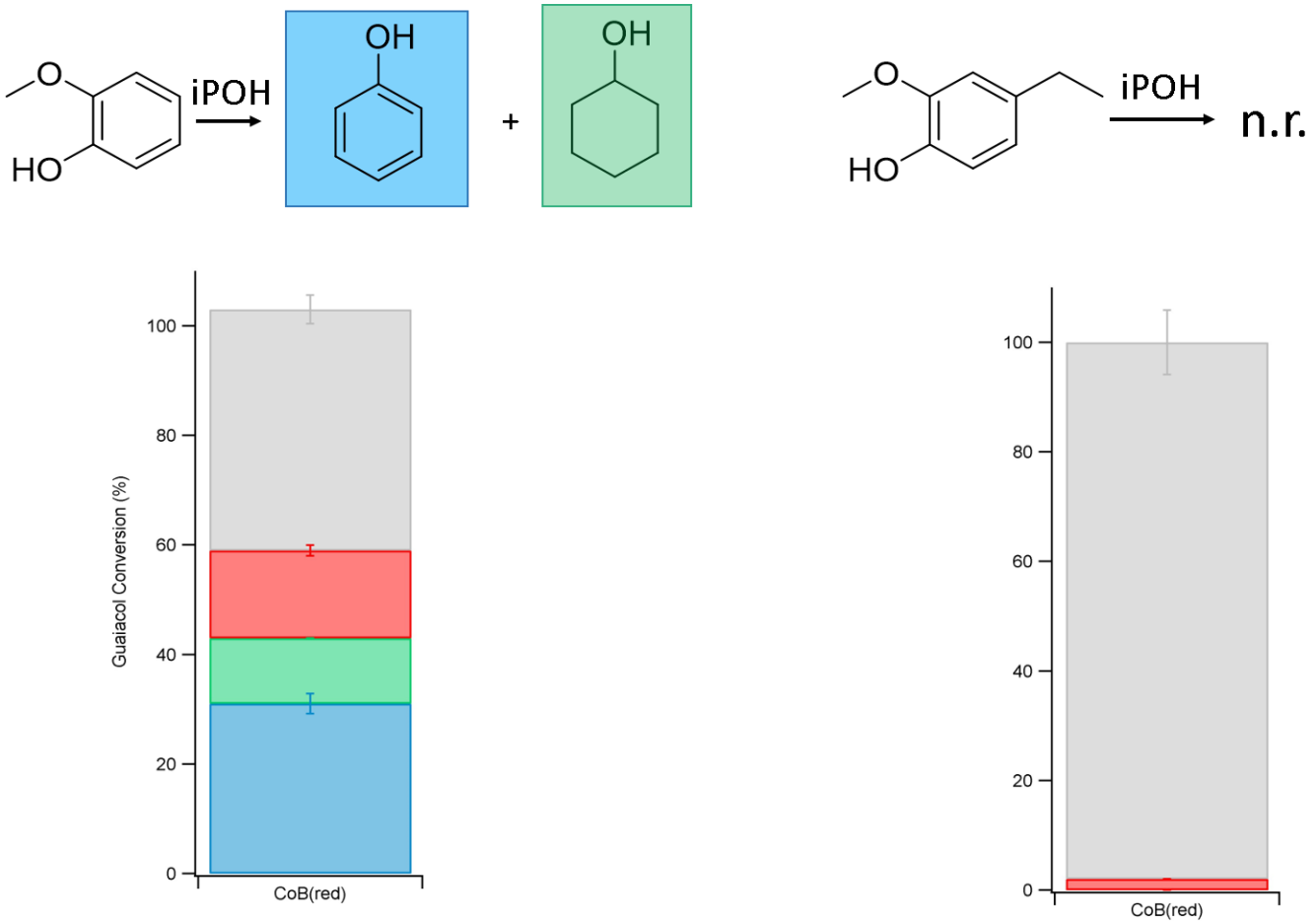


Figure 60. Catalytic results showing comparison between 4-ethylguaiacol and guaiacol as substrates at 200 °C in the presence of CoB_{red}. Conditions: 10 mg CoB_{red}, 0.5 mmol substrate, 2 mL i-PrOH, 15 minutes.

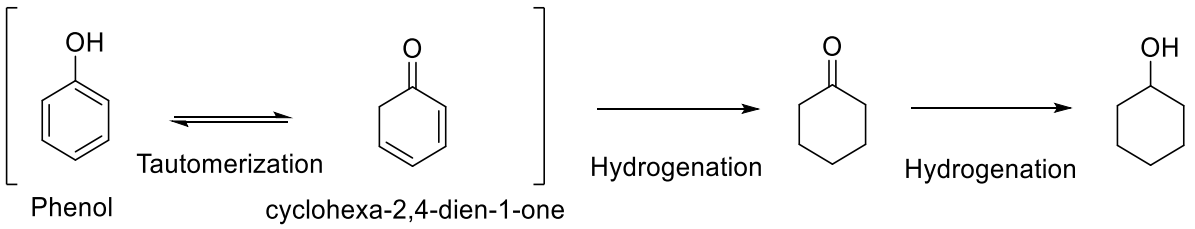


Figure 61. Tautomerization of phenol to cyclohexa-2,4-diene-1-one and subsequent hydrogenation to cyclohexanone and cyclohexanol.

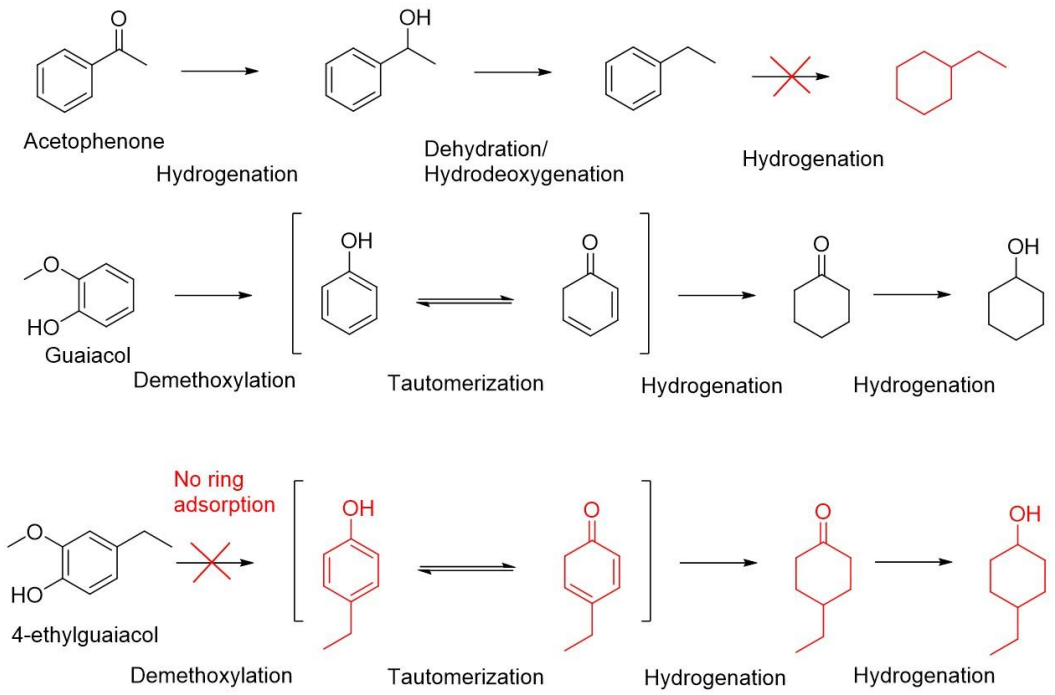


Figure 62. Proposed reduction schemes showing the major products formed from each substrate at 200 °C for 15 min in i-PrOH.

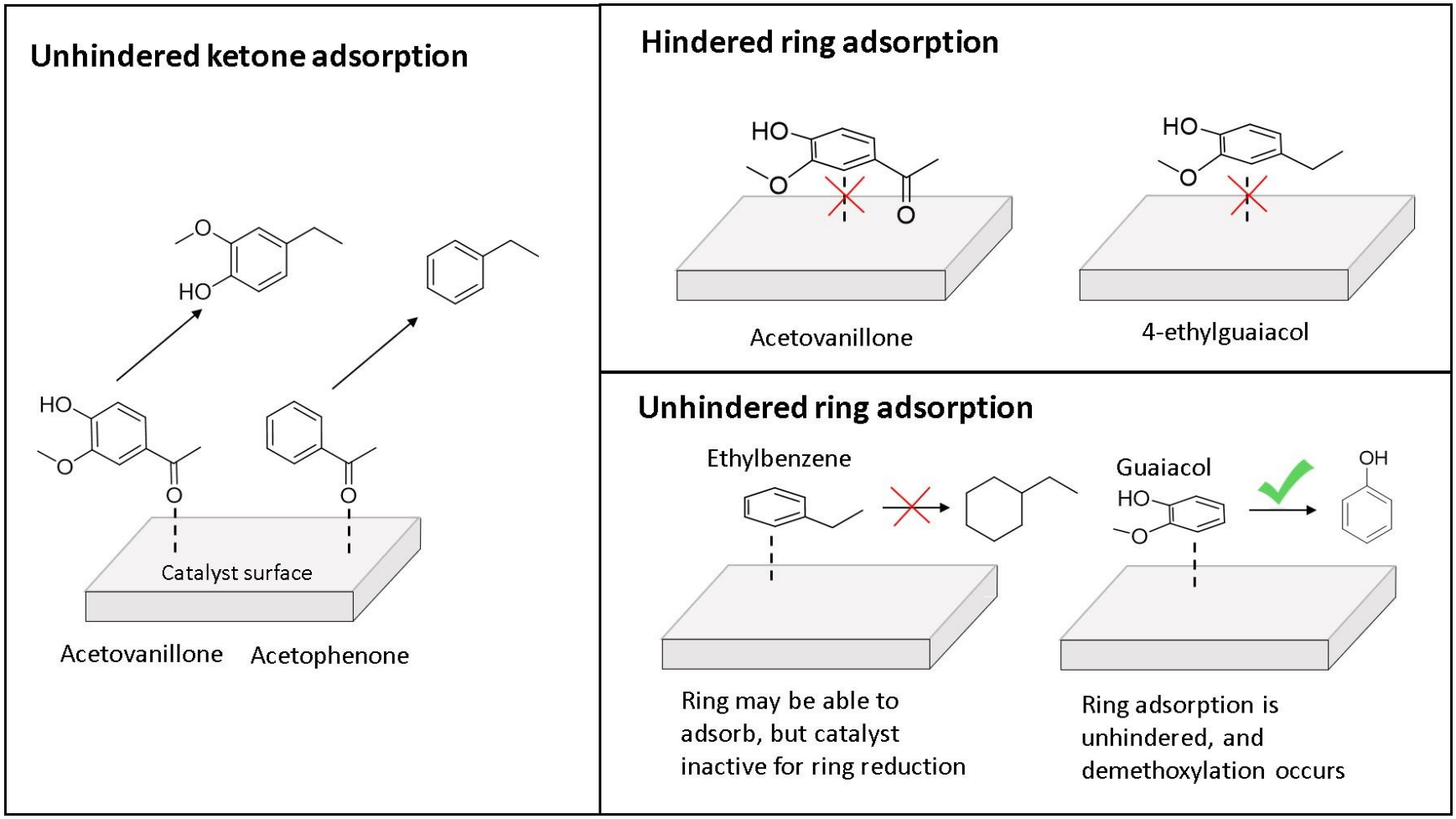


Figure 63. Illustration of possible surface interactions of various functional groups of each substr

aromaticity *via* a tautomerization mechanism in which a cyclohexadienone intermediate is formed and the ring hydrogenated, and 3) in the case of guaiacol,removal of the adjacent methoxy group is necessary to allow (2), which suggests that methoxy group serves as a "gatekeeper" to further aromatic ring reduction. These results highlight important selectivity differences in which the presence or absence of certain reducible functional groups significantly impacts activity of CoB catalysts towards aromatic ring reduction. In the context of lignin upgrading, para-alkyl substituted phenolic monomers are frequently the primary products of lignin reduction, which suggests that CoB catalysts would be selective for preserving the aromaticity of these products.

Finally, CoB_{red} generally shows high activity whereas CoB_{oxi} and commercially purchased Co powder shows little or no conversion. However, as will be discussed later, pretreatment of CoB_{oxi} with *i*-PrOH under reducing conditions leads to significant enhancement of its activity. A simple rationalization for this observation is that *i*-PrOH at elevated temperatures transforms the oxidized surface into a more reduced and more active one. Taken together, these points suggest that boron plays an important role in promoting transfer hydrogenation reactions, and the presence of a surface oxide layer inhibits substrate reduction. As previously described, ICP-OES analysis indicates significant amounts of oxygen is present, and EDX indicates the oxygen content is localized on the surface. The oxygen content is likely in the form of various formulations of cobalt oxides, boron oxides, or cobalt-boron oxides (e.g. Co_xO_y, B_xO_y, or $Co_xB_yO_z$). With respect to the classic MPV reduction mechanism, surface boron species may act the necessary Lewis basic sites required to deprotonate the donor alcohol and promote reductions with an adjacent Lewis acidic cobalt site. It is also possible that transformation occurs *via* a hydride mechanism in which the donor molecule directly donates hydrogen to the surface to form hydride intermediate species. These mechanisms are illustrated in Figure 64.

Reduction of Acetophenone, Acetovanillone, and Guaiacol in EtOH

Although i-PrOH is a powerful hydrogen donor and one of the most commonly used reagents for catalytic transfer hydrogenation reactions, most of the i-PrOH produced in the world is ultimately derived from propene, which is a petroleum-derived product. EtOH, however, is considered a "green" solvent as it can be derived from plant biomass and is relatively non-toxic. CoB_{oxi} and CoB_{red} were tested for catalytic transfer hydrogenation of acetophenone, acetovanillone, and guaiacol with EtOH as the H-donor instead of i-PrOH. Reactions were performed at 200 °C for 3 hours and 18 hours. Figure 65 shows the catalysis results of acetophenone, acetovanillone, and guaiacol in the presence of CoB_{oxi} and CoB_{red}

at 200 °C for 3 hours. Table 7 summarizes the numerical results. For both catalysts and all substrates, low conversion was observed under these conditions. Thus, the reactions were repeated for 18 hours.

Figure 66 shows the catalysis results for acetophenone, acetovanillone, and guaiacol in the presence of CoB_{oxi} and CoB_{red} at 200 °C for 18 hours. For acetophenone, CoB_{oxi} and CoB_{red} both exhibited almost complete conversion of acetophenone. However, CoB_{red} showed nearly quantitative yield for ethylbenzene. CoB_{oxi} showed only modest selectivity for ethylbenzene, with formation of a significant amount of butylbenzene and minor amounts of 1-phenyl-1-butanone. For acetovanillone, CoB_{oxi} showed some conversion of acetovanillone to 4-ethylguaiacol but showed significant yield for unidentified other products. CoB_{red} however showed quantitative conversion to 4-ethylguaiacol. For guaiacol, CoB_{oxi} showed some conversion of guaiacol to unidentified other products, whereas CoB_{red} showed no conversion.

In conclusion, CoB_{oxi} and CoB_{red} are both active for reduction of carbonyl moieties, but CoB_{red} shows significantly higher selectivity, whereas CoB_{oxi} shows significantly lower selectivity, as non-selective products were formed. Interestingly, CoB_{red} did not show activity towards reduction of guaiacol under these conditions, but CoB_{oxi} showed some conversion to unidentified products. Thus, by using EtOH as the H-donor with CoB_{red}, the rates of conversion appear much lower as compared to i-PrOH, but CoB_{red} shows excellent selectivity towards reduction of the acetyl carbonyl moiety with preservation of the aromatic ring and its substituents. These data indicate that CoB_{red} and EtOH are the preferred catalyst and solvent for reduction of carbonyl moieties without reduction of the aromatic ring and its substituents.

Stability of CoB_{red} for Conversion of Acetophenone

Figure 67 shows the graphical results of 10 catalytic runs with acetophenone in the presence of CoB_{red}, and Table 8 shows the numerical values. All reactions were done at 165 °C for 15 minutes. CoB_{red} remained highly active over the course of ten runs, with 85% conversion of acetophenone at run 1 and 80% conversion by run 10. Interestingly, the selectivity of 1-phenylethanol gradually decreased from run 1 (37% yield) to run 5 (11% yield). From runs 5-10, the yield of 1-phenylethanol was approximately the same (11 – 15%). For ethylbenzene, the yield was 26%, but increased to 40% by run 2. From runs 2-10 the yields for ethylbenzene were approximately the same, ranging from 30 – 40% yield in each case. The total yield for undetected products was approximately the same in all cases, ranging from 22% at run 1 to 26% by run 10. These results show that CoB_{red} is highly stable for conversion of acetophenone under

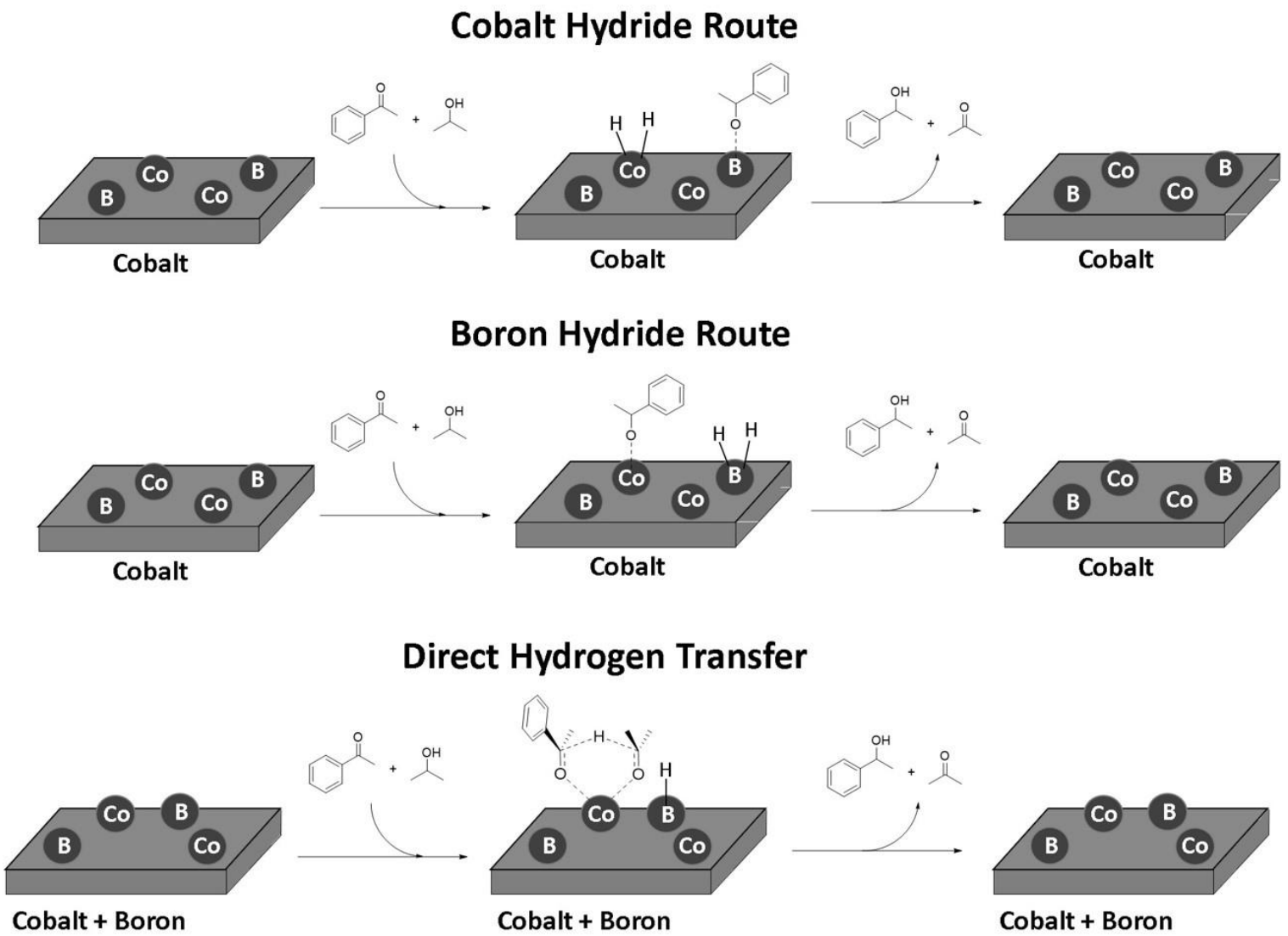


Figure 64. Possible reduction pathways over CoB catalysts.

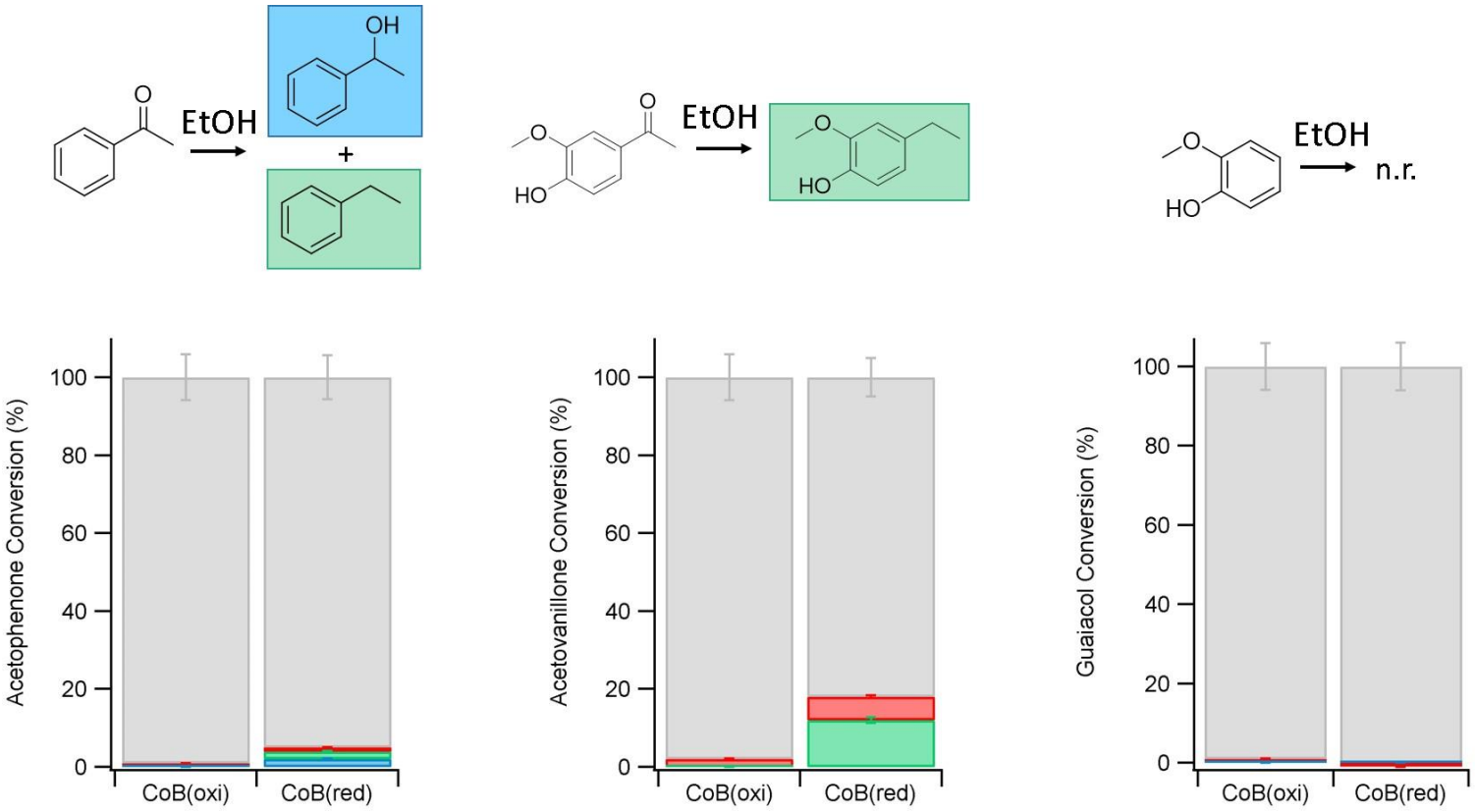


Figure 65. Catalysis results with acetophenone, acetovanillone, and guaiacol in the presence of CoB_{red} at 200 °C. Conditions: Conditions: 10 mg CoB_{red}, 0.5 mmol substrate, 2 mL EtOH, 3 hours. n.r. = "no reaction." Numerical values shown in Table 7.

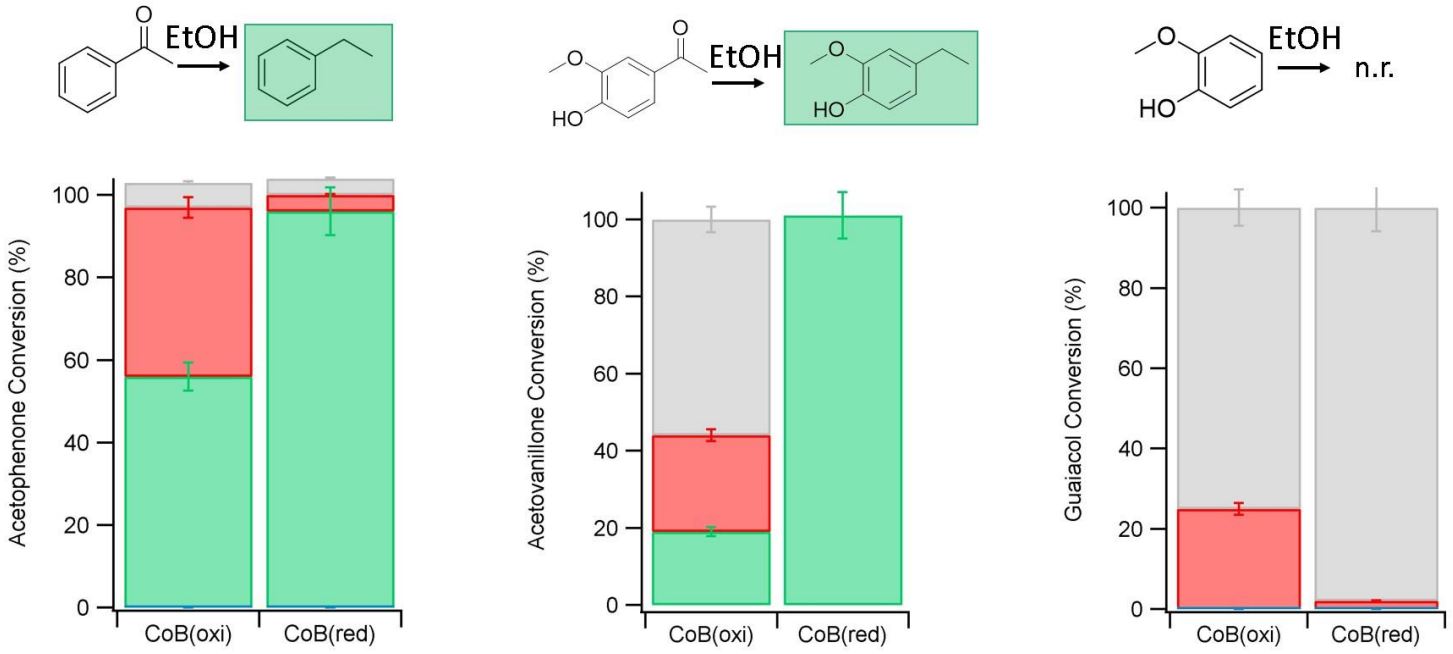
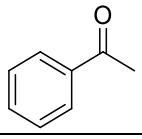
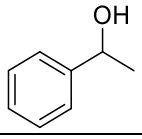
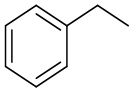
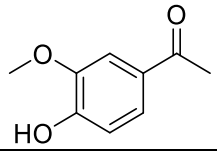
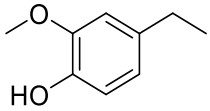
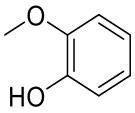
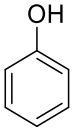
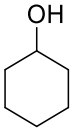


Figure 66. Catalysis results with acetophenone, acetovanillone, and guaiacol in the presence of CoBoxi or CoBred at 200 °C. Conditions: Conditions: 10 mg catalyst, 0.5 mmol substrate, 2 mL EtOH, 18 hours. Numerical values shown in Table 7.

Table 7. Catalytic screening of acetophenone, acetovanillone, and guaiacol in EtOH with CoB_{red}

Catalyst[a]	t (hr)	X (%)[b] 	Y (%)[c] 	Y (%) 
CoB_{oxi}	3	1 ± 1	0	0
CoB_{red}	3	5 ± 1	2 ± 1	2 ± 1
CoB_{oxi}	18	94 ± 6	0	38 ± 2
CoB_{red}	18	100 ± 6	N.D.[d]	96 ± 6
				
CoB_{oxi}	3	2 ± 1	0	
CoB_{red}	3	18 ± 1	12 ± 1	
CoB_{oxi}	18	44 ± 3	19 ± 1	
CoB_{red}	18	100 ± 6	101 ± 6	
				
CoB_{oxi}	3	1	0	0
CoB_{red}	3	1 ± 1	N.D.	N.D.
CoB_{oxi}	18	25 ± 2	0	0
CoB_{red}	18	0	N.D.	N.D.

[a] Reaction conditions: 10 mg catalyst, 0.5 mmol substrate, 2 mL EtOH, 200 °C, 3 or 18 hr.

[b] Conversion (X) was measured with GC/MS using hexadecane as the internal standard.

[c] Yield (Y) was measured as above.

[d] N.D. = not detected.

these conditions and can be recycled multiple times without significant loss of either activity or selectivity.

Pretreatment with I-PrOH: Activation of CoB_{oxi} and CoB_{red}

Figure 68 shows the catalytic results of CoB_{oxi} and CoB_{red} with acetophenone, acetovanillone, and guaiacol after pretreatment with i-PrOH at 250 °C for 1 hour, and Table 9 shows the numerical values. Catalytic runs were done at 165 °C for 15 minutes. For acetophenone after catalyst pretreatment, CoB_{oxi} showed 68 ± 4% conversion, 2 ± 1% yield for 1-phenylethanol, 48 ± 3% yield for ethylbenzene, and 10±1% yield for unidentified other products. CoB_{red} showed 100 ± 6% conversion of acetophenone with 102 ± 6% yield for ethylbenzene. Without pretreatment with i-PrOH, CoB_{oxi} showed only 2 ± 1% conversion with 2 ± 1% yield for ethylbenzene, and CoB_{red} showed 85 ± 5% conversion with 37 ± 2% yield for 1-phenylethanol, 26 ± 2% yield for ethylbenzene and 22 ± 2% yield for unidentified other products.

For acetovanillone after catalyst pretreatment, CoB_{oxi} showed 34 ± 2% conversion with 24 ± 2% yield for 4-ethylguaiacol and 11 ± 1% yield for unidentified other products, whereas CoB_{red} showed 61 ± 4% conversion with 50 ± 3% yield for 4-ethylguaiacol. Without pretreatment, CoB_{oxi} showed 2 ± 1% conversion with 2 ± 1% yield for 4-ethylguaiacol and 1 ± 1% yield for unidentified other products, and CoB_{red} showed 17 ± 2% conversion with 14 ± 2% yield for 4-ethylguaiacol.

For guaiacol after catalyst pretreatment, CoB_{oxi} showed 7 ± 1% conversion with 4 ± 1% yield for phenol, and CoB_{red} showed 18 ± 2% conversion with 3 ± 1% yield for phenol and 4 ± 1% yield for cyclohexanol. Without pretreatment, CoB_{oxi} showed 8 ± 1% conversion of guaiacol with 8 ± 1% yield for unidentified other products, and CoB_{red} showed 30 ± 2% conversion with 5 ± 1% yield for phenol, 13 ± 1% yield for cyclohexanol, and 12 ± 1% yield for unidentified other products.

To test whether longer pretreatment time leads to further catalyst activation, CoB_{oxi} and CoB_{red} were then pretreated with i-PrOH for 2 hours and tested for their activity towards conversion of acetophenone (Figure 69). Table 10 shows the numerical values. CoB_{oxi} showed 60 ± 4% conversion with 8 ± 1% yield for 1-phenylethanol, 40 ± 2% yield for ethylbenzene, and 12 ± 1% yield for unidentified other products. CoB_{red} showed 100 ± 6% conversion and 103 ± 6% yield for ethyl benzene. No significant difference in activity was observed after 2 hours of pretreatment instead of only 1 hour. This suggests that either at or before 1 hour of activation, transformation of CoB_{oxi} into the more active form is complete.

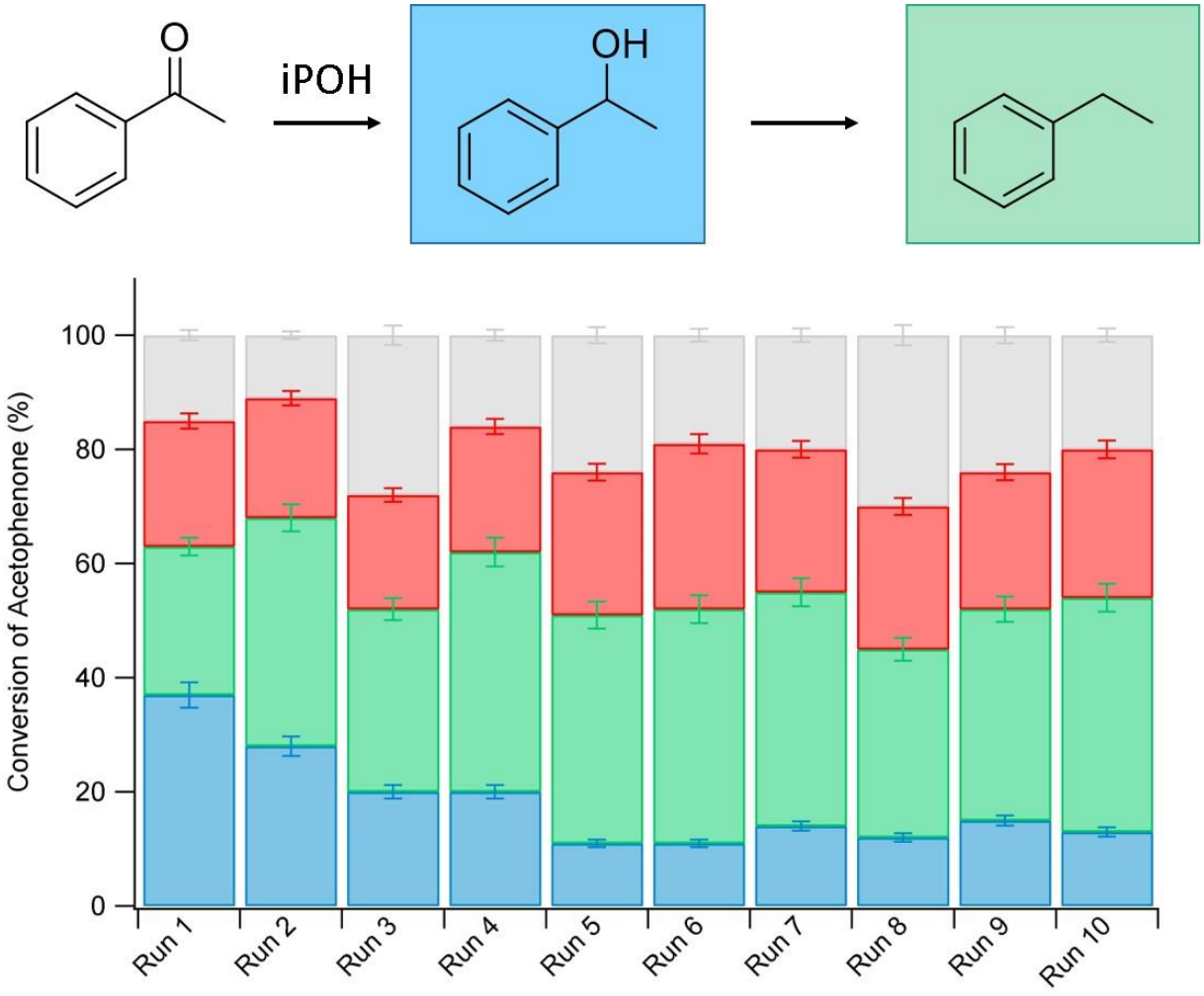
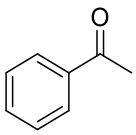
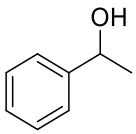
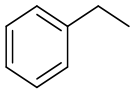


Figure 67. Recycling of CoB_{red} over 10 runs. Conditions: 10 mg catalyst, 0.5 mmol acetophenone, 2 mL i-PrOH, 165 °C, 15 minutes. Numerical values shown in Table 8.

Table 8. Recycling study over 10 runs with CoB_{red} and acetophenone substrate.

Run #[a]	X (%)[b] 	Y (%)[c] 	Y (%) 
1	85 ± 5	37 ± 2	26 ± 2
2	89 ± 5	28 ± 2	40 ± 2
3	72 ± 4	20 ± 2	32 ± 2
4	84 ± 5	20 ± 2	42 ± 2
5	76 ± 5	11 ± 1	40 ± 2
6	81 ± 5	11 ± 1	41 ± 2
7	80 ± 5	14 ± 1	41 ± 2
8	70 ± 4	12 ± 1	33 ± 2
9	76 ± 5	15 ± 1	37 ± 2
10	80 ± 5	13 ± 1	41 ± 2

[a] Reaction conditions: 10 mg CoB_{red}, 0.5 mmol acetophenone, 2 mL i-PrOH, 165 °C.
[b] Conversion (X) was measured with GC/MS using hexadecane as the internal standard.
[c] Yield (Y) was measured as above.

For both CoB_{oxi} and CoB_{red}, activity towards reduction of the carbonyl moiety of acetophenone and acetovanillone increased significantly after pretreatment relative to untreated catalysts. For guaiacol, neither CoB_{oxi} nor CoB_{red} showed increased activity towards conversion of guaiacol after pretreatment. Interestingly, in the case of acetophenone, CoB_{oxi} after activation showed a similar degree of conversion as CoB_{red} without activation, but CoB_{oxi} showed higher selectivity for ethylbenzene, whereas CoB_{red} showed lower selectivity for ethyl benzene but higher selectivity for 1-phenylethanol.

Overall, CoB_{red} after pretreatment shows the highest activity, though both catalysts show significantly increased activity relative to their non-pretreated precursors. One rationale for the observed enhancement in activity is that exposure of CoB_{red} or CoB_{oxi} to i-PrOH at elevated temperatures transforms the surface of both catalysts to a more reduced derivative that is significantly more active towards hydrogenation and hydrodeoxygenation of C=O and C-OH moieties than the more oxidized derivative. Future investigations into the effects of pretreatment will involve use of X-ray photoelectron spectroscopy (XPS), which may allow us to probe and quantify the oxidation states of Co, B, O, and other elements that may be present in the catalysts. This may help us further correlate the role of oxidation states to activity and selectivity for catalysts with and without pretreatment. However, one disadvantage of XPS is that samples frequently must be exposed to air which may make interpretation of the results challenging.

Comparison of CoB_{oxi} and CoB_{red} for Catalysis at 100 °C

Figure 70**,** Figure 71, and Figure 72 show the catalytic results of CoB_{oxi} and CoB_{red} for conversion of acetophenone, acetovanillone, and guaiacol, respectively, at 100 °C for 18 hours with and without pre-activation with i-PrOH. Table 11 shows the numerical values. With activation, CoB_{oxi} showed 93 ± 6% conversion of acetophenone with 44 ± 3% yield for 1-phenylethanol, 32 ± 2% yield for ethylbenzene, and 18 ± 1% yield for unidentified other products. CoB_{red} showed 100 ± 6% conversion of acetophenone with 102 ± 6% yield for ethylbenzene.

Without activation, CoB_{oxi} showed 52 ± 3% conversion of acetophenone with 48 ± 3% yield for 1-phenylethanol, 4 ± 1% yield for ethylbenzene, and 1 ± 1% yield for unidentified other products. CoB_{red} showed 93 ± 6% conversion of acetophenone with 72 ± 4% yield for 1-phenylethanol, 8 ± 1% yield for ethylbenzene, and 14 ± 1% yield for unidentified other products.

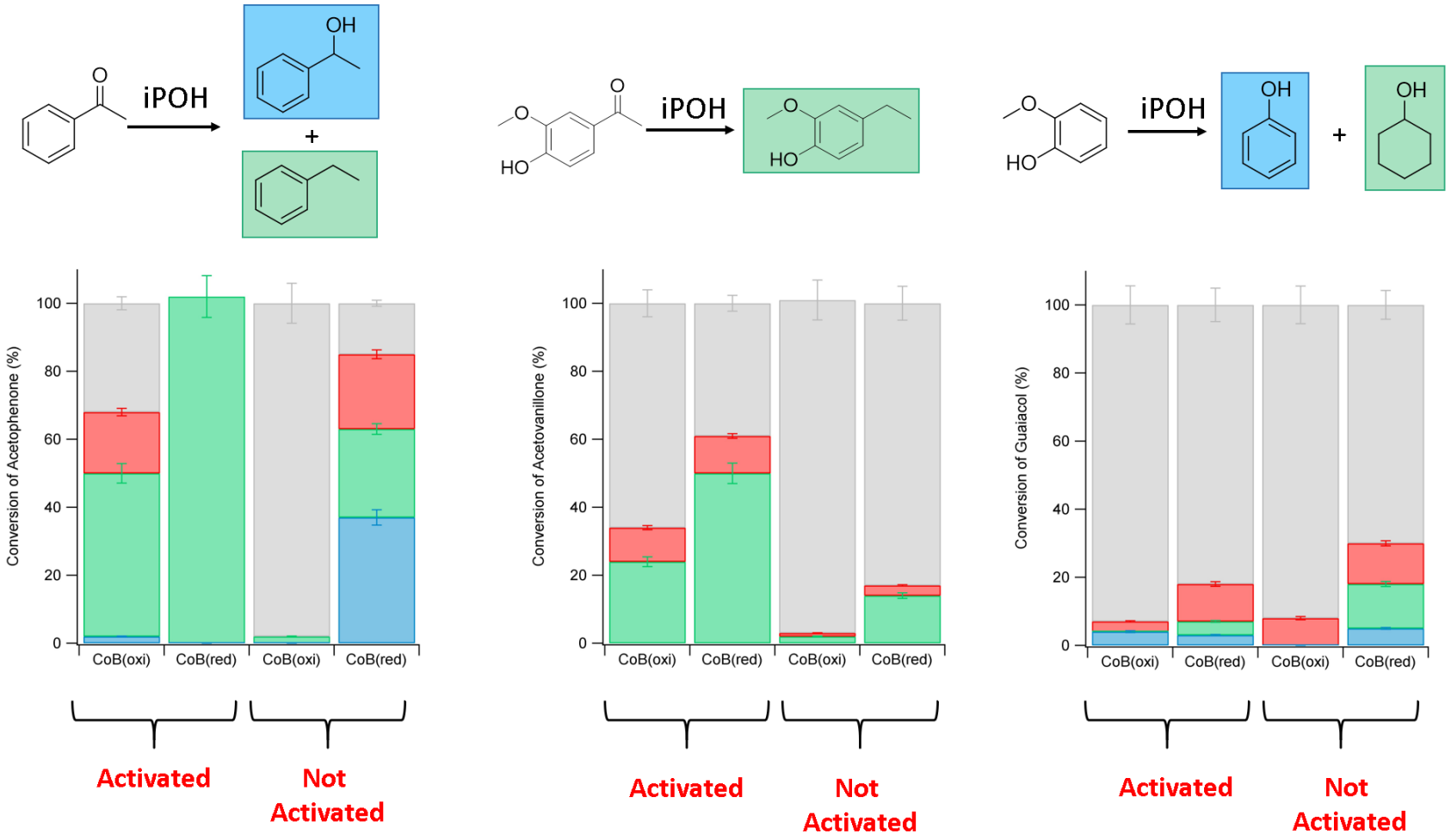
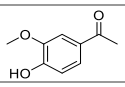
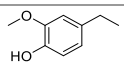
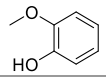


Figure 68. Comparison of CoB_{oxi} and CoB_{red} after activation with isopropanol at 250 °C for 1 hour, and no activation for conversion of acetophenone (left), acetovanillone (middle), and guaiacol (right). Conditions: 10 mg catalyst, 0.5 mmol substrate, 2 mL i-PrOH, 165 °C, 15 minutes. Numerical values shown in Table 9.

Table 9. Comparison of CoB_{oxi} and CoB_{red} with and without pretreatment with i-PrOH.

Catalyst[a,b]	**X (%)**[c] 	**Y (%)**[d] 	**Y (%)** 
CoB_{oxi}	2 ± 1	N.D.[e]	2 ± 1
CoB_{red}	85 ± 5	37 ± 2	26 ± 2
CoB_{oxi}-Activated	68 ± 4	2 ± 1	48 ± 3
CoB_{red}-Activated	100 ± 6	N.D.	102 ± 6
			
CoB_{oxi}	2 ± 1	2 ± 1	
CoB_{red}	17 ± 2	14 ± 2	
CoB_{oxi}-Activated	34 ± 2	24 ± 2	
CoB_{red}-Activated	61 ± 4	50 ± 3	
			
CoB_{oxi}	8 ± 1	8 ± 1	N.D.
CoB_{red}	30 ± 2	5 ± 1	13 ± 1
CoB_{oxi}-Activated	7 ± 1	4 ± 1	N.D.
CoB_{red}-Activated	18 ± 2	3 ± 1	4 ± 1

[a] Activation pretreatment conditions: 10 mg catalyst, 2 mL i-PrOH, 250 °C, 1 hr.

[b] Reaction conditions: 10 mg catalyst, 0.5 mmol substrate, 2 mL i-PrOH, 165 °C, 15 min.

[c] Conversion (X) was measured with GC/MS using hexadecane as the internal standard.

[d] Yield (Y) was measured as above.

[e] N.D. = not detected.

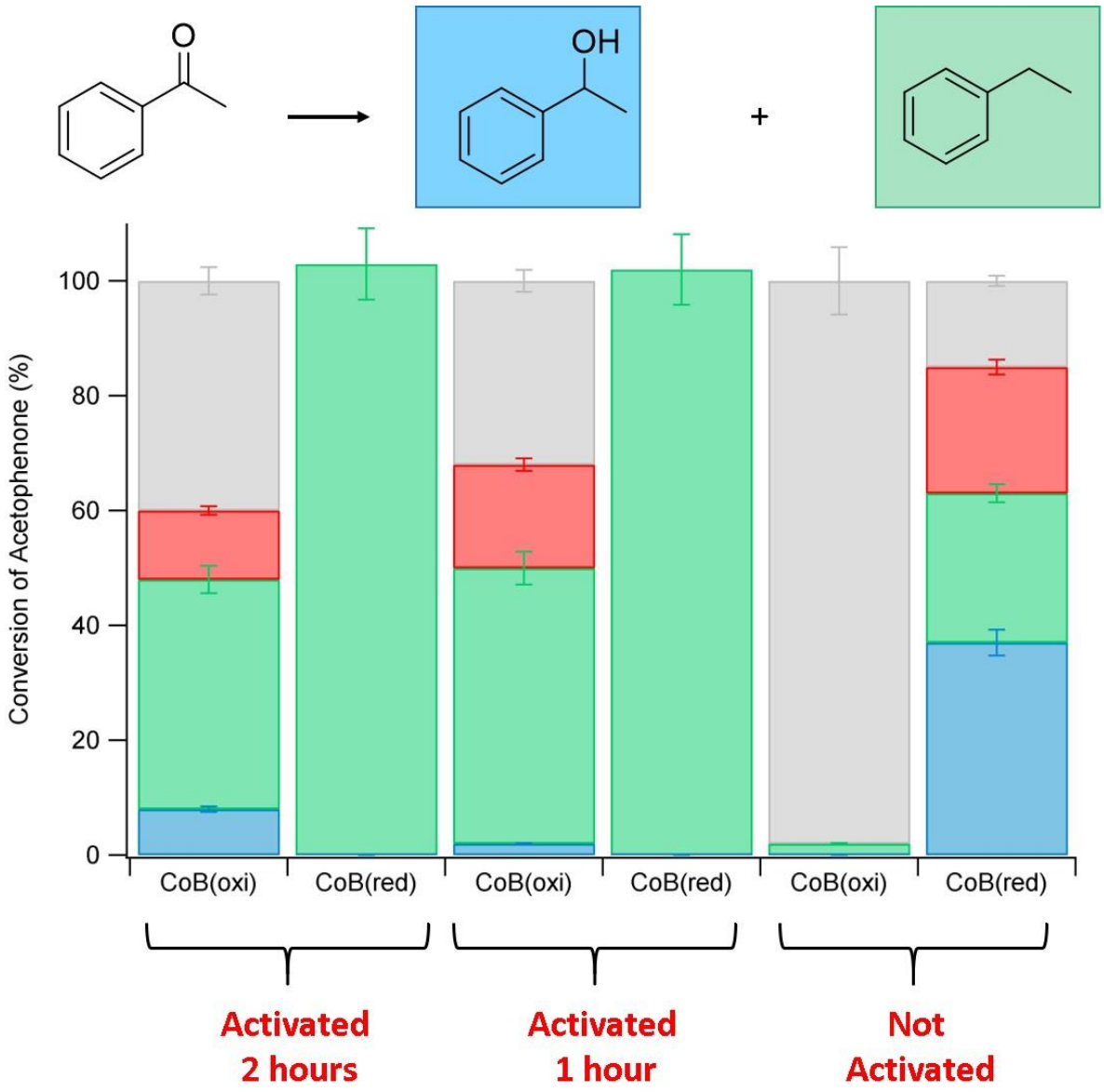


Figure 69. Comparison of activity of CoB_{oxi} and CoB_{red} with acetophenone after 2 hours of pretreatment at 250 °C, 1 hour of pretreatment at 250 °C, and no pretreatment. Catalysis conditions: 10 mg catalyst, 0.5 mmol acetophenone, 2 mL i-PrOH, 165 °C, 15 minutes. Numerical values shown in Table 10.

Table 10. Comparison of CoB_{red} and CoB_{oxi} after 0, 1, and 2 hours of pretreatment with i-PrOH.

Catalyst[a,b]	**Pretreatment time (hr)**	**X (%)**[c] 	**Y (%)**[d] 	**Y (%)** 
CoB_{oxi}	0	2 ± 1	N.D.[e]	2 ± 1
CoB_{red}	0	85 ± 5	37 ± 2	26 ± 2
CoB_{oxi}-Activated	1	68 ± 4	2 ± 1	48 ± 3
CoB_{red}-Activated	1	100 ± 6	N.D.	102 ± 6
CoB_{oxi}-Activated	2	60 ± 4	8 ± 1	40 ± 2
CoB_{red}-Activated	2	100 ± 6	N.D.	103 ± 6

[a] Activation pretreatment conditions: 10 mg catalyst, 2 mL i-PrOH, 250 °C, 1 or 2 hr.

[b] Reaction conditions: 10 mg catalyst, 0.5 mmol substrate, 2 mL i-PrOH, 165 °C, 15 min.

[c] Conversion (X) was measured with GC/MS using hexadecane as the internal standard.

[d] Yield (Y) was measured as above.

[e] N.D. = not detected.

With or without pre-activation, CoB_{oxi} and CoB_{red} show high conversion of acetophenone. After activation, CoB_{oxi} shows lower selectivity for ethylbenzene than CoB_{red} but higher selectivity for 1-phenylethanol. Without activation, CoB_{oxi} and CoB_{red} both showed some conversion, and showed much higher selectivity for 1-phenylethanol than ethylbenzene than the pre-activated catalysts. With activation, both CoB catalysts show higher activity towards deoxygenation to ethylbenzene whereas without activation, high selectivity for 1-phenylethanol is observed. This result shows that the selectivity towards the alcohol or alkyl derivatives in the case of acetophenone is a sensitive function of the activation protocol.

For acetovanillone and without pretreatment, CoB_{red} showed only 2 ± 1% conversion with 3 ± 1% yield for 4-ethylguaiacol, whereas CoB_{oxi} showed 24 ± 1% conversion, 6 ± 1% yield for 4-ethylguaiacol and 18 ± 2% yield for unidentified other products. With activation, both catalysts showed moderate conversion with high selectivity for 4-ethylguaiacol. CoB_{oxi} showed 42 ± 1% conversion with 44 ± 3% yield for 4-ethylguaiacol and CoB_{red} showed 61 ± 4% conversion with 63 ± 4% yield for 4-ethylguaiacol. Finally, for guaiacol, none of the catalysts tested were active for conversion under these conditions.

It is noteworthy that CoB_{oxi} shows activity for ketone reduction under these conditions whereas in previous studies in which reactions were conducted in only 15 minutes, little or no activity was observed. This is true for both EtOH and i-PrOH as H-donors when reactions were run over long time periods. A simple rationale for the observed difference in activity is that the necessary removal of a catalytically inactive surface oxide layer occurs, which exposes a catalytically active surface.

Comparison with Other Heterogeneous Cobalt Catalysts for Reduction of Acetophenone

Finally, CoB catalysts were compared to a few other heterogeneous Co catalysts reported in the literature for reduction of C=O groups. Table 12 shows comparisons of the catalysts based on time, temperature, conversion, and yields. Many reported catalysts generally require either addition of KOH to promote transfer hydrogenation or used molecular H_2 as the hydrogen source. Further, with one exception none of the catalysts compared contain precious metals. For comparison of CoB catalysts, acetophenone is used for comparing CoB with the other catalysts. Most CoB catalysts exhibit comparable yields to those of several other heterogeneous Co catalysts reported in the literature after reaction over the specified times and temperatures. CoB_{red} in particular shows the highest yields for C=O reduction products without the addition of base.

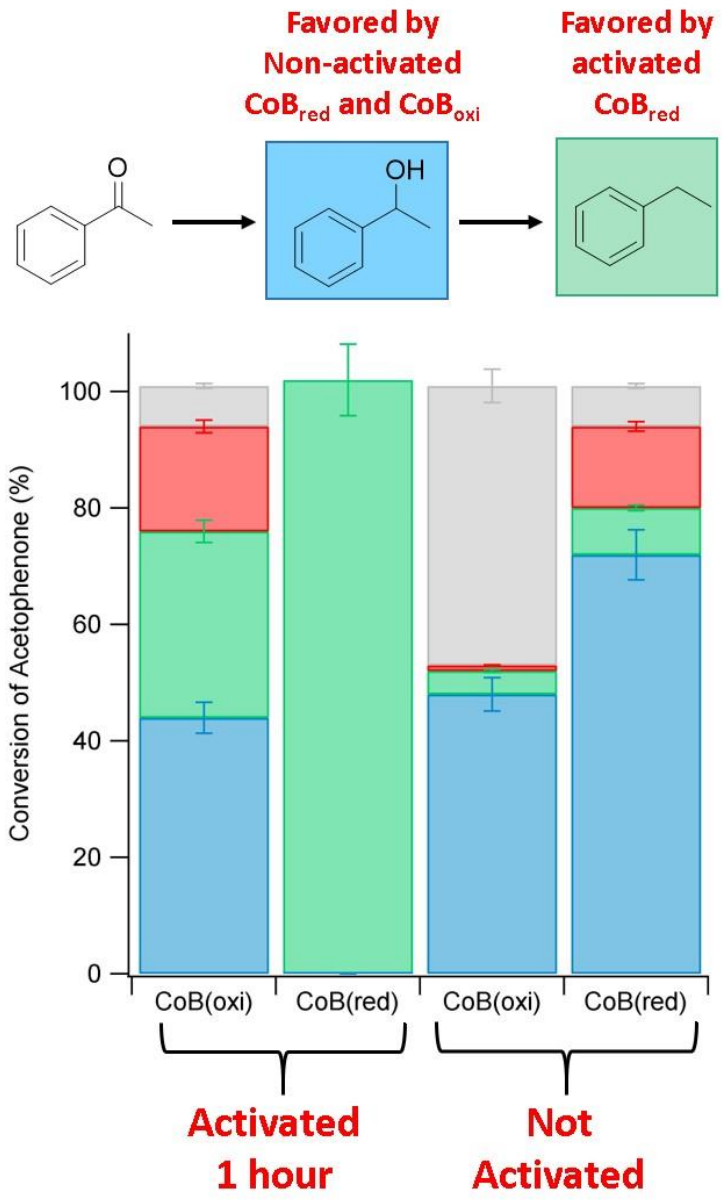


Figure 70. Comparison of CoB_{oxi} and CoB_{red} for conversion of acetophenone with and without pre-activation with isopropanol. Catalysis conditions: 10 mg catalyst, 0.5 mmol acetophenone, 2 mL i-PrOH, 100 °C, 18 hours. Numerical values shown in Table 11.

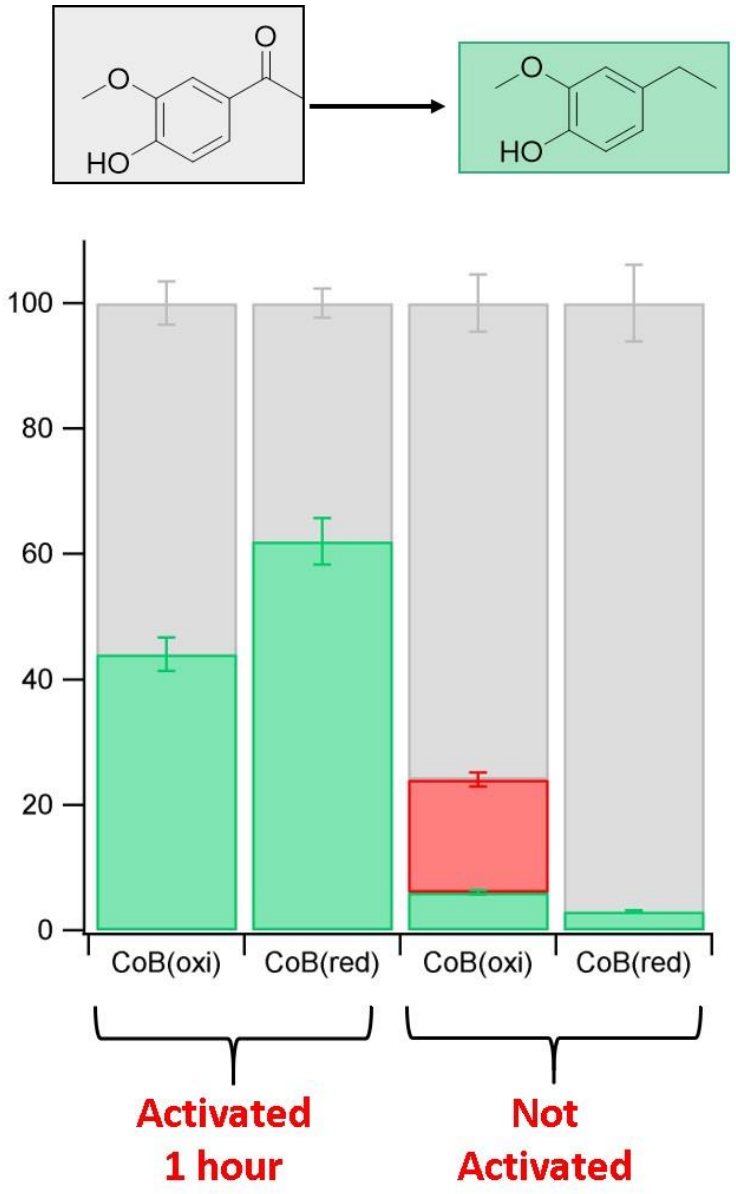


Figure 71. Comparison of CoB_{oxi} and CoB_{red} for conversion of acetovanillone with and without pre-activation with isopropanol. Catalysis conditions: 10 mg catalyst, 0.5 mmol acetovanillone, 2 mL i-PrOH, 100 °C, 18 hours. Numerical values shown in Table 11.

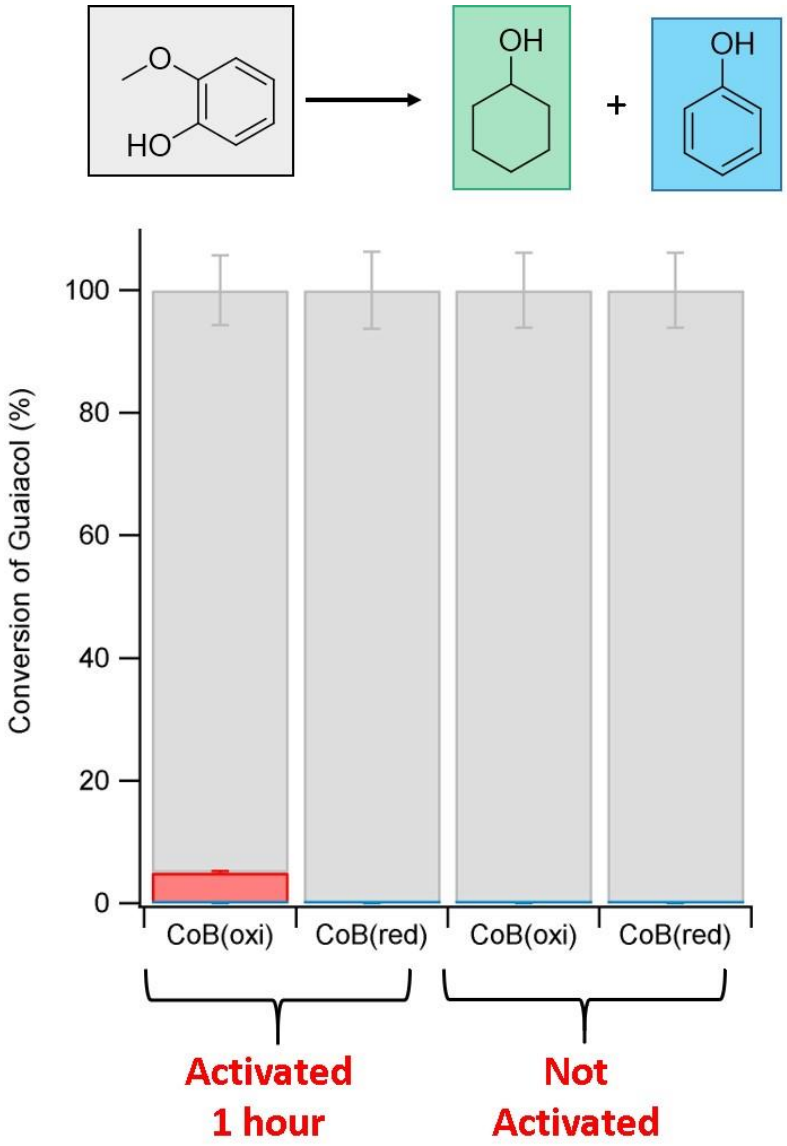
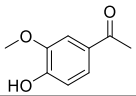
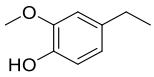
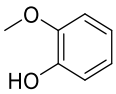


Figure 72. Comparison of CoB_{oxi} and CoB_{red} for conversion of guaiacol with and without pre-activation with isopropanol. Catalysis conditions: 10 mg catalyst, 0.5 mmol guaiacol, 2 mL i-PrOH, 100 °C, 18 hours. Numerical values shown in Table 11.

Table 11. Comparison of CoB_{red} and CoB_{oxi} with acetophenone, acetovanillone, and guaiacol at 100 °C with and without pretreatment with i-PrOH.

Catalyst[a,b]	**X (%)**[c] 	**Y (%)**[d] 	**Y (%)** 
CoB_{oxi}	52 ± 3	48 ± 3	1 ± 1
CoB_{red}	93 ± 6	72 ± 4	8 ± 1
CoB_{oxi}-Activated	93 ± 6	44 ± 3	32 ± 2
CoB_{red}-Activated	100 ± 6	N.D.[e]	102 ± 6
			
CoB_{oxi}	24 ± 1	6 ± 1	
CoB_{red}	2 ± 1	3 ± 1	
CoB_{oxi}-Activated	42 ± 1	44 ± 3	
CoB_{red}-Activated	61 ± 4	63 ± 4	
			
CoB_{oxi}	-1 ± 1	N.D.	N.D.
CoB_{red}	-1 ± 1	N.D.	N.D.
CoB_{oxi}-Activated	4 ± 1	N.D.	N.D.
CoB_{red}-Activated	0	N.D.	N.D.

[a] Activation pretreatment conditions: 10 mg catalyst, 2 mL i-PrOH, 250 °C, 1 hr.
[b] Reaction conditions: 10 mg catalyst, 0.5 mmol substrate, 2 mL i-PrOH, 100 °C, 18 hr.
[c] Conversion (X) was measured with GC/MS using hexadecane as the internal standard.
[d] Yield (Y) was measured as above.
[e] N.D. = not detected.

Here it was also demonstrated that CoB_{red} is highly selective for carbonyl reduction using EtOH as the H-donor instead of i-PrOH, although higher temperatures and reaction times were required to promote conversion. It was also demonstrated that the selectivity for conversion of acetophenone to either 1-phenylethanol or ethylbenzene can be tuned by pretreating the catalysts with i-PrOH as described before. It is possible that this pretreatment strategy could be used with other catalysts as well as a simple strategy for tuning activity and selectivity. Use of the i-PrOH pretreatment strategy is not necessarily limited to the CoB catalysts in this work and could feasibly be utilized with other catalysts to modify their catalytic properties.

Chapter Summary

Two types of CoB catalysts were synthesized by facile aqueous reduction of Co^{2+} with BH_4^-. Figure 73 shows a flow chart summarizing all CoB catalysts that were synthesized and studed in this work. The as-synthesized CoB catalyst was partitioned into two batches: one that was stored in an inert atmosphere glovebox to prevent oxidation by ambient air, (CoB_{red}) and one which was removed from the glovebox and allowed to oxidize in the presence of air (CoB_{oxi}). CoB_{red} and CoB_{oxi} were then compared with Co powder and the catalyst-free blank for their catalytic efficiency towards reduction of acetophenone, acetovanillone, and guaiacol. The reactions were run at 300 °C, 200 °C, and 165 °C for 15 min.

Characterization of CoB_{oxi} and CoB_{red} revealed that the materials consist of aggregated amorphous nanoparticles comprised of a relatively uniform mixture of Co and B with atomic ratios of $Co_{1.7}BO_{1.7}$ and $Co_{1.7}B$, respectively. The catalysts were also characterized post-reaction. PXRD did not reveal significant differences of CoB_{oxi} or CoB_{red} after reaction compared to their as-synthesized counterparts. TEM images of pre- and post-reaction catalysts for both CoB_{oxi} and CoB_{red} showed evidence of crystalline Co and Co_3O_4, though it is unclear what role, if any, these phases play in catalysis. EDX revealed however that the elemental distribution of Co and B remains the same before and after catalysis.

At 300 °C the non-catalyzed conversion of substrate to products occurs in some cases, thus activity studies were done at lower temperatures. A series of blanks and controls were also tested at 200 °C for 15 min with only acetophenone as the substrate. None of the controls showed conversion under these conditions, which reveals the unique catalytic properties of the CoB catalysts. CoB_{red} was shown to be the most active catalyst in all cases, showing high conversion of substrate as low as 165 °C in 15 minutes. In most cases CoB_{red} and CoB_{oxi} both showed high selectivity for carbonyl reduction in the

Table 12. Comparison of CoB catalysts in this work with some other reported heterogeneous Co catalysts for reduction of C=O bonds.

Catalyst	H-source	Solvent	Base	Time (h)	T (°C)	Yield (%)	Ref.
Co NPs@HCC	i-PrOH	i-PrOH	KOH	18	90	72-98	78
$Pd_{36}Co_{64}$@HCC	i-PrOH	i-PrOH	KOH	10	90	92-99	100
CoHMA	i-PrOH	i-PrOH	KOH	1.5-5	83	67-96	101
Co@C-N-900-15h	i-PrOH	i-PrOH	-	12-60	80-100	95-99	76
([$Co(OAc)_2$/Phen@ α-Al_2O_3]-800	H_2 (15-40 bar)	EtOH	-	15-20	100-130	60-99	74
Co@$P123_{0.8}$	H_2 (10 bar)	Hexane	-	23	120	94	75
Co-Cu/SBA-15	H_2 (20 bar)	i-PrOH	-	4	170	62-80	102
CoB_{oxi}[b]	i-PrOH	i-PrOH	-	18	100	48[c] (4[d])	This work
CoB_{red}[b]	i-PrOH	i-PrOH	-	18	100	72[c] (8[d])	This work
CoB_{oxi}-activated[b]	i-PrOH	i-PrOH	-	18	100	44[c] (32[d])	This work
CoB_{red}-activated[b]	i-PrOH	i-PrOH	-	18	100	0[c] (102[d])	This work
CoB_{oxi}[b]	EtOH	EtOH	-	18	200	0[c] (38)[d]	This work
CoB_{red}[b]	EtOH	EtOH	-	18	200	0[c] (96)[d]	This work

[a] Activity reported as turnover numbers (TON).

[b] Catalytic data derived from conversion of acetophenone to 1-phenylethanol and ethylbenzene.

[c]Yield corresponds to 1-phenylethanol.

[d]Yield corresponds to ethylbenzene.

cases of acetophenone and acetovanillone, whereas reduction of guaiacol readily produced the demethoxylated and ring-saturated derivatives.

It was also observed that 4-ethylguaiacol, which differs from guaiacol by possessing an ethyl moiety in the para-position to the phenol hydroxyl group, did not show conversion at 200 °C, whereas a significant amount of guaiacol was converted under the same conditions. This suggests that the ethyl substituent hinders the demethoxylation and ring hydrogenation steps, possibly by hindering adsorption of the molecule to the surface.

CoB_{oxi} and CoB_{red} were also tested for their catalytic performance using EtOH as an H-donor. The conditions used were 200 °C for 3 and 18 hours. After 3 hours, low conversion was observed for all three substrates for CoB_{red}, whereas CoB_{oxi} showed no conversion. After 18 hours with CoB_{red}, acetophenone and acetovanillone were quantitatively converted to ethylbenzene and 4-ethylguaiacol, respectively, whereas guaiacol showed no significant conversion. CoB_{oxi} also exhibited high conversion but was significantly less selective in all cases. For EtOH as the H-donor, high selectivity for carbonyl reduction without demethoxylation or aromatic ring hydrogenation was observed. These results highlight the potential of CoB_{red} and EtOH as a more selective H-donor for carbonyl reduction.

Investigations into the pre-activation of CoB_{oxi} and CoB_{red} showed that the activities of both catalysts can be significantly enhanced by pretreatment with neat i-PrOH at 250 °C for 1 hour. After treatment, both catalysts showed significantly higher activity than their respective non-activated counterparts. CoB_{red} after activation was the most active catalyst among all catalysts tested. To test whether longer activation times would lead to even more active catalysts, the catalysts were activated at 250 °C for 2 hours and compared for their activity for conversion of acetophenone. At either 1 hour or 2 hour activation, both catalysts appear to perform similarly, thus indicating that activation is complete either at or before 1 hour. These results reveals that, although the activity of CoB_{oxi} is significantly lower than CoB_{red}, CoB_{oxi} can be transformed into a much more active catalyst by the pretreatment protocol, and does not need to be stored under air-free conditions.

Finally, the catalytic activity of CoB_{red} and CoB_{oxi}, both activated and not activated, for conversion of acetophenone, acetovanillone, and guaiacol at 100 °C for 18 hours was compared. For acetophenone, all catalysts showed high conversion over the timeframe. However their selectivities differed significantly in several cases. For activated CoB_{oxi}, lower selectivity for ethylbenzene was observed compared to CoB_{red}, which showed complete conversion to ethylbenzene. Activated CoB_{oxi} exhibited higher selectivity for 1-phenylethanol. In both non-activated cases, high conversion was

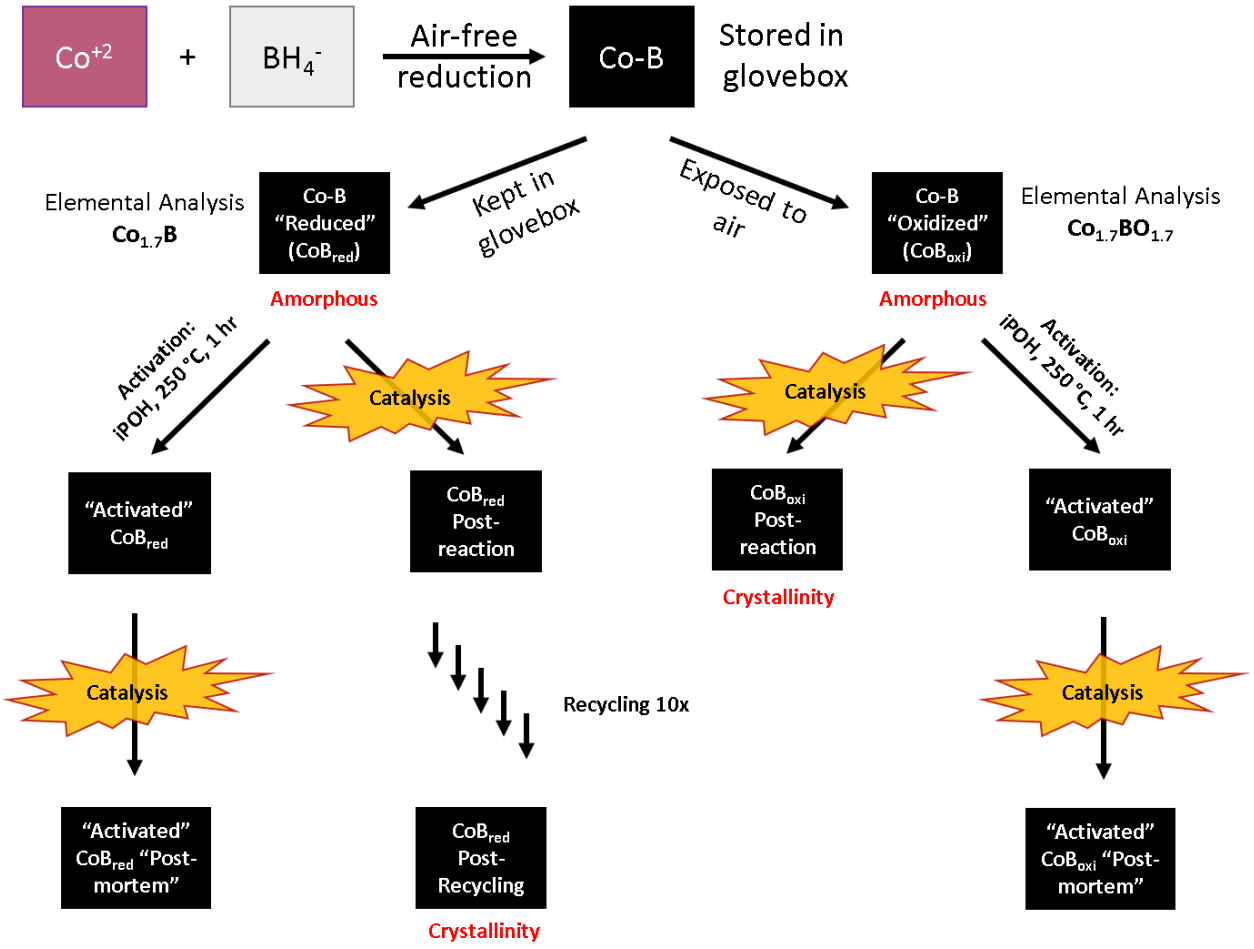


Figure 73. Flow-chart summary of CoB catalysts that were studied in this work. Red text indicates which samples were amorphous and which samples showed crystalline features as determined by TEM.

observed, but with low selectivity for ethylbenzene, with near quantitative selectivity for 1-phenylethanol. These results reveal that the selectivity of CoB catalysts can be tuned by the pretreatment protocol in the case of acetophenone. For acetovanillone, low conversion was observed for the non-activated catalysts whereas moderate conversion was observed in the activated cases with high selectivity for 4-ethylguaiacol. For guaiacol, none of the catalysts were active for its conversion.Chapter 5. Conclusions and Future Work

General Conclusions

This work described the synthesis, characterization, and reactivity of boron-containing cobalt catalysts for catalytic transfer hydrogenation. This work was performed in the interest of developing inexpensive, earth-abundant catalysts for catalytic transfer hydrogenation of several model compounds containing lignin-relevant reducible moieties. CoB catalysts can be rapidly synthesized on large scale and are active and selective for reduction of C=O groups in the cases of acetophenone and acetovanillone using i-PrOH as the H-donor. Using CoB_{red} with EtOH as the H-donor also revealed that CoB_{red} is quantitatively selective for carbonyl reduction without reduction of the aromatic rings, even in the case of guaiacol, though higher temperatures and longer reaction times are required as compared to using i-PrOH as the H-donor. The activation protocol in which catalysts are exposed to i-PrOH under reducing conditions leads to more active catalysts for C=O reduction for both CoB_{oxi} and CoB_{red}, which suggests that the active site(s) may be more reduced surface species. Further, the selectivity of the catalysts is tunable in the case of acetophenone by use of the pretreatment protocol. These results reveal the potential for CoB materials as efficient earth-abundant and green catalysts for applications in transfer hydrogenolysis reactions and lignin upgrading.

Future Work

The Role of Oxidation States in Catalysis: X-Ray Photoelectron Spectroscopy (XPS)

Initial catalytic screening revealed that CoB_{red} is unanimously the most active species for reduction of the putative substrates described in this work. Exposure of CoB_{red} to air to form CoB_{oxi} clearly results in a dramatic drop in activity, which is likely due to formation of more inert oxide species on the surface. A simple rationale is that lower valent surface species such as Co(0) or Co(I) are ultimately responsible for the transformations observed. The oxidation states of each element present in each catalyst, CoB_{oxi}, CoB_{red}, activated CoB_{oxi}, and activated CoB_{red}, could be revealed using XPS which would allow us to correlate oxidation state to activity and selectivity. This technique would also be used

in tandem with gas chemisorption techniques, in gas-phase probe molecules are adsorbed to the catalyst surface to determine, for example, the number of reduced, basic, or acidic catalytic sites. This information would further reveal the nature of the active site(s).

The Role of Boron in Catalysis

As previously mentioned, although boron is present in all CoB catalysts, it is still unclear whether it plays a role (if any) in catalysis. However, several reports in the literature have indicated that boron can help protect the catalysts from sulfur poisoning. Li *et. al.*[103] compared the effects of sulfur poisoning on TiO_2-supported Co (Co/TiO_2) catalysts with and without modification with boron. Their results show that by adding 0.1 wt% B, only 35% of activity was lost in the presence of 500 ppm sulfur as opposed to 80% activity loss for Fischer-Tropsch reactions, and the addition of B did not itself impede activity. Wang *et.*[104] *al.* also demonstrated that SiO_2-supported boron-containing Ni catalysts (NiB/SiO_2) are much more sulfur resistant than the analogous catalysts without boron. Thus, it may be important to perform poisoning studies with catalysts that do and do not contain boron.

Counting the Active Sites: Gas Chemisorption Analysis

A common strategy to characterize active sites involves *gas chemisorption*, in which catalyst material is exposed to probe gases such as CO, CO_2, NH_3 which bind to surface atoms, as opposed to *physisorption* where gas molecules weakly interact with the surface *via* dispersive forces. Each of these gases are strongly adsorbing molecules and can be used to quantify different types of surface sites. CO can be used to determine the number of reduced metal surface sites, CO_2 is often used to probe surface basic sites, and NH_3 is often used to probe surface acid sites. Once the number of active sites is determined, important parameters such as turnover frequencies can be determined.

Catalytic turnover frequencies are important parameters for evaluating catalytic efficiency. Catalytic turnovers are typically calculated by taking the ratio of the number of moles of active site with the number of moles of substrate that was converted per unit of time. However, one of the major challenges in heterogeneous catalysis is that determining the exact number of active sites is difficult and often not possible. For this reason, as is frequently done in heterogeneous catalysis, the catalytic activities of the materials in this work were compared by showing the amounts of substrate converted under identical reaction conditions on a per-weight basis of catalyst. However, while this simplified strategy is useful for preliminary comparisons of catalysts, it is not necessarily indicative of the number of active sites present on each catalyst surface.

For example, CoB_{red} was shown to be more active than CoB_{oxi} in all cases. This may be due to the possibility that CoB_{red} simply possesses a greater number of active sites on its surface than CoB_{oxi}. Another possibility is that CoB_{red} and CoB_{oxi} possess *different* active sites, such that the active sites present on CoB_{red} are more active than those present on CoB_{oxi}. A third explanation is a combination of these two possibilities.

Other Chemical Transformations

Though the focus of this work was on transfer hydrogenation reactions in the context of lignin upgrading, CoB catalysts are not necessarily limited to only the substrates and functional group transformations described in this work. Thus, it would be pertinent to explore other possible CTH transformations that could enhance the chemist's synthetic toolbox. One example is the reduction of amide groups. Amide reduction is conventionally mediated by reactive metal hydrides such as lithium aluminum hydride (LAH) or promoted through catalytic hydrogenation at elevated temperatures and pressures. An analogous reaction is reduction of an ester to an ether.

Continuous Flow Reactor

In this work, catalytic studies were carried out using batch reactors because they are inexpensive, easily assembled, disassembled and cleaned, and allow for rapid catalyst screening. However, batch systems generally do not out allow reactions to be monitored *in situ*. Changing conditions such as reagent concentrations or catalyst evolution in the batch reactor as the reaction progresses may also obfuscate information on the inherent kinetics of the catalyst. For these reasons, continuous flow reactors are generally preferable for kinetic analysis. Although continuous flow systems are much more operationally complex than batch reactors, they allow reactions to be continuously monitored *in situ*. Further, they allow for steady-state conditions in which the temperature, pressure, and initial substrate concentrations are kept constant over the course of the reaction.

Attacking Lignin: Evaluating CoB Catalysts with Real Lignin Feedstocks

As described in Chapter 2, future work will involve upgrading lignin by combining flow reactor technology and the aldehyde protection strategy with catalytic transfer hydrogenation. This strategy combines the advantages of flow reactors with transfer hydrogenation, which does not require the addition of exogenous hydrogen gas to promote hydrogenolysis reactions.

Nanocrystalline Metal Borides

This work focused on the preparation of amorphous boron-containing materials for transfer hydrogenation applications. However, while these materials are efficient catalysts, their amorphous nature obfuscates elucidation of the active site(s), as characterizing amorphous materials is difficult. Post-catalysis TEM analysis of these catalysts showed formation of crystalline domains, which may provide clues to the nature of the active site. However, it is still unclear what role (if any) these crystalline domains play in catalysis. What phases are they comprised of, and do they hinder or enhance activity, or are the domains catalytically inert? Answering these questions for amorphous materials is a formidable challenge. Thus, investigations of nanocrystalline to study their catalytic properties have been initiated. Crystalline materials are generally easier to characterize than amorphous materials, as crystal structures can be determined using X-ray crystallographic techniques.

Crystalline borides are often synthesized by reacting the metal or metal oxide precursor with elemental boron at extremely high (>1000 °C) temperatures, but these temperatures can result in material annealing which leads to macroscopic, low-surface area materials. Routes toward nanocrystalline metal borides have been brought to light in recent years.[85] Our group has recently begun synthesizing nanocrystalline metal borides using a salt flux method developed by Portehault *et. al.*[105] In this method, a metal chloride and sodium borohydride are thoroughly mixed together in a eutectic salt mixture and heated to >800 °C under air-free conditions. The authors successfully synthesized nano-sized Nb, Hf, Ce, Mo, Fe, and Mn borides. Thus, investigations are now underway using this salt flux strategy to create Co borides and investigate their catalytic properties, and to aid investigations into the nature of the catalytic active site.

References

1 Hsu, C. S. & Robinson, P. R. Practical advances in petroleum processing. (2006).
2 Zeng, F. & Hohn, K. L. Modeling of three-way catalytic converter performance with exhaust mixture from natural gas-fueled engines. *Appl Catal B-Environ* **182**, 570-579, doi:10.1016/j.apcatb.2015.10.004 (2016).
3 Koltsakis, G. C. & Stamatelos, A. M. Catalytic automotive exhaust aftertreatment. *Prog Energ Combust* **23**, 1-39, doi:Doi 10.1016/S0360-1285(97)00003-8 (1997).
4 Vengosh, A., Jackson, R. B., Warner, N., Darrah, T. H. & Kondash, A. A Critical Review of the Risks to Water Resources from Unconventional Shale Gas Development and Hydraulic Fracturing in the United States. *Environ Sci Technol* **48**, 8334-8348, doi:10.1021/es405118y (2014).
5 Albrecht, M. & van Koten, G. Platinum group organometallics based on "Pincer" complexes: Sensors, switches, and catalysts. *Angew Chem Int Edit* **40**, 3750-3781, doi:Doi 10.1002/1521-3773(20011015)40:20<3750::Aid-Anie3750>3.3.Co;2-Y (2001).
6 Phan, C. M. & Nguyen, H. M. Role of Capping Agent in Wet Synthesis of Nanoparticles. *J Phys Chem A* **121**, 3213-3219, doi:10.1021/acs.jpca.7b02186 (2017).
7 Finney, E. E. & Finke, R. G. Nanocluster nucleation and growth kinetic and mechanistic studies: A review emphasizing transition-metal nanoclusters. *J Colloid Interf Sci* **317**, 351-374, doi:10.1016/j.jcis.2007.05.092 (2008).
8 Lamer, V. K. Nucleation in Phase Transitions. *Ind Eng Chem* **44**, 1270-1277 (1952).
9 Thanh, N. T. K., Maclean, N. & Mahiddine, S. Mechanisms of Nucleation and Growth of Nanoparticles in Solution. *Chem Rev* **114**, 7610-7630, doi:10.1021/cr400544s (2014).
10 Shan, W. J. *et al.* Oxidative steam reforming of methanol on Ce0.9Cu0.1OY catalysts prepared by deposition-precipitation, coprecipitation, and complexation-combustion methods. *J Catal* **228**, 206-217, doi:10.1016/j.jcat.2004.07.010 (2004).
11 Klein, L. C. & Garvey, G. J. Kinetics of the Sol-Gel Transition. *J Non-Cryst Solids* **38-9**, 45-50, doi:Doi 10.1016/0022-3093(80)90392-0 (1980).
12 Narula, C. K., Rokosz, M., Allard, L. F., Kudla, R. J. & Chattha, M. S. Sol-gel processed silica-alumina materials for diesel engine emission reduction catalysts. *Langmuir* **16**, 3818-3822, doi:DOI 10.1021/la991090s (2000).
13 Delattre, L. & Babonneau, F. O-17 solution NMR characterization of the preparation of sol-gel derived SiO2/TiO2 and SiO2/ZrO2 glasses. *Chem Mater* **9**, 2385-2394, doi:DOI 10.1021/cm970372f (1997).
14 Vioux, A. Nonhydrolytic sol-gel routes to oxides. *Chem Mater* **9**, 2292-2299, doi:DOI 10.1021/cm970322a (1997).
15 Styskalik, A., Skoda, D., Barnes, C. E. & Pinkas, J. The Power of Non-Hydrolytic Sol-Gel Chemistry: A Review. *Catalysts* **7**, doi:ARTN 16810.3390/catal7060168 (2017).
16 Arnal, P., Corriu, R. J. P., Leclercq, D., Mutin, P. H. & Vioux, A. Preparation of anatase, brookite and rutile at low temperature by non-hydrolytic sol-gel methods. *J Mater Chem* **6**, 1925-1932, doi:DOI 10.1039/jm9960601925 (1996).
17 Joo, J., Kwon, S. G., Yu, J. H. & Hyeon, T. Synthesis of ZnO nanocrystals with cone, hexagonal cone, and rod shapes via non-hydrolytic ester elimination sol-gel reactions. *Adv Mater* **17**, 1873-+, doi:10.1002/adma.200402109 (2005).
18 Hayashi, H. & Hakuta, Y. Hydrothermal Synthesis of Metal Oxide Nanoparticles in Supercritical Water. *Materials* **3**, 3794-3817, doi:10.3390/ma3073794 (2010).
19 Vogt, E. T. C. & Weckhuysen, B. M. Fluid catalytic cracking: recent developments on the grand old lady of zeolite catalysis. *Chem Soc Rev* **44**, 7342-7370, doi:10.1039/c5cs00376h (2015).
20 Ennaert, T. *et al.* Potential and challenges of zeolite chemistry in the catalytic conversion of biomass. *Chem Soc Rev* **45**, 584-611, doi:10.1039/c5cs00859j (2016).

21 Ghasemi, Z., Sourinejad, I., Kazemian, H. & Rohani, S. Application of zeolites in aquaculture industry: a review. *Rev Aquacult* **10**, 75-95, doi:10.1111/raq.12148 (2018).
22 Franus, M., Wdowin, M., Bandura, L. & Franus, W. Removal of Environmental Pollutions Using Zeolites from Fly Ash: A Review. *Fresen Environ Bull* **24**, 854-866 (2015).
23 Ozekmekci, M., Salkic, G. & Fellah, M. F. Use of zeolites for the removal of H2S: A mini-review. *Fuel Process Technol* **139**, 49-60, doi:10.1016/j.fuproc.2015.08.015 (2015).
24 Cundy, C. S. & Cox, P. A. The hydrothermal synthesis of zeolites: Precursors, intermediates and reaction mechanism. *Micropor Mesopor Mat* **82**, 1-78, doi:10.1016/j.micromeso.2005.02.016 (2005).
25 Cundy, C. S. & Cox, P. A. The hydrothermal synthesis of zeolites: History and development from the earliest days to the present time. *Chem Rev* **103**, 663-701, doi:10.1021/cr020060i (2003).
26 Caputo, D., Liguori, B. & Colella, C. Some advances in understanding the pozzolanic activity of zeolites: The effect of zeolite structure. *Cement Concrete Comp* **30**, 455-462, doi:10.1016/j.cemconcomp.2007.08.004 (2008).
27 Csicsery, S. M. Shape Selective Catalysis in Zeolites. *Chem Brit* **21**, 473-& (1985).
28 Ross, J. (Elsevier).
29 Argyle, M. D. & Bartholomew, C. H. Heterogeneous Catalyst Deactivation and Regeneration: A Review. *Catalysts* **5**, 145-269, doi:10.3390/catal5010145 (2015).
30 Bradley, M. K., Woodruff, D. P. & Robinson, J. Adsorbate-induced surface stress, surface strain and surface reconstruction: S on Cu(100) and Ni(100). *Surf Sci* **613**, 21-27, doi:10.1016/j.susc.2013.02.018 (2013).
31 Grossmann, A., Erley, W. & Ibach, H. Adsorbate-Induced Surface Stress and Surface Reconstruction - Oxygen, Sulfur and Carbon on Ni(111). *Surf Sci* **337**, 183-189, doi:Doi 10.1016/0039-6028(95)00615-X (1995).
32 Bartholomew, C. H. Mechanisms of catalyst deactivation. *Appl Catal a-Gen* **212**, 17-60, doi:Doi 10.1016/S0926-860x(00)00843-7 (2001).
33 Xie, J. *et al.* Size and Promoter Effects in Supported Iron Fischer-Tropsch Catalysts: Insights from Experiment and Theory. *Acs Catal* **6**, 3147-3157, doi:10.1021/acscatal.6b00131 (2016).
34 Shen, W. M., Dumesic, J. A. & Hill, C. G. Criteria for Stable Ni Particle-Size under Methanation Reaction Conditions - Nickel Transport and Particle-Size Growth Via Nickel Carbonyl. *J Catal* **68**, 152-165, doi:Doi 10.1016/0021-9517(81)90048-8 (1981).
35 Bartholomew, C. H. Reduction of Nitric-Oxide by Monolithic-Supported Palladium-Nickel and Palladium-Ruthenium Alloys. *Ind Eng Chem Prod Rd* **14**, 29-33, doi:DOI 10.1021/i360053a006 (1975).
36 Abbet, S. *et al.* Acetylene cyclotrimerization on supported size-selected Pd-n clusters (1 <= n <= 30): one atom is enough! *J Am Chem Soc* **122**, 3453-3457, doi:DOI 10.1021/ja9922476 (2000).
37 Hlatky, G. G. Heterogeneous single-site catalysts for olefin polymerization. *Chem Rev* **100**, 1347-1376, doi:DOI 10.1021/cr9902401 (2000).
38 McKeown, N. B. & Budd, P. M. Exploitation of Intrinsic Microporosity in Polymer-Based Materials. *Macromolecules* **43**, 5163-5176, doi:10.1021/ma1006396 (2010).
39 Sun, Q., Dai, Z. F., Meng, X. J. & Xiao, F. S. Porous polymer catalysts with hierarchical structures. *Chem Soc Rev* **44**, 6018-6034, doi:10.1039/c5cs00198f (2015).
40 Sun, Q., Dai, Z. F., Meng, X. J., Wang, L. & Xiao, F. S. Task-Specific Design of Porous Polymer Heterogeneous Catalysts beyond Homogeneous Counterparts. *Acs Catal* **5**, 4556-4567, doi:10.1021/acscatal.5b00757 (2015).
41 Liu, F. J., Kong, W. P., Qi, C. Z., Zhu, L. F. & Xiao, F. S. Design and Synthesis of Mesoporous Polymer-Based Solid Acid Catalysts with Excellent Hydrophobicity and Extraordinary Catalytic Activity. *Acs Catal* **2**, 565-572, doi:10.1021/cs200613p (2012).

42 Li, G. Z., Wang, L. C., Ni, H. L. & Pittman, C. U. Polyhedral oligomeric silsesquioxane (POSS) polymers and copolymers: A review. *J Inorg Organomet P* **11**, 123-154, doi:Unsp 1053-0495/01/0900-0123/0Doi 10.1023/A:1015287910502 (2001).

43 Haddad, T. S., Viers, B. D. & Phillips, S. H. Polyhedral oligomeric silsesquioxane (POSS)-styrene macromers. *J Inorg Organomet P* **11**, 155-164, doi:Unsp 1053-0495/01/0900-0155/0, Doi 10.1023/A:1015237627340 (2001).

44 Moriarty, P. & Honnery, D. What is the global potential for renewable energy? *Renew Sust Energ Rev* **16**, 244-252, doi:10.1016/j.rser.2011.07.151 (2012).

45 De Wild, P. J., Huijgen, W. J. J. & Gosselink, R. J. A. Lignin pyrolysis for profitable lignocellulosic biorefineries. *Biofuel Bioprod Bior* **8**, 645-657, doi:10.1002/bbb.1474 (2014).

46 Li, C. Z., Zhao, X. C., Wang, A. Q., Huber, G. W. & Zhang, T. Catalytic Transformation of Lignin for the Production of Chemicals and Fuels. *Chem Rev* **115**, 11559-11624, doi:10.1021/acs.chemrev.5b00155 (2015).

47 Ragauskas, A. J. *et al.* Lignin Valorization: Improving Lignin Processing in the Biorefinery. *Science* **344**, 709-+, doi:ARTN 124684310.1126/science.1246843 (2014).

48 Rinaldi, R. *et al.* Paving the Way for Lignin Valorisation: Recent Advances in Bioengineering, Biorefining and Catalysis. *Angew Chem Int Edit* **55**, 8164-8215, doi:10.1002/anie.201510351 (2016).

49 Thakur, V. K. & Thakur, M. K. Recent advances in green hydrogels from lignin: a review. *Int J Biol Macromol* **72**, 834-847, doi:10.1016/j.ijbiomac.2014.09.044 (2015).

50 Upton, B. M. & Kasko, A. M. Strategies for the Conversion of Lignin to High-Value Polymeric Materials: Review and Perspective. *Chem Rev* **116**, 2275-2306, doi:10.1021/acs.chemrev.5b00345 (2016).

51 Jensen, C. U., Guerrero, J. K. R., Karatzos, S., Olofsson, G. & Iversen, S. B. Fundamentals of Hydrofaction((TM)): Renewable crude oil from woody biomass. *Biomass Convers Bior* **7**, 495-509, doi:10.1007/s13399-017-0248-8 (2017).

52 Van den Bosch, S., Schutyser, W. & Sels, B. Reductive lignocellulose fractionation into soluble lignin-derived phenolic mono- and dimers and processable carbohydrate pulp. *Abstr Pap Am Chem S* **250** (2015).

53 Vanholme, R., Demedts, B., Morreel, K., Ralph, J. & Boerjan, W. Lignin Biosynthesis and Structure. *Plant Physiol* **153**, 895-905, doi:10.1104/pp.110.155119 (2010).

54 Huang, Y. *et al.* Lignin-first biorefinery: a reusable catalyst for lignin depolymerization and application of lignin oil to jet fuel aromatics and polyurethane feedstock. *Sustain Energ Fuels* **2**, 637-647, doi:10.1039/c7se00535k (2018).

55 Bali, G., Meng, X. Z., Deneff, J. I., Sun, Q. N. & Ragauskas, A. J. The Effect of Alkaline Pretreatment Methods on Cellulose Structure and Accessibility. *Chemsuschem* **8**, 275-279, doi:10.1002/cssc.201402752 (2015).

56 Howe, D. T. *et al.* Steam gasification of a thermally pretreated high lignin corn stover simultaneous saccharification and fermentation digester residue. *Energy* **119**, 400-407, doi:10.1016/j.energy.2016.12.094 (2017).

57 Zhang, B., Huang, H. J. & Ramaswamy, S. Reaction kinetics of the hydrothermal treatment of lignin. *Appl Biochem Biotech* **147**, 119-131, doi:10.1007/s12010-007-8070-6 (2008).

58 Prado, R. *et al.* Depolymerisation of lignin by oxidation in ionic liquids. *Abstr Pap Am Chem S* **251** (2016).

59 Liu, C. J., Wang, H. M., Karim, A. M., Sun, J. M. & Wang, Y. Catalytic fast pyrolysis of lignocellulosic biomass. *Chem Soc Rev* **43**, 7594-7623, doi:10.1039/c3cs60414d (2014).

60 Zakzeski, J., Jongerius, A. L., Bruijnincx, P. C. A. & Weckhuysen, B. M. Catalytic Lignin Valorization Process for the Production of Aromatic Chemicals and Hydrogen. *Chemsuschem* **5**, 1602-1609, doi:10.1002/cssc.201100699 (2012).
61 Anderson, E. M. *et al.* Reductive Catalytic Fractionation of Corn Stover Lignin. *Acs Sustain Chem Eng* **4**, 6940-6950, doi:10.1021/acssuschemeng.6b01858 (2016).
62 Renders, T., Van den Bosch, S., Koelewijn, S. F., Schutyser, W. & Sels, B. F. Lignin-first biomass fractionation: the advent of active stabilisation strategies. *Energ Environ Sci* **10**, 1551-1557, doi:10.1039/c7ee01298e (2017).
63 Anderson, E. M. *et al.* Flowthrough Reductive Catalytic Fractionation of Biomass. *Joule* **1**, 613-622, doi:10.1016/j.joule.2017.10.004 (2017).
64 Shuai, L. *et al.* Formaldehyde stabilization facilitates lignin monomer production during biomass depolymerization. *Science* **354**, 329-333, doi:10.1126/science.aaf7810 (2016).
65 Meemken, F. & Baiker, A. Recent Progress in Heterogeneous Asymmetric Hydrogenation of C=O and C=C Bonds on Supported Noble Metal Catalysts. *Chem Rev* **117**, 11522-11569, doi:10.1021/acs.chemrev.7b00272 (2017).
66 Lindqvist, M. *et al.* Chiral Molecular Tweezers: Synthesis and Reactivity in Asymmetric Hydrogenation. *J Am Chem Soc* **137**, 4038-4041, doi:10.1021/ja512658m (2015).
67 Nishiguchi, T., Tachi, K. & Fukuzumi, K. Transfer Hydrogenation and Transfer Hydrogenolysis .5. Hydrogen Transfer from Amines, Ethers, Alcohols, and Hydroaromatic Compounds to Olefins Catalyzed by Chlorotris(Triphenylphosphine)Rhodium(I). *J Org Chem* **40**, 237-240, doi:DOI 10.1021/jo00890a019 (1975).
68 Aleman-Vazquez, L. O., Torres-Mancera, P., Ancheyta, J. & Ramirez-Salgado, J. Use of Hydrogen Donors for Partial Upgrading of Heavy Petroleum. *Energ Fuel* **30**, 9050-9060, doi:10.1021/acs.energyfuels.6b01656 (2016).
69 Gilkey, M. J. & Xu, B. J. Heterogeneous Catalytic Transfer Hydrogenation as an Effective Pathway in Biomass Upgrading. *Acs Catal* **6**, 1420-1436, doi:10.1021/acscatal.5b02171 (2016).
70 Wang, D. & Astruc, D. The Golden Age of Transfer Hydrogenation. *Chem Rev* **115**, 6621-6686, doi:10.1021/acs.chemrev.5b00203 (2015).
71 Saidi, M. *et al.* Upgrading of lignin-derived bio-oils by catalytic hydrodeoxygenation. *Energ Environ Sci* **7**, 103-129, doi:10.1039/c3ee43081b (2014).
72 Zakzeski, J., Bruijnincx, P. C. A., Jongerius, A. L. & Weckhuysen, B. M. The Catalytic Valorization of Lignin for the Production of Renewable Chemicals. *Chem Rev* **110**, 3552-3599, doi:10.1021/cr900354u (2010).
73 Luo, H. *et al.* Total Utilization of Miscanthus Biomass, Lignin and Carbohydrates, Using Earth Abundant Nickel Catalyst. *Acs Sustain Chem Eng* **4**, 2316-2322, doi:10.1021/acssuschemeng.5b01776 (2016).
74 Chen, F. *et al.* Stable and Inert Cobalt Catalysts for Highly Selective and Practical Hydrogenation of C N and C=O Bonds. *J Am Chem Soc* **138**, 8781-8788, doi:10.1021/jacs.6b03439 (2016).
75 Zhang, P. *et al.* Ultra-Stable and High-Cobalt-Loaded Cobalt@Ordered Mesoporous Carbon Catalysts: All-in-One Deoxygenation of Ketone into Alkylbenzene. *ChemCatChem* **10**, 3299-3304, doi:doi:10.1002/cctc.201800358 (2018).
76 Long, J. L., Zhou, Y. & Li, Y. W. Transfer hydrogenation of unsaturated bonds in the absence of base additives catalyzed by a cobalt-based heterogeneous catalyst. *Chem Commun* **51**, 2331-2334, doi:10.1039/c4cc08946d (2015).
77 Chen, F. *et al.* Selective cobalt nanoparticles for catalytic transfer hydrogenation of N-heteroarenes. *Chem Sci* **8**, 6239-6246, doi:10.1039/c7sc02062g (2017).

78 Kumar, B. S., Amali, A. J. & Pitchumani, K. Heterogenization of cobalt nanoparticles on hollow carbon capsules: Lab-in-capsule for catalytic transfer hydrogenation of carbonyl compounds. *Mol Catal* **448**, 153-161, doi:10.1016/j.mcat.2018.01.036 (2018).
79 Pei, Y. *et al.* Synthesis and catalysis of chemically reduced metal–metalloid amorphous alloys. *Chem Soc Rev* **41**, 8140-8162, doi:10.1039/C2CS35182J (2012).
80 Liu, Y. *et al.* Structure and electrochemical behaviors of a series of Co-B alloys. *Electrochim Acta* **53**, 2265-2271, doi:10.1016/j.electacta.2007.09.052 (2008).
81 Chen, Y. Z. & Wu, K. J. Hydrogenation Activity and Selectivity of Cobalt Borides. *Appl Catal* **78**, 185-197, doi:Doi 10.1016/0166-9834(91)80105-6 (1991).
82 Wang, W. Y., Yang, Y. Q., Luo, H. A. & Liu, W. Y. Characterization and hydrodeoxygenation properties of Co promoted Ni-Mo-B amorphous catalysts: influence of Co content. *React Kinet Mech Cat* **101**, 105-115, doi:10.1007/s11144-010-0201-3 (2010).
83 Wang, W. Y., Yang, Y. Q., Luo, H. A., Hu, T. & Liu, W. Y. Amorphous Co-Mo-B catalyst with high activity for the hydrodeoxygenation of bio-oil. *Catal Commun* **12**, 436-440, doi:10.1016/j.catcom.2010.11.001 (2011).
84 Li, H., Yang, H. X. & Li, H. X. Highly active mesoporous Co-B amorphous alloy catalyst for cinnamaldehyde hydrogenation to cinnamyl alcohol. *J Catal* **251**, 233-238, doi:10.1016/j.jcat.2007.07.022 (2007).
85 Carenco, S., Portehault, D., Boissiere, C., Mezailles, N. & Sanchez, C. Nanoscaled Metal Borides and Phosphides: Recent Developments and Perspectives. *Chem Rev* **113**, 7981-8065, doi:10.1021/cr400020d (2013).
86 Axelbaum, R. L. *et al.* Gas-phase combustion synthesis of titanium boride (TiB2) nanocrystallites. *J Mater Res* **11**, 948-954, doi:Doi 10.1557/Jmr.1996.0119 (1996).
87 Maynadie, J. *et al.* Cobalt Growth on the Tips of CdSe Nanorods. *Angew Chem Int Edit* **48**, 1814-1817, doi:10.1002/anie.200804798 (2009).
88 Gonzalez-Carballo, J. M., Sadasivan, S., Landon, P. & Tooze, R. P. Synthesis of cobalt nanodumbbells and their thermal stability under H-2, H-2/CO and O-2 atmospheres. *Mater Charact* **118**, 519-526, doi:10.1016/j.matchar.2016.06.031 (2016).
89 Li, C. *et al.* Mesoporous nanostructured Co3O4 derived from MOF template: a high-performance anode material for lithium-ion batteries. *J Mater Chem A* **3**, 5585-5591, doi:10.1039/c4ta06914e (2015).
90 Cazacu, A. *et al.* Self-Organization and/or Nanocrystallinity of Co Nanocrystals Effects on the Oxidation Process Using High-Energy Electron Beam. *Advanced Functional Materials* **24**, 164-170, doi:doi:10.1002/adfm.201301465 (2014).
91 Lee, S., Zaborenko, N. & Varma, A. Acetophenone hydrogenation on Rh/Al2O3 catalyst: Flow regime effect and trickle bed reactor modeling. *Chem Eng J* **317**, 42-50, doi:10.1016/j.cej.2017.02.002 (2017).
92 Verma, D. *et al.* Ga-doped Cu/H-nanozeolite-Y catalyst for selective hydrogenation and hydrodeoxygenation of lignin-derived chemicals. *Green Chem* **20**, 3253-3270, doi:10.1039/c8gc00629f (2018).
93 Shafaghat, H., Rezaei, P. S. & Daud, W. M. A. W. Catalytic hydrogenation of phenol, cresol and guaiacol over physically mixed catalysts of Pd/C and zeolite solid acids. *Rsc Adv* **5**, 33990-33998, doi:10.1039/c5ra00367a (2015).
94 Fang, H. H. *et al.* Product tunable behavior of carbon nanotubes-supported Ni-Fe catalysts for guaiacol hydrodeoxygenation. *Appl Catal a-Gen* **529**, 20-31, doi:10.1016/j.apcata.2016.10.011 (2017).
95 Liu, X. Y., An, W., Wang, Y. X., Turner, C. H. & Resasco, D. E. Hydrodeoxygenation of guaiacol over bimetallic Fe-alloyed (Ni, Pt) surfaces: reaction mechanism, transition-state scaling

relations and descriptor for predicting C-O bond scission reactivity. *Catal Sci Technol* **8**, 2146-2158, doi:10.1039/c8cy00282g (2018).

96 Lee, K., Gu, G. H., Mullen, C. A., Boateng, A. A. & Vlachos, D. G. Guaiacol Hydrodeoxygenation Mechanism on Pt(111): Insights from Density Functional Theory and Linear Free Energy Relations. *Chemsuschem* **8**, 315-322, doi:10.1002/cssc.201402940 (2015).

97 de Souza, P. M. *et al.* Hydrodeoxygenation of Phenol over Pd Catalysts. Effect of Support on Reaction Mechanism and Catalyst Deactivation. *Acs Catal* **7**, 2058-2073, doi:10.1021/acscatal.6b02022 (2017).

98 de Souza, P. M. *et al.* Role of Keto Intermediates in the Hydrodeoxygenation of Phenol over Pd on Oxophilic Supports. *Acs Catal* **5**, 1318-1329, doi:10.1021/cs501853t (2015).

99 Teles, C. A. *et al.* The Effect of Metal Type on Hydrodeoxygenation of Phenol Over Silica Supported Catalysts. *Catalysis Letters* **146**, 1848-1857, doi:10.1007/s10562-016-1815-5 (2016).

100 Kumar, B. S., Puthiaraj, P., Amali, A. J. & Pitchumani, K. Ultrafine Bimetallic PdCo Alloy Nanoparticles on Hollow Carbon Capsules: An Efficient Heterogeneous Catalyst for Transfer Hydrogenation of Carbonyl Compounds. *Acs Sustain Chem Eng* **6**, 491-500, doi:10.1021/acssuschemeng.7b02754 (2018).

101 Mohapatra, S. K., Sonavane, S. U., Jayaram, R. V. & Selvam, P. Heterogeneous catalytic transfer hydrogenation of aromatic nitro and carbonyl compounds over cobalt (II) substituted hexagonal mesoporous aluminophosphate molecular sieves. *Tetrahedron letters* **43**, 8527-8529 (2002).

102 Srivastava, S. *et al.* Cr-free Co–Cu/SBA-15 catalysts for hydrogenation of biomass-derived α-, β-unsaturated aldehyde to alcohol. *Chinese Journal of Catalysis* **36**, 933-942, doi:https://doi.org/10.1016/S1872-2067(15)60870-1 (2015).

103 Li, J. L. & Coville, N. J. Effect of boron on the sulfur poisoning of Co/TiO2 Fischer-Tropsch catalysts. *Appl Catal a-Gen* **208**, 177-184, doi:Doi 10.1016/S0926-860x(00)00705-5 (2001).

104 Wang, W. J., Li, H. X. & Deng, J. F. Boron role on sulfur resistance of amorphous NiB/SiO2 catalyst poisoned by carbon disulfide in cyclopentadiene hydrogenation. *Appl Catal a-Gen* **203**, 293-300, doi:Doi 10.1016/S0926-860x(00)00501-9 (2000).

105 Portehault, D. *et al.* A General Solution Route toward Metal Boride Nanocrystals. *Angew Chem Int Edit* **50**, 3262-3265, doi:10.1002/anie.201006810 (2011).

Vita

Michael Kandziolka was born in Pottstown, PA, but grew up in Augusta, GA where he graduated from Evans High School in May 2007. He then enrolled at Augusta University in 2007, and transferred to the University of Tennessee at Knoxville in 2009 with a Bachelor's of Science in Chemistry (ACS Certification) in May 2012.

Michael then participated in the Science Undergraduate Laboratory Internship (SULI) Program at Oak Ridge National Laboratory in Oak Ridge, TN for two separate appointments in Fall 2012 and Spring 2013. In Fall of 2012 he conducted research under Dr. Aditya Savara on the interaction of surface-grafted aromatic moieties with neighboring surface silanols of SBA-15. In Spring 2013 he then conducted research under Dr. Nickolay Lavrik and Dr. Michael Sepaniak on silicon nanopillars for enhanced fluorescent detection.

In Fall 2013 he then pursued a doctoral degree in inorganic chemistry at the University of Tennessee at Knoxville in Knoxville TN under the guidance of Dr. Craig E. Barnes and co-advisor Dr. Stephen C. Chmely. His graduate work focused on an ongoing project involving synthesis of boron-containing cobalt catalysts for catalytic transfer hydrogenolysis of lignin model compounds.